FEDERAL UNIVERSITY OF PARÁ
INSTITUTE OF TECHNOLOGY
POST-GRADUATE PROGRAM IN ELECTRICAL ENGINEERING

DENIS LIMA DO ROSÁRIO

CROSS-LAYER OPTIMIZATIONS FOR MULTIMEDIA DISTRIBUTION OVER WIRELESS MULTIMEDIA SENSOR NETWORKS AND FLYING AD-HOC NETWORKS WITH QUALITY OF EXPERIENCE SUPPORT

TD 04/2014

July - 2014

FEDERAL UNIVERSITY OF PARÁ
INSTITUTE OF TECHNOLOGY
POST-GRADUATE PROGRAM IN
ELECTRICAL ENGINEERING

UNIVERSITY OF BERN
FACULTY OF SCIENCES
INSTITUTE OF COMPUTER SCIENCES
AND APPLIED MATHEMATICS

DENIS LIMA DO ROSÁRIO

CROSS-LAYER OPTIMIZATIONS FOR MULTIMEDIA DISTRIBUTION OVER WIRELESS MULTIMEDIA SENSOR NETWORKS AND FLYING AD-HOC NETWORKS WITH QUALITY OF EXPERIENCE SUPPORT

PhD thesis submitted to the Examining Board to obtain a joint-supervision PhD degree by the Federal University of Pará and the University of Bern

Advisor: Professor Dr. Eduardo Coelho Cerqueira

Co-Advisor: Professor Dr. Torsten Ingo Braun

July - 2014

Dados Internacionais de Catalogação-na-Publicação (CIP)

Rosário, Denis Lima do , 1986-
Cross-layer optimizations for multimedia distribution over wireless multimedia sensor networks and flying ad-hoc networks with quality of experience support / Denis Lima do Rosário. - 2014.

Orientador: Eduardo Coelho Cerqueira;
Coorientador: Torsten Ingo Braun.
Tese (Doutorado) - Universidade Federal do Pará, Instituto de Tecnologia, Programa de Pós-Graduação em Engenharia Elétrica, Belém, 2014.

1. Sistemas multimídia. 2. Redes de sensores. 3. Redes ad hoc (redes de computadores). 4. Comunicações digitais. I. Título.

CDD 23. ed. 006.7

CROSS-LAYER OPTIMIZATIONS FOR MULTIMEDIA DISTRIBUTION OVER WIRELESS MULTIMEDIA SENSOR NETWORKS AND FLYING AD-HOC NETWORKS WITH QUALITY OF EXPERIENCE SUPPORT

Inauguraldissertation
der Philosophisch-naturwissenschaftlichen Fakultät
der Universität Bern

vorgelegt von

Denis Lima do Rosário

von Brazil

Leiter der Arbeit:
Professor Dr. Eduardo Coelho Cerqueira
Federal University of Pará
Professor Dr. Torsten Braun
Institut für Informatik und angewandte Mathematik

CROSS-LAYER OPTIMIZATIONS FOR MULTIMEDIA DISTRIBUTION OVER WIRELESS MULTIMEDIA SENSOR NETWORKS AND FLYING AD-HOC NETWORKS WITH QUALITY OF EXPERIENCE SUPPORT

Inauguraldissertation
der Philosophisch-naturwissenschaftlichen Fakultät
der Universität Bern

vorgelegt von

Denis Lima do Rosário

von Brazil

Leiter der Arbeit:
Professor Dr. Eduardo Coelho Cerqueira
Federal University of Pará
Professor Dr. Torsten Braun
Institut für Informatik und angewandte Mathematik

Von der Philosophisch-naturwissenschaftlichen Fakultät angenommen.

Bern, 16.7.2014

Der Dekan:
Prof. Dr. Silvio Decurtins

FEDERAL UNIVERSITY OF PARÁ
INSTITUTE OF TECHNOLOGY
POST-GRADUATE PROGRAM IN
ELECTRICAL ENGINEERING

UNIVERSITY OF BERN
FACULTY OF SCIENCES
INSTITUTE OF COMPUTER SCIENCES
AND APPLIED MATHEMATICS

CROSS-LAYER OPTIMIZATIONS FOR MULTIMEDIA DISTRIBUTION OVER WIRELESS MULTIMEDIA SENSOR NETWORKS AND FLYING AD-HOC NETWORKS WITH QUALITY OF EXPERIENCE SUPPORT

DENIS LIMA DO ROSÁRIO

This PhD thesis was considered as appropriate and accepted in its final version to obtain the joint-supervision PhD degree in Electrical Engineering, Area of Concentration in Applied Computing by the Post-graduate Program of Electrical Engineering of the Federal University of Pará, as well as in Computer Science by the Institute of Computer Sciences and Applied Mathematics of University of Bern.

Aproved at: __/__/____

PhD Thesis Examination-Board

Prof. Professor Dr. Eduardo Coelho Cerqueira
(Federal University of Pará – Advisor)

Prof. Professor Dr. Torsten Ingo Braun
(University of Bern – Co-Advisor)

Prof. Dr. Aldebaro Barreto da Rocha Klautau Júnior
(Federal University of Pará – President of the Jury)

Prof. Dr. Aldri Luiz dos Santos
(Federal University of Paraná – Member of the Jury)

Prof. Dr. Augusto José Venâncio Neto
(Federal University of Rio Grande do Norte – Member of the Jury)

Analyzed:

Prof. Dr. Evaldo Gonçalves Pelaes
Coordinator of the Post-graduate Program in Electrical Engineering at UFPA

Prof. Dr. Silvio Decurtins
Dean of the Faculty of Science at University of Bern

To my parents.

Acknowledgements

Firstly, thank God, because he is the responsible for everything that happens in my life.

Secondly, I would like to thank my family, especially to my parents, José Everaldo do Rosário and Waldeci Rosário, and also to my sisters, Danielle and Denise do Rosário. Although we stayed far away during my PhD, they always encourage me to continue and finish my studies. For my parents and sisters, I will translate my acknowledgements for them to Portuguese. Em especial para os meus pais e irmãs irei traduzir meus agradecimentos para português: "Gostaria de agradecer a minha família, especialmente aos meus pais, José Everaldo do Rosário e Waldeci Rosário, bem como para as minhas irmãs, Danielle e Denise do Rosário. Embora tenhamos ficado longe durante boa parte do meu doutorado, vocês sempre me incentivaram a continuar meus estudos e sem o incentivo de vocês não seria possível terminar. Amo vocês!"

Next, I would like to express a deep gratitude to Hilda Rosa Freitas (in the near future Mrs. Hilda Rosário :)). Although we stayed far away during my visiting researcher at University of Bern, Switzerland, we never stayed far away mentally. She always gave me support and encouragement during the difficult moments of this thesis. Finally, without her patience, encouragement, and support, I could never tolerate to stay in Bern and also I could never finish this work.

I also would like to express my gratitude to my PhD advisor Eduardo Coelho Cerqueira and PhD co-advisor Torsten Braun for the outstanding supervision leading towards this work, and in special for the patience for teach me. During my PhD work, both have a fundamental importance to help me to improve my work, for their very interesting suggestions and critics, and also to teach me how to write this thesis and my research papers. I am so thankful for so many things that I learned from both, and also for the time spent together in some meetings, happy hours, CDS Stammtischs, lunch time, or any other events. Finally, I would like to thank both for seeing the usefulness of my work and for their considerable efforts to make my work more visible to the research community.

I would also thank Aldri Santos for his contribution for this thesis and for the uncountable Skype meetings that we had together discussing.

I would like to thank all Federal University of Pará (Brazil) and the University of Bern (Switzerland) employees that were responsible for the establishment of the cooperation agreement for the joint-supervision of doctoral theses between UFPA and the University of Bern. In special, I would like to thank Prof. Eduardo Cerqueira, Leila Assef Mendes, and Emmanuel Tourinho from UFPA, and also to Prof. Torsten Braun, Zoe Ghielmetti, and Dr. Silvio Decurtins from University of Bern, which made a lot of effort to establish the contract to provide me the joint-supervision PhD degree.

I would like to thank CNPq and University of Bern by their financial resources allocated during my PhD.

I would like to express my appreciation to Rodrigo Costa, Claudio Silva, Helder Paranese, Tales Mousinho, and Philipe Terroso for their implementation efforts that contributed significantly to the results presented in this work. Their efforts were made in the context of their Bachelor or Master works.

I would like to thank my colleges from UFPA and University of Bern for sharing of knowledge and mainly for the great moments spent together, namely Thiêgo Maciel, Roberto Sato, Kássio Machado, André Riker, Zhongliang Zhao, Zan Li, Carlos Anastasiades, and Desi. I also would like to thank my friend Cloudo Luis by encouragement and support during my PhD period.

Finally, I would like to thank to someone that I forgot to mention, which might help me directly or indirectly during this work.

Abstract

Abstract of the PhD thesis presented to UFPA and University of Bern as a partial fulfilment to obtain the joint-supervision PhD degree in Electrical Engineering by the Post-graduate Program of Electrical Engineering of the Federal University of Par, as well as in Computer Science by the Institute of Computer Sciences and Applied Mathematics of University of Bern.

Cross-layer Optimizations for Multimedia Distribution over Wireless Multimedia Sensor Networks and Flying Ad-Hoc Networks with Quality of Experience Support

Advisor: Professor Dr. Eduardo Coelho Cerqueira
Co-advisor: Professor Dr. Torsten Ingo Braun
Keywords: Energy-efficiency; FANETs; Reliability; Robustness; Scalability; QoE support; and WMSNs.

The proliferation of multimedia content and the demand for new audio or video services have fostered the development of a new era based on multimedia information, which allowed the evolution of Wireless Multimedia Sensor Networks (WMSNs) and also Flying Ad-Hoc Networks (FANETs). In this way, live multimedia services require real-time video transmissions with a low frame loss rate, tolerable end-to-end delay, and jitter to support video dissemination with Quality of Experience (QoE) support. Hence, a key principle in a QoE-aware approach is the transmission of high priority frames (protect them) with a minimum packet loss ratio, as well as network overhead. Moreover, multimedia content must be transmitted from a given source to the destination via intermediate nodes with high reliability in a large scale scenario. The routing service must cope with dynamic topologies caused by node failure or mobility, as well as wireless channel changes,

in order to continue to operate despite dynamic topologies during multimedia transmission. Finally, understanding user satisfaction on watching a video sequence is becoming a key requirement for delivery of multimedia content with QoE support. With this goal in mind, solutions involving multimedia transmissions must take into account the video characteristics to improve video quality delivery.

The main research contributions of this thesis are driven by the research question how to provide multimedia distribution with high energy-efficiency, reliability, robustness, scalability, and QoE support over wireless ad hoc networks. The thesis addresses several problem domains with contributions on different layers of the communication stack. At the application layer, we introduce a QoE-aware packet redundancy mechanism to reduce the impact of the unreliable and lossy nature of wireless environment to disseminate live multimedia content. At the network layer, we introduce two routing protocols, namely video-aware Multi-hop and multi-path hierarchical routing protocol for Efficient VIdeo transmission for static WMSN scenarios (MEVI), and cross-layer link quality and geographical-aware beaconless OR protocol for multimedia FANET scenarios (XLinGO). Both protocols enable multimedia dissemination with energy-efficiency, reliability and QoE support. This is achieved by combining multiple cross-layer metrics for routing decision in order to establish reliable routes.

Resumo

Resumo da tese de doutorado apresentada à UFPA e à Universidade de Berna como um cumprimento parcial para obtenção do grau de doutor com dupla titulação em Engenharia Elétrica pelo Programa de Pós-Graduação de Engenharia Elétrica da Universidade Federal do Pará, bem como em Ciência da Computação pela do Instituto de Ciências da Computação e Matemática Aplicada da Universidade de Berna.

Otimizações em Múltiplas Camada para Distribuição Multimídia em Redes de Sensores Sem Fio Multimídia e Redes Ad-Hoc Formadas por VANTs com Suporte à Qualidade de Experiência

Orientador: Professor Dr. Eduardo Coelho Cerqueira
Co-orientador: Professor Dr. Torsten Ingo Braun
Palavras-chave: Confiabilidade; Eficiência energética; Escalabilidade; FANETs; suporte à QoE; Robustez; e RSSFM.

A proliferação de conteúdo multimídia bem como a demanda por novos serviços de áudio ou vídeo promoveram o desenvolvimento de uma nova era baseada em informações multimídia, o que permitiu a evolução das Redes de Sensores Sem Fio Multimídia (RSSFM) e também das redes ad-hoc desenvolvimento formadas por VANTs (FANETs). Desta forma, serviços multimídia em tempo real requerem transmissões de vídeo em tempo real com uma baixa taxa de perda de quadros, atraso fim-a-fim tolerável, para apoiar a disseminação de vídeo com qualidade de Experiência (QoE) assegurada. Desta forma, um princípio fundamental de uma abordagem ciente de QoE é a transmissão de quadros de vídeo com alta prioridade, baixa taxa de perda de pacotes, bem como baixa sobrecarga

da rede, a fim de protegê-los. Além disso, o conteúdo multimídia devem ser transmitidos a partir de um determinado nó de origem para um nó de destino através de nós intermediários com alta confiabilidade em um cenário de grande escala. O serviço de roteamento deve lidar com topologias dinâmicas causadas por falha de um nó ou a mobilidade do mesmo, bem como as mudanças no canal sem fio, a fim de continuar a operar mesmo em casos de mudanças de topologia durante a transmissão multimídia. Por fim, o mapeamento da satisfação do usuário ao assistir um determinado vídeo está se tornando um requisito fundamental para a entrega de conteúdos multimídia com suporte à QoE. Com estes objetivos em mente, soluções envolvendo transmissões multimídia deve levar em conta as características de vídeo e do usuário para melhorar a entrega de vídeo com qualidade assegurada.

As principais contribuições desta tese são conduzidos pela seguinte questão de pesquisa: como para fornecer distribuição de multimídia com alta eficiência energética, confiabilidade, robustez, escalabilidade e suporte à QoE em redes sem fio ad hoc. A tese aborda vários domínios de problemas com contribuições em diferentes camadas da pilha de comunicação. Na camada de aplicação, apresentamos um mecanismo de redundância de pacotes ciente de QoE para reduzir o impacto da não confiabilidade do canal sem fio, e assim prover disseminação de conteúdo multimídia em tempo real com suporte à QoE. Na camada de rede, apresentamos dois protocolos de roteamento, ou seja, o *video-aware Multi-hop and multi-path hierarchical routing protocol for Efficient VIdeo transmission for static WMSN scenarios (MEVI)* e o *cross-layer link quality and geographical-aware beaconless OR protocol for multimedia FANET scenarios* (XLinGO). Ambos os protocolos de roteamento permitem a disseminação de conteúdo multimídia com eficiência energética, confiabilidade e suporte à QoE. Isto é alcançado através da combinação de métricas de múltiplas camadas para a tomada de decisão para o roteamento de pacotes, e assim estabelecer rotas confiáveis.

Contents

1 Introduction .... p. 1

1.1 Overview .... p. 1

1.2 Problem Statement .... p. 3

1.2.1 Scalability .... p. 3

1.2.2 Unreliable Nature of Wireless Channels .... p. 4

1.2.3 Robustness .... p. 4

1.2.4 Energy-efficiency .... p. 5

1.2.5 QoE Requirements .... p. 5

1.2.6 Buffer Control .... p. 6

1.3 Thesis Contributions .... p. 6

1.3.1 Application-Level Packet Redundancy Mechanism .... p. 7

1.3.2 Hierarchical Routing Protocol for Static Wireless Multimedia Sensor Networks Scenarios .... p. 7

1.3.3 Opportunistic Routing Protocol for Multimedia Flying Ad-Hoc Network Scenarios .... p. 8

1.4 Thesis Outline .... p. 9

2 Related Work .... p. 11

2.1 Video Characteristics .... p. 11

2.1.1 Spatial or Intra-frame Compression .... p. 12

2.1.2 Temporal or Inter-frame Compression .... p. 14

2.1.3 Group of pictures (GoP) . . . . p. 16

2.2 Error Correction Schemes . . . . p. 17

2.2.1 Automatic Repeat Request Schemes . . . . p. 18

2.2.2 Link-layer Forward Error Correction Schemes . . . . p. 18

2.2.3 Packet-Level Redundancy Mechanisms . . . . p. 19

2.3 Routing Protocols for Static WMSNs . . . . p. 22

2.3.1 Low-Energy Adaptive Clustering Hierarchy for WSNs . . . . p. 22

2.3.2 Hierarchical Routing Algorithm for WMSNs . . . . p. 23

2.3.3 Multi-path Routing for WMSNs . . . . p. 24

2.3.4 Ant-based Hierarchical Routing Algorithm for WMSNs . . . . p. 24

2.3.5 Final Considerations of Different Hierarchical Routing Protocols for WMSN Scenarios . . . . p. 25

2.4 Opportunistic Routing Protocols for Multimedia FANET Scenarios . . . . p. 26

2.4.1 Beacon-based OR Protocols . . . . p. 26

2.4.2 Beaconless OR Protocols . . . . p. 27

2.4.3 Final Considerations of Existing OR Protocols for Multimedia FANET Scenarios . . . . p. 29

3 QoE-aware Packet-Level Redundancy Mechanism . . . . p. 31

3.1 Motivation . . . . p. 32

3.2 Problem Statement . . . . p. 32

3.3 QoE-aware Packet Redundancy Mechanism Description and Operation Principles . . . . p. 33

3.4 Summary . . . . p. 36

4 A Multi-hop Hierarchical Routing Protocol for Efficient Video Communication . . . . p. 37

4.1 Motivation . . . . p. 38

4.2 Network Model . . . . p. 40

4.3 Problem Statement . . . . p. 42

4.4 MEVI Design and Operation Principles . . . . p. 42

4.4.1 Intra-Cluster Communication . . . . p. 43

4.4.2 Inter-Cluster Communication ... p. 46
4.4.2.1 Operational Modes: Normal or Event Mode ... p. 47
4.4.2.2 Node-disjoint Multiple Route Discovery ... p. 49
4.4.2.3 Video-aware Multimedia Transmission ... p. 55
4.5 Summary ... p. 57

5 A Cross-layer Link quality and Geographical-aware beaconless OR protocol ... p. 59
5.1 Motivation ... p. 60
5.2 Network Model ... p. 62
5.3 Problem Statement ... p. 64
5.4 XLinGO Design and Operation Principles ... p. 64
5.4.1 Contention-based Forwarding Mode ... p. 65
5.4.1.1 Complexity and Overhead Analysis of the Contention-based Forwarding Mode Algorithm ... p. 69
5.4.1.2 Metrics for the Contention-based Forwarding Mode ... p. 70
5.4.1.3 Contention-based Forwarding Mode Example ... p. 77
5.4.2 Persistent Route Mode ... p. 77
5.4.2.1 Recovery Mechanism for the Persistent Route Mode ... p. 78
5.4.2.2 Complexity and Overhead Analysis of the Persistent Route Mode Algorithm ... p. 81
5.5 Summary ... p. 81

6 Performance Evaluation ... p. 83
6.1 Mobile MultiMedia Wireless Sensor Network (M3WSN) OMNeT++ Framework ... p. 84
6.2 Performance Metrics ... p. 87
6.2.1 Video Quality Assessment ... p. 87
6.2.2 Energy-Efficiency Assessment ... p. 89
6.3 Performance Evaluation of the MEVI Protocol over Static WMSN Scenarios p. 89
6.3.1 Simulation Scenarios ... p. 90
6.3.2 Simulation-Based Result Analysis ... p. 94

6.3.2.1 Scalability Assessment .... p. 94
6.3.2.2 Reliability Assessment .... p. 100
6.3.2.3 Energy-efficiency Assessment .... p. 102
6.3.3 Summary .... p. 103
6.4 Performance Evaluation of the QoE-aware Redundancy Mechanism .... p. 104
6.4.1 Simulation Scenarios .... p. 104
6.4.2 Simulation-Based Result Analysis .... p. 106
6.4.2.1 QoE-aware Redundancy Mechanism Parameters Definition .... p. 107
6.4.2.2 Simulation Results for Scenario 1 .... p. 110
6.4.2.3 Simulation Results for Scenario 2 .... p. 111
6.4.3 Summary .... p. 116
6.5 Performance Evaluation of the XLinGO Protocol over Multimedia FANET Scenarios .... p. 116
6.5.1 Simulation Scenarios .... p. 116
6.5.2 Simulation-Based Result Analysis .... p. 120
6.5.2.1 XLinGO Parameters under Conditions of Scenario 1 .... p. 120
6.5.2.2 Impact of Transient and Permanent Node Failures under Conditions of Scenario 1 .... p. 123
6.5.2.3 Impact of the Mechanism to Recover from Route Failures under Conditions of Scenario 1 .... p. 126
6.5.2.4 Impact of Node Mobility and Number of Video Flows under Conditions of Scenario 2 .... p. 128
6.5.2.5 Signalling Overhead Evaluation under Conditions of Scenario 1 .... p. 132
6.5.2.6 Subjective Video Quality Evaluation .... p. 132
6.5.3 Summary .... p. 135
6.6 Performance Evaluation Summary .... p. 136

7 Conclusions and Outlook .... p. 139
7.1 Main Contributions and Thesis Summary .... p. 140
7.2 Outlook .... p. 144

References .... p. 147

List of Acronyms

WMSNs	Wireless Multimedia Sensor Networks
FANETs	Flying Ad-Hoc Networks
IoT	Internet of Things
BS	Base Station
UAVs	Unmanned Aerial Vehicles
QoE	Quality of Experience
LQE	Link Quality Estimator
PRR	Packet Reception Ratio
RSSI	Received Signal Strength Indicator
SNR	Signal to Noise Ratio
LQI	Link Quality Indicator
WSNs	Wireless Sensor Networks
QoE-aware redundancy	QoE-aware Packet-Level Redundancy Mechanism
MEVI	video-aware Multi-hop and multi-path hierarchical routing protocol for Efficient VIdeo transmission for static WMSN scenarios
OR	Opportunistic Routing
XLinGO	Cross-layer Link quality and Geographical-aware beaconless OR protocol for multimedia FANET scenarios
codec	Coder-decoders
MPEG	Moving Picture Experts Group
DCT	Discrete Cosine Transform
I-Frames	Intra-coded frames
P-Frames	Predictive coded frames
B-Frames	Bi-directionally predictive coded frames
GoP	Group of Pictures

ARQ	Automatic Repeat Request
FEC	Forward Error Correction
EC	Erasure Coding
ECC	Error Correcting Code
BCH	Bose-Hocquenghem-Chaudhuri
RS	Reed-Solomon
DGR	Directional Geographical Routing
SR	Sensing Relevance
FL-FEC	Forward-looking Forward Error Correction
AHECM	Adaptive Hybrid Error Correction Model
RTT	Round-Trip Time
LEACH	Low-Energy Adaptive Clustering Hierarchy
CH	Cluster Heads
TDMA	Time Division Multiple Access
PEMuR	Power Efficient Multimedia Routing protocol
SHPER	Scalable Hierarchical Power Efficient Routing
ARCH	Adaptive Reliable Routing Based on a Cluster Hierarchy for WMSNs
EEQAR	Energy Efficiency QoS Assurance Routing in WMSNs
AOMDV	Ad-hoc On-demand Multi-path Distance Vector protocol
S-AOMDV	Ad-hoc On-Demand Multipath distance Vector routing for MWSNs
EEPMQR	Energy Efficient Prioritized Multipath QoS Routing
ASAR	Ant-based Service-Aware Routing algorithm for WMSNs
AMRA	Ant-based Mobile Routing Architecture
TAP	Topology Abstracting Protocol
MABR	Mobile Ants-Based Routing
StPF	Straight Packet Forwarding
DFD	Dynamic Forwarding Delay
BLR	Beaconless Routing protocol
BOSS	Beaconless On-demand geographic routing Strategy
RTS	Request to Send
EBGR	Energy-efficient Beaconless Geographic Routing
EAOR	Energy Aware Opportunistic Routing protocol
MRR	Multipath Routeless Routing protocol
FIFO	First In First Out
SN	Source Node
RREQ	Route REQuest

RREP	Route REPly
EO	Event Occurrence
MT	Multimedia Transmission
RD	Route Discovery
SA	Send Aggregate packets
MR	Multimedia Request
LQ	Link Quality
PQ	Path Quality
PPA	Positive Progress Area
NPA	Negative Progress Area
ACK	acknowledgment message
PSNR	Peak Signal to Noise Ratio
MSE	Mean Squared Error
SSIM	Structural Similarity Index Metric
VQM	Video Quality Metric
MOS	Mean Opinion Score
QoS	Quality of Service
M3WSN	Mobile MultiMedia Wireless Sensor Network Framework
FoV	Field of view
VQMT	Video Quality Measurement Tool
ITU-T	International Telecommunication Union - Telecommunication Standardization Sector
SS	Single Stimulus
DS	Double Stimulus
EQI	Energy-Quality Index
QCIF	Quarter Common Intermediate Format
CIF	Common Intermediate Format
LIVE	Link Validity time Estimation

List of Symbol

M_{GoP}	Distance between successive P-frames
N_{GoP}	The distance between adjacent I-frames
K	A set of coded packets
n_{pkts}	A set of original video packets
r	Number of redundant packets created by the redundancy mechanism, where $r = K - n_{pkts}$
X_1	Number of P-frames that need packet redundancy
p	Relative frame position within the GoP
n	Number of nodes in the network, $n = \|V\|$
i	Individual identity, where 1 $<$ i $<$ n
$G(V, E)$	Graph representing the routing topology
V	Set of the nodes in the network topology
E	Set of the edges connecting nodes
v_i	A given node with an individual node identity i
e_j	Edge j connecting two nodes within the radio range of each other, were $1 < j < m$
$w(e_j)$	Weight value for each e_j, were $w(e_j)_{min} < w(e_j) < w(e_j)_{max}$
$w(e_j)_{min}$	Minimal weight value for a given link e_j
$w(e_j)_{max}$	Maximum weight value for a given link e_j
Q	Queue for a given node v_i, where $0 < Q < Q_{max}$
Q_{max}	Maximum queue capacity
Q_{length}	Current queue length
P	Battery for a given node v_i, where $P_0 < P < P_{max}$
P_0	Initial battery power
P_{max}	Maximum battery power
RE_t	Remaining energy in a given time t

P_{tx}	Power required to transmit a packet
P_{rx}	Power required to receive a packet
P_{sense}	Power required either to retrieve a video frame or to sense physical scalar sensor measurements
SN_i	A subset of nodes v_i used to transmit physical scalar sensor data measurements
CN_i	A subset of nodes v_i used to transmit multimedia data
DN	Destination Node
$P_{SN,DN}$	A path connecting any pair of SN and DN via multiple CN_i
adv	Advertisement period during the intra-cluster communication
slot_k	A set of time-slots for the intra-cluster communication, were $1 < k < \text{n}_{slot}$
t_{slot}	time-slot duration
n_{slot}	Number of time-slots in each superframe
R	Total amount of time for intra- and inter-cluster communications
candidate_{id}	Candidate CN_i identifier
LQI_{avg}	Exponential average for the LQI perceived in the last w beacons
w	The window size of the exponential average
$candidateList$	CN_k candidate list
o	Size of $candidateList$
type	It is used to identify the message type. RERQ messages are marked with the value equal to 1
src_{addr}	Source address for a given RREQ or RREP message
$dest_{addr}$	Destination address for a given RREQ or RREP message
$RREQ_{seq}$	RREQ sequence number
$route_{id}$	Route identifier
HC	Number of hops for a given RREQ message
DL	Number of disconnected links for a given RREQ message
CL	Number of connected links for a given RREQ message
type	It is used to identify the message type. RERQ messages are marked with the value equal to 2
$RREP_{seq}$	RREQ sequence number
LQI_{bad}	LQI threshold used to define a disconnected link
LQI_{good}	LQI threshold used to define a connected link
ω_{energy}	Energy relevance used to compute the LQ
ω_{LQE}	Link quality relevance used to compute the LQ
ω_{HC}	Hop count relevance used to compute the LQ
LQI_{max}	Maximum value for LQI
HC_{max}	Maximum number of hops

ϕ_{CL}	Coefficient used to give priority to the number of connected links when computing the PQ
ϕ_{DL}	Coefficient used to give priority to the number of disconnected links when computing the PQ
ϕ_{energy}	Coefficient used to give priority to energy when computing the PQ
ϕ_{LQE}	Coefficient used to give priority to link quality when computing the PQ
PQ_{min}	Minimal PQ value to consider a given path as a reliable alternative path
N	Number of paths
$\mathrm{N}(v_i)$	Subset of neighbours within the radio range of a given node v_i
t	A given time
P_v	Power required to move with a certain speed
s_{vi}	Node moving speed
dir	Node moving direction
s_{min}	Minimum speed limit
s_{max}	Maximum speed limit
F	Forwarding node
pkt_{id}	Packet identifier
DFD_{max}	Maximum DFD value
RN_i	Possible relay nodes
E_{th}	Energy threshold used to indicate the total amount of energy required to transmit packets and to move
E_{tx}	Total amount of energy required to transmit a given set of packets
E_v	Total amount of energy required to move at a certain speed
Φ_{LQE}	Coefficient used to give priority to the link quality to compute the DFD
$\Phi_{progress}$	Coefficient used to give priority to the progress when computing the DFD
Φ_{energy}	Coefficient used to give priority to the energy when computing the DFD
Φ_{queue}	Coefficient used to give priority to the queue length when computing the DFD
linkQuality	Link quality calculation part of the DFD function
progress	Progress calculation part of the DFD function
energy	Energy calculation part of the DFD function
queueLength	Queue length calculation part of the DFD function
$w(e_j)_{bad}$	Threshold used to define that a given link e_j provides multimedia dissemination with poor quality level
$w(e_j)_{good}$	Threshold used to define that a given link e_j provides multimedia dissemination with good quality level
X	Parameter to determine the center of the sigmoid output
c	Coefficient to regulate the slope or "growth rate"
RR	Radio Range

$D(RN_i, DN)$	Euclidian distance between a given RN_i and DN
$P(RN_i, DN)$	Geographical advance of a given RN_i towards the DN
$P_1(RN_i)$	Projection of the distance travelled from SN to any RN_i
$P_2(RN_i)$	Projection of line RN_i-RN_i' onto line SN-DN
$nFlow$	Number of video flows
$dataRate_{in}$	Packets per second required for each video flow
$rate_{out}$	Packets per second that a given node is transmitting
Q_{t+1}	Predicted queue size
V	Direction of the camera for FoV definition
θ	Angle of view for FoV definition
d	Depth of view for FoV definition
$\Delta SSIM$	Video quality achieved normalized with a number of hops
E	Spent energy to achieve a given video quality level

List of Algorithms

Algorithm 1 QoE-aware Redundancy Mechanism ... p. 35
Algorithm 2 MEVI Cluster Formation ... p. 45
Algorithm 3 Contention-based Forwarding Mode for SN ... p. 66
Algorithm 4 Contention-based Forwarding Mode for N(SN) ... p. 68
Algorithm 5 Persistent Route Mode ... p. 80

List of Figures

Figure 1 WMSN and Multimedia FANET Application Scenario 2

Figure 2 Thesis Contributions Overview 6

Figure 3 Example of Video Coding and Encoding in a Wireless Network 12

Figure 4 Transform Coding, Quantization and Run-length Coding 13

Figure 5 Complexity Level for Different Video Frames 14

Figure 6 Motion Level for Different Video Frames 15

Figure 7 Group of Pictures Structure 16

Figure 8 Different Strategies for Error Correction 18

Figure 9 Packet-level Redundancy Mechanism 19

Figure 10 Cluster-based Network Architecture 22

Figure 11 Forwarding Area for BLR 28

Figure 12 Forwarding Area for MRR 29

Figure 13 QoE-aware Redundancy Mechanism Overview 33

Figure 14 QoE-aware Redundancy Mechanism Example 36

Figure 15 Hierarchical Network Architecture for Static WMSNs 38

Figure 16 Network Model for Static WMSNs 41

Figure 17 Superframe Structure 43

Figure 18 Intra-cluster Communication Structure 43

Figure 19 Activity Diagram for Inter-Cluster Communication 48

Figure 20 Inter-Cluster Communication Structure 49

Figure 21 Route Request Message 50

Figure 22 Route Reply Message 50

Figure 23 Multi-Path Route Discovery 51

Figure 24 Network Configuration and Results for Reception Regions Evaluation . 53

Figure 25 Activity diagram for Video-aware Multimedia Transmission 56

Figure 26 Load Balancing Scheme Used by MEVI 56

Figure 27 Multimedia FANET Deployed in an Emergency Situation 60

Figure 28 XLinGO Network Model 63

Figure 29 XLinGO Forwarding Decisions 65

Figure 30 Forwarding Area and Strategy 67

Figure 31 Contention-based Forwarding Mode Overview 69

Figure 32 DFD Values for Different progress and linkQuality Values Following the Eq. 5.2 with $\Phi_{queue} = 0$, $\Phi_{LQE} = 0.5$, and $\Phi_{progress} = 0.5$ 71

Figure 33 Irregular Radio Range (left) and Resultant PRR Distribution (right) .. 72

Figure 34 Network Configuration and Results for Video Quality Evaluation 73

Figure 35 Example of an Exponential Distribution 74

Figure 36 Definition of Progress with Potential RN_i 75

Figure 37 Queue Length Monitoring 76

Figure 38 Routing Example with XLinGO in Contention-based Forwarding Mode 78

Figure 39 Time Diagram of the Mechanism Employed to Recover from Route Failures 81

Figure 40 M3WSN Framework Architecture 85

Figure 41 Sensing Range and Object Detection 86

Figure 42 Video Transmission Procedure 87

Figure 43 Simulation Topology for Different Hierarchical Routing Protocols for Static WMSN Scenarios 92

Figure 44 Network Stack for the Performance Evaluation of Different Hierarchical Routing Protocol for Static WMSN Scenarios 92

Figure 45 Video Quality Level According to the Distance Between SN and DN for

Scenario 1 95

Figure 46 Video Quality Level According to the Distance Between SN and DN for Scenario 2 96

Figure 47 SSIM in Colour Scale for Each Node that Composes Scenarios 1 and 2 97

Figure 48 Frame number 266 from Container Video Sequence Transmitted from a Given Node via Different Hierarchical Routing Protocols 99

Figure 49 SSIM for all Frames that Composes the Container Video Sequence Transmitted by a Specific Node under Conditions of Scenario 1 99

Figure 50 SSIM According to Different PQ Value 100

Figure 51 Video Quality Level According to the Number of Hops for Scenario 2 . 101

Figure 52 Frame number 257 from Container Video Sequence Transmitted from a Given Node via Different Hierarchical Routing Protocols 102

Figure 53 Network Lifetime 103

Figure 54 EQI According to the Number of Hops for Scenario 2 103

Figure 55 Network Stack for the Performance Evaluation of Different Redundancy Mechanisms 106

Figure 56 Possible Configurations for the QoE-aware Redundancy Mechanism ... 108

Figure 57 SSIM According to the Distance for Different Configurations of the QoE-aware Redundancy Mechanism 109

Figure 58 Video Quality Level According to the Distance Between SN and DN for Scenario 1 110

Figure 59 Packet Overhead Introduced by Different Redundancy Mechanisms ... 111

Figure 60 Video Quality Level According to the Number of Hops for Scenario 2 . 112

Figure 61 Energy Consumption According to the Number of Hops for Scenario 2 113

Figure 62 EQI According to the Number of Hops for Scenario 2 114

Figure 63 SSIM for all the Frames that Composes the Hall Video Sequence Transmitted by a Specific Node under Conditions of Scenario 2 114

Figure 64 Frame Number 258 for the Hall Video Sequence Transmitted for a Given Node with Different Redundancy Mechanisms for Scenario 2 115

Figure 65 Snapshots of the Selected Videos 119

Figure 66 Network Stack for the Performance Evaluation of Different Beaconless OR Protocol for Multimedia FANETs 119

Figure 67 Video Quality Level for Different XLinGO Coefficient Combinations .. 122

Figure 68 Impact of Redundancy Mechanism for Different Beaconless OR Protocols 122

Figure 69 Network Topology Composed of 30 Static Nodes 123

Figure 70 Video Quality in Presence of Transient Node Failures with $LIVE$ Value of 2 and Different Number of Nodes 125

Figure 71 Video Quality in Presence of Permanent Node Failures with $LIVE$ Value of 2 and Different Number of Nodes 125

Figure 72 SSIM for All Frames for the Compose the Hall and UAV_1 Video Sequence Transmitted by a Specific SN under Conditions of Scenario 1 with Transient Node Failures 127

Figure 73 Overall Video Quality for Hall and UAV_1 Video Sequences Transmitted by a Specific SN under Conditions of Scenario 1 with Transient Node

Failures 128

Figure 74 Video Quality for a Scenario with a Different Number of Multimedia SN, Moving Speed, and Videos with Different Motion and Complexity Levels 130

Figure 75 Frame Loss Ratio for Videos Transmitted in a Scenario with s_{max} equals to 20m/s and with 2 Simultaneous Video Flows Transmissions 131

Figure 76 Number of Dropped Packets at Intermediate Buffers for a Scenario with Different Number of Multimedia Source Nodes and Moving Speeds 131

Figure 77 Signalling Overhead for a Scenario with Different Number of Multimedia Source Nodes and Moving Speeds 133

Figure 78 Subjective Video Quality Evaluation 133

Figure 79 Frame Number 143 from UAV Video Sequence Transmitted from a Given Node via Different Beaconless OR for Scenario 2 134

Figure 80 SSIM for All Frames for the Compose the UAV_1 Video Sequence Transmitted by a Specific SN 135

Figure 81 Overall Video Quality for the UAV_1 Video Sequences Transmitted by a Specific SN 136

List of Tables

Table 2 Comparison Between Different Routing Protocols for WMSNs 26

Table 3 Comparison Between Each OR Protocols for FANETs 30

Table 4 Routing Table Example 54

Table 5 MOS Scale According to ITU-R BT.500-11 Recommendations [141] 89

Table 6 Simulation Parameters for Different Hierarchical Routing Protocols 91

Table 7 Comparison Among Different Hierarchical Routing Protocols Based on Conducted Simulation Experiments 104

Table 8 Simulation Parameters for Different Packet Redundancy Mechanisms .. 105

Table 9 Possible Configurations for the QoE-aware Redundancy Mechanism 107

Table 10 Comparison Among Different Packet Redundancy Mechanisms Based on Conducted Simulation Experiments 116

Table 11 Simulation Parameters for Different Beaconless OR Protocols 117

Table 12 Coefficient Combinations for DFD function 121

Table 13 Comparison Among Different Beaconless OR Protocols Based on Conducted Simulation Experiments 136

CHAPTER 1

Introduction

This chapter briefly introduces the key concepts about Wireless Multimedia Sensor Networks (WMSNs) and Flying Ad-Hoc Networks (FANETs), portrays the fundamental challenges faced in the different parts of the thesis, summarizes the essential contributions, and outlines the course of the subsequent chapters.

1.1 Overview

The proliferation of multimedia content and the demand for new audio or video services in Internet of Things (IoT) applications [1–3] have fostered the development of a new era based on multimedia information. Those applications allowed the evolution of WMSNs [4–7] and also FANETs [8–10]. Those networks enable a large class of scenarios in both civilian and military areas, which require visual and audio information, such as, environmental monitoring, intruder detection, video surveillance, safety & security, smart parking, traffic control, natural disaster recovery, smart cities, and other IoT applications. Multimedia content in those applications has the potential to enhance the level of collected information compared to simple scalar data. For instance, it enables the end user or end system to take appropriate actions and be aware of the environmental conditions based on rich visual information.

The above scenarios consist of several distributed static or mobile nodes, and also a Base Station (BS), as depicted in Figure 1. In this context, nodes are usually deployed across a wide area to monitor, gather, process, and send a set of sensed data to the BS, i.e. nodes are collecting multimedia or physical scalar sensor data from the environment. The BSs communicate with the network nodes over wireless links, and it is connected to the Internet in order to deliver the collected data to any IoT platforms for further processing and analysis, such as provided by the semantic system [11], sensor4cities [12,13], i-SCOPE, Sight Machine, and others. In this context, physical scalar sensor data can be used to predict event occurrence, by means of existing models or methods defined by an expert [14]. On the other hand, multimedia content in such applications gives support to the end-users (or systems) to visually verify the real impact of events, and be aware of what is happening in the environment with the aid of rich visual information [15, 16].

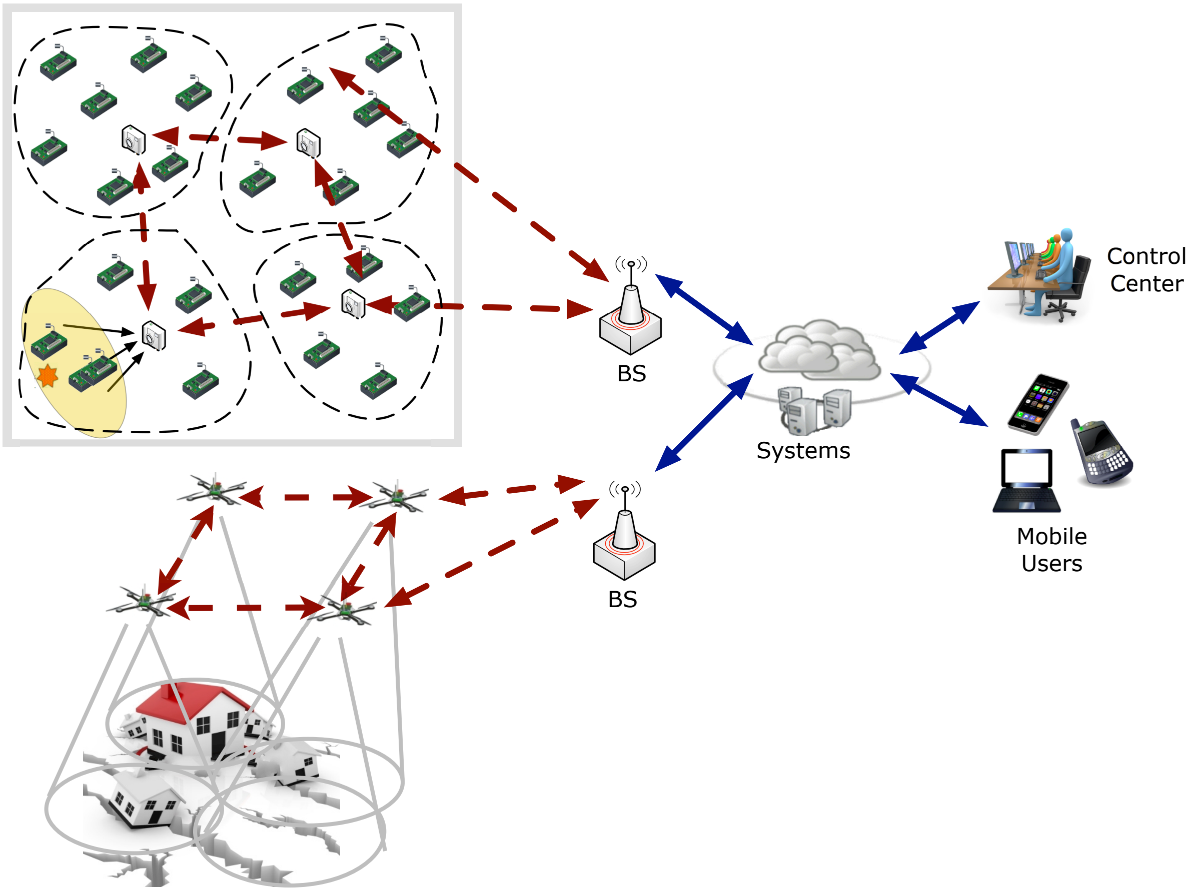

Figure 1: WMSN and Multimedia FANET Application Scenario

Let us consider a WMSN application that relies on fixed network infrastructure to accurately monitor a part of a river with fast velocity and a high water levels. Such application can be composed of a set of nodes sensing the river flow by means of physical scalar measurements, and also by using another set of nodes collecting multimedia data in the case of an event occurrence [17–20]. As soon as an event occurs, it might be interesting to see whether additional objects, such as wood or thrash, are floating on the river surface. This is because these objects might affect the behaviour of the river, in particular when they block the normal river flow, and thus the river dams up.

Moreover, in case of a natural disaster, e.g., earthquake or hurricane, the recovery process demands a rapid deployment of a communication system to monitor the hazard area that rescuers cannot reach easily. This is because the standard communication infrastructure might be damaged or does not work anymore. In this scenario, a group of Unmanned Aerial Vehicles (UAVs) equipped with video camera could be used to set up a multimedia FANET with the aims of explore, sense, and also send multimedia data from the hazardous area, enabling humans in the control center to be aware of what is happening in the environment, as well as take action based on rich visual information.

In this context, live multimedia services require real-time video transmissions with a low frame loss rate, tolerable end-to-end delay, and jitter to support video dissemination with Quality of Experience (QoE) support. Multimedia content should be delivered with, at least, a minimum video quality level from the user's point-of-view [21, 22]. Further, frames with different priorities compose a compressed video, and from a human's experience, the loss of high priority frames causes severe video distortions. Thus, a key principle in a QoE-aware approach is the transmission of high priority frames (protect them) with a minimum packet loss, as well as network overhead.

Moreover, the routing service must find a set of reliable routes between the source and the destination nodes via multiple forwarding nodes with a minimal overhead. The protocol must prevent the selection of forwarding nodes with heavy traffic load or low residual energy. It also has to adapt to topology changes and be aware of QoE requirements in order to recover or maintain the video quality with acceptable level, providing robustness under scenarios with topology changes.

1.2 Problem Statement

In this thesis, we focus only on optimizing video transmission over multi-hop wireless ad-hoc networks. We addressed several challenges in the context of WMSN and multimedia FANET communication in order to provide multimedia dissemination with QoE assurance, scalability, reliability, energy-efficiency, and also load balancing. Our contributions tackle issues relating to the following problem domains.

1.2.1 Scalability

WMSN and FANET scenarios are usually composed of a set of nodes deployed either inside the phenomenon or very close to it. The node density in the region of interest ranges from a few to hundreds of nodes deployed to cover the whole monitored area. In this context, scalability is one of the main design issues that routing protocols must encompass. Thus, routing protocols should provide an efficient multi-hop communication between any pair of source and destination nodes, in order to deliver the collected data from any part of the monitored area. The multi-hop communication must be scalable without requiring user intervention, and also independently of the number of nodes or field size [15].

1.2.2 Unreliable Nature of Wireless Channels

Low-power radios cause links unreliable and unpredictable, because they are very sensitive to noise, interference, and multipath distortion. In this context, Link Quality Estimator (LQE) is a fundamental building block in the design of routing protocols for WMSN and multimedia FANET scenarios, since a reliable routing protocol must consider the LQE as a metric to help in the selection of high quality routes for multimedia dissemination. In this way, the accuracy of the LQE greatly impacts the efficiency and reliability of the routing protocol [23].

LQE can be classified as either hardware-based or software-based. Most of software-based LQEs either count or approximate the Packet Reception Ratio (PRR), as well as the average number of packet transmissions or re-transmissions. However, software-based LQEs include overhead and delay to estimate the link quality for a given link. On the other hand, hardware-based LQEs, such as Received Signal Strength Indicator (RSSI), Signal to Noise Ratio (SNR), and Link Quality Indicator (LQI), are directly read from the radio transceiver (e.g., the CC2420) upon the reception of a packet, making calculation of LQE less time and resource consuming.

1.2.3 Robustness

The routing protocol must cope with dynamic topologies caused by node failure or mobility, as well as wireless channel changes, in order to continue to operate despite dynamic topologies during multimedia transmission [24]. Hence, reliable and robust multimedia transmissions in wireless networks are challenging tasks, due to the time-varying characteristics of low-power wireless links, node failure and mobility, and also wireless interference [25].

In the fault tolerance domain, whenever a node cannot forward its data packets towards the sink, it can benefit from an available alternative route to deliver its data packets, even if node or link failures happen. Through this mechanism, as long as an alternative path is available from the pair of source and destination node, data forwarding can be continued without any interruption even in the case of path failure [26].

The routing protocol must have mechanisms to detect and recover from route failures, which can be periodically route reconstruction or transmitting acknowledgment messages. For the latter one, whenever a certain number of consecutive packets are not acknowledged, the routing protocol must consider the route as broken, remove the failed node from the neighbour table, and re-establish the route. In this way, it is possible to cope with route failures, as well as continue operating even in the presence of dynamic topologies caused by node failures or mobility [27].

The error-prone nature of wireless links can be very severe for a compressed multimedia streams, which are vulnerable to transmission errors due to the predictive nature of coding standards. Node constraints, such as bandwidth, also increase the effects of wireless channel errors. Hence, error correction schemes must be used to deal with wireless transmission errors in real-time multimedia applications, and also to enhance their resilience and robustness [28].

1.2.4 Energy-efficiency

Similar to Wireless Sensor Networks (WSNs), energy consumption is also prime concern in WMSNs and FANETs, which consist of battery-powered nodes with limited energy resources. In this way, the development of energy-efficient communication protocols is one of the main goals to increase network lifetime. The nodes consume energy in tasks such as sensing, communication, data processing, and also movements. Data communication involves both data transmission and reception. We consider sensing as collecting physical measurements data from any scalar sensor, and also retrieving video frames from camera sensors. The energy cost for node movements depends on the moving speed.

Nodes equipped with rechargeable battery or solar power is the best way of overcoming energy drawbacks [29]. For instance, a permanent 24/7 solar-operated network for fire detection and localization has been installed in the Asturias region in the north of Spain [30], where nodes are permanently attached to trees to continuously measure temperature and humidity conditions to detect fire. However, equipping all network nodes with renewable energy sources may not be feasible, or at least, not appropriate. Hence, mechanisms have been developed to extend network lifetime, especially by designing energy-conserving communication protocols on the MAC and routing layer.

In this context, the routing protocol must reduce message overhead required for route discovery and cluster formation. Therefore, multimedia transmission in WMSNs should be based on either the query-driven or the event-driven model, which reduces energy consumption required to both retrieve video frames and to transmit multimedia packets. For instance, we can trigger the multimedia transmission based on the sensing relevance [31, 32]. This is because periodic multimedia transmission involves the delivery of irrelevant multimedia content when there is not any event occurrence, causing wasteful expenditure of energy and bandwidth [25]. Route discovery must prevent the selection of relay nodes with low residual energy, to avoid route failures. Finally, source nodes may also avoid adding redundant packets for low-priority packets, reducing local energy consumption and indirectly preserving energy of intermediate nodes [7].

1.2.5 QoE Requirements

During video transmission over wireless networks, packets can be corrupted or dropped caused by shortcomings in the wireless link quality and congestion, which decreases the video quality level. In addition, live multimedia dissemination requires real-time video transmissions with low frame loss rate, tolerable end-to-end delay, and jitter to support video delivery with QoE support. In this way, multimedia content should be delivered with, at least, a minimum video quality level from the user's point-of-view [33].

Understanding users' satisfaction on watching a video sequence is becoming a key requirement for delivery of multimedia content with QoE support [34–36]. With this goal in mind, solutions involving multimedia transmissions must take into account the video characteristics to improve video quality. Moreover, users' experience must be measured and integrated into networking components to enhance the overall performance of multimedia systems, and also to provide QoE-awareness.

1.2.6 Buffer Control

Multimedia dissemination usually involves a set of nodes transmitting multiple video flows simultaneously. This scenario leads to a higher degree of network congestion, buffer overflow, and packet loss ratio, which reduces the quality level of the delivered video flows [37].

In this context, the routing protocol must prevent the selection of relay nodes with heavy traffic load, while avoiding route failure, queue congestions, packet loss, delay, and jitter. Moreover, as soon as intermediate nodes on a given path detect buffer overflow, the queue policy algorithm must discard less relevant packets, reducing the impact on the quality of the received video from the users' perspective [38]. The source node can also react to congestion by avoiding transmission of less relevant packets.

1.3 Thesis Contributions

In this thesis, we introduce novel mechanisms and protocols in different layers of communication stack of three nodes involved in a communication process, which provide multimedia dissemination with QoE assurance, scalability, reliability, energy-efficiency, and also load balancing. More specifically, Figure 2 schematically indicates the contributions of this thesis, and also depicts the protocol stacks of three nodes involved in the communication process: a source node, an intermediate node, and a destination node.

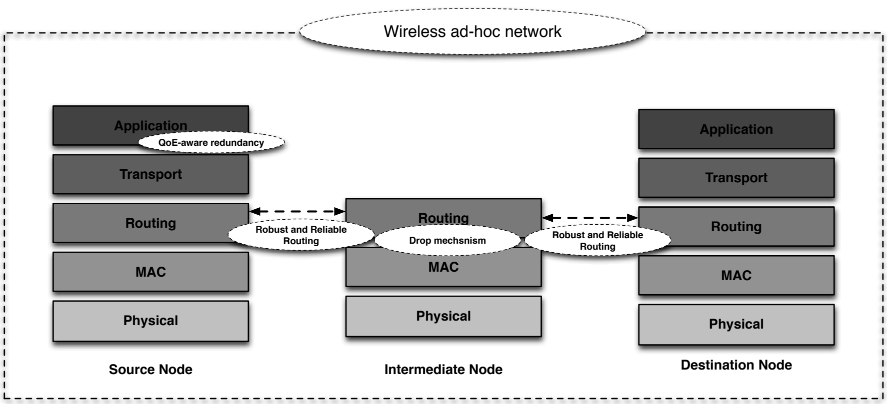

Figure 2: Thesis Contributions Overview

1.3.1 Application-Level Packet Redundancy Mechanism

The compressed multimedia streams are vulnerable to transmission errors due to the predictive nature of coding standards. Moreover, solutions involving multimedia transmission must take into account the video characteristics based on users' experience to support the delivery of high quality live video sequences, and to increase users' satisfaction on watching a given video, as well as to provide QoE-awareness.

Error correction schemes deal with wireless transmission errors in real-time multimedia applications to enhance their resilience and robustness. Among the existing error control schemes to handle packet losses in real-time multimedia communication, application-level redundancy mechanisms offer a suitable solution to provide video delivery with quality level assurance, without adding delay and considering end-to-end routes [39]. Hence, multimedia content must be delivered to the destination node with minimal quality level support from the user's perspective, while, at the same time, the network overhead must be reduced.

With the introduction of the QoE-aware Packet-Level Redundancy Mechanism (QoE-aware redundancy) in Chapter 3, we reduce the impact of the unreliable and lossy nature of wireless environment to disseminate live multimedia content. It considers the frame priority based on users' perspective to add redundant packets, and thus protects them during losses or link error periods. In this way, we reduce the number of redundant packets (overhead) to save network resources, such as bandwidth, while keeping the video quality level high. We also reduce the local energy consumption and indirectly preserving energy of intermediate nodes, since we add redundant packets only to priority frames.

1.3.2 Hierarchical Routing Protocol for Static Wireless Multimedia Sensor Networks Scenarios

Routing protocols can be classified into flat, location-based and hierarchical architectures [25]. For WMSN applications, where it is possible to rely on a fixed network infrastructure, hierarchical network architectures with heterogeneous nodes have proved to be more beneficial than flat architectures in terms of lower energy consumption, greater functionality, better scalability, and reliability. In this context, the advantages of using a hierarchical architecture with heterogeneous nodes are as follows: i) nodes have different roles or functionalities to reduce energy consumption; ii) some nodes perform data aggregation, avoiding unnecessary data transmission; and iii) a set of nodes may turn-off the radio after transmitting their data packets, and as a result, reduce their energy consumption and avoid communication conflicts, such as interferences and congestions [4, 5, 7].

In Chapter 4, we take these considerations into account to propose the video-aware Multi-hop and multi-path hierarchical routing protocol for Efficient VIdeo transmission for static WMSN scenarios, called of MEVI. The proposed hierarchical routing protocol provides scalability, energy-efficiency, and load balancing, as well as delivers multimedia content over WMSN scenarios with reliability and quality level support.

MEVI relies on cluster formation with low overhead, providing scalability, and also energy-efficiency. It finds multiple node-disjoint paths, and evaluates each possible path by means of cross-layer end-to-end link quality estimation, supporting multimedia transmissions with reliability and scalability. We also combined frame relevance with a multi-path scheme to schedule multimedia dissemination, enabling load balancing, as well as increasing the video quality level from the user's perspective. Finally, MEVI takes into account either the query-driven or the event-driven model to start multimedia transmission. More specifically, it triggers video transmissions according to sensed data, supporting energy-efficiency for multimedia transmissions.

1.3.3 Opportunistic Routing Protocol for Multimedia Flying Ad-Hoc Network Scenarios

Protocols that rely on end-to-end routes and also on a fixed network infrastructure cannot be used as soon as the standard fixed network infrastructure are not available due to some natural disaster. This is because to deploy a fixed network infrastructure takes time, and thus multimedia FANET appears as a feasible solution. Moreover, end-to-end routes might be subject to frequent interruptions or may not exist at all times in case of node mobility or wireless channel variations, such as experienced in FANET scenarios. In this context, Opportunistic Routing (OR) does not require a stable end-to-end connection from the source to the destination, and the packets are forwarded even during topology changes. This is because OR improves communication performance by exploiting the broadcast nature and spatial diversity of the wireless medium, and nodes forward the packet to the destination based on a hop-by-hop routing decisions.

We contribute to the research field of OR for multimedia transmission over FANET scenarios by introducing the cross-layer link quality and geographical-aware beaconless OR protocol for multimedia FANET scenarios (XLinGO), which we describe in detail in Chapter 5. XLinGO provides efficient multimedia dissemination with reliability, robustness, load balancing, as well as QoE assurance.

XLinGO is a stateless routing method, since the nodes do not need to be aware of their neighbours. This avoids beacon transmission compared to other position-based protocols, saving scarce resources, e.g., battery and bandwidth. It takes a set of cross-layer and human-related parameters into account to establish a robust and reliable persistent route, namely PRR, QoE, queue length, link quality, geographical location, and residual energy. With the introduction of queue length for routing decisions, we cope with the problem of buffer overflow and also to provide load balancing in a scenario with simultaneous multi-flow video transmissions. XLinGO avoids the selection of forwarding nodes with heavy traffic load. Furthermore, we introduce a recovery mechanism to deal with route failures, providing robustness, and smoother operation in harsh wireless environments and mobile networks.

1.4 Thesis Outline

The remainder chapters of this thesis are structured as follows.

- Chapter 2 outlines the most significant related work about application-level packet redundancy mechanism, hierarchical routing, as well as OR. We also describe their drawbacks to provide scalability, reliability, energy-efficiency, load balancing, and also the transmission of multimedia content with quality level support from the users' perspective.
- Chapter 3 discusses our motivations and contributions toward an application-level packet redundancy mechanism.
- Chapter 4 describes our proposed hierarchical routing protocol for static WMSNs, the MEVI protocol.
- Chapter 5 presents our contributions on OR for multimedia dissemination over FANETs, the XLinGO protocol.
- Chapter 6 introduces the simulation environment, the metrics used to evaluate our contributions, the performance evaluation, and analyses the achieved results.
- Chapter 7 concludes the thesis, summarising the main contributions and results by this thesis. It also motivates potential topics for future research.

CHAPTER 2

Related Work

In this chapter, we give an overview of the important and significant existing work in the field of this thesis. We divided this chapter in a way such that each section corresponds to one of the main three contributions of this thesis.

We start with Section 2.1 reviews the main concepts and definitions needed to understand the video characteristics. Hereafter, Section 2.2 discussing error correction schemes to handle packet loss in real time video transmissions. Among the existing error correction schemes, we describe the state-of-the-art for packet-level redundancy mechanisms, and their main drawbacks to achieve resilient, robust, and reliable video transmissions with minimal overhead. Section 2.3 discusses the research field of hierarchical routing protocols for static WMSN scenarios. We categorize the existing approaches with their advantages and drawbacks compared to our contributions in this field, and conclude the section by giving an outlook about future trends and developments. In Section 2.4, we give a comprehensive overview of existing OR protocol multimedia FANET scenarios, on which we build upon for designing our beaconless OR strategy.

2.1 Video Characteristics

Video compression techniques aim to reduce the amount of data required to store digital video images, and use both image compression and motion compensation techniques. This is because a video recorded with no compression generates a large file, being hard to manipulate and distribute through wireless networks. To avoid this problem, video compression generates smaller files, which increases its storage efficiency and also enables it to be distributed through the network [40]. This is especially needed in network scenarios with limited resources, i.e., bandwidth, energy, and memory space, such as experienced in WMSNs and FANETs [41].

Figure 3 shows a generic example for video coding and decoding in a wireless network. At the sender side, the codec (coder-decoder) encodes the video provided by either a live source camera or stored video repository before transmitting it. Thus, the encoding process removes redundant information and converts the video into an intermediate format (bitstream) so that it can be distributed through the network. The intermediate format is a set of bits created by the encoder in accordance with well-defined standards, such as Moving Picture Experts Group (MPEG) or H.264 [42]. Video coding standards specify the bitstream format and the decoding process for a given video sequence, where each flow starts with a sequence header, followed by a GoP header, and then by one or more coded frames. At the receiver side, the codec decodes the received data, and converts it from an intermediate format to a video sequence [43].

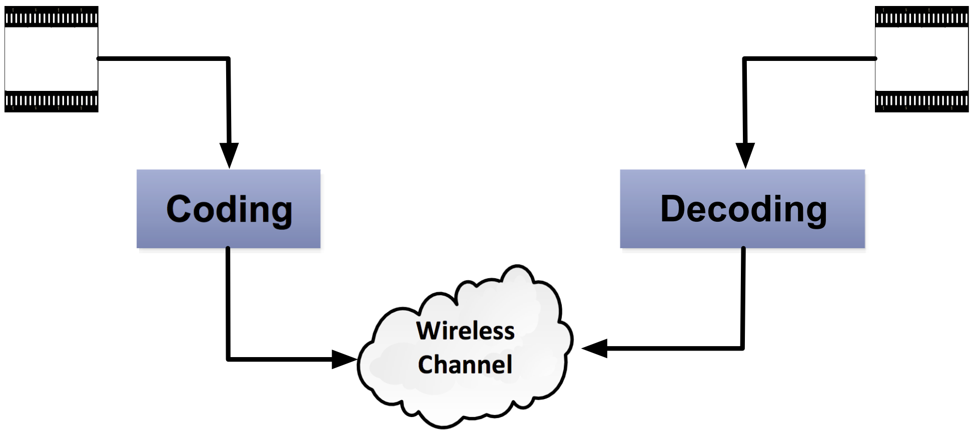

Figure 3: Example of Video Coding and Encoding in a Wireless Network

Both video coding and transmission processes have an impact on the final video quality at the receiver side [44]. Although, this thesis only focuses on optimising the video transmission over multi-hop wireless ad-hoc networks, it is necessary to discuss video characteristics from the user perspective to understand how video characteristics affect the video quality. Hierarchical video coding schemes, such as MPEG or H.264, convert and compress a video signal into a series of pictures or frames. In this way, the encoder significantly compresses the video, allowing the transmission only of differences between consecutive frames [45].

2.1.1 Spatial or Intra-frame Compression

Intra-frame compression removes redundant information within frames by taking advantage of the fact that pixels within a single frame are related to their neighbours. This process includes signal transformation, quantisation, and entropy encoding, which is very similar to that of a JPEG still image encoder [45]. The intra-frame compression process consists of three stages: computation of the transform coefficients; quantization of the transform coefficients; and conversion of the transform coefficients into pairs after the data has been rearranged in a zigzag scanning order (see Figure 4) [46].

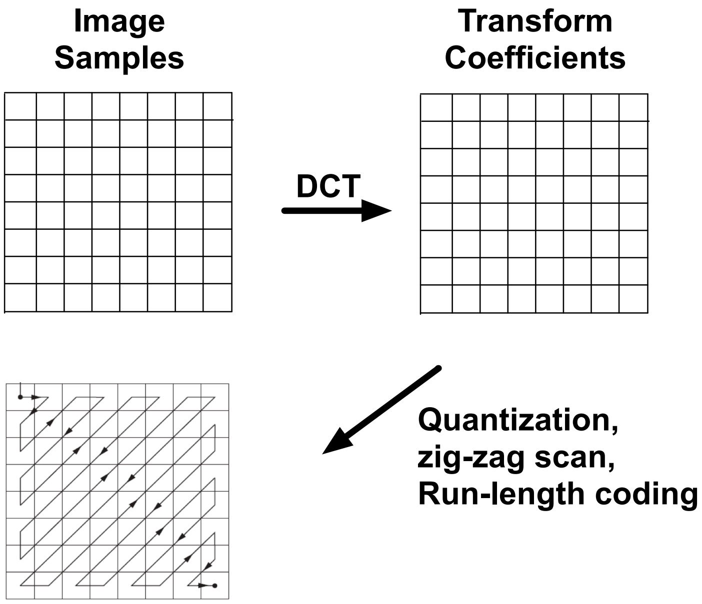

Figure 4: Transform Coding, Quantization and Run-length Coding

Intra-frame compression uses Discrete Cosine Transform (DCT) derived from still image compression to extract signals into a sum of cosine functions. This is because spatial compression performs frequency analysis in a given frame to find the dominant frequencies, which is carried out by converting frames to the frequency domain by means of transform techniques [47]. The DCT result is pre-multiplied by the quantisation scale code and divided by the element-wise quantisation matrix. The processed result usually generates a matrix with values primarily in the upper left-hand corner. The zigzag ordering groups all non-zero values. This basic intra-frame compression greatly reduces the size of the data storage.

Figure 5 illustrates the complexity level for different video sequences downloaded from a well-known video source library [48]. Figures 5(a) and 5(d) show a given frame from the Flower and Hall video sequences, respectively. Furthermore, macroblocks can be observed in both frames, which are the basic unit for video frame compression. Each macroblock divides each frame into small blocks for further handling, and uses the YUV system, i.e., a common used colour space that takes account of human perceptions when encoding an image or a video. It was initially used in the H.261 standard, and nowadays it is the basis for all previous and current video-coding standards.

The size of the macroblock is variable, but the standard size comprises an array of 8x8 pixels. The DCT transform is applied to each macroblock, and produces a coefficient for each pixel macroblock. In this way, each macroblock has 64 pixels (8x8), i.e., the DCT transform produces an 8x8 matrix containing 64 coefficients. To illustrate this process, Figures 5(b) and 5(e) show macroblocks obtained after the DCT transform has been applied in Figures 5(a) and 5(d), respectively. In seeking to give a better explanation of the results of the DCT transform, we used coefficient values in black and white colour scale, where black represents lower coefficient values, while white represents higher coefficient values. It can be seen that the Hall frame has more macroblocks with a colour closer to white, which explains the higher number of coefficient values in 5(b) than in Figure 5(e).

Figures 5(c) and 5(f) show the horizontal and vertical DCT coefficients from two specific macroblocks from Figures 5(b) and 5(e), respectively. In the matrix containing the coefficients of a given macroblock, frequency increases from the left to the right and from the top to the bottom. On the basis of these observations, MPEG saves the coefficients in a vector with an ascending order of frequency.

Hence, coefficients with higher frequencies and values closer to zero cannot be transmitted without affecting the level of video quality. In this way, spatial compression reduces the number of bits required to represent a given video frame. However, spatial compression rates provided by the DCT transform changes, since it depends on the frequency of the image. For example, the Hall frame in Figure 5(b) has lower coefficient values for higher frequencies than the coefficients of the Flower frame in Figure 5(e). Hence, by calculating the number of DCT coefficients, it is possible to infer the spatial compression rate for a given video.

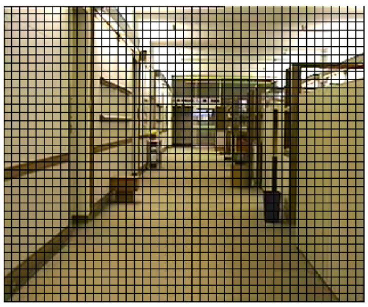

(a) Hall Video Frame with Macroblocks Division

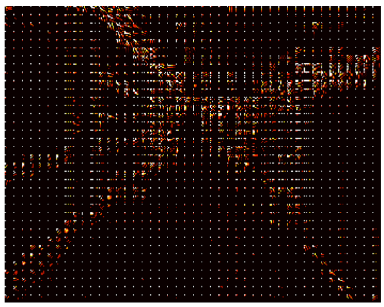

(b) DCT Coefficients for Each Macroblocks for the Hall Frame

(c) A Single Macroblocks of the Hall Video Frame

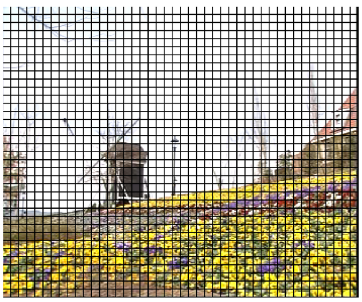

(d) Flower Video Frame with Macroblocks Division

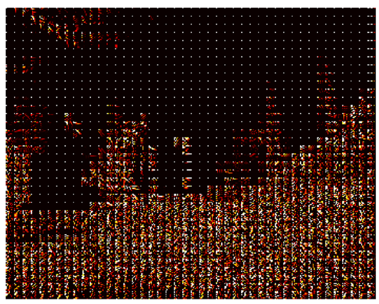

(e) DCT Coefficients for Each Macroblocks for the Flower Frame

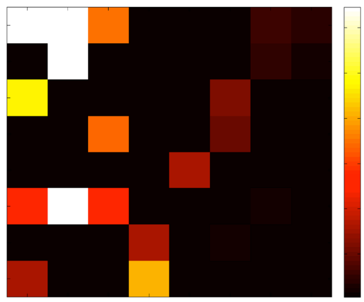

(f) A Single Macroblocks of the Flower Video Frame

Figure 5: Complexity Level for Different Video Frames

2.1.2 Temporal or Inter-frame Compression

Temporal or inter-frame compression tries to remove redundancies existing in consecutive frames, obtaining a high compression ratio. In this way, it creates a frame based on the previous frame, by eliminating the common parts of the frames. Motion causes the differences between different video frames. Thus, the video frame size is reduced by removing the unnecessary parts in the related video frames, and also by only encoding the motion parts. Hence, it is possible to transmit only the differences between the frames.

For instance, it is possible to obtain the frame-difference, as shown in Figure 6(c), by extracting the motion difference from the News frames 1 and 2 [48], i.e., denoted as frame #2 - frame #1. The black portion represents the common parts in both frames, and the other parts represent the variation between them. Thus, it is possible to reconstruct the frame #2 based on the frame #1 and the frame-difference.

In a similar way, Figure 6(f) shows the frame-difference obtained by extracting the motion difference from Figures 6(d) and 6(e). First of all, it is possible to observe that Figure 6(f) has fewer parts in black than Figure 6(c), suggesting that this video has higher level of motion. Second, the rate of time compression is lower for videos with a high motion level. Third, with motion compensation, only the filtered video frame is stored instead of the original frame, which reduces the video size, since the filtered video frame contains less information. To decode a given video, the motion vector search algorithm must match the motion part in the previous reference video frame to decode the current video frame. The algorithm for locating the motion part is the key part of video coding.

(a) Frame #1 from News Video Sequence

(b) Frame #2 from News Video Sequence

(c) Motion Difference for Frame #1 and #2 from News Video Sequence

(d) Frame #1 from Football Video Sequence

(e) Frame #2 from Football Video Sequence

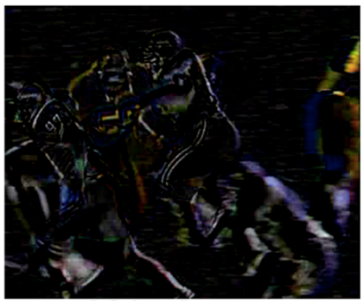

(f) Motion Difference for Frame #1 and #2 from Football Video Sequence

Figure 6: Motion Level for Different Video Frames

2.1.3 Group of pictures (GoP)

A given video sequence contains a series of video frames, and each frame includes information about the whole picture. MPEG/h.264 employs a hierarchical structure composed of 3 types of frames, namely, Intra-coded frames (I-Frames), Predictive coded frames (P-Frames), and Bi-directionally predictive coded frames (B-Frames) [49]. The macroblock from I-, P-, and B-frames uses spatial compression. On the other hand, temporal compression is only applied to the macroblocks from the P- and B-frames. The macroblocks of the P-frames use as reference the macroblocks from the previous I- or P-frames, as shown in Figure 7. The macroblocks of the B-frames use as reference the macroblocks of previous or future I- or P-frames [50].

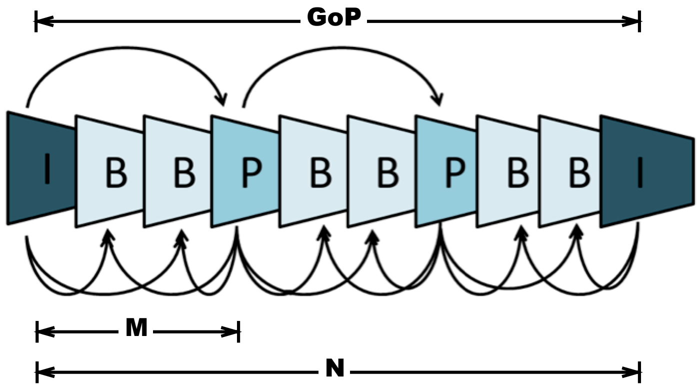

Figure 7: Group of Pictures Structure

These frames are arranged into sequences called Group of Pictures (GoP). A GoP contains all the information required to decode a given video sequence within a period of time, which can be used for optimization procedure. An important factor of MPEG encoding is the GoP size, which indicates the frequency of I-frames in a given video. Each GoP includes an I-frame and all the subsequent P- and B-frames leading up to the next I-frame, as shown in Figure 7. For example, a GoP length of 10 frames means a GoP that starts with an I-frame, followed by a sequence of 9 P- or B-frames. For each GoP, M_{GoP} represents the distance between successive P-frames, and N_{GoP} defines the distance between adjacent I-frames. As a result, this structure is flexible, and the frame types and their location within the GoP can be adjusted to the encoding type. Hence, the MPEG/h.264 standard provides a hierarchically GoP structured, and some frames are more important than others. In this way, a packet loss has different impact depending on the user's perspective.

The frequency of the I-frames in the compressed video defines the size and quality of a video stream. The video bit rate can be reduced by decreasing the frequency of the I-frames when encoding a given video, also degrades the video quality. On the other hand, more I-frames should be added during the encoding process, whenever a higher video quality level is required, and this results in a video with higher video bit rates.

The I-frame contains complete information for a specific video picture, and it is coded without any reference to other frames. In addition, it is known as the key frame for a GoP, since it provides the reference point for decoding a received video stream, i.e., it serves as a reference for all the other frames. It might use spatial compression, and not temporal compression. By removing spatial redundancy, the size of the encoded frame is reduced, and predictions can be used at the decoder to reconstruct the frame. The size of the I-frame is usually higher than the P- or B-frames, since it is the least compressible.

P-frames predict the frame that has to be coded from the previous I-frame or P-frame by using temporal compression, i.e., unlike the preceding I- or P-Frame, P-frames contain changes of the actual frame. P-frames provide a higher rate of compression than I-Frames, typically 20 – 70 % the size of an I-frame. Finally, B-frames consider both the previous and the next I-frame or P-frame as their reference points for motion compensation. In this way, B-frames provide further compression, typically 5 – 40 % the size of an associated I-frame [51].

As a result of the hierarchical structure of MPEG/h.264, packet loss might affect the level of the video quality in different ways, depending on the lost information [52]. The loss of an I-frame affects the other B- or P-frames within the same GoP. Thus, errors propagate in other frames until a new I-frame reaches the receiver. In the case of a P-frame lost, the error propagates in the remaining P- and B-frames in a GoP. In addition, P-frames that appear earlier in the GoP cause impairments over a longer period, since subsequent frames are directly or indirectly impaired until the decoder receives the next I-frame. Finally, in the case of B-frame loss, the error does not propagate, since B-frames are not used as a reference-point for the other frames [53]. It is important to notice that not all packets are equal or have the same degree of importance. Hence, we can use this information to perform optimization procedures, such as human/QoE-aware packet redundancy schemes.

2.2 Error Correction Schemes

Node constraints, such as bandwidth, increase the effects of wireless channel errors. Moreover, as soon as video packets are lost or arrive late, there is a significant decline in the resulting video quality based on user experience. In this context, error correction techniques can be applied to provide resilient and robust video transmission over unreliable wireless communication channels. Error control mechanisms that deal with wireless transmission errors in multimedia streaming applications include Automatic Repeat Request (ARQ), Forward Error Correction (FEC), and Erasure Coding (EC) [28]. A graphical representation of ARQ, FEC, and packet-level redundancy for error control mechanism in wireless networks is presented in Figure 8. In this figure, the packet error occurs during transmission from node 3 to node 4.

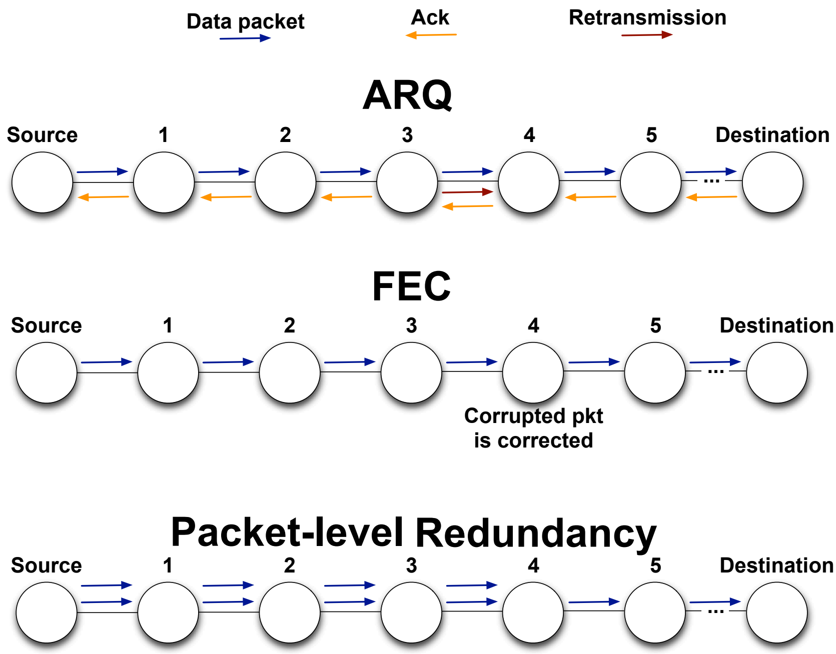

Figure 8: Different Strategies for Error Correction

2.2.1 Automatic Repeat Request Schemes

ARQ mechanisms can be used either in the application or data on link layers. ARQ mechanisms achieve robust video transmission by re-transmitting packets that fail to reach the destination node or arrive in a damaged state. In this way, the sender has to re-transmit a given packet when it does not receive an acknowledgement from the destination node on time, due to packet loss. The sender must also retransmit a given packet when it receives a retransmission request from the destination, due to the arrival of erroneous packets [54]. In the example of Figure 8, node 3 does not receive the acknowledgement from node 4, and thus it retransmitted the packet. However, the ARQ mechanism introduces overhead, delay, energy consumption costs, and also requires an end-to-end bidirectional channel. In addition, when a packet arrives late at the destination node, it misses the playback deadline and can be considered as a lost packet.

2.2.2 Link-layer Forward Error Correction Schemes

In link-layer FEC schemes, the sender node adds some data redundancy to the source packets, and transmits them to the destination node. In this way, it can cope with the problem of packet corruption and provides a fixed network delay, but consumes more bandwidth. More specifically, the sender computes the parity information in accordance with the applied Error Correcting Code (ECC) over the data bits, and adds this redundant information to the payload. At the receiver, the decoder of the applied ECC checks for errors in the received data bits, by taking the parity information into account. Hence, the redundant information detects and corrects errors at the receiver, and the destination node is able to receive error-free packets even if some transmission bit errors occur, depending on the amount and structure of the redundancy. In the example of Figure 8, node 4 uses redundant information to correct errors, and thus it transmits the packet to node 5 correctly. The two most widely-used schemes in FEC are block codes, such as Bose-Hocquenghem-Chaudhuri (BCH) and Reed-Solomon (RS) codes, as well as convolutional codes [55]. However, error recovery by correction codes may add complexity to source and intermediate nodes without success guarantees. FEC schemes are also highly susceptible to burst losses, which are very common in wireless channels.

2.2.3 Packet-Level Redundancy Mechanisms

Erasure coding is an error control scheme for packet-level FEC to handle losses at the application layer in real-time communications. Figure 9 shows how EC is applied to a set of video packets that have to be transmitted to the destination node. Packet-level FEC creates $(K - n_{pkts})$ redundant packets at the application layer, to protect a set of n_{pkts} original video packets. The decoder recovers the set of n_{pkts} original video packets by receiving any n_{pkts} packets out of the K coded packets. The redundant packets are used to reconstruct a corresponding video frame, which can be considered as a lost frame in a scenario that does not add redundant packets. Hence, the packet-level redundancy mechanism provides robust and reliable multimedia dissemination over unreliable wireless channel. Moreover, this scheme does not introduce jitter problems, since there is no acknowledgment mechanism.

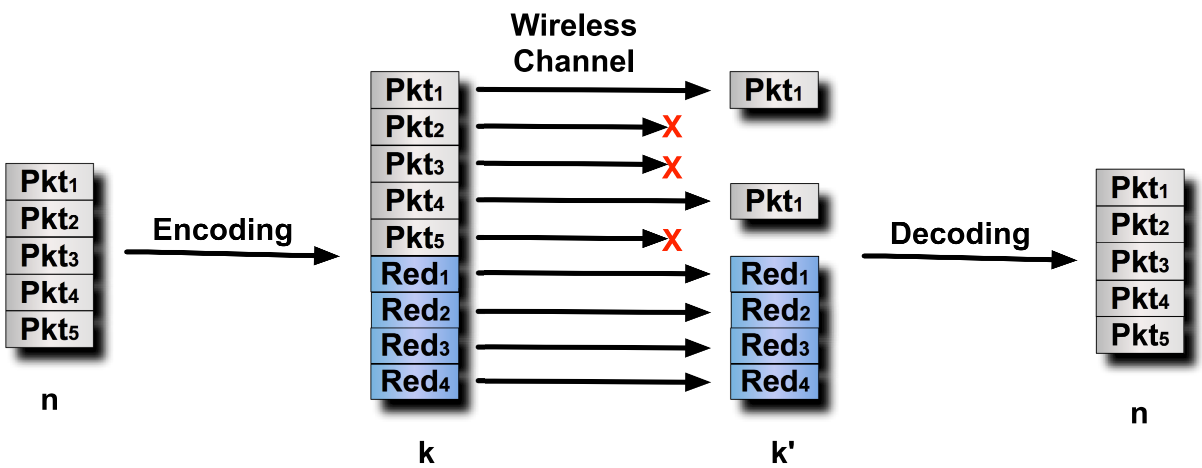

Figure 9: Packet-level Redundancy Mechanism

Packet-level redundancy mechanisms protect video streaming from channel errors without an extra delay. This is because such mechanisms act in a completely different way than link-layer mechanisms, and it has been employed due to its suitability for multimedia communications, as well as the nature of the error coding at the application layer. Moreover, ARQ uses the bandwidth in an efficient way compared with the FEC techniques, although ARQ incurs additional latency costs, which can not be tolerated for live video sequences [56]. Hence, among the existing error control schemes to handle packet losses in real-time multimedia communication, application-level redundancy mechanisms offer a suitable solution to provide video delivery with quality level assurance, as well as without adding delay and considering end-to-end reverse channel.

In this context, Sarisaray-Boluk et al. [57] presented an error compensation technique, which uses packet redundancy and multi-path transmission. The redundancy mechanism employs a modified version of a wavelets based error concealment algorithm, and then the source transmits the image through diverse paths to improve perceptual quality of the received image at the destination. In this way, multiple paths facilitate load balancing, bandwidth aggregation, and fast packet delivery.

Yang el al. [58] proposed a cross-layer approach to enable reliable block transfer of variable-length coded data in WMSNs. This scheme combines FEC techniques at the physical layer, transport, and application layers. More specifically, this work applied symmetrical reversible variable-length codes at the application layer, the recursive systemic convolutional codes at the physical layer, and generating redundant packets, corresponding to the transport layer FEC technique. Redundant packets are utilized as soft information in the decoding process, overcoming packet loss in multi-hop transmissions. In this way, it not only provides strong bit error correcting capability to the variable-length coded data, but also it is capable of overcoming packet loss.

Chen et al. [59] combined multipath routes with packet redundancy in a protocol called Directional Geographical Routing (DGR). DGR implements a redundancy scheme proposed in [60], where K - n_{pkts} redundant packets are generated to protect n_{pkts} data packets of a given video frame. In this way, DGR tackles the unreliability of wireless links to deliver video content with quality level assurance.

Costa et al. [31] introduced the idea of compute the Sensing Relevance (SR) of source nodes, since source nodes may have different importance for the monitoring functions of the applications according to the monitoring requirements and the current sensors poses. For instance, in intrusion detection systems, some source nodes may be monitoring highly critical areas, demanding prioritized transmissions to the sink. Hence, the differentiation of the monitoring relevancy of source nodes may be exploited to optimize network operation in different ways. The SR values are assigned to each source node according to the significance of the retrieved visual data for the application and available monitoring resources in the source nodes, which is represented by a numeric value referred as SR index. The significance of the retrieved visual data is used to classify each source node in a group of relevance, e.g., a numeric index between 0 and 4. In addition, the available monitoring resources of the nodes can be camera resolution, processing resources, and coding algorithms. Later, Costa et al. [61] explored the SR to assure transmissions with high reliability by adding redundant packets only to most relevant source nodes for the application. On the other hand, packets from low-relevant source nodes are transmitted without packet redundancy, saving energy over the network with potential low impact to the overall monitoring quality.

Tsai et al. [62] introduced a forward-looking forward error correction (FL-FEC) mechanism to recover lost packets in order to improve video quality level. The redundancy mechanism encodes n_{pkts} packets with (K - n_{pkts}) redundant packets to form a block with K packets at the sender. Then, the mechanism can tolerate the loss of (K - n_{pkts}) packets in networks and recover the K packets from the FEC block at the receiver. The proposed redundancy mechanism recovers not only the lost packet from its block, but also the previous block from the recovered packet. Thereupon, the FL-FEC mechanism can recover another lost packet from the previous block just recovered, until all lost packets are recovered at the receiver. More specifically, the mechanism selects non-continuous source packets in previous blocks to generate packet redundancy within the current block. Hence, the FL-FEC mechanism can efficiently work against burst packet loss.

Later, Tsai et al. [63] combined ARQ and FEC mechanisms into an adaptive HARQ mechanism, called the Adaptive Hybrid Error Correction Model (AHECM). AHECM finds appropriate parameters, i.e., maximum retransmission threshold and packet redundancy, to avoid network congestion and also reduce the number of redundant packets by predicting the effective packet loss rate. More specifically, AHECM collects meta-information about the average packet loss rate, the average Round-Trip Time (RTT), and the available bandwidth at the receiver. As soon as the meta-information changes due to channel or network conditions, the AHECM makes the receiver send the meta-information to the sender in order to adjust parameters of the AHECM. Hence, the AHECM at the sender chooses the appropriate redundancy for different video frame types when the sender transmits video streaming to the receiver over wireless networks. With information about the average RTT and tolerable end-to-end delay provided by the receiver, the AHECM at the sender finds the maximum retransmission time and retransmits the lost packet to the receiver in time to reduce the packet redundancy. With information about the average packet loss rate and the available bandwidth provided by the receiver, the AHECM at the sender calculates the appropriate parameter to avoid network congestion and the unnecessary packet redundancy.

From the packet-level redundancy mechanisms analysis, we conclude that existing redundancy mechanisms [57–63] add redundant packets in a black-box manner, i.e., without considering the frame importance from a user's perspective, which increases the overhead and the usage of scarce resources, such as battery and bandwidth. The usage of energy resources is due to the hierarchical structure of video coding schemes, where in case of loss of high priority frames, some packets with low priority frames cannot be played on the receiving side after the decoding process. In this case, intermediate nodes spend energy to forward a packet that is not useful to reconstruct the video received at the destination node. In addition, the mechanism proposed by Tsai et al. [63] includes additional delay and overhead for the retransmission scheme, and requires a reverse channel to the destination sends control packet to the sender in order to update meta-information about the average packet loss rate, the average RTT, and the available bandwidth. Finally, redundancy mechanisms [58, 61, 63] lack QoE-based assessment to show the real impact of those mechanisms based on user's experience. Hence, a QoE-aware scheme to add redundant packets based on frame importance is a promising solution. In this way, the source node protects only key frames during loss or link error periods, which reduces overhead and brings many benefits to a resource-constrained system.

2.3 Routing Protocols for Static WMSNs

Routing protocols can be classified into flat, location-based and hierarchical architectures [25]. For WMSN applications, where it is possible to rely on a fixed network infrastructure, hierarchical network architectures with heterogeneous nodes have proved to be more beneficial than flat architectures in terms of lower energy consumption, greater functionality, better scalability, and reliability. In this context, the advantages of using a hierarchical architecture with heterogeneous nodes are as follows: i) nodes have different roles or functionalities to reduce energy consumption; ii) some nodes perform data aggregation, avoiding unnecessary data transmission; and iii) a set of nodes may turn off the radio after transmitting their data packets, and as a result, reduce their energy consumption and avoid communication conflicts [4, 5, 7].

2.3.1 Low-Energy Adaptive Clustering Hierarchy for WSNs

Heinzelman et al. [64] proposed the Low-Energy Adaptive Clustering Hierarchy routing protocol (LEACH). LEACH is the main precursor of hierarchical routing protocols for WSNs, and it achieves low energy dissipation and latency without sacrificing application-specific quality for WSNs. LEACH divides protocol operation into rounds, and each round is subdivided into two phases, namely setup and steady-state phase. In the setup phase, the nodes create clusters, as depicted in Figure 10.

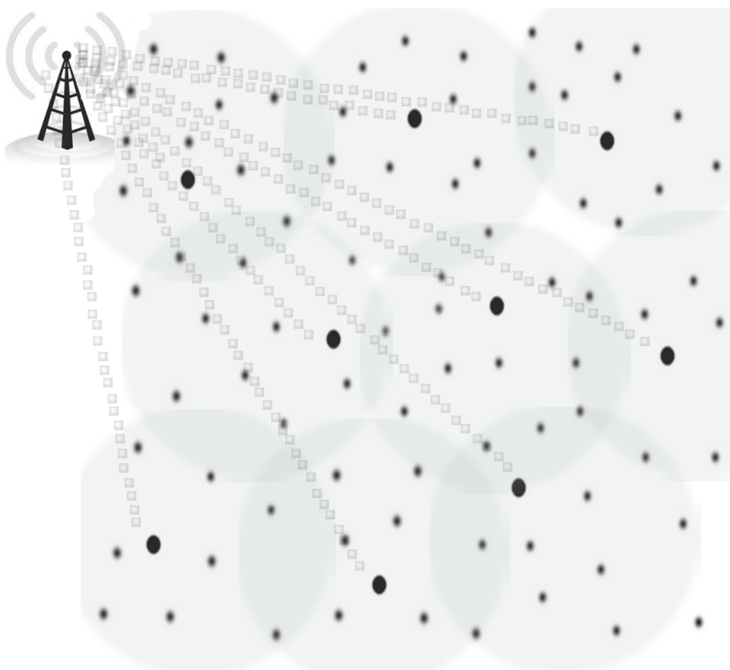

Figure 10: Cluster-based Network Architecture

In the setup phase, nodes also elect Cluster Heads (CH) in a distributed way by choosing a random number between 0 and 1. A given node becomes CH for the current round, as soon as the random number is less than a given threshold $T(n)$ (Eq. 2.1).

After CH election, nodes form clusters by using a distributed scheme, which involves the transmission of beacon, join, and schedule messages. In this way, CHs must schedule the transmission of non-CHs according to a TDMA (Time Division Multiple Access) scheme. On the other hand, non-CH nodes elect the CH on the basis of minimum energy communication.

$$T(n) = \begin{cases} \frac{P}{1-P\left(r \ mod \ \frac{1}{P}\right)} & \text{if n} \in \text{G} \\ 0 & \text{otherwise} \end{cases} \tag{2.1}$$

In the case of the steady state phase, each non-CH transmits the sensed data to its CH. The CH receives the data, aggregates it into a single packet, and then forwards it directly to the BS. After a certain period of time (determined a priori), the network returns to the setup phase to create new clusters.

The main drawback of LEACH concerns the use of a single-hop communication between CHs and BS, which is not suitable for large-scale WMSNs. Periodic data transmissions are unnecessary, causing an ineffective expenditure of energy. Moreover, this approach generates high signalling overhead to create clusters, which decreases the network lifetime and consumes scarce resources.

2.3.2 Hierarchical Routing Algorithm for WMSNs

Kandris et al. [65] introduced the Power Efficient Multimedia Routing protocol (PEMuR), which extends the Scalable Hierarchical Power Efficient Routing protocol (SHPER) [66], by combining routing with video packet scheduling models to support efficient video communication in WMSNs. Nodes create clusters in a centralized way by using beacon, schedule, advertisement, identifier, and join messages. To select the best route, PEMuR considers only the remaining energy to find routes (not link quality).

Each node decides which video packets should be dropped to reduce its current transmission rate, as soon as the bandwidth required from the node exceeds the capacity limit of the shared wireless channel. However, PEMuR relies on a centralized scheme to create clusters, which is not realistic in a large-scale WMSN scenario, and also reduces the scalability. It includes high signalling overhead for cluster formation, while decreasing network lifetime. In addition, it only uses the remaining energy to select the best routes and not end-to-end link quality estimation, limiting transmission of multimedia content with QoS or QoE support due to the unreliable nature of the low-power wireless links.

Lin et al. [67] developed the Adaptive Reliable Routing Based on a Cluster Hierarchy for WMSNs (ARCH) to balance energy consumption and meet required reliability, adjusting the transmission power, together with an energy prediction mechanism. Afterwards, Lin et al. [68] introduced the Energy Efficiency QoS Assurance Routing in WMSNs (EEQAR), which employs social network analysis to optimize network performance. Nevertheless, both ARCH and EEQAR implement multi-hop communication inside a cluster, adding extra overhead for route discovery. Further, they do not consider link quality for route selection, neither the usage of multiple paths. These solutions also lack QoE-based evaluation.

2.3.3 Multi-path Routing for WMSNs

Larri et al. [69] combined a scheduling scheme with the Ad-hoc On-demand Multipath Distance Vector protocol (AOMDV), in a protocol called S-AOMDV. It searches for node-disjoint multi-paths, and considers free buffer size, residual energy, hop-count, and packet loss rate to score and classify each possible path. Paths with better conditions achieve higher scores and are used to transmit higher priority video packets.

Jayashree et al. [70] proposed the Energy Efficient Prioritized Multipath QoS Routing (EEPMQR). It analyses the image to find some common regions (overlapping) and some non-common regions (non-overlapping). The path with the highest score has the best condition for sending packets from overlapped area. However, both S-AOMDV and EEPMQR consider a flat network architecture, which reduces the network lifetime [25]. Moreover, route selection does not take into account the end-to-end link quality estimation, leading to multimedia content without QoS or QoE support. EEPMQE also carries out image processing, which consumes time and energy.

Politis et al. [71] introduced a modified version of the LEACH protocol to allow the establishment of multiple routes among the elected CHs. This work employed two packet scheduling algorithms to transmit video packets over multi-paths dependent on their priorities. Further, a scheduling mechanism drops packets according to their effect on the overall video distortion. This work, however, does not take into account the end-to-end link quality estimation and node-disjoint multiple paths.

2.3.4 Ant-based Hierarchical Routing Algorithm for WMSNs

Sun et al. [72] proposed an Ant-based Service-Aware Routing algorithm for WMSNs, called of ASAR. It considers three kinds of services: (i) event-driven (R-service), where applications tend to be both delay and error intolerant. This service should meet higher real-time and reliability requirements; (ii) data query (D-service) is a service with both error intolerant and query-specific delay tolerant applications. It needs to be supplied with required data that is as reliable as possible. However, it tolerates query-specific delays; and (iii) stream queries (S-service), where applications tend to be delay intolerant. ASAR takes into account four QoS requirements (latency, packet loss, energy consumption, and bandwidth). Thus, it aims to maximize network utilization and improve network performance by selecting an optimal path. The ASAR algorithm is running in all CH to find three available paths for those three types of services.

Cobo et al. [73] introduced AntSensNet to meet QoS requirements for multimedia applications by choosing a path that achieves the desired QoS goals for maximizing network utilization. AntSensNet uses an efficient multi-path video packet scheduling to obtain minimum video distortion. Both ASAR and AntSensNet do not evaluate the quality level of multimedia transmissions from the user perspective. Additionally, ant-colony networking solutions require a long time to react to topology changes and need a lot of messages for route discovery, which increases the energy consumption, and thus these kinds of proposals have not been explored in real applications.

Heissenbüttel et al. [74–76] proposed an Ant-based Mobile Routing Architecture (AMRA), which aims to find more optimal paths than other position-based protocols by memorizing past data traffic. AMRA is a two-layered framework with three independent protocols. Two protocols are used on the upper layer, namely Topology Abstracting Protocol (TAP) and Mobile Ants-Based Routing (MABR). In addition, Straight Packet Forwarding (StPF) is situated on the lower layer and functions as an interface to the physical network for MABR.

More specifically, in MABR, each node maintains a probabilistic routing table, which depends on its current view on the network, its past locations, and overheard packets. Hence, each node determines the estimated average delay. Furthermore, nodes operate in promiscuous mode such that the routing table is not only updated when a packet is received, but also is also updated for all overheard packets to expedite the dissemination of routing information. Furthermore, ants can be transmitted periodically to explore new paths if there is only little data traffic in the network.

2.3.5 Final Considerations of Different Hierarchical Routing Protocols for WMSN Scenarios

From the related work analysis, we conclude that hierarchical routing protocols should create low overhead for cluster formation, and also the multimedia transmissions should be triggered only in case of event occurrence, which increases network lifetime. Moreover, node-disjoint multiple path routing protocols, together with a route selection scheme that considers cross-layer end-to-end link quality estimation with a minimal signalling overhead improves scalability, reliability, and energy-efficiency.

In addition, a video-aware mechanism to protect priority frames in loss or link error periods enhances video quality from the human's experience. However, existing hierarchical routing protocols for WMSNs [64–76] do not take into account all of these relevant characteristics for a single hierarchical routing proposal to support QoE-aware multimedia transmissions, while achieving scalability, robustness, and energy-efficiency. Finally, Table 2 summarizes the main features for each hierarchical routing protocol.

Table 2: Comparison Between Different Routing Protocols for WMSNs

Protocols	Network architecture	Data transmission model	Network overhead	Route selection metrics	Bio inspired approach
LEACH [64]	Hierarchical	Periodically	High overhead for cluster formation	Single-hop	No
PEMuR [65]	Hierarchical	Event-driven	High overhead for cluster formation	Residual Energy	No
ARCH [67]	Hierarchical	Periodically	Overhead for route discovery for intra-cluster communications	QoS Metrics	No
EEQAR [68]	Hierarchical	Periodically	Overhead for route discovery intra-cluster communications	QoS Metrics	No
ASAR [72]	Hierarchical	Event or query based based	Ant-base protocol require high number of messages	QoS Metrics	Ant-colony
AntSensNet [73]	Hierarchical	Periodically or Event based	Ant-base protocol require high number of messages	QoS Metrics	Ant-colony
AMRA [74]	Flat	Periodically	Ant-base protocol introduce overhead	Average delay	Ant-colony
S-AOMDV [69]	Flat	Periodically	No	buffer size, hop-count packet loss rate, and residual energy	No
EEPMQR [70]	Flat	Periodically	No	minimum residual energy minimum buffer size, and hop count	No
Politis et al. [71]	Hierarchical	Periodically	High overhead for cluster formation	Energy and QoS Metrics	No

2.4 Opportunistic Routing Protocols for Multimedia FANET Scenarios

In contrast to other routing protocols that rely on existing end-to-end routes, in OR forwarding decisions are not taken by the sender of a packet, but in a completely distributed manner at the possible relay nodes. In OR protocols, the sender sends a packet not only to a single next-hop, but to multiple neighbours simultaneously. Afterwards, one or more of the receiving nodes forward the packet towards the destination, based on a coordination method to select the best candidate to forward packets. Hence, the routing mechanism forwards the packet towards the destination on a based on hop-by-hop routing decision at the receiver side. More specifically, OR relies on a coordination method to pick up the best candidate to forward packets. We consider both beacon-based and beaconless modes as promising OR coordination methods for multimedia FANET applications, since they do not require a stable end-to-end route, which enables packet transmission even if the topology continuously changes.

2.4.1 Beacon-based OR Protocols

Beacon-based OR protocols select and prioritize a set of candidate nodes by transmitting beacon messages before packet transmission. This enables OR to create and order a relay candidate list prior to packet transmission according to a certain criteria, such as expected transmission count. Then, depending on the candidate priority, neighbour nodes decide to forward the received packet.

Mao et al. [77] presented an energy-efficient OR strategy, which focuses on selecting and prioritizing the forwarder list to optimize network performance. Furthermore, Lu et al. [78] introduced an analytical model to study the performance of multi-hop video streaming. In addition, Seferoglu et al. [79] proposed a video-aware opportunistic network, which considers decodability of network codes by several receivers and the importance of video packet deadlines.

However, beacon-based OR schemes [78, 79] do not provide robustness and QoE support in presence of node failure or mobility, as well as wireless channel changes. This is because those protocols rely on creating a candidate list by sending beacon messages, which increases the signalling overhead. In addition, the candidate list is determined before sending packets, and may not reflect the real situation at the moment of packet transmission. Finally, some works [78, 79] lack QoE-based evaluation to show the real impact of their schemes based on users's perception.

2.4.2 Beaconless OR Protocols

In beaconless OR protocols, the sender does not need to be aware of its neighbours and, consequently, nodes do not have to proactively transmit beacons, such as performed in other position-based protocols. Forwarding decisions are performed by the receiver of a packet based only on information contained in the packet, as well as in local information, such as node position and direction. Hence, the coordination method relies on a Dynamic Forward Delay (DFD) calculation at the receiver side to select the forwarding node, i.e., the candidate node with best conditions compute the shortest DFD value, and thus such node transmits the packet faster, creating the persistent route.

Heissenbüttel et al. [80–82] introduced the concept of DFD as a forwarding decision in the Beaconless Routing protocol (BLR). The BLR protocol selects a forwarding node in a distributed manner among all its neighbouring based only on information contained in the packet. In this way, BLR has three main operational modes: greedy mode, backup mode, and unicast mode. In the greedy mode, the source node broadcasts a data packet, and before forwarding the received packet, possible relays within a forwarding area compute a DFD value based on location information. More specifically, the DFD is calculated by Eq. 2.2 with r as the transmission radius of a node, p the node's progress towards the destination, and maxDFD as a system parameter. Afterwards, possible relays wait during the corresponding time interval, i.e. DFD, to forward the received packet.

$$DFD = maxDFD \times \frac{r - p}{r} \tag{2.2}$$

In addition, BLR considers that only nodes located within the forwarding area participate in the forwarding process as shown in Figure 11, preventing the destination node to receive many duplicated packets. As result of DFD calculation, the node closest to the destination generates the shortest DFD and forwards the packet first. Neighbour nodes recognize the occurrence of relaying, and cancel their scheduled transmission for the same packet that they overhear. After a given node has detected through passive acknowledgment the successful reception, it sends subsequent packets via unicast to the node that relayed the packet. Moreover, BLR defines a backup strategy when the greedy mode fails. In this case, the node broadcasts a control message and all of its neighbours reply with another control message indicating their positions. Then, the node chooses the possible candidate closer to the destination to unicast the subsequent packets.

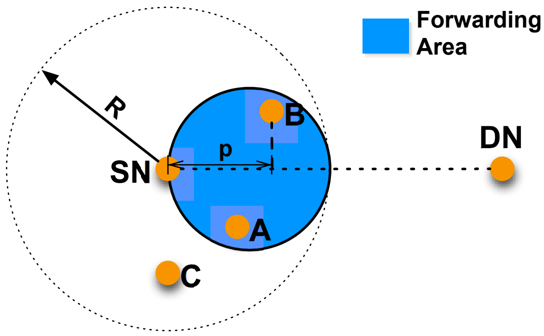

Figure 11: Forwarding Area for BLR

Sanchez et al. [83, 84] proposed the Beaconless On-demand geographic routing Strategy (BOSS), which extends BLR by introducing a different forwarding area, DFD, and applying a three-way handshake mechanism. It assumes a full data payload for the Request to Send (RTS) message size, since selecting a forwarder using short control messages may lead to the choice of a forwarder unable to receive larger data packets. Moreover, the proposed DFD function combines a uniform distribution that depends on the geographical advance towards the destination with a random value.

Zhang and Shen [85] introduced an Energy-efficient Beaconless Geographic Routing (EBGR), where each node calculates its ideal next-hop relay position on the straight line towards the sink to minimize energy consumption required to transmit packets. Each forwarder selects the neighbour closest to its ideal next-hop relay position by using a three-way handshake mechanism.

Spachos and Hatzinakos [86] presented the Energy Aware Opportunistic Routing protocol (EAOR), which considered a three-way handshake mechanism to establish a path between the source and the destination. The proposed DFD function is computed based on the distance and the sensing relevance introduced by Costa et al. [31]. Nodes also prioritize transmission of packets with high sensing relevance.

Chen et al. [59] combined a packet-level redundancy mechanism with a multipath routing scheme in DGR. DGR relies on a three-way handshake mechanism to select the forwarding node, and computes the DFD based on a uniform distribution that depends on the geographical location with a random value. The multiple paths in DGR facilitate load balancing, bandwidth aggregation, and fast packet delivery.

Al-Otaibi et al. [87,88] proposed a Multipath Routeless Routing protocol (MRR), which defines a forwarding area as a rectangle and combines multiple metrics to compute the DFD. MRR uses received signal strength, remaining energy, and location information to set DFD and thereby determine which nodes are most eligible for forwarding the subsequent packets in unicast fashion. It defines the forwarding area as a rectangle and tries to find paths closer to the rectangle borders, as depicted in Figure 12. According to the proposed DFD calculation, nodes receiving packet with weaker signals, located closer to the boundaries of the forwarding area, and having more remaining energy transmit the received packet faster. By preferring nodes located close to the borders of the forwarding area, MRR finds at least two routes existing without interference.

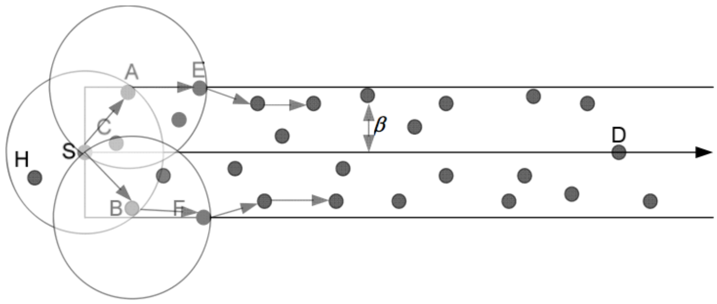

Figure 12: Forwarding Area for MRR

Several beaconless OR protocols [59, 80–84, 86] rely only on distance to compute the DFD. However, computing DFD based only on distance increases packet loss ratio and reduces video quality, since the most distant node might suffer from bad connectivity [89]. Other OR protocols [59, 83–86] include message overhead and also delay for the three-way handshake mechanism. In addition, protocols [59, 85, 86] consider small size for the RTS message, leading to the selection of a forwarding node unable to receive larger data packets as they are expected in video transmissions.

MRR [87] selects a forwarding node that receives a packet with weaker signals, reducing system reliability and increasing the packet loss ratio. Hence, MRR delivers video with poor quality. In addition, MRR gives priority to select forwarding nodes closer to the boundaries of the forwarding area, which does not mean that the node provides geographical advance towards the destination node. In this way, it increases the number of hops, interferences, and buffer overflow, and thus decreases video quality.

Certain protocols [59,80–86] rely on periodic route reconstruction to detect topology changes. But, when one of the forwarding nodes from a given route is no longer available to forward packets, a burst of packets might be lost until the protocol re-establishes the route. Hence, video quality becomes worse during the interval of route reconstruction, reducing transmission robustness. These protocols also do not preclude the selection of forwarding nodes with heavy traffic load or low residual energy.

2.4.3 Final Considerations of Existing OR Protocols for Multimedia FANET Scenarios

From the analysis of existing OR, a beaconless OR approach appears as a promising routing scheme for FANET applications. This is because nodes do not need to proactively broadcast beacon messages to be aware of their neighbours, which saves scarce resources, such as battery and bandwidth, and reduces delay. We also concluded that it is essential to consider multiple metrics for forwarding decisions in order to assure robust and reliable video dissemination, which involves being aware of QoE requirements and quickly detecting and responding to topology changes. However, so far not all of these key features have been provided in a unified beaconless OR protocol. In addition, existing OR protocols also lack robustness and QoE assurance over FANET multimedia applications. Finally, Table 3 summarizes the main features for each OR protocol.

Table 3: Comparison Between Each OR Protocols for FANETs

OR protocols	Coordination method	Route selection metrics	3-way handshake mechanism	Route reconstruction
Mao et al. [77]	Beacon-based	Energy	No	Periodic
Seferoglu et al. [79]	Beacon-based	Network coding and video characteristics	No	Periodic
BLR [80]	Beaconless	Distance	No	Periodic
BOSS [83]	Beaconless	Distance	Yes	Periodic
EBGR [85]	Beaconless	Location and Energy	Yes	Periodic
EAOR [86]	Beaconless	Distance and SR index	No	Periodic
DGR [59]	Beaconless	Distance	Yes	Periodic
MRR [87]	Beaconless	Energy, Distance, and Link quality	No	Periodic

CHAPTER 3

QoE-aware Packet-Level Redundancy Mechanism

Multimedia dissemination over wireless networks has been attracting research interest and encouraging the development of new video application services for static and mobile devices. In this context, multimedia content must be delivered to the destination node with a minimal quality level assurance from the user's perspective, while, at the same time, the network overhead must be reduced. Among existing error control schemes to handle packet loss in real-time communication, application-level redundancy mechanisms offer a suitable solution to improve the video quality level assurance, without adding delay and an end-to-end reverse channel.

In this chapter, we introduce our proposed QoE-aware packet level redundancy scheme [90,91], which adds redundant packets based on frame importance from the user's experience. The proposed QoE-aware redundancy mechanism enables video dissemination with a similar video quality level compared to standard packet-level redundancy mechanisms. At the same time, our proposal reduces the number of redundant packets needed for the decoding process, bringing many benefits to a resource-constrained system.

This chapter is structured into four sections. Section 3.1 explains the rationale behind the development of a QoE-aware redundancy mechanism. Section 3.2 introduces the problem statement addressed by our QoE-aware redundancy mechanism. Section 3.3 describes the proposed QoE-aware packet redundancy mechanism, which adds redundant packets based on the frame importance from the user's experience. Section 3.4 summarizes the main advantages of the proposed QoE-aware redundancy mechanism.

3.1 Motivation

Compressed multimedia streams are vulnerable to transmission errors due to the predictive nature of coding standards. Moreover, node constraints, such as bandwidth and battery, increase effects of wireless channel errors. Hence, error correction schemes must be used to deal with wireless transmission errors in real-time multimedia streaming applications, and also to enhance their resilience and robustness [28].

Live multimedia services require real-time video transmissions with a low frame loss rate, tolerable end-to-end delay, and jitter to support video dissemination with QoE support. Multimedia content should be delivered with, at least, a minimum video quality level from the user's point-of-view [21, 22]. This is required in scenarios ranging across diverse areas, including safety & security, environmental monitoring, natural disaster recovery applications, and others [1].

As explained later, I-, P- and B-frames compose a compressed video, and those frames have different priorities. The loss of high priority frames causes severe video distortion, since some received packets cannot be decoded on the receiver side. In this way, nodes also waste scarce network resources, such as bandwidth and energy. For instance, energy cost is because intermediate nodes spend energy to forward frames that are not useful to reconstruct the video received at the destination node [61]. Based on the above considerations, solutions involving multimedia dissemination must take into account the video characteristics to optimize video transmission with energy-efficiency and QoE support, and improve the user's satisfaction on watching a given video, as well as provide QoE-awareness.

Among existing error control schemes, packet-level redundancy mechanisms achieve robust video distribution by transmitting redundant packets together with the original sequence. Thus, when the original packet is lost, it can be recovered from redundant packets. Recovered packets help to reconstruct a corresponding video frame, which might be considered as a lost frame in a scenario that does not add redundant packets. However, existing redundancy mechanisms [57–63] add redundant packets in a black-box manner, i.e., they do not take into account the video characteristics to add redundant packets only to priority frames based on user experience, which increase the overhead, as well as the usage of scarce resources, such as battery and bandwidth. This is because a key principle for QoE-aware multimedia dissemination is the need to protect high priority frames during loss or link error periods.

3.2 Problem Statement

In this chapter, we address the following issues:

- We enhance the robustness and also the video delivery in wireless ad-hoc networks by means of a packet redundancy mechanism. In this way, we combat the unreliable nature of multimedia transmissions over wireless networks, while increasing the user experience on watching a given video.

- Our proposed packet redundancy mechanism considers the video characteristics to add redundant packets only to priority frames based on the user experience. Hence, we reduce the number of redundant packets (overhead), while keeping the video quality level high, which reduces energy and bandwidth consumption.

3.3 QoE-aware Packet Redundancy Mechanism Description and Operation Principles

In this section, we introduce our QoE-aware packet redundancy mechanism [90, 91]. The proposed mechanism achieves resilient, robust, and reliable video transmission over a bandwidth-limited unreliable networking environment, such as experienced in many wireless ad-hoc network environments.

Figure 13 depicts how the proposed mechanism can be applied to a set of source multimedia packets, before being transmitted through a wireless channel to the destination node. Existing non-QoE redundancy approaches [57–63] add redundant packets in a black-box manner, i.e., without considering the frame importance from the user perspective, which increases the overhead and the usage of scarce resources, such as battery and bandwidth. In contrast to that the proposed QoE-aware redundancy mechanism considers frame importance based on the user perspective to add redundant packets, which only protect priority frames in loss or link error periods.

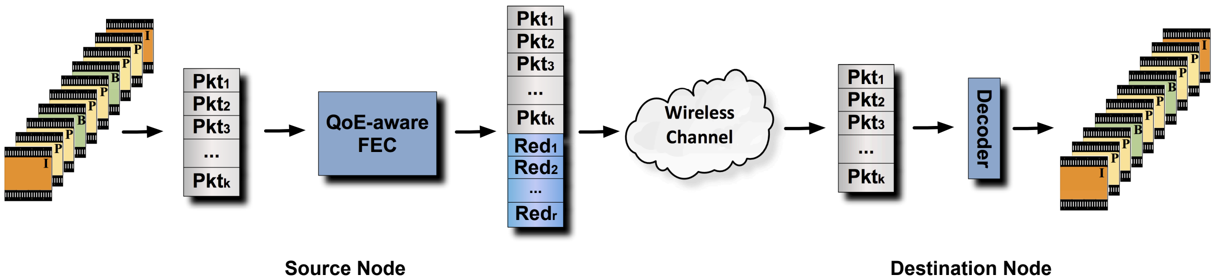

Figure 13: QoE-aware Redundancy Mechanism Overview

Source nodes avoid the transmission of low-priority frames, which reduce local energy consumption, as well as indirectly preserve the energy at intermediate nodes. This is because intermediate nodes spend energy to forward frames that are not useful to reconstruct the video received at the destination node. Hence, the proposed mechanism supports QoE-aware multimedia transmissions. In addition, it enables video dissemination with a similar video quality level compared to non-QoE packet-level redundancy mechanisms, but with reduced overhead, leading to many benefits for a resource-constrained system, such as reduced energy and bandwidth consumption.

The proposed mechanism applies RS coding to encode the set of n_{pkts} original video packets. This is because RS deals with burst errors more effectively, has low computational complexity, and consumes less energy than other coding techniques, as required for many multimedia applications [92, 93]. The QoE-aware redundancy mechanism adds r redundant packets to a set of original video packets, i.e., it encodes n_{pkts} original video packets into a set of K coded packets by producing $(r = K - n_{pkts})$ additional packets. Thus, whenever the destination node receives any n out of the K packets correctly, it may decode the frame immediately and drop the subsequent redundant packets.

Algorithm 1 shows the pseudo-code for the proposed QoE-aware redundancy mechanism used by the source nodes, before transmitting multimedia packets. The proposed algorithm requires a default value for the percentage of redundancy (r) to apply for a set of n_{pkts} original video packets, and also the number of P-frames that requires packet redundancy (X_1) (lines 1 and 2). This is because P-frames that appear earlier in the GoP causes impairments over a longer period, since subsequent P-frames are directly or indirectly impaired until the decoder receives the next I-frame. For instance, X_1 equals 50% means that the proposed redundancy mechanism adds r redundant packet only to 50% of P-frames in each GoP.

For every incoming video frame, the mechanism must know some video information, namely the relative frame position within the GoP (p), the number of packets after fragmentation (n_{pkts}), and the frame type (line 3 to 5). To obtain this information, a deep packet inspection algorithm enables to extract information about the frame type and intra-frame dependency for each video packet, since each video flow starts with a sequence header followed by a GoP header (as presented in the MPEG standard), and then by one or more coded frames. Hence, the proposed redundancy mechanism adds r redundant packets to a set of n_{pkts} original packets depending on the frame type and the location of the P-frame within the GoP.

As mentioned earlier, frame loss might affect the video quality in different ways depending on the user experience. In this way, I-frames, and also P-frames earlier in the GoP, i.e., P-frames with a relative position p lower than X_1, have their packets encoded by using RS coding to add r% of packet redundancy for the set of n_{pkts} original packets (lines 6 to 13). This is because losses of these frames cause greater video impairment, as presented by Greengrass et al. [45,53]. Hence, these frames require robust and resilient transmission, which is achieved by adding redundant packets, and this enables the destination node to decode the frame even if packet losses occur.

P-frames later in a GoP, i.e., P-frames with a relative position p higher than X_1, and each B-frame is sent without any packet redundancy (line 14 to 19). This is because loss of these packets creates less video distortion for a given user watching the video sequence. It should be noted that X_1 is defined based on video motion and complexity levels. This is because a GoP may be composed of video frames with different sizes, depending on the spatial and temporal levels in the video content. For instance, a given video sequence with larger I-frames will be fragmented into several packets, e.g., videos with high spatial complexity, such as the Flower video sequence downloaded from the

YUV library [48]. In this context, the dropping probability of an I-frame increases, which produces different impact based on user perception. The same process occurs with P- and B-frames for videos with high temporal complexity, such as the Football video sequence downloaded from the YUV library. Aguiar et al. showed that the video called Mobile has the biggest I-frame size and, consequently, has a highest spatial complexity, while the video Football has the smallest ones [51].

Algorithm 1 QoE-aware Redundancy Mechanism

Startup
Let r = redundancy measured in %
Let X_1 = number of P-frames that need packet redundancy
on receiving a given video $frame$ from the application layer
Let frameType ← getFrameType($frame$)
Let p ← getRelativePosition($frame$) // relative frame position within the GoP
Let n_{pkts} ← getNumberOfPaackets($frame$) // number of packets after frame fragmentation
if frameType = I **then**
    addRedundancy (n_{pkts}, r); //add packet redundancy using RS coding
    SendWithRedundancy(k, n_{pkts})
end if
if frameType = P and p <= X_1 **then**
    addRedundancy (n_{pkts}, r); // add packet redundancy using RS coding
    SendWithRedundancy (k, n_{pkts})
end if
if frameType = P and p > X_1 **then**
    SendWithoutRedundancy (n_{pkts})
end if
if FrameType = B **then**
    SendWithoutRedundancy (n_{pkts})
end if

Let us illustrate the behaviour of the proposed mechanism by means of Figure 14. In this example, we assume r equals to 100%, i.e., the proposed redundancy mechanism adds n_{pkts} for each set of n_{pkts} original packets. Moreover, let us assume X_1 equals 50%, i.e., the mechanism adds redundant packets only to 50% of earlier P-frames in each GoP. Finally, we consider a video sequence with GoP size of 18 frames and 2 B-frames between successive P-frames, i.e., a GoP has the following frame sequence $IBBPBBPBBPBBPBBPBB$. Hence, the proposed QoE-aware redundancy mechanism adds n_{pkts} redundant packets for each set of n_{pkts} original packets for each I-frame and the first two P-frames within each GoP.

Our proposed QoE-aware redundancy mechanism provides the following advantage, such as expected for many wireless multimedia applications. It protects priority frames during loss or link error periods, as well as achieves high resilience and reliability without wasting more bandwidth and energy. Moreover, it reduces the overhead compared with non-QoE redundancy mechanisms, which also minimizes delay, since it reduces the number coded packets that have to be buffered before the encoding and decoding process at the application layer, as well as in intermediate forwarding nodes. Finally, it decreases energy consumption at the source node, as well as indirectly preserving energy of intermediate nodes.

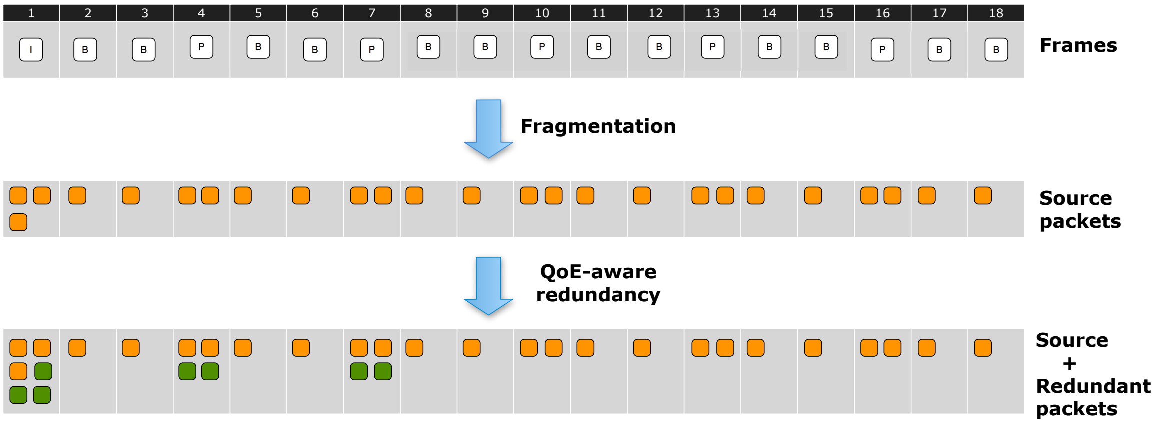

Figure 14: QoE-aware Redundancy Mechanism Example

Hereafter, we analyse the frame overhead introduced by the proposed QoE-aware redundancy mechanism (communication overhead), and also the memory usage and algorithm complexity (computational complexity).

- *Communication overhead:* based on the example of Figure 14, the proposed QoE-aware redundancy mechanism adds redundant packets only to 3 frames out of 18 frames for each GoP, i.e., the I-frame and the first two P-frames. In other words, the proposed redundancy mechanism transmits the GoP with the following frame $II'BBPP'BBPP'BBPBBPBBPBB$. This is because the source node only adds redundant packets to priority frames, reducing the overhead compared to existing non-QoE approaches. Hence, we conclude that the parameters r and X_1 dictate the communication overhead for the proposed QoE-aware redundancy mechanism. It is important to mention that the number of redundant packets depends on the frame size and the fragmentation size. In addition, the frame size depends on the video motion and complexity levels, as introduced by Aguiar et al. [94].
- *Computational complexity:* Algorithm 1 adds redundant packets based on their frame priorities, which can be done using a small number of float point operations.

3.4 Summary

In this chapter, we introduced the concepts of error correction schemes to handle packet loss in real-time wireless communications, as well as examining the video characteristics. On the basis of these observations, we proposed a QoE-aware redundancy mechanism, which targets the reduction of the number of redundant packets to save network resources, such as bandwidth, while keeping transmitted videos at a good quality. More specifically, the proposed mechanism adds redundant packets depending on the frame type and the location of the P-frame within the GoP, protecting those frames during losses or link error periods, such as expected for many wireless multimedia environments.

CHAPTER 4

A Multi-hop Hierarchical Routing Protocol for Efficient Video Communication

This chapter introduces our contributions towards an efficient and reliable hierarchical routing protocol for static WMSNs, the MEVI protocol [95–97]. MEVI provides scalability, reliability, energy-efficiency, load balancing, and also improves the transmission of multimedia content over WMSN scenarios with video quality level support from the user's perspective.

In our initial work [95], we proposed cluster formation with low overhead, providing scalability, and also energy-efficiency. Later, we proposed to trigger multimedia transmission according to sensing relevance, supporting energy-efficiency for multimedia transmissions [96]. In following works [98, 99], we introduced end-to-end link quality estimation, but in these studies we do not consider a hierarchical architecture, multiple node-disjoint paths, and requirements to provide multimedia dissemination with QoE support. In our recent work [97], we proposed to find multiple node-disjoint paths, and evaluated each possible path by means of a cross-layer end-to-end link quality estimation, supporting multimedia transmissions with high packet delivery rate. In such work [97], we also combined frame relevance with a multi-path scheme to schedule the multimedia dissemination, enabling load balancing, as well as increasing the video quality level from the user perspective.

The remainder of this chapter is structured as follows. Section 4.1 highlights the motivations to propose MEVI. Section 4.2 introduces the network model for the static WMSNs network scenario considered by MEVI. Section 4.3 presents the problem statement addressed by MEVI. Section 4.4 describes the basic design and operating principles of the MEVI protocol. Section 4.5 concludes the chapter.

4.1 Motivation

Figure 15 shows a WMSN application example, where a fixed network infrastructure is available. In such case, some nodes are able to continuously monitor physical scalar sensor data to predict an event occurrence, by means of existing models or methods and defined by an expert [14]. As soon as there is an event occurrence, another set of nodes must transmit multimedia data, e.g., audio and video streaming, with QoE assurance to headquarters or IoT platforms, such as provided by the semantic system [11], sensor4cities [12, 13], i-SCOPE [100], and other IoT platforms. In this context, multimedia content provides more precise information than simple scalar data, enabling specialists, mobile users, or computer vision software to visually verify the real impact of the event, avoid false-positive alarms, take consciousness of what is happening in the environment, plan actions, detect objects or intruders, and analyse scenes. Sensor4cities [12, 13] is an example of a tool that can be used to allow the users to request scalar or multimedia data from the monitored area via webpages and social networks, e.g., Twitter or Facebook. After receiving scalar or real-time multimedia flows, sensor4cities can share them with a control center or mobile user for further analysis. However, in this chapter, we focus only on how to disseminate video flows and physical scalar sensor data with QoS or QoE assurance, robustness, and reliability to feed smart cities or IoT platforms for static WMSN scenarios.

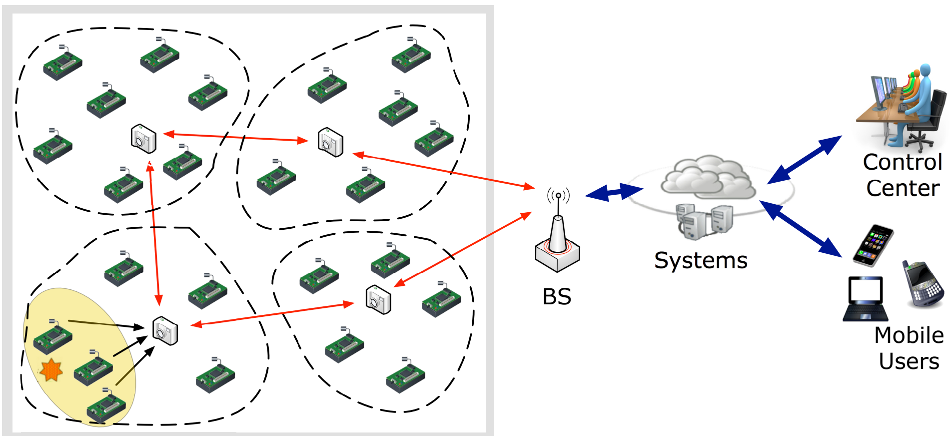

Figure 15: Hierarchical Network Architecture for Static WMSNs

We consider a river monitoring application [17–19] composed of a set of nodes sensing the river flow by means of physical scalar measurements, and also using another set of nodes collecting multimedia data in the case of an event occurrence. As soon as a river has fast velocity and high water level, it might be useful to see whether additional objects, such as wood or thrash are floating on the surface of the river. This is because these objects might affect the behaviour of the river flow, in particular when they block the normal flow of the river, and thus the river dam up. However, this phenomenon cannot be detected by measuring simple scalar data. Hence, live video flows must be collected to enable such task to be carried out. This scenario description is also desirable for many WMSN applications, such as safety & security, environmental monitoring, smart parking, traffic control, and other smart cities applications.

Physical scalar sensor data measurement requires transmission reliability and tolerable end-to-end delay. On the other hand, multimedia dissemination demands a high bandwidth, real-time transmission, lower frame loss, tolerable end-to-end delay and jitter. In addition, applications involving multimedia dissemination should support QoS and QoE to deliver video content with, at least, a minimum level of video quality from the user's perspective, together with energy-efficiency and scalability [21,101]. These factors impose considerable constraints and design challenges to design an energy-efficient, scalable, and reliable routing protocol for WMSNs.

Routing protocols for WMSNs can be classified into flat, location-based, and hierarchical architectures [25]. Hierarchical network architectures with heterogeneous nodes have been proven to be more beneficial than flat network architectures for WMSNs in terms of lower energy consumption, greater functionality, better scalability, and reliability. The advantages of using a hierarchical architecture are as follows: i) nodes have different roles or functionalities to reduce energy consumption; ii) some nodes perform data aggregation, avoiding unnecessary data transmission; and iii) a set of nodes may turn-off the radio after transmitting their data packets, and as a result, reduce their energy consumption and avoid communication conflicts [4, 5, 7].

Energy constraints in WMSNs are even stricter than in WSNs, because multimedia content creates a huge amount of data that has to be processed, transmitted, and forwarded, as well as it requires the use of network resources. In this context, continuous multimedia delivery requires the transmission of multimedia content gathered at a specified rate independent of any event or user query. Moreover, in most WMSN applications, periodic multimedia transmissions involve the delivery of irrelevant multimedia content without any event occurrence, causing wasteful expenditure of energy and bandwidth [102]. On the other hand, in the event-driven and query-driven models, the transmission of video content is triggered only when an event occurs or a query is generated. Therefore, the routing protocol for WMSNs should be based on either the query-driven or the event-driven model in order to reduce the waste of scarce network resources [25]. Finally, a hierarchical routing protocol should minimize the signalling overhead required for the cluster formation to increase the network lifetime.

Scalability is another key issue for a hierarchical routing protocol in WMSNs, which is achieved by an efficient multi-hop routing scheme [25]. Moreover, multi-path communications allow the routing service to provide load balancing, bandwidth aggregation, and reduced delay compared to single-path communication [26]. However, the routing protocol must find node-disjoint multiple paths that avoid common nodes (or hot spot) among different paths. This is because node-disjoint multi-path routing mitigates the problem of packet losses at intermediate forwarding nodes with restricted buffer capacity, and thus improves the video quality level.

Low-power radios used in WMSNs are very sensitive to noise, interference, and multipath distortion, which causes link unreliability. Significant link quality fluctuations and weak connectivity also have serious effects on the quality of wireless communication. In this context, the link quality estimation accuracy greatly impacts the efficiency and reliability of the routing protocols. In this context, many routing protocols rely on link quality estimation to help in the selection of high quality routes for communications [103].

To ensure efficient and reliable routing decisions, nodes must have knowledge about the remaining energy of their neighbour nodes, and also the number of hops required to reach the destination node for each possible path. However, reliable route selection must consider both cross-layer information and end-to-end link quality estimation with minimum overhead to find node-disjoint multi-path [104]. Hence, the routing protocol is able to select QoS/QoE-aware multi-path routes to transmit multimedia or scalar data with high packet delivery rate.

As introduced in Section 2.1, frames with different priorities compose a compressed video. From a human's standpoint, the loss of high priority frames causes severe video distortion. Hence, a key principle in a QoE-aware routing protocol for WMSNs is to have the ability to schedule high priority frames through better paths, and less important frames via alternative paths. In this way, it protects key frames during losses and link error period [45, 53]. However, so far, current hierarchical routing protocols for WMSNs have failed to take into account of all of these key features outlined in this section into a single proposal. These features are needed to support scalability, reliability, energy-efficiency, and QoE-aware multimedia transmission.

4.2 Network Model

We consider a network composed of n static nodes deployed in the monitored area. Those nodes have an individual identity ($i \in [1, n]$) and are represented in a dynamic graph $G(V, E)$, where vertices $V = \{v_1, v_2, ..., v_n\}$ create a finite set of nodes, and edges $E = \{e_1, e_2, ..., e_m\}$ build a finite set of asymmetric wireless links between them. Each node v_i is able to estimate network conditions at the physical layer for a given link e_j, $j = 1, ..., m$. For instance, the physical layer of CC2420 radio chip provides LQI, RSSI, and SNR to compute the LQE for each received packet [89]. In this chapter, $w(e_j) \in [w(e_j)_{min}, w(e_j)_{max}]$ denotes the LQE for a given link e_j.

Each node v_i has a queue $(Q) \in [0,\ Q_{max}]$, which has a maximum queue capacity (Q_{max}) and current queue length (Q_{length}). The queue policy schedules the packet transmission using the First In First Out (FIFO) algorithm, and drops packets by using the drop tail algorithm in case of buffer overflow. Moreover, each node v_i has a battery (P) with initial power (P_0) and maximum power (P_{max}), and it is able to estimate the remaining energy (RE_t) at any time t. A given node v_i requires power (P_{tx}) to transmit a packet, (P_{rx}) to receive a packet, and (P_{sense}) either to retrieve a video frame or to sense physical scalar sensor measurements.

MEVI relies on a hierarchical network architecture with heterogeneous nodes, as expected for many WMSN scenarios. This is because hierarchical architectures has been proven to be more effective than flat architectures in terms of lower energy consumption, greater functionality, better scalability, and reliability [4, 5, 7]. In this context, nodes v_i can be categorized as follows: Sensor Nodes (SN_i, i = 1, 2, ..., n') $\subset V$; and Camera Nodes (CN_i, i = 1, 2, ..., n") $\subset V$, as illustrated in Figure 16. Every SN_i is equipped with a radio transceiver and a scalar sensor, but they are restricted in terms of energy supply, processing, and memory space. On the other hand, every CN_i is equipped with a radio transceiver, an alternative energy source, a camera, and an image encoder. For instance, each CN_i can be equipped with rechargeable battery or solar power, such as introduced by Abu-Baker et al. [29] and Solobera [30]. Solobera proposed a permanent 24/7 solar-operated network for fire detection and localization in the Asturias region in the north of Spain.

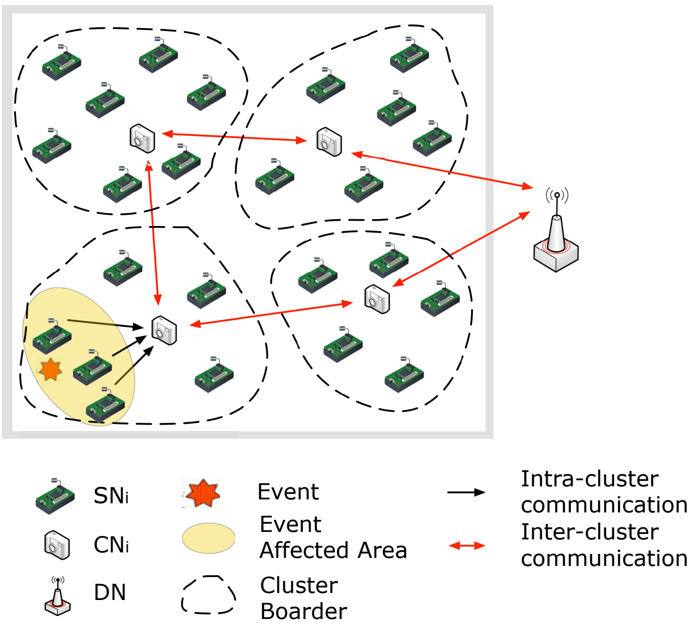

Figure 16: Network Model for Static WMSNs

We consider a network composed of one Destination Node (DN) equipped with a radio transceiver, an image decoder, and unlimited energy supply. For convenience of notation, we denote $SN \subset CN_i$ (Source Node) as the CN_i responsible for capturing video flows and transmitting them to the DN in a multi-hop fashion. Each CN_i encodes the video stream before distributing, and the DN decodes the received packets by converting them from an intermediate format to a video sequence, as introduced in Section 2.1.

In a similar way to existing hierarchical routing protocols for WMSNs, MEVI considers that every SN_i performs simple tasks, such as collecting physical scalar measurements in the monitored area, and transmitting them to CN_i in a given time-slot. Each SN_i can be deployed in a uniform or random way, depending on application requirements or cost issues. However, node deployment is out of scope of this thesis. On the other hand, each CN_i carries out more complex tasks, such as routing, slot allocation, synchronizing SN_i transmissions, multimedia retrieval, and data aggregation. Moreover, each SN must establish a route $P_{SN,DN} = \{SN, CN_i, ..., DN\}$ connecting any pair of SN and

DN via multiple CN_i. Each CN_i locations is pre-defined by the network administrator, in accordance with the physical characteristics of the environment or local policies.

Each CN_i or DN processes the physical scalar sensor measurements by means of existing models or methods with the aim of predicting an event occurrence, such as flooding, fire, detecting intruders, or any other event [14, 31, 32]. As soon as a given CN_i detects an event in the monitored are, it must start multimedia retrieval and transmission to provide more precise visual information about the monitored environment than simple scalar data does. Thus, real-time multimedia transmission enables the end-user (or system) to visually identify the real effects of the event, take consciousness of what is happening in the environment, plan actions, analyse scenes, and also help to detect objects or intruders [15, 16].

4.3 Problem Statement

In this chapter we address the following issues.

- We introduce a cluster formation with low overhead, while at the same time we provide efficient and reliable intra-cluster communication.
- We find a subset of reliable camera nodes CN_i to establish multiple paths $P_{SN,DN} = \{SN, CN_i, ...DN\} \subset V$, connecting a SN to a DN via multiple CN_i. In particular, the subset of optimal CN_i must provide high packet delivery rate.
- We trigger multimedia transmission according to the SR index, avoiding the transmission of unnecessary video content and saving scarce network resources, such as energy and bandwidth.
- We schedule multimedia transmission via multi-paths according to the frame relevance, providing load balancing and QoE-awareness.

4.4 MEVI Design and Operation Principles

This section outlines our proposed MEVI protocol, a hierarchical routing protocol, which considers two phases for data transmission: (i) single-hop communication between SN_i and CN_i to create clusters, called intra-cluster communication; and (ii) multi-hop communication between CN_i and DN, called inter-cluster communication. The intra and inter-cluster communication comprises a superframe, as illustrated in Figure 17. Moreover, MEVI triggers the multimedia transmission according to the sensed information about the environment. It also takes into account a multi-path routing scheme and frame relevance to provide load balance, robustness, and QoE-aware video transmission.

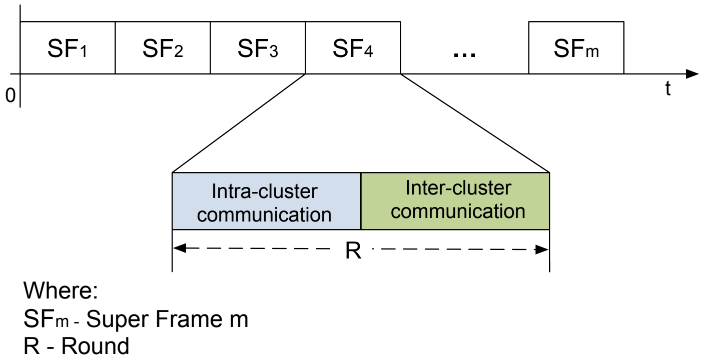

Figure 17: Superframe Structure

4.4.1 Intra-Cluster Communication

The advertisement period (adv) and a set of slots (slot$_k$, k = 1, 2, ..., n$_{slot}$) compose the intra-cluster communication, as depicted in Figure 18. During intra-cluster communication, nodes SN_i and CN_i create clusters with low signalling overhead, and each SN_i transmits the sensed scalar physical measurements in a specific slot$_k$ to a given CN_i. Furthermore, each CN_i receives the data packets from a set of SN_i, aggregates them into a single packet, and assigns slot$_k$ for each SN_i according to the TDMA schedule.

MEVI contains a set of parameters for intra-cluster communication: (i) time-slot duration (t$_{slot}$) indicates the time interval that a given SN_i takes to transmit its data packets; (ii) n$_{slot}$ indicates the number of contained time-slots in each superframe; and (iii) Round (R) denotes the total amount of time for intra- and inter-cluster communications. All superframes contain the same values for the parameters n$_{slot}$ and t$_{slot}$, and these values depend on the application requirements. For instance, each SN_i must allocate enough slots to satisfy the required bandwidth and delay.

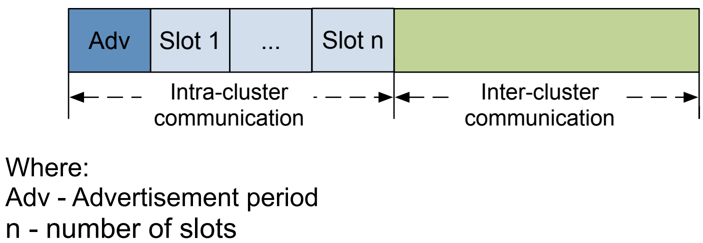

Figure 18: Intra-cluster Communication Structure

Existing hierarchical routing protocols considers that each CN_i and SN_i have to exchange at least beacon, join, and schedule messages, before sending their data packets. In contrast to those protocols, the beacon message in MEVI includes the TDMA schedule, and the data packet behaves as a join message. This is because before each SN_i tries to allocate a given slot$_k$ in a CN_i, it has to wait for a beacon message sent by CN_i, and then the SN_i must send its data packet within the selected slot$_k$. In this way, MEVI provides a cluster formation scheme with a low overhead.

Algorithm 2 shows the pseudo-code for cluster formation proposed for intra-cluster communication. Each SN_i remains in sleep mode until the beginning of a new superframe, which is started by each CN_i broadcasting a beacon message. Before transmitting the beacon message, each CN_i must include each slot$_k$ status, i.e., idle or busy, in the *slotStatus* field (lines 7 – 13). Hence, compared with existing hierarchical routing protocols, such as LEACH [64] and PEMuR [65], the beacon message in MEVI integrates the schedule and beacon messages, which contains the following fields:

- CN_k: camera node address;
- *timestamp*: timestamp for the current beaconMessage; and
- *slotStatus*: a queue to report the TDMA schedule;

MEVI takes into account the link quality estimation for a given link e_j between any pair CN_k and SN_j, as the metric to enable each SN_j in order to select a reliable CN_k to transmit its data packet. LQE can be classified as either hardware-based or software-based [105]. Software-based LQEs enable to either count or approximate the PRR or the average number of packet transmissions or re-transmissions. For instance, the PRR counts the Packet Reception Ratio as the ratio of the number of successfully received packets to the number of transmitted packets, for each window of w received packets. However, software-based LQEs include overhead and delay to estimate the link quality $w(e_j)$ for a given link e_j. On the other hand, hardware-based LQEs, such as LQI, RSSI, and SNR, are directly read from the radio transceiver (e.g., the CC2420) upon the reception of a packet. Gomez et al. [106] compared the performance of RSSI and LQI in terms of reliable transmission, and as a result found that LQI can improve the reliability of a single-hop link. Hence, we considered the LQI values to estimate the link quality $w(e_j)$ for a given link e_j between any pair CN_k and SN_j.

As soon as a given SN_i receives a beacon message from each CN_i, it extracts the candidate$_{id}$, and derives the LQI value. It should be stressed that MEVI takes into account the degree of variability of wireless links, since each SN_i computes the exponential average for the LQI (LQI$_{avg}$) perceived in the last (w) beacon messages from each CN_i. Thus, MEVI gives more importance to recent LQI values. In contrast to existing hierarchical routing protocols, where each SN_i sends a join message for a given CN_i, each CN_i chooses a slot$_k$ for each SN_i, and then the CN_i sends a schedule message. In MEVI, each SN_i becomes aware of idle slot$_k$ by analysing the *slotStatus* field contained in a beacon message, and then it randomly selects one of the idle slots (*selectedSlot*). Once a given SN_i has those information for each received beacon, it must add them into a CN_k candidate list (*candidateList*) (lines 14 – 23), which contains the following information:

- $candidate_{id}$: camera node address;
- *selectedSlot*: the selected slot to send the collected data;
- LQI_{temp}: a queue to save the last w LQI values; and

- LQI_{avg}: exponential average for the LQI perceived in the last w beacon messages.

After transmitting a beacon, every SN_i must select a given CN_i with the highest LQI_{avg} from the $candidateList$. This is because the selected CN_i should be the candidate node with the best communication quality, reducing waste of energy and the number of lost packets (lines 24 – 28). Following this, each SN_i waits for its selected slot$_k$, and sends the collected physical sensor data measurements to the chosen CN_i (lines 29 – 32). In the case of each data packet received by a given CN_i, it must decide about the slot allocation for each SN_i and perform data aggregation (lines 33 – 36).

Algorithm 2 MEVI Cluster Formation

StartUp
1: Let t$_{slot}$ = slot$_k$ duration
2: Let n$_{slot}$ = number of slot$_k$
3: Let R = total amount of time for intra- and inter-cluster communication
4: Let *slotStatus* = queue to report the TDMA schedule
5: Let $aggPkt$ = queue to aggregate data packet
6: Let *candidateList* = CN_k candidate list
Start the advertisement period
7: **if** v_i is CN_i **then**
8: broadcast beaconMessage(CN_k, *slotStatus*)
9: **end if**
10: **if** v_i is SN_i **then**
11: turn the radio on
12: **end if**
13: Restart the advertisement period at R
on receiving a $beaconMessage$
14: **if** v_i is CN_i **then**
15: drop message
16: **end if**
17: **if** v_i is SN_i **then**
18: c.cadidate$_{id}$ ← getSourceId($beaconMessage$)
19: c.LQI_{temp} ← getLQI($beaconMessage$)
20: c.LQI_{avg} ← computeExponetialAverage(c.LQI_{temp})
21: c.selectedSlot ← selectSlot($beaconMessage$.*slot*[]) // randomly select an available slot from $beaconMessage$.*slotStatus*
22: ADD c to *candidateList*
23: **end if**
End of the advertisement period
24: **if** v_i is SN_i AND *candidateList* is not empty **then**
25: *candidateList* order by LQI_{avg}
26: set the *sendData* timer to fire at currentTime + *candidateList*[0].*slot* * t$_{slot}$
27: turn the radio off
28: **end if**
On *sendData* timer timeout
29: turn the radio on
30: data ← getSensorData() // sense physical sensor data measurement
31: sendData(data, *candidateList*[0].cadidate$_{id}$)
32: turn the radio off
on receiving a $dataPacket$
33: schedulingDecision($dataPacket$)
34: **if** successfully slot$_k$ allocation **then**
35: aggPkt.enqueue(dataPacket)
36: **end if**

For slot allocation decision, i.e., $schedulingDecision(dataPacket)$, a given CN_i must successfully assign slot$_k$ when only one SN_i tries to allocate such slot$_k$. On the other hand, when multiple SN_i attempt to use the same slot$_k$, the CN_i randomly allocates slot$_k$ to one of those candidates. Moreover, a given CN_i considers any slot$_k$ as idle, when it discovers that one of slot$_k$ has not been used for the last y super-frames (called the idleness of a time-slot).

Each SN_i must wait for the next beacon message to find out if the selected slot$_k$ was successfully allocated. If this holds, it must keep sending the collected physical environmental data using the same slot$_k$, until it finds that the LQI_{avg} of another CN_i in the *candidateList* is higher than the current CN_i. Otherwise, each SN_i must repeat this procedure until obtaining a slot. It should be noted that each SN_i only turns the radio on in the beacon transmission period and in its own time-slot.

Hereafter, we analyse the memory usage and algorithm complexity (computational complexity), and also the signalling overhead (communication overhead) introduced by the MEVI intra-cluster communication algorithm.

- *Communication overhead:* the communication complexity of our algorithm is n, where n is the number of camera nodes deployed in the network. This is because each camera node broadcasts only one beacon message per round. MEVI adds low byte overhead compared to existing solutions, since it includes only the *slotStatus* field into the beacon message. Hence, we conclude that our proposed cluster formation algorithm adds low byte and message overhead compared to existing hierarchical routing protocols.

- *Computational complexity:* the proposed algorithm has a computational complexity value of $O(n)$. This is explained because as soon as there is an incoming beacon message, each SN_i has to search for an available slot$_k$ in the *slotStatus* field, which has a size of n$_{slot}$ (line 21). Moreover, each SN_i has to order the *candidateList* from higher LQI_{avg} to lower LQI_{avg} values, and the *candidateList* has the size of o (line 25). It can be concluded that the algorithm has a computational complexity with a cost of $O(n)$, since the *candidateList* size o and the number of slot$_k$ n$_{slot}$ have quite similar values.

4.4.2 Inter-Cluster Communication

The inter-cluster communication consists of a route discovery period, where MEVI explores a reactive scheme to find on demand multiple paths $P_{CN_i,DN}$ between any pair of CN_i and DN. The route discovery process involves each CN_i broadcasting route request (RREQ) and reply (RREP) messages, searching for available multi-paths. Hence, each CN_i forwards the aggregated and multimedia data packets to the DN, and the DN can also request multimedia content to a given CN_i in case of event occurrence.

4.4.2.1 Operational Modes: Normal or Event Mode

When an event occurs in the monitored field, any SN_i located in the event region generates data packets with scalar environmental information of the event. A given SN_i closer to the event has a higher Sensing Relevance (SR) than any other SN_i, because it can generate more accurate and detailed information from the event area [31]. For instance, in temperature or fire monitoring applications, a given SN_i that senses a higher temperature value must have a higher SR, because it generates urgent information [32].

We defined that the SR of each sensor node SN_i into three categories, representing the potential of each SN_i to provide relevant physical scalar sensor data for the monitoring application. In such way, the SR depends on the application requirements. The SR categories are the following.

- **Irrelevant.** It may happen after random deployment that a given SN_i has no relevant scalar physical measurements for the monitoring application, i.e., a given SN_i collects only values lower than a defined soft threshold. In this case, the corresponding CN_i should turn off their camera, since no visual information should be transmitted. Hence, in such case, the camera node acts only as relay node.

- **Medium relevance.** Based on the scalar physical measurements, e.g., temperature, humidity, or any other measurement, visual information should be sent by the CN_i, but the DN decides if the CN_i should start to transmit multimedia data or not. Hence, a given CN_i with low relevance may be transmitting complementary visual information in order to confirm that an event occurred in the monitored area, and also to identify its real impact on the basis of valuable visual information.

- **High relevance.** It indicates that an event already happened, and thus the retrieved visual information is highly critical. Moreover, some CN_i have higher relevance for the application, requiring prioritized treating in packet processing, congestion control, error recovery, and multipath selection algorithms. In most cases, lost of information from high relevant CN_i may harm the monitoring quality of the application.

In this context, MEVI relies on existing models or methods [14] to process the scalar physical measurements to help each CN_i to choose the operational mode for inter-cluster communication. For instance, in case of high or medium SR, the CN_i must send multimedia content to the DN. This is because multimedia data provides more precise visual information about the monitored environment than simple scalar data does.

Figure 19 shows the activity diagram for inter-cluster communication. During the Event Occurrence (EO) period, each CN_i analyses received data packets from every SN_i to detect if one of the sensed data measurement has a higher SR, i.e., when one of the data measurements is higher than a hard threshold. For instance, for temperature or fire monitoring applications, temperature higher than 90 °C indicates that an event has already occurred, and the CN_i must provide as much visual information as possible. In this way, as soon as a given CN_i detects that the collected data from any SN_i has a higher SR, it must start the event mode. It should be underlined that such CN_i does not need to save energy in case of important data to be sent, since the users or civil authorities need visual information to be aware of what is happening in the environment, and depending on the event, e.g., a fire or flooding, the network nodes might quickly die or be destroyed.

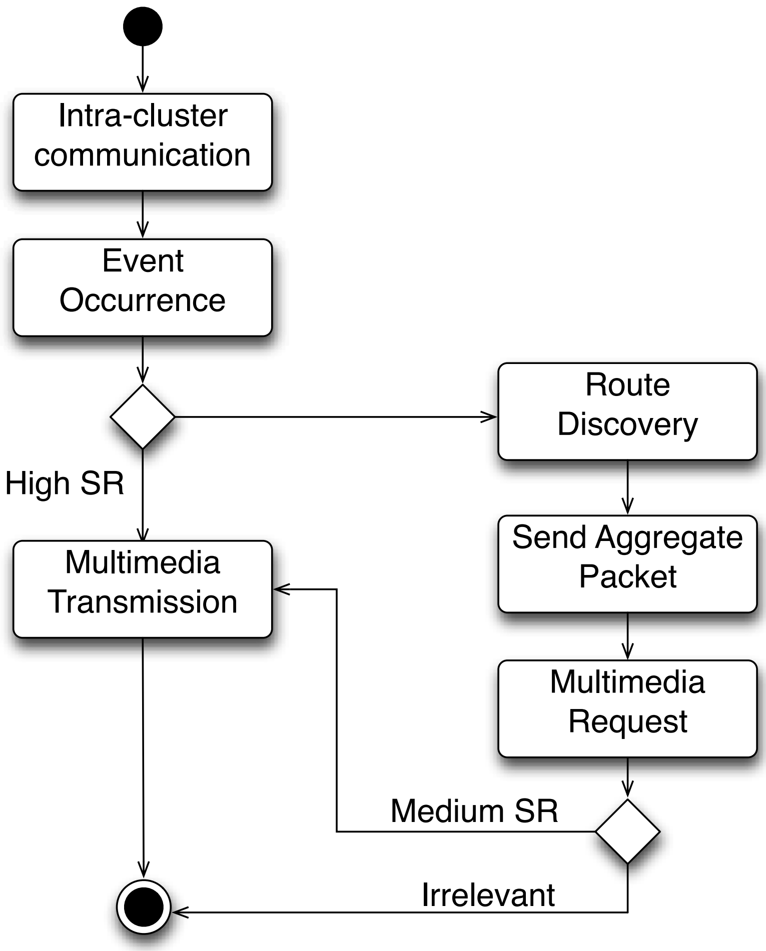

Figure 19: Activity Diagram for Inter-Cluster Communication

Any CN_i should start the event mode by sending an event message through the path $P_{CN_i,DN}$ that connects the CN_i to the DN via multiple CN_i. Hence, it is possible to avoid interference, and also give priority to multimedia transmissions from the monitored area with high SR. As soon as every CN_i that composes the path $P_{CN_i,DN}$ becomes aware of the event mode, Multimedia Transmission (MT) period starts.

In normal mode, i.e., in case of medium or irrelevant SR, any CN_i only transmits video content when the DN requests it, since there is a low risk of event occurrence, and also during the normal mode every CN_i aims to save scarce resources, such as energy and bandwidth. As soon as a given CN_i has an aggregate packet to send to the DN, it must search for available paths $P_{CN_i,DN}$ to reach the DN via multiple CN_i within the Route Discovery (RD) period. After the RD period, each CN_i must send the aggregate packet to the DN during the Send Aggregate packets (SA) period.

On receiving an aggregate packet, the DN must analyse the SR of the received data by means of existing models or methods. The DN requests a video sequence from a given CN_i within the Multimedia Request (MR) period, as soon as the DN detects that one of the sensed values from such CN_i is higher than a defined soft threshold, i.e., the data has medium SR. For instance, again in temperature or fire monitoring applications, temperature higher than 60 °C might indicate a possible event occurrence. Hence, multimedia data can be used to confirm that an event occurred in the monitored area, and also to identify its real impact on the basis of valuable visual information. On the other hand, no visual information should be transmitted in case of low SR for the monitored data. Figure 20 illustrates periods that comprise inter-cluster communication.

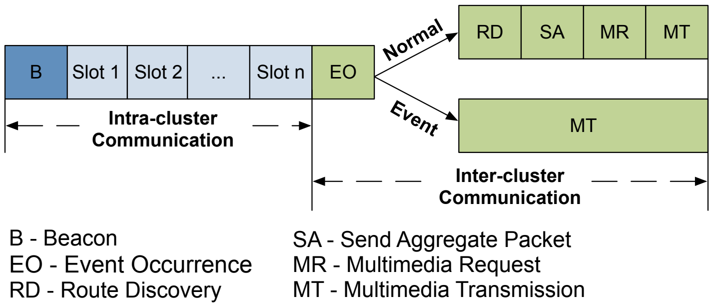

Figure 20: Inter-Cluster Communication Structure

4.4.2.2 Node-disjoint Multiple Route Discovery

MEVI finds on-demand multiple node-disjoint paths $P_{SN,DN}$ between any pair of SN and DN via multiple CN_i by transmitting RREQ and RREP messages. The RREQ message corresponds to the beginning of the route discovery process. Figure 21 shows the fields that compose the RREQ message in MEVI.

- type: It is used to identify the message type. RERQ messages are marked with the value equal to 1;
- src_{addr}: Source node address for a given RREQ message;
- $dest_{addr}$: Destination node address for a given RREQ message;
- $RREQ_{seq}$: RREQ sequence number;
- $route_{id}$: Route identifier;
- HC: Number of hops for a given RREQ message;
- DL: Number of disconnected links for a given RREQ message;
- CL: Number of connected links for a given RREQ message;

- RE_t: Remaining energy of a given next-hop.

```
 0                   1                   2                   3
 0 1 2 3 4 5 6 7 8 9 0 1 2 3 4 5 6 7 8 9 0 1 2 3 4 5 6 7 8 9 0 1
+-+-+-+-+-+-+-+-+-+-+-+-+-+-+-+-+-+-+-+-+-+-+-+-+-+-+-+-+-+-+-+-+
|     Type      |    RREQ ID    |   Route ID    |   Hop Count   |
+-+-+-+-+-+-+-+-+-+-+-+-+-+-+-+-+-+-+-+-+-+-+-+-+-+-+-+-+-+-+-+-+
|                         Source address                        |
+-+-+-+-+-+-+-+-+-+-+-+-+-+-+-+-+-+-+-+-+-+-+-+-+-+-+-+-+-+-+-+-+
|                      Destination address                      |
+-+-+-+-+-+-+-+-+-+-+-+-+-+-+-+-+-+-+-+-+-+-+-+-+-+-+-+-+-+-+-+-+
|      CL       |      DL       |    Energy     |
+-+-+-+-+-+-+-+-+-+-+-+-+-+-+-+-+-+-+-+-+-+-+-+-+
```

Figure 21: Route Request Message

The RREQ message is part of the route discovery process, and represents a response to a route request, which contains information describing the route. The RREP message in MEVI contains the following fields, as shown in Figure 22.

- type: It is used to identify the message type. RERP messages are marked with the value equal to 2;
- src_{addr}: Source node address for a given RREP message;
- $dest_{addr}$ Destination node address for a given RREP message;
- $RREP_{seq}$: RREP sequence number;
- $route_{id}$: route identifier;
- HC: Number of hops for a given RREP message;
- CL: Number of connected links for a given RREP message;
- DL: Number of disconnected links for a given RREP message;
- RE_t: remaining energy of a given next-hop.

```
 0                   1                   2                   3
 0 1 2 3 4 5 6 7 8 9 0 1 2 3 4 5 6 7 8 9 0 1 2 3 4 5 6 7 8 9 0 1
+-+-+-+-+-+-+-+-+-+-+-+-+-+-+-+-+-+-+-+-+-+-+-+-+-+-+-+-+-+-+-+-+
|     Type      |    RREP ID    |   Route ID    |   Hop Count   |
+-+-+-+-+-+-+-+-+-+-+-+-+-+-+-+-+-+-+-+-+-+-+-+-+-+-+-+-+-+-+-+-+
|                         Source address                        |
+-+-+-+-+-+-+-+-+-+-+-+-+-+-+-+-+-+-+-+-+-+-+-+-+-+-+-+-+-+-+-+-+
|                      Destination address                      |
+-+-+-+-+-+-+-+-+-+-+-+-+-+-+-+-+-+-+-+-+-+-+-+-+-+-+-+-+-+-+-+-+
|      CL       |      DL       |    Energy     |
+-+-+-+-+-+-+-+-+-+-+-+-+-+-+-+-+-+-+-+-+-+-+-+-+
```

Figure 22: Route Reply Message

The proposed protocol assigns an identifier ($route_{id}$) for each possible path $P_{SN,DN}$ in order to name each possible path, and thus it helps MEVI to find node-disjoint multi-paths. More specifically, the SN broadcasts the RREQ message with $route_{id}$ field empty, then the first node that rebroadcasts the RREQ message adds its identifier into the $route_{id}$ field of the RREQ message. Figure 23(a) illustrates the route discovery operation, where the SN broadcasts a RREQ message to find possible node-disjoint multiple paths $P_{SN,DN}$, i.e., paths with different $route_{id}$. In this example, the RREQ message traverses by three possible paths to reach the DN with different $route_{id}$, i.e., $route_{id}$ equals to 1, 4, and 6. Hence, each RREQ arriving via a different neighbor of the SN has a different $route_{id}$, defining a node-disjoint path.

It should be pointed out that a given CN_i never rebroadcasts duplicate RREQs, so any two RREQs arriving at given CN_i via a different neighbor of the SN could not have traversed the same node, and thus RREQ duplicates are discarded in intermediate CN_i. For example, node 7 receives RREQs with $route_{id}$ 4 and 6, and thus it knows that these paths are not node-disjoint. In this case, node 7 does not rebroadcast the RREQ with $route_{id}$ 4, and it adds only the path with $route_{id}$ 6 into the routing table.

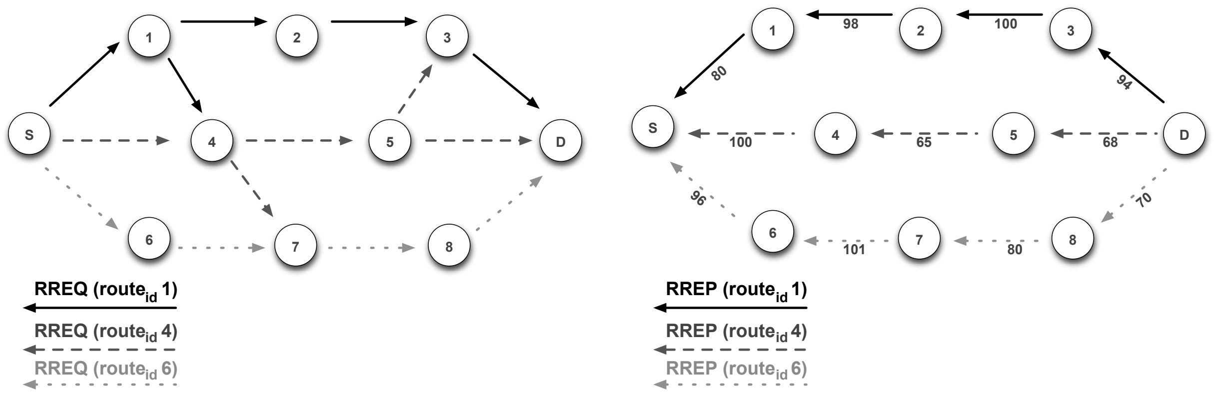

(a) Route request (b) Route reply

Figure 23: Multi-Path Route Discovery

As soon as the RREQ message has reached the DN, it creates a new entry into the routing table for each incoming request from every SN, even when the received RREQs have a different $route_{id}$. Afterwards, the DN must send a corresponding RREP message for every incoming RREQ message. This is because MEVI aims to establish a full bi-directional multi-path $P_{SN,DN}$, as depicted in Figure 23(b). The RREP message travels back to reach the SN, which creates new path entries in the routing table for every incoming RREP. The routing table in each CN_i contains the following information:

- src_{addr}: source node address for a given path $P_{SN,DN}$;
- $dest_{addr}$: destination node address for a given path $P_{SN,DN}$;
- $route_{id}$: route identifier;
- HC: Number of hops to reach the DN;
- CL: Number of connected links to reach the DN;
- DL: Number of disconnected links to reach the DN;
- PQ: path quality for a given path $P_{SN,DN}$.

Existing studies classify each possible path $P_{SN,DN}$ according to hop-count or single-hop metrics. In contrast to those studies, MEVI evaluates the end-to-end link quality communication by using regions of connectivity presented by Baccour et al. [105], which classified links by means of the experienced Packet Reception Ratio (PRR) into three regions of connectivity, namely connected (PRR higher than 90%), transitional (PRR between 10% and 90%), and disconnected (PRR lower than 10%), as depicted in Figure 24(b). Based on this information, MEVI attempts to find routes composed of connected links to support multimedia transmissions with high packet delivery rate. In addition, as explained in the following section, MEVI schedules packet transmission via multiple paths by using frame priority from the user experience, protecting key frames during loss or link error periods.

To estimate the end-to-end link quality during route discovery in MEVI, each CN_i must count the number of disconnected (DL) and connected (CL) links for a given path $P_{SN,DN}$. These counters are included into two fields within the RREQ and RREP messages, namely the DL and CL fields. In this context, two thresholds, i.e., LQI_{bad} and LQI_{good}, define the boundaries of the disconnected and connected regions, as shown in Figure 24(b). Those thresholds must be defined according to performed calibration experiments, which consist of establishing a rich set of single-links exhibiting different qualities, regardless of any external factors, such as collisions and routing. It is important to mention that end-to-end link quality estimation was first introduced in our studies [98, 99], but without considering the requirements to provide multimedia dissemination with QoE support, hierarchical architecture, and multiple node-disjoint paths. For instance, in our initial studies [98, 99], we do not count the number of connected links, i.e., reliable links, but we only count the number of disconnected links. In addition, in such works [98, 99], we do not integrate the number of disconnected links into a formula to score each possible path $P_{SN,DN}$.

As recommended by Baccour et al. [107], 40 nodes are deployed for the calibration experiments, which have different distances and directions from the DN, as depicted in Figure 24(a). This is because distance and direction directly affect the link quality. Nodes were placed in a circle around the DN, where we divided nodes into 8 sets with different radius. Each set contains 4 nodes, all placed in a circle around the DN. The distance between two consecutive sets is equal to 1 meter. Each node had an exclusive time-slot defined according to a TDMA scheme, enabling each one to transmit a burst of n_{pkts} packets to the DN without collision and interference. Hence, based on exchanged data, the link quality of each unidirectional link has been estimated. Figure 24(b) presents the PRR as a function of the LQI, where it is possible to defined two thresholds, i.e., LQI_{bad} and LQI_{good}, which represent the boundaries of the disconnected and connected regions.

After calibration experiments have been carried out, we can correlate the PRR and LQI provided by each link e_j. For instance, a given link e_j is considered as a disconnected link, when it has LQI lower than LQI_{bad}. A video sequence transmitted via a disconnected link might have a reduced video quality level, since this link has a high packet loss rate. In addition, a given link e_j with LQI higher than LQI_{good} provides a connected link, enabling multimedia transmission with packet delivery guarantee, such as expected for multimedia applications with QoE support. Finally, a given link e_j with LQI between LQI_{bad} and LQI_{good} is considered as a transitional link, which is not stable to transmit video packets, since the same LQI might have PRR raging from 10% to 90%. Hence, after receiving a RREQ or RREP message, a given CN_i must derive the LQI value, and classify the links into disconnected and connected based on the LQI_{bad} and LQI_{good} thresholds. After that, it must update the values of disconnected and connected fields of RREQ/RREP messages.

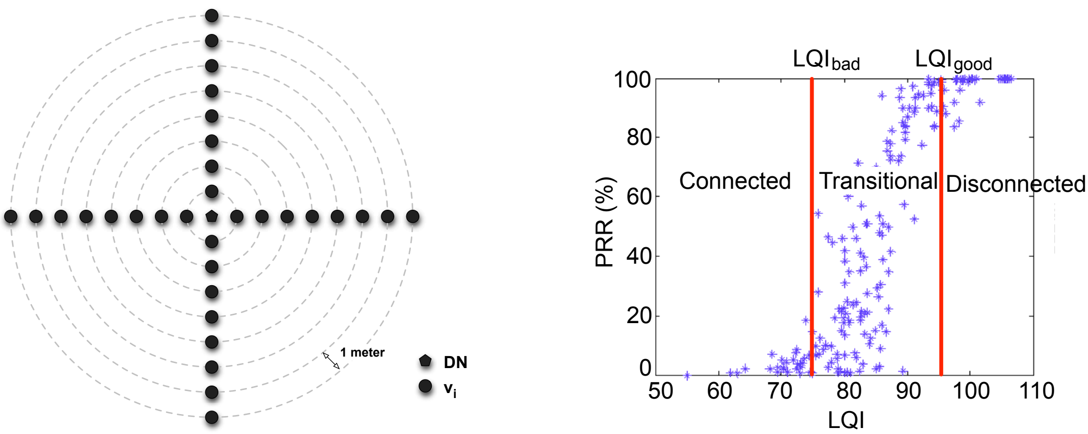

(a) Network Topology (b) Regions of Connectivity

Figure 24: Network Configuration and Results for Reception Regions Evaluation

Initially, we considered the **Link Quality (LQ)** $\in$ [0, 1] to score and classify each possible path $P_{SN,DN}$ in MEVI [95,96]. Later, we introduced the **Path Quality (PQ)** $\in$ [0, 1] in MEVI to score and classify each possible path $P_{SN,DN}$ [97], because PQ enables to score each possible path based on end-to-end link quality estimation. When MEVI considers LQ to score and classify each possible path $P_{SN,DN}$, a given CN_i computes the LQ based on Eq. 4.1 by taking into account multiple cross-layer single-hop metrics, namely energy (RE_t), link quality (LQI), and number of hops (HC). The proposed LQ considers tree weights (ω_{energy}, ω_{LQE}, ω_{HC}) to assign a different degrees of relevance for each of those metrics, which can be adjusted according to different application requirements.

$$LQ = \omega_{energy} \times \frac{RE_t}{E_0} + \omega_{LQE} \times \frac{LQI}{LQI_{max}} + \omega_{HC} \times \frac{HC_{max} - HC}{HC_{max}} \tag{4.1}$$

The sum of weights is equal to 1. E_0 represents the initial energy for a given CN_i, LQI_{max} represents the maximum value for LQI, and the maximum Hop Count (HC_{max}) depends on the network diameter. Each possible path $P_{SN,DN}$ has a LQ value ranging from 0 to 1. In this way, a given CN_i searches for the most reliable next-hop candidate with enough energy to forward the multimedia packets, and also the path $P_{SN,DN}$ with a low number of hops. According to LQ calculation, the path $P_{SN,DN}$ with the highest score has the next hop with the best network conditions for transmitting packets.

PQ is computed according to Eq. 4.2, which considers cross-layer single-hop metrics, i.e., RE_t and LQI, and also end-to-end link quality metrics, i.e., DL and CL. Moreover, PQ considers coefficients (ϕ_{CL}, ϕ_{DL}, ϕ_{energy}, ϕ_{LQE}) to give different degrees of priority to each metric. The sum of coefficients is equal to 1, and the values have to be adjusted according to scenario characteristics or application requirements.

$$PQ = \phi_{CL} \times \frac{CL}{HC} + \phi_{DL} \times \frac{HC - DL}{HC} + \phi_{energy} \times \frac{RE_t}{E_0} + \phi_{LQE} \times \frac{LQI}{LQI_{max}} \tag{4.2}$$

The proposed PQ function considers end-to-end link quality metrics, since it returns a high value for a path $P_{SN,DN}$ composed of hops with a higher number of connected links and a smaller number of disconnected links. It also considers single-hop metrics, because the next-hop may also have enough energy and a reliable link to forward the multimedia packets. As result of the PQ calculation, each possible path $P_{SN,DN}$ between a pair of SN and DN has a PQ value ranging from 0 to 1. Hence, a given path $P_{SN,DN}$ with a high PQ value provides efficient and reliable end-to-end multimedia transmission.

Figure 23(b) illustrates route selection based on end-to-end information compared with route selection based on single-hop metrics. For this example, it is assumed that the link quality threshold LQI_{bad} equals to 75 and LQI_{good} equals to 95, which are defined according to the performed calibration experiment results of Figure 24(b). Table 4 shows the values for HC, LQ (Eq. 4.1), and PQ (Eq. 4.2) for each possible path $P_{SN,DN}$ between the pair SN and DN. MEVI must select $route_{id}$ 4 to transmit multimedia packets, when it considers the lowest number of hops for the routing decision. However, this route has two bad links, which causes a higher packet loss rate, and thus reduced video quality level. On another hand, by taking into account the LQ for the routing decision, MEVI considers $route_{id}$ 4 as the best route and $route_{id}$ 6 as an alternative route. However, these routes contain two bad links, which also cause a higher packet loss rate. Finally, MEVI selects $route_{id}$ 1 when it considers PQ for the routing decision, since this route has reliable end-to-end links, and thus enables MEVI to deliver video content with a higher quality level support.

Table 4: Routing Table Example

$route_{id}$	Possible Paths	PQ	LQ	HC
1	S-1-2-3-D	0.74	0.36	4
4	S-4-5-D	0.63	0.58	3
6	S-6-7-8-D	0.73	0.44	4

In the following, we briefly analyse the communication overhead and the computational complexity included by the inter-cluster communication algorithm used by the proposed MEVI protocol.

- *Communication overhead.* The communication overhead to find multiple paths $P_{SN,DN}$ by our algorithm is n, where n is the number camera nodes deployed in the network. This is because in the worst case, each camera node broadcasts one RREQ and one RREP message to find multiple paths $P_{SN,DN}$ between each pair of SN and DN via multiple CN_i. In addition, MEVI adds low byte overhead compared to existing solutions, since it includes only four additional fields into RREQ/RREP messages, namely, $route_{id}$, DL, CL, and RE_t. Hence, we conclude that our proposed algorithm adds low overhead to find multiple paths $P_{SN,DN}$ compared to existing hierarchical routing protocols.

- *Computational complexity.* The proposed algorithm to find multiple paths $P_{SN,DN}$ has a computational complexity value of $O(n)$. This is explained because each CN_i has to order the $routingTable$ from higher PQ to lower PQ values, and the $routingTable$ has the size of n. Hence, it can be concluded that the algorithm has a computational complexity cost of $O(n)$.

4.4.2.3 Video-aware Multimedia Transmission

MEVI schedules packet transmissions via multiple paths by using frame priority information and also PQ, as explained in the following. Thus, it protects key frames during loss or link error periods. The goal of the video-aware multimedia transmission used by MEVI is first to send priority frames through better paths, while enhancing their successful transmission probability. The second goal is to provide load balancing, which reduces network congestion and prolong network lifetime.

The video-aware multimedia transmission used by MEVI considers the following three attributes to schedule the packets: next-hop CN_i candidate list, PQ, and frame importance. Before the SN transmits each multimedia packet, it must acquire the possible next-hop CN_i from the routing table, and also the PQ for each possible path. A deep packet inspector collects information about the frame type, which is described in the video sequence and GoP headers.

Figure 25 depicts the activity diagram for the video-aware multimedia transmission used by MEVI. The SN must order each possible path $P_{SN,DN}$ from the highest PQ to the lowest PQ value. In this way, it considers a given path $P_{SN,DN}$ with the highest PQ value as the best path, since this path has better network conditions to provide reliable end-to-end multimedia transmission. Moreover, it considers the next path $P_{SN,DN}$ as an alternative path. However, in some cases, an alternative path is unable to provide reliable multimedia transmissions, since it experiences a higher packet loss rate. Hence, as soon as MEVI detects that an alternative path has a PQ value lower than a minimal PQ (PQ_{min}), it only considers one path.

Figure 26 also illustrates how MEVI schedules the transmission of video frames and aggregated packets by the SN. The simplest case for the load balancing mechanism

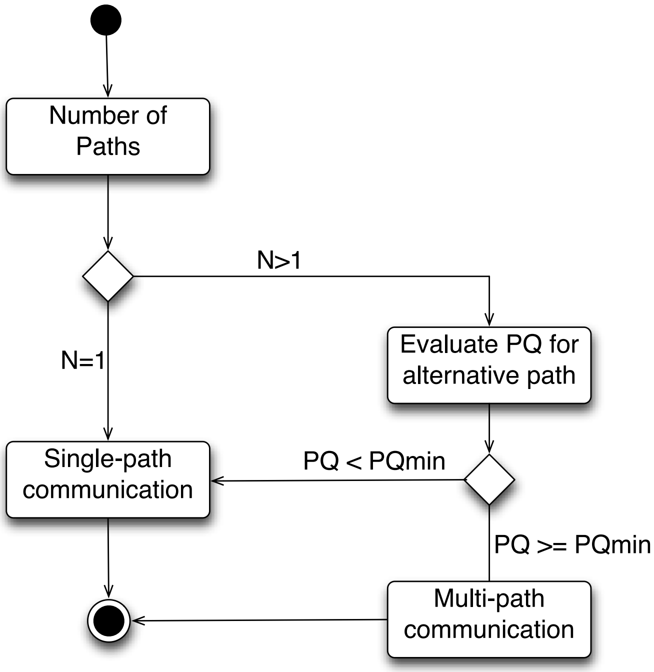

Figure 25: Activity diagram for Video-aware Multimedia Transmission

is when there is only one reliable path, i.e., $N = 1$, as shown in Figure 26(a). In this case, the SN sends both aggregate packets and multimedia packets through a single-path transmission. In the case that the load balancing has two paths, i.e., $N = 2$, as shown in Figure 26(b), it schedules the transmission of priority frames, i.e., the I-frame and the first P-frames, and also the aggregated packets via the best path, since this is a reliable path for transmitting frames with packet delivery guarantee. On the other hand, the SN sends other frames, i.e., B-frames and the remaining P-frames, via an alternative path. In this way, MEVI ensures minimum packet loss for priority frames based on human's experience, as well as being able to provide robustness and load balancing.

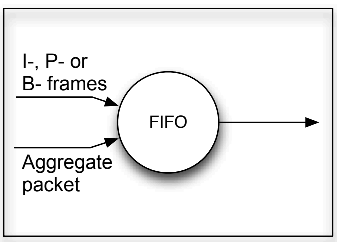

(a) N = 1

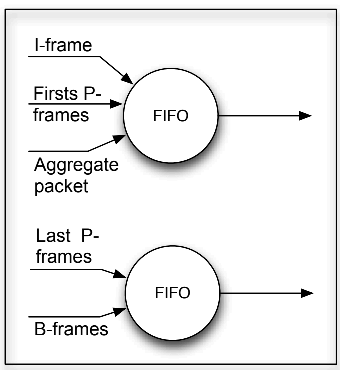

(b) N = 2

Figure 26: Load Balancing Scheme Used by MEVI

4.5 Summary

In this section, we introduced the MEVI routing protocol to provide load balancing and multimedia transmission with QoE support, while achieving energy-efficiency. In specific terms, it provides a cluster formation scheme with low overhead and multi-hop communication between CN_i and DN. A given CN_i triggers multimedia transmission in accordance with the sensed physical environmental conditions from a SN_i. Moreover, MEVI searches for node-disjoint multiple paths, and also evaluates the paths according to cross-layer end-to-end link quality estimation. Hence, it selects the most reliable route to send priority frames based on the user's perspective, and alternative routes to distribute lower priority frames.

CHAPTER 5

A Cross-layer Link quality and Geographical-aware beaconless OR protocol

A reliable and robust routing service for multimedia FANETs must be able to adapt to topology changes, and also to recover the quality level of the delivered multiple video flows under dynamic environments, caused by node failure or mobility. User experience on watching live video sequences must also be satisfactory, even in scenarios with node mobility, network congestion, buffer overflow, and unreliable wireless network environment, as experienced in many FANET multimedia applications. In this context, beaconless OR improves network performance by supporting routing decisions in a completely distributed manner, even if the topology continuously changes. However, cross-layer optimization in beaconless OR protocols based on information from the network and link layers, as well as user's experience are open issues. To the best of our knowledge, existing beaconless OR protocols [59, 81, 84–87] do not establish persistent multi-hop routes with robustness and reliability, and do not prevent the selection of forwarding nodes with heavy traffic load or low residual energy. In addition, those protocols rely on periodic route reconstruction, and also they do not consider QoE requirements for multimedia dissemination. These factors preclude the ability to achieve multimedia transmission with reliability, QoE assurance, and robustness.

With the introduction of the Cross-layer Link quality and Geographical-aware beaconless OR protocol (XLinGO) in [108], we have targeted the designing of an efficient and reliable beaconless OR protocol. XLinGO relies on a beaconless OR approach to establish a reliable persistent route, and takes multiple metrics into account to establish it, including link quality, geographical information, and remaining energy. Later in [109, 110], we integrated XLinGO with the QoE-aware redundancy mechanism [90, 91] to increase XLinGO's reliability and resilience, and at the same time, provide multimedia dissemination over FANET scenarios with QoE support. In both studies, we evaluated the effects of different parameters on the video quality level, namely, temporary and permanent node failures, node mobility with different moving speeds, as well as the transmission of videos with different characteristics. Furthermore in [111,112], we introduced a recovery mechanism to deal with route failures, providing smoother operation in harsh environments and mobile networks. We also considered new metrics for routing decisions, namely packet delivery ratio, QoE, and queue length. For the last study, we evaluated the video quality level provided by XLinGO in a scenario with mobile nodes and simultaneous multi-flow video transmissions.

This chapter is structured as follows. Section 5.1 sets out the need for an efficient, reliable and robust OR protocol for mobile network scenarios. Section 5.2 introduces the network model for FANET network scenario considered by target application. Section 5.3 introduces the problem statement addressed by XLinGO. Section 5.4 describes the proposed XLinGO protocol. With Section 5.5, the chapter concludes the chapter.

5.1 Motivation

In case of a natural disaster, such as Hurricane Sandy in New York/USA (2012), flooding in Rio de Janeiro/Brazil (2013) or any other disaster environments, the standard telecommunications infrastructure might be damaged or does not exist anymore. In such scenario, the recovery process demands an efficient and rapid deployment of a multimedia communication system to monitor the hazardous area that rescue teams cannot easily reach. Hence, a group of UAVs equipped with cameras can be used to set up a temporary multimedia FANET [8–10], as shown in Figure 27. This description could also be applied to various multimedia applications, such as safety & security, environmental monitoring, natural disaster recovery, and others.

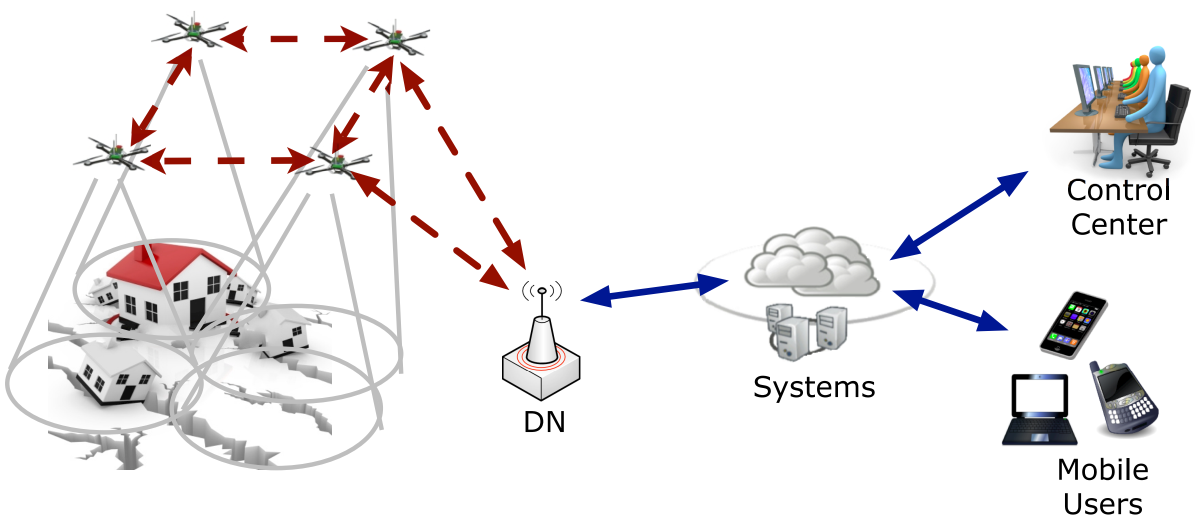

Figure 27: Multimedia FANET Deployed in an Emergency Situation

For such Multimedia FANET scenario description, video flows collected by a given UAV must be transmitted with QoE assurance to headquarters or computer systems for further processing, analysis, and dissemination [22]. Multimedia dissemination over FANETs plays an important role in a future mobile IoT and smart city scenarios [1]. For instance, it enables humans in the control center to take action to explore a hazardous area, which rescuers are unable to reach easily and quickly. In addition, it provides image processing by computer systems, which extracts valuable information, such as object or intruder detection. It also allows the end-users to determine the real impact of an event, and be aware of what is happening in the environment based on rich visual information.

In this context, the distribution of multimedia content for the above applications requires real-time transmission, lower frame loss, as well as tolerable end-to-end delay and jitter. It also requires QoE support to deliver video content with, at least, a minimal video quality from the user's perspective [101]. Moreover, multimedia dissemination usually involves a set of nodes transmitting multiple video flows simultaneously. This scenario leads to a higher degree of network congestion, buffer overflow, and packet loss ratio, which reduces the quality level of the delivered video flows [37]. Hence, sharing multimedia data over FANETs imposes more constraints and design challenges to deliver real-time simultaneous video flows with QoE support. This makes the design of an efficient, reliable, and robust routing protocol for multimedia FANET applications a nontrivial task.

Several routing protocols have been proposed to meet the requirements of delivering video flows with robustness and QoE support over FANET scenarios [25, 68, 95–97, 113–115]. These protocols, including MEVI [95–97], rely on route discovery to find end-to-end routes to forward packets, and adopt flat, hierarchical, or location-based approaches. However, end-to-end routes might be subject to frequent interruptions or may not exist at all times due to node mobility or wireless channel variations, which is not desirable for FANET multimedia applications. Moreover, for the above scenario description, a rescue operation requires a temporary communication system during or after a natural disaster, but to deploy a fixed network infrastructure takes time.

OR increases network performance by making a distributed hop-by-hop routing decision based on protocol-specific characteristics [116]. OR postpones forwarding selection decisions to the receiver side, and relies on a coordination method to pick up the best candidate to forward packets. We consider both beacon-based and beaconless modes as promising OR coordination methods, since they do not require a stable end-to-end route. This enables packet transmission even if the topology continuously changes.

Beacon-based OR methods [77–79] select and prioritize a set of candidate nodes by transmitting beacon messages before sending packets. This enables OR to create and order a relay candidate list prior to packet transmission, and then a given relay node is selected to forward the packets according to certain criteria, such as expected transmission count (ETX) [117]. However, a beacon-based OR increases signalling overhead, and also the predefined candidate list found before sending packets may not reflect the real situation at the moment of packet transmission. This is because node mobility or failure, as well as wireless channel changes. On another hand, beaconless OR [59, 80, 83, 85–87] is a stateless method, since the nodes do not need to be aware of their neighbours. This avoids beacon transmission compared to other position-based protocols, saving scarce resources, e.g., battery and bandwidth. In particular, the receiver of a given packet performs forwarding decisions based on information contained in the packet and inside the node itself only. Unlike in the other routing protocols, forwarding decisions are not made by the sender of a packet, but in a completely distributed manner at the nodes that received the packet.

Let us consider a given source-destination pair, the goal of an efficient and reliable beaconless OR is to find reliable relay nodes to create a persistent route. In particular, the forwarding selection mechanism must find a subset of optimal forwarders to provide multimedia transmission with high packet delivery rate. The optimal set of relay nodes must provide a greater geographical advance towards the destination, together with a reliable link, and enough energy and buffer availability to transmit video packets with low packet loss rate. However, the use of a cross-layer optimization scheme in beaconless OR protocol is still an open issue. In addition, the routing service must detect and recover from route failures, so that it can enable a smoother operation in mobile networks, which is not addressed by existing beaconless OR protocols.

To the best of our knowledge, most existing beaconless OR protocols [59, 81, 84–87] do not establish persistent multi-hop routes with robustness and reliability, and fail to meet QoE requirements for a scenario with simultaneous multiple video flows transmission and mobile nodes, as seen in many FANET multimedia applications. Those that address the question of reliable persistent multi-hop routes, such as in our earlier studies [108–110], do not enable efficient simultaneous multi-flow video transmissions. Our earlier studies combined link quality, geographical information, and energy for routing decisions, as well as taking into account dynamic topologies. But, they only deal with node failures and channel quality variations. Moreover, beaconless OR protocols [59, 81, 84–87], including our initial efforts in [108–110], do not prevent the selection of forwarding nodes with heavy traffic load or low residual energy, which cause route failure, queue congestions, packet loss, delay, and jitter. Finally, they rely on periodic route reconstruction, introducing a long time to detect and respond to topology changes, reducing system robustness, and also increasing packet loss ratio. These factors preclude the possibility of achieving multimedia transmission with reliability, robustness, and QoE assurance in scenarios with multiple video flows and mobile nodes.

5.2 Network Model

XLinGO considers a network composed of n mobile nodes deployed in the monitored area, as illustrates Figure 28. Each node has an individual identity ($i \in [1, n]$), and these nodes are represented in a dynamic graph $G(V, E)$, where vertices $V = \{v_1, v_2, ..., v_n\}$ represent a finite set of nodes, and edges $E = \{e_1, e_2, ..., e_m\}$ create a finite set of wireless links between the mobile nodes (v_i). We define $\mathrm{N}(v_i) \subset V$ as a subset of neighbours within the radio range of a given node v_i. We assume a network scenario composed of one static Destination Node (DN) $\subset V$ equipped with a radio transceiver, an image decoder, and unlimited energy supply. Moreover, each mobile node v_i is equipped with a camera, an image encoder, a radio transceiver, and a limited energy supply. For convenience of notation, we denote $SN \subset V$ (Source Node) as the node v_i responsible for capturing video flows and transmitting them to the DN in a multi-hop fashion. Each SN encodes the video flow before distributing, and the DN decodes the received packets by converting them from an intermediate format to a video sequence, as introduced in Section 2.1.

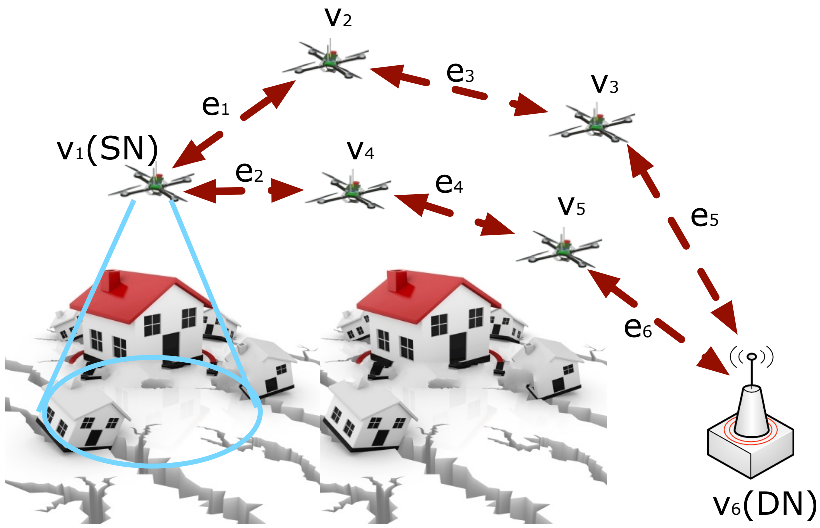

Figure 28: XLinGO Network Model

Each link e_j, $j = 1, ..., m$ has a weight value associated ($w(e_j) \in [w(e_j)_{min}$, $w(e_j)_{max}]$), which is equivalent to the link quality perceived by a given node v_j for each received packet from a node v_i. For instance, the physical layer of the CC2420 radio chip provides the RSSI, SNR, and LQI values for each received packet, which are usually used to estimate the link quality for a given link e_j [89]. Each node v_i has a queue $Q \in [0$, $Q_{max}]$ with a maximum queue capacity (Q_{max}) and current queue length (Q_{length}). The queue policy schedules the packet transmission by using the FIFO algorithm, and drops packets using the Drop Tail algorithm in case of buffer overflow.

Each node v_i has a battery P with initial power P_0 and maximum power P_{max}, and it is able to estimate the remaining energy (RE_t) at any time t. Each node v_i requires power (P_{tx}) to transmit each packet, (P_{rx}) to receive each packet, and also (P_v) to move with a certain speed (s_{vi}) $\in [s_{min}, s_{max}]$. It moves toward a certain direction (dir) with the speed ranging between a minimum (s_{min}) and a maximum (s_{max}) limit. Each node v_i is aware of its own location by means of GPS, Galileo, or any other positioning service [118]. The DN location is known a priori by each node v_i, since we assume a static DN.

FANET scenarios might involve dynamic topologies caused by the failure, damage, or mobility of an individual node or set of nodes [8]. For instance, a given node v_i might have a physical (hardware) fault caused by natural phenomena without human intervention, or it could run out of energy resources, and thus cause topology changes. Moreover, the topology may also change due to node movement, whenever a given node v_i moves out of the transmission range of its neighbour v_j [27].

Wireless channel variations also cause topology changes, since wireless transmissions often experience link error periods, and thus neighbour nodes $N(v_i)$ of a given node v_i stop to overhear each other's transmission. This is because several factors affect the propagation of wireless signals, leading to channel impairments. In addition, wireless transmissions suffer from interference caused by concurrent transmissions, coexisting networks, and other electromagnetic sources. Hardware transceivers may also distort the received or sent signals because of their internal noise [103].

The persistence of node failures can be classified into permanent and transient, depending on the duration of node failure. Transient failure occurs when a given node v_i resumes its operations after a failure. Otherwise, the node failure is considered as permanent node failure. For example, transient failures occur when nodes move out of each other's transmission range or use up their energy resources with battery replacement, as well as because of channel variability. Furthermore, permanent failures are caused when nodes stop working permanently due to natural faults or run out of energy resources without battery replacement [119].

5.3 Problem Statement

In this chapter we address the following issues:

- We find a subset of reliable forwarders F to establish a persistent route $P_{SN,DN} = \{SN, F_1, ..., F_n, DN\} \subset V$, connecting the pair of SN to DN via multiple relays F. In particular, the subset of optimal F provides high packet delivery rate, enabling video delivery with high video quality level from the user's experience.

- We prevent the selection of a possible relay RN_i with heavy traffic load or low residual energy from being selected as a forwarder F. In this way, we provide load balancing and energy-efficiency, as well as reduce queue congestions, packet loss, delay, and jitter.

- We determine whether one of the forwarders F_i from a given persistent route $P_{SN,DN}$ might be no longer available or still reliable to forward packets. Hence, we enable a smoother operation in mobile networks, which provide robust and reliable multimedia transmission, such as expected in multimedia FANET applications.

5.4 XLinGO Design and Operation Principles

This section introduces the Cross-layer Link quality and Geographical-aware beaconless OR protocol (XLinGO), which provides an efficient, robust, and reliable simultaneous multi-flow video dissemination together with QoE support in FANET multimedia scenarios. XLinGO includes forwarding and MAC functionalities. In this way, it assumes a CSMA/CA mechanism, and relies on beaconless OR with two operational modes to establish robust and reliable persistent routes, namely contention-based forwarding and persistent route modes.

XLinGO relies on a beaconless OR approach, since the receiver of a given packet performs forwarding decisions based only on information contained in the packet and in itself information. In XLinGO, forwarding decisions are not made by the sender of a packet, but in a completely distributed manner at receivers, i.e., XLinGO forwards packets towards the DN based on completely distributed hop-by-hop routing decisions. Hence, it is not necessary to have a stable end-to-end connection from the SN to the DN, and packets are forwarded even if the topology continuously changes.

More specifically, XLinGO considers two operational modes (i.e., contention-based forwarding and persistent route modes) to establish a persistent route $P_{SN,DN}$ between the SN and DN via multiple forwarding node. It combines a set of cross-layer and human-related parameters for routing decisions, namely packet delivery rate, QoE, queue length, link quality, geographical location, and residual energy, as depicted in Figure 29. XLinGO relies on a recovery mechanism to deal with route failures, providing a smoother operation in harsh environments and mobile networks.

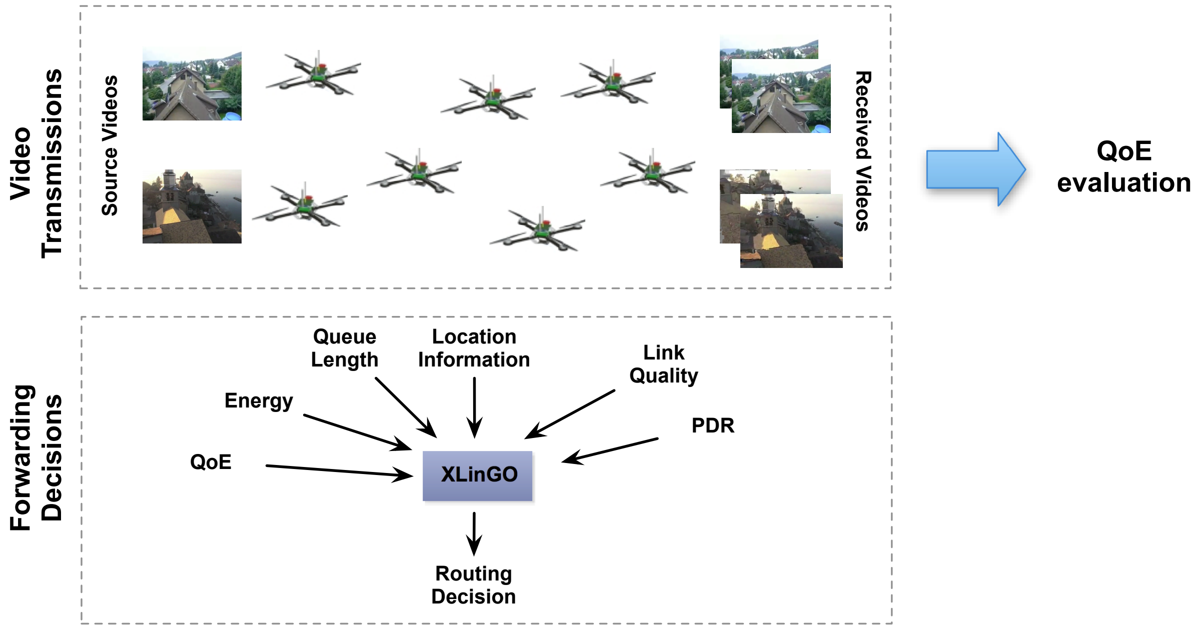

Figure 29: XLinGO Forwarding Decisions

5.4.1 Contention-based Forwarding Mode

Whenever a given SN wants to send a video flow, it triggers the contention-based forwarding mode. Since the SN does not have any knowledge of its neighbouring nodes N(SN), the only thing it can do is to broadcast the video packet to its neighbours N(SN). In this way, it establishes a persistent route $P_{SN,DN}$ between itself and DN via multiple forwarding nodes (F) in order to unicast the subsequent video packets. Algorithm 3 describes the main operations for the contention-based forwarding mode for the SN.

Before the SN transmits a video packet, it must determine its own location (x_{SN}, y_{SN}) and include it into the packet header. The packet header contains the following information: $< x_{SN}, y_{SN}, pkt_{id}, src_{addr}, dest_{addr} >$. After broadcasting the video packet, SN may set a *waiting* timer, and then wait for its neighbours N(SN) to decide about forwarding the received packet based on protocol-specific characteristics, which are explained in the following section (lines 5 – 12).

Algorithm 3 Contention-based Forwarding Mode for SN

StartUp
1: Let t = current time
2: Let *waiting* = a timer used for a given SN waits for its neighbours decide about forwarding the received packet
3: Let DFD$_{max}$ = maximum DFD value
4: Let buffer = a queue to store the packets until the SN establishes the persistent route
On SN receiving a multimedia packet from application layer
5: $SNlocation \leftarrow$ getLocation()
6: pkt.$SNlocation \leftarrow SNlocation$
7: **if** *waiting* timer is not started **then**
8:     broadcast(pkt, src$_{addr}$, dest$_{addr}$)
9:     *waiting* $\leftarrow$ a timer to fire at t + DFD$_{max}$
10: **else**
11:     buffer.equeue(pkt)
12: **end if**
On *waiting* timer timeout
13: goto line 4

Within the *waiting* timer, SN neighbours N(SN), e.g., RN_1, RN_2, RN_3, RN_4, and RN_5 depicted in Figure 30 compete to forward the received packets in a completely distributed manner, and XLinGO attempts to ensure that only one node forwards the packet. This is accomplished by N(SN) computing: the DFD; the required energy to move at a certain speed s and to transmit a given number of packets; and also restricting the area in which nodes are allowed to forward the packet, called forwarding area. It should be noted that in the worst case scenario, the SN overhears the packet coming from the F within DFD_{max}. This is because, DFD_{max} is the maximum DFD value that a given node requires to make a decision about forwarding the received packet.

Neighbours of SN, i.e., N(SN), decide to forward the received packet based only on information contained in the packet and information inside the node itself. Algorithm 4 describes the main operations for the contention-based forwarding mode. In particular, as soon as N(SN) receive a packet, they can extract the SN location from the packet header. In addition, N(SN) are aware of their own locations and the DN location (as explained in Section 5.2). Based on these three positions, a given node v_i can easily determine if it is located within a specific area relative to the SN in the direction of the DN. More specifically, XLinGO divides the forwarding area into: Positive Progress Area (PPA) and Negative Progress Area (NPA).

PPA comprises the forwarding area, where each N(SN) is closer to DN than

SN. NPA comprises the rest of the forwarding area, where the neighbour nodes are not closer to DN than SN, as shown in Figure 30. Each N(SN) located within NPA must immediately drop the received packets, since they are further away from DN than SN, e.g., nodes RN_1 and RN_2 depicted in Figure 30. On the other hand, the nodes within the PPA are considered as possible Relay Nodes ($RN_i \in$ N(SN)), e.g., nodes RN_3, RN_4, and RN_5 depicted in Figure 30.

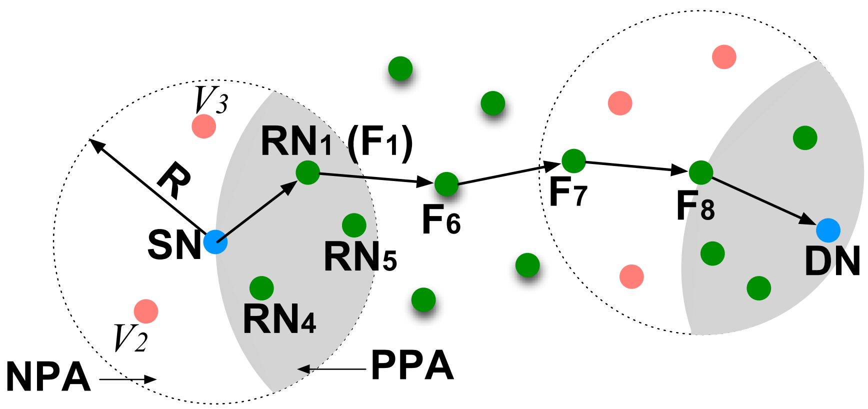

Figure 30: Forwarding Area and Strategy

Battery-powered mobile nodes should consider Residual Energy (RE_t) for forwarding decisions. In this context, XLinGO prevents the selection of a forwarding node with low RE_t. This is accomplished by each node of N(SN) within the PPA, where it computes the energy threshold (E_{th}), and checks if RE_t is above E_{th}. E_{th} indicates the total amount of energy required to transmit packets (E_{tx}) and to move (E_v). Specifically, each RN_i requires ($E_{tx} = k' \times P_{tx}$) to send a given number of k' packets. They also need ($E_v = s_{vi} \times P_v$) to move at a certain speed s_{vi}. Hence, a given RN_i only becomes a candidate, if it has enough RE to forward subsequent video packets, and to move back to the control centre for battery replacement, such as expected in multimedia FANET scenarios with battery replacement support. In this way, it prevents the selection of forwarding nodes with a low residual energy.

Instead of immediately forwarding the received packet, each RN_i must compute the DFD value in the interval $[0, DFD_{Max}]$ to add a short additional delay prior to relaying the received packet, which helps to pick up the best RN_i in a completely distributed manner in order to unicast the subsequent packets without additional delay. Afterwards, they must set a *contention* timer according to the DFD value, and wait for the conclusion of this timer to transmit the received packet (lines 13 – 20). In this way, the RN_i that generates the smallest DFD value replaces the SN location with its own location in the packet header, and thus it forwards the packet first. In this thesis, this node is called forwarder node ($F \in$ N(SN)).

By overhearing a retransmission coming from F, each RN_i must cancel its sched-

Algorithm 4 Contention-based Forwarding Mode for N(SN)

StartUp
1: Let t = current time
2: Let *contention* = a timer used for each RN_i waits before forwarding the received packet
3: Let DFD$_{max}$ = maximum DFD value
4: Let Φ_{LQE}, $\Phi_{progress}$, Φ_{energy}, and Φ_{queue} = a set of coefficient values
5: Let $DNlocation \leftarrow$ getLocation(DN)
6: Let buffer = a queue to store the packets until establishment of $P_{SN,DN}$
On N(SN) receiving the multimedia packet with pkt_{id} from SN
7: $SNlocation \leftarrow$ getSourceLocation(pkt)
8: $w(e_j) \leftarrow$ getLinkQuality(pkt)
9: $itSelfLocation \leftarrow$ getLocation()
10: $RE_t \leftarrow$ getRemainingEnergy()
11: forwardingArea($itSelfLocation$, $SNlocation$)
12: $E_{th} \leftarrow E_{tx} + E_v$
13: **if** RN_i is within PPA AND RN_i did not processed the pkt_{id} AND $RE_t > E_{th}$ **then**
14: compute DFD according to Eq. 5.2 or 5.1
15: buffer.equeue(pkt)
16: *contention* $\leftarrow$ timer to fire at t + DFD
17: **else**
18: drop received packet
19: **end if**
On *contention* timer timeout
20: pkt $\leftarrow$ buffer.dequeue()
21: pkt.$SNlocation \leftarrow itSelfLocation$
22: broadcast(pkt, src$_{addr}$, dest$_{addr}$) //this node is denoted as F
On a N(F) receiving the multimedia packet with pkt_{id} from F
23: **if** node v_i is part of the $P_{SN,DN}$ **then**
24: **if** *waiting* timer is started AND it has not F **then**
25: cancel *waiting* timer
26: nextHop$_{addr} \leftarrow$ F$_{addr}$ //passive acknowledgment
27: switch to persistent route mode
28: **while** buffer is not empty **do**
29: pkt $\leftarrow$ buffer.dequeue()
30: unicast(pkt, src$_{addr}$, dest$_{addr}$, nextHop$_{addr}$)
31: **end while**
32: **else**
33: drop the received packet
34: **end if**
35: **else**
36: **if** *contention* timer has been started for the same pkt_{id} **then**
37: cancel *contention* timer
38: buffer.clear()
39: **else**
40: goto line 6
41: **end if**
42: **end if**

uled transmission with the same packet identifier (pkt_{id}), and also delete the buffered packet (lines 35 – 38). At the same time, XLinGO uses the transmitted packet for passive acknowledgement [120], i.e., it helps to acknowledge the SN about which RN_i has the best network conditions to become forwarder F (lines 23 – 33). Hence, XLinGO saves one acknowledgment transmission per hop by using passive acknowledgments, which helps to save scarce network resources, such as battery and bandwidth. As soon as the SN receives the passive acknowledgment, it must unicast subsequent packets explicitly addressed to F without any additional delay. The contention-based forwarding mode continues until the packet reaches DN, which is the last node on the path and does not forward the packet further. Thus, it must send an explicit acknowledgment (ACK) message to the previous F. In this way, XLinGO establishes a reliable persistent route $P_{SN,DN}$ to connect a pair of SN and DN via multiple F. Hence, nodes that compose the $P_{SN,DN}$ unicast subsequent packets until some of them detect that the $P_{SN,DN}$ is not reliable or does not exist anymore caused by network conditions changes or node mobility.

Nevertheless, the hidden terminal problem might appear, and the SN may be unable to overhear the packet relaying from F, preventing the SN from establishing a persistent route. Route creation may also fail when there is no RN_i inside the PPA, i.e., an empty PPA, as well as due to node mobility. Hence, as soon as the SN does not detect the relaying of a previously broadcasted packet from any RN_i after the DFD_{Max}, it must repeat the contention-based forwarding mode until it establishes the route $P_{SN,DN}$ to unicast the subsequent packets. Figure 31 depicts the general overview of the contention-based forwarding mode. In this example, RN_2 forwards pkt_i first, but SN does not overhear this transmission, and thus SN stays in contention mode and broadcasts pkt_{i+1} after DFD_{max}. RN_1 forwards pkt_{i+1} first. SN overhears this transmission, and thus SN unicasts subsequent packets to RN_1, i.e., it switches to backbone-based forwarding mode.

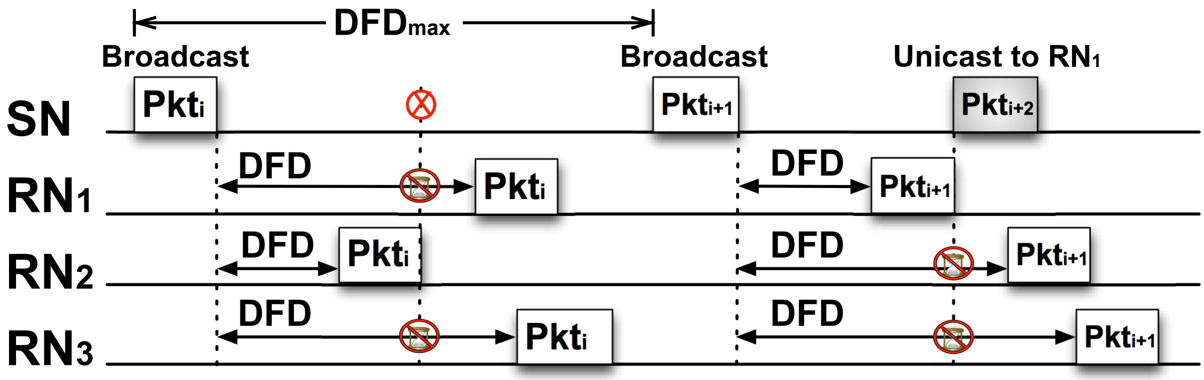

Figure 31: Contention-based Forwarding Mode Overview

5.4.1.1 Complexity and Overhead Analysis of the Contention-based Forwarding Mode Algorithm

In this section, we briefly analyse the communication overhead and computational complexity of the XLinGO contention-based forwarding mode algorithm introduced in this section.

- *Communication overhead.* XLinGO is a stateless approach, since the nodes do not need to be aware of their neighbours. This avoids beacon transmissions compared to other position-based protocols, saving scarce resources, e.g., battery and bandwidth. In this way, XLinGO does not include any message overhead, and thus the communication overhead of our contention-based forwarding mode algorithm is zero.

- *Computational complexity.* As introduced above, Algorithms 3 and 4 establish a persistent route $P_{SN,DN}$ between the pair of SN and DN via a multiple forwarding node. These procedures are simple and can be done using a small number of floating point operations.

5.4.1.2 Metrics for the Contention-based Forwarding Mode

As mentioned earlier, XLinGO postpones the forwarding decision to the receiver side, and thus each RN_i applies a concept of DFD to add a short delay in the interval $[0, DFD_{Max}]$ before relaying the received packet. More specifically, each RN_i computes the **DFD** based on Eq. 5.1 or 5.2, which take multiple metrics into account, namely link quality, geographical information, energy, and queue length. The proposed DFD function includes coefficients (Φ_{LQE}, $\Phi_{progress}$, Φ_{energy}, and Φ_{queue}) to give different degrees of importance to each metric, and the sum of the coefficients must be equal to 1.

$$\mathrm{DFD} = DFD_{Max} \times (\Phi_{LQE} \times \mathrm{linkQuality} + \Phi_{progress} \times \mathrm{progress} + \Phi_{energy} \times \mathrm{energy}) \tag{5.1}$$

$$\mathrm{DFD} = DFD_{Max} \times (\Phi_{LQE} \times \mathrm{linkQuality} + \Phi_{progress} \times \mathrm{progress} + \Phi_{queue} \times \mathrm{queueLength}) \tag{5.2}$$

With our first DFD definition [108–110, 121], i.e., Eq. 5.1, XLinGO selects forwarder nodes closer to the destination with a reliable link, as well as sufficient remaining energy to forward subsequent packets, but without considering the requirements to provide video dissemination with simultaneous multi-flow. On the other hand, with our second DFD definition [111, 112], i.e. Eq. 5.2, XLinGO aims to select forwarder nodes closer to the destination with a reliable link, as well as sufficient queue capacity to forward packets from simultaneous multi-flows and mobile nodes with a reduced packet loss ratio.

In the following, we explain how each RN_i computes linkQuality, progress, energy, and queueLength metrics. Moreover, our initial studies [108–110,121] compute each metric according to a linear distribution. This basic function must be replaced by more advanced functions, which have been considered in our recent studies [111, 122], where we defined each metric by means of an exponential distribution. This is because an exponential distribution reduces the number of responses compared to linear distributed, which leads to a lower latency and better feedback suppression [81, 123].

Let us consider only progress and linkQuality with the same coefficient for both metrics to compute the DFD function. Figure 32 shows the result of such DFD calculation. We can see that the DFD value decreases as soon as both metrics (progress and linkQuality) decrease. In this way, a given node with low progress and linkQuality receives priority to forward the packet faster.

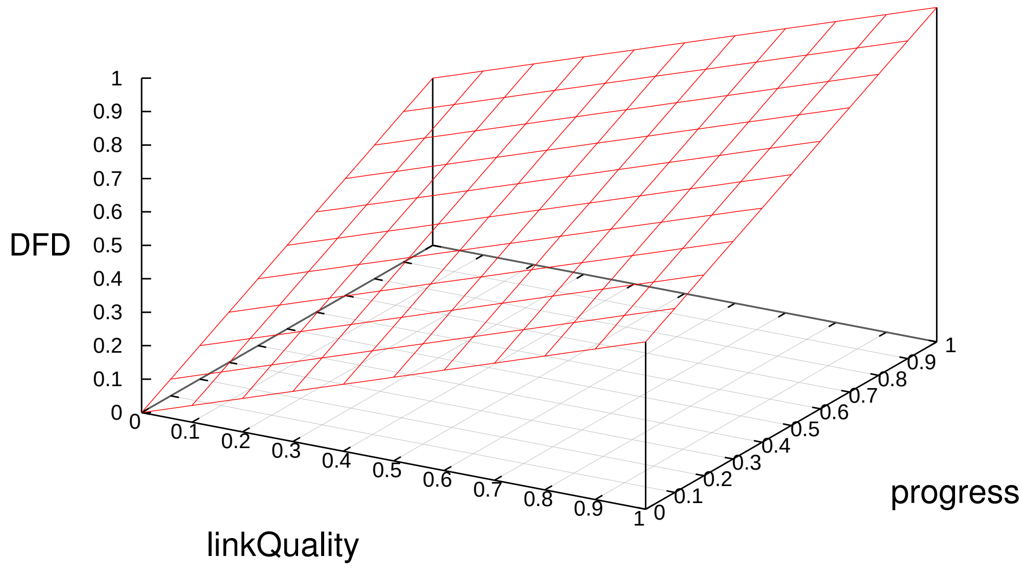

Figure 32: DFD Values for Different progress and linkQuality Values Following the Eq. 5.2 with $\Phi_{queue} = 0$, $\Phi_{LQE} = 0.5$, and $\Phi_{progress} = 0.5$

Link Quality

Existing beaconless OR protocols consider the transmission range as a circle, since they assume successful transmissions as long as two nodes are within the transmission range of each other. However, this is not a realistic assumption for wireless multimedia FANET applications, since the transmission range of wireless links is normally irregular. This irregularity is caused by the unreliable nature of wireless links, which results in a non-uniform PRR distribution and significantly affects the system's performance [124], as shown in Figure 33.

In this context, XLinGO considers link quality as part of the DFD function, and hence it ensures that the selected forwarding node F provides multimedia transmission with high packet delivery support, as expected in many multimedia applications [125]. In particular, each link e_j has a weight value $w(e_j) \in [w(e_j)_{min}, w(e_j)_{max}]$ associated, which represents a single value for the immediate link quality computed at the received side, such as provided by RSSI, SNR, or LQI. Our previous work [108–110, 121, 122] classifies links according to PRR, such as introduced by Baccour et al. [105]. This work classifies links according to the values of PRR perceived by a given link e_j within three regions of connectivity, namely connected (PRR values higher than 90%), transitional (PRR values between 10% and 90%), and disconnected (PRR values lower than 10%).

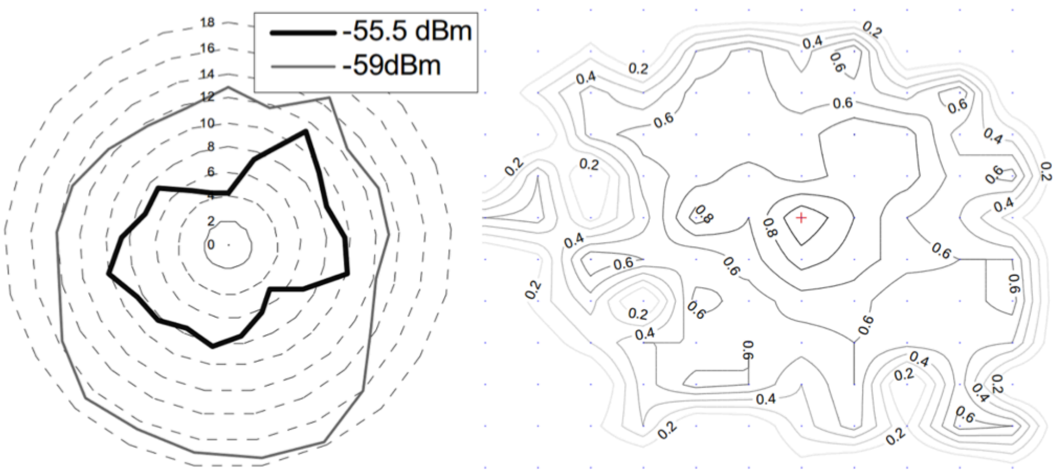

Figure 33: Irregular Radio Range (left) and Resultant PRR Distribution (right)

In contrast to our preliminary works [108–110, 121, 122], our recent work [111] classifies each link e_j in terms of the video quality level that a particular link e_j could provide. In this way, XLinGO selects a QoE-aware forwarder node F to compose the persistent route $P_{SN,DN}$. More specifically, we performed calibration experiments to identify the video quality level provided by a given link e_j. Calibration experiments involve establishing a rich set of single-hop links with different link qualities, and independently of any external factors, such as collisions and routing. In this way, we can analyse when a given link e_j provides multimedia dissemination with bad or good video quality level.

In a similar way to the calibration experiments performed for MEVI and discussed in Section 4.4.2.2, we also deployed 40 nodes with different distances and directions from the DN, as shown in Figure 34(a). This is because distance and direction directly affect the link quality level. In contrast to the calibration experiments of MEVI that analysed the PRR as a function of the link quality $w(e_j)$, the calibration experiments of XLinGO analysed the video quality as a function of the link quality $w(e_j)$, since XLinGO aims to select QoE-aware forwarder nodes F to compose the persistent route $P_{SN,DN}$.

For calibration experiments, nodes were placed in a circle around the DN by dividing nodes into 8 sets with different radius. Each set contains 4 nodes, all placed in a circle around the DN. The distance between two consecutive sets is equal to 1 meter. Each node had its own time-slot defined according to a TDMA scheme, in order to use its time-slot to transmit a video sequence to the DN without collision and interference. Based on exchanged data packets, the link quality $w(e_j)$ measured by means of LQI for each unidirectional link has been estimated. In addition, we computed the final quality level of each transmitted video sequence measured by means of a well-known QoE objective metric, i.e., Structural Similarity (SSIM). Figure 34(b) presents the SSIM as a function of the $w(e_j)$, where it is possible analyse the video quality with the link quality $w(e_j)$.

We defined two link quality $w(e_j)$ thresholds according to the calibration experiment results, namely $w(e_j)_{bad}$ and $w(e_j)_{good}$. These thresholds help to define when a given link e_j provides multimedia dissemination with bad or good video quality level, and thus the node receives low, medium or intermediate priority to forward the received packet faster, such as explained in the following. A given RN_i must immediately drop the received packet, as soon as it receives a packet with a link quality $w(e_j)$ lower than $w(e_j)_{bad}$. This is because our calibration experiments showed that this link provides video transmission with a poor video quality, i.e., SSIM lower than 0.5. On the other hand, the *linkQuality* function returns 0 to the DFD function, i.e., Eq. 5.1 or 5.2, when a given RN_i receives a packet with link quality $w(e_j)$ higher than $w(e_j)_{good}$. The reason for this is that such node provides multimedia dissemination with QoE assurance, i.e., SSIM higher than 0.9. Hence, XLinGO must support such node more likely to forward the received packet faster, which allows XLinGO to select QoE-aware forwarder nodes.

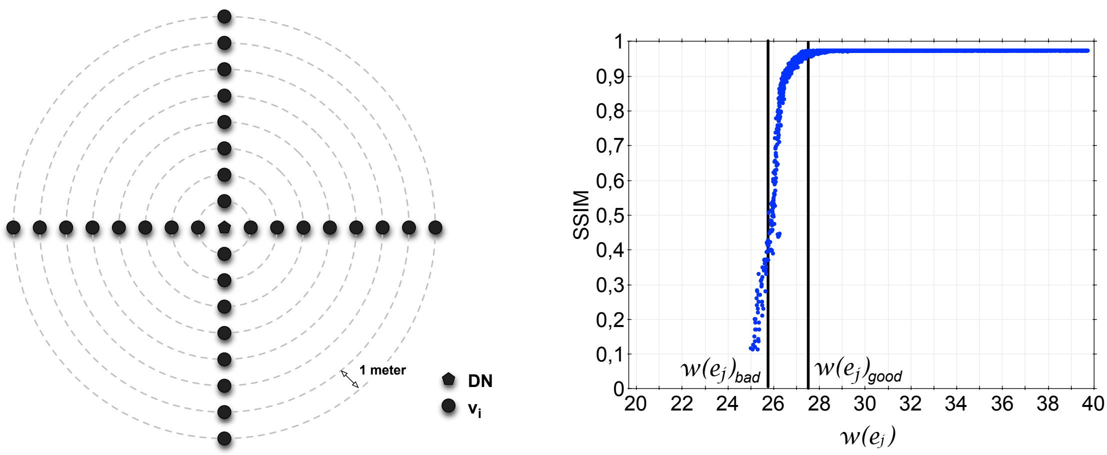

(a) Network Topology (b) Link Quality vs. Video Quality

Figure 34: Network Configuration and Results for Video Quality Evaluation

For the case where the link quality $w(e_j)$ ranges between $w(e_j)_{bad}$ and $w(e_j)_{good}$, the *linkQuality* value is computed in the interval [0, 1] based on an exponential distribution computed according to Eq. 5.3. As a result of the proposed *linkQuality* function, as soon as a given RN_i receives a packet with low link quality $w(e_j)$, it computes a higher *linkQuality* value for the proposed DFD function, i.e., Eq. 5.1 or 5.2. In this way, XLinGO reduces the likelihood of choosing this particular RN_i. This is because such node cannot provide multimedia dissemination with high quality level assurance, as showed by calibration experiments displayed in Figure 34(b).

$$\text{linkQuality} = \begin{cases} 0 & \text{if } w(e_j) > w(e_j)_{good} \\ \frac{1}{1+e^{-c(w(e_j)-X)}} & \text{if } w(e_j)_{Bad} < w(e_j) < w(e_j)_{Good} \\ -1 & \text{if } w(e_j) < w(e_j)_{bad} \end{cases} \tag{5.3}$$

We employed the sigmoid function to represent the exponential distribution of *linkQuality*, as well as for the *progress* and *queueLength* metrics. The sigmoid function requires two float parameters, namely, X determines the center of the sigmoid output, and c regulates the slope or "growth rate" of the sigmoid during its rising portion, as shown in Figure 35(b). We used a negative value for the parameter c, enabling large values of $w(e_j)$ to generate output closer to 0. Hence, high link quality $w(e_j)$ values produce low values for the *linkQuality* metric, as depicted in Figure 35(b). In this way, high link quality $w(e_j)$ values add low contribution to the DFD function, increasing the likelihood of the packet being relayed faster.

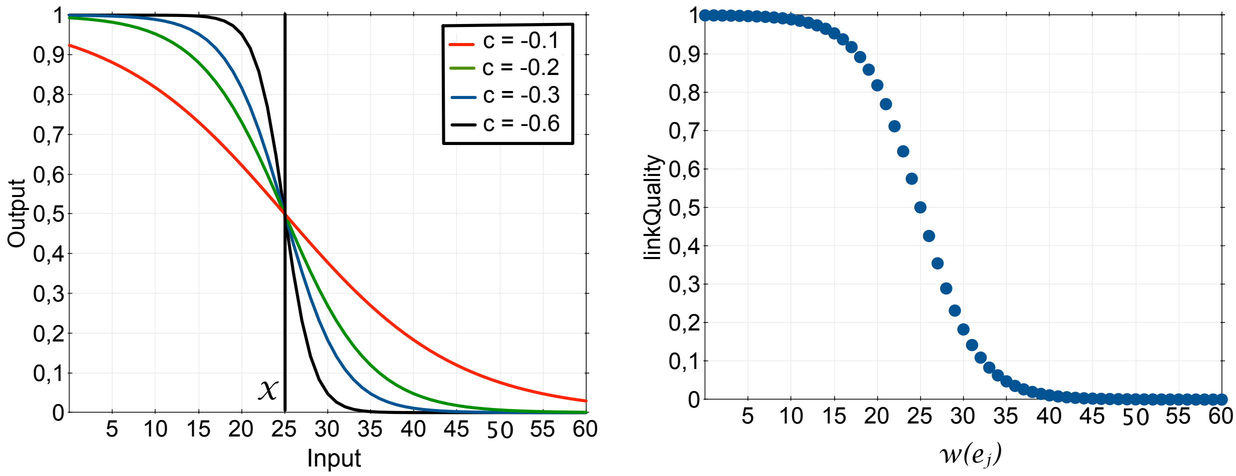

(a) Exponential Distribution with Different X and c Parameters

(b) linkQuality Output with Exponential Distribution, $X = 25$ and $c =$ -0.3

Figure 35: Example of an Exponential Distribution

Progress

Through this metric, we attempt to minimize the number of hops, since longer routes reduce the packet delivery rate. For this reason, it is suitable to select the F closer to the DN. Hence, a given RN_i with a larger geographical advance towards DN generates a smaller *progress* value in order to add to the proposed DFD function, i.e., 5.1 or 5.2. Each RN_i computes the $progress\ in$ $[0, 1]$ value according to:

$$\text{progress} = \begin{cases} \frac{1}{1+e^{(-c(P(RN_i,DN)-R))}} & \text{if } D(RN_i, DN) > RR \\ 0 & \text{if } D(RN_i, DN) < RR \end{cases} \tag{5.4}$$

The RR means the radio range value for a given node v_i. In terms of practical implementation, we assume a fixed RR for all nodes. However, this assumption might not be valid in realistic scenarios, since the RR value might dynamically change as a result of shadowing effects, attenuation from buildings, etc. Thus, an on-line algorithm to compute the RR can be used to deal with this problem, such as proposed by Palazzi et al. [126].

We denote $D(RN_i, DN)$ as the Euclidian distance between a given RN_i and DN, and define $P(RN_i, DN)\ in\ [0, 2 \times RR]$ equals to the sum of $P_1(RN_i)$ and $P_2(RN_i)$. More specifically, $P_1(RN_i)$ *in* $[0,\ RR]$ is the projection of the distance travelled from SN to any RN_i, onto the line from SN to DN. Moreover, the projection of the line RN_i-RN_i' onto line SN-DN defines $P_2(RN_i)$ *in* $[0,\ RR]$. According to our definition, $P(RN_i, DN)$ means the geographical advance of a given RN_i towards DN, i.e., how close to the DN a given RN_i reaches, as depicted in Figure 36(a).

Existing works [59, 81, 84] defined $P(RN_i, DN)$ as $P_1(RN_i)$, which may cause collisions. This is because multiple RN_i may have the same $P(RN_i, DN)$ value, i.e., $P_1(RN_1) = P_1(RN_2)$, as shown in Figure 36(b). In this way, both nodes transmit the packet at the same time. XLinGO solves this problem by applying our definition of progress $P(RN_i, DN)$. For instance, RN_2 is closer to the line SN-DN, and this increases the $P(RN_i, DN)$ value in our definition. Moreover, SN can also transmit packets to DN via RN_2 with only one hop, which cannot be achieved by selecting RN_1 as the next-hop.

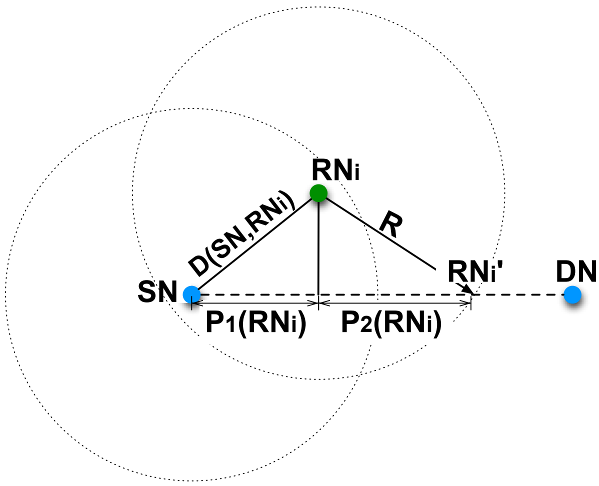

(a) Progress Definition

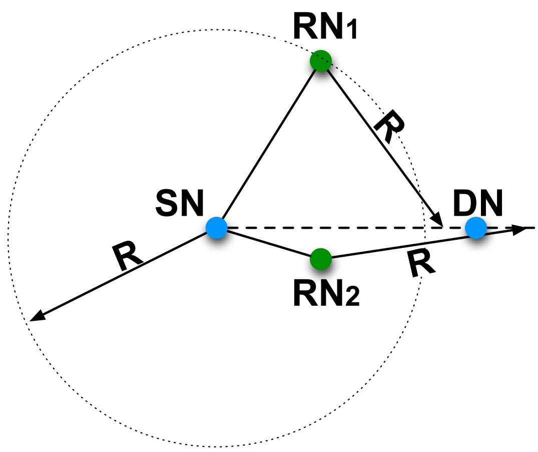

(b) Multiple RN_i

Figure 36: Definition of Progress with Potential RN_i

According to the proposed *progress* function (Eq. 5.4), as soon as a given RN_i is able to directly reach the DN, it receives priority to forward the packet first, i.e., the *progress* function adds 0 to the proposed DFD. In this way, XLinGO reduces the number of hops for a given persistent route. This is because relaying packets by intermediate nodes is often not more energy-efficient than through direct transmission [85]. Otherwise, a given RN_i with less progress adds a larger contribution to the DFD value than a node with more progress. Consequently, a given RN_i with the most progress could forward the received packet faster.

Queue Length

In a scenario with simultaneous multi-flow video transmission, buffer overflow might often occur in the intermediate F. Figure 37 depicts a logical representation of packet transmission by a given forwarding node F, where multiple flows are received simultaneously. As soon as the number of flows increasing, the forwarder F receives heavy traffic, which indicates a poor distribution of flows in the network. This can cause multiplexing, buffer overflow, delay, packet loss, leading to degradation of the video quality perceived by the user when watching video flows.

To cope with this problem, XLinGO also considers queue length as part of the DFD function, since it allows the establishment of a persistent route that avoids the selection of F with heavy traffic load. Hence, the *queueLength* metric helps to prevent buffer overflow, minimizing packet loss, delay, and jitter, as well as providing load balancing. It is important to mention that the *queueLength* metric is only part of our recent DFD function (i.e., Eq. 5.1).

Each RN_i must take into account the number of video flows that it will forward when computing the *queueLength* value $\in [0, 1]$, $(nFlow)$, if it becomes the forwarder for a new video flow. It must also consider the packets per second required for each video flow $(dataRate_{in})$. In this way, a given RN_i is able to estimate the incoming data rate that it will receive for all the video flows according to Eq. 5.5.

$$rate_{out} = nFlow \times dataRate_{in} \tag{5.5}$$

In addition, each RN_i knows the number of packets per second that it is transmitting, i.e. $rate_{out}$. Hence, a given RN_i predicts the queue size (Q_{t+1}) according to Eq. 5.6, considering that it will become the forwarder for a new video flow.

$$Q_{t+1} = rate_{out} - rate_{out} \tag{5.6}$$

Each RN_i must compute the *queueLength* metric with the aid of Eq. 5.7. The proposed *queueLength* function adds a small value to the DFD function, as long as the Q_{t+1} in a given RN_i is not closer to the Q_{max}. In this way, XLinGO increases the probability that a given RN_i with high queue availability forward the packet faster, in order to become the forwarding node.

$$queueLength = \frac{1}{1 + e^{(-c(Q_{t+1} - Q_{max}/2))}} \tag{5.7}$$

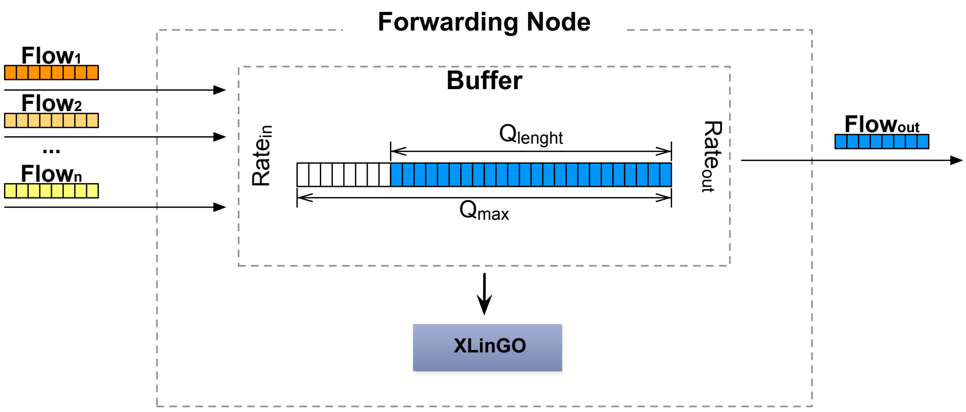

Figure 37: Queue Length Monitoring

Energy

Battery-powered mobile nodes, such as UAVs, must take into account energy for the forwarder selection in order to support energy-efficiency. Thus, we propose to compute the *energy in* $[0, 1]$ value according to Eq. 5.8, which is only a part of our initial DFD function (Eq. 5.2).

$$energy = \frac{P_0 - RE_t}{P_0} \tag{5.8}$$

According to the proposed *energy* function, a given RN_i has priority to forward the packet faster, as soon as it has enough remaining energy to forward subsequent video packets, and also to move back to the control centre for battery replacement.

5.4.1.3 Contention-based Forwarding Mode Example

Let us use Figure 38 to give a brief example on how the contention-based forwarding mode is performed with XLinGO. In Figure 38(a), the source node S broadcasts the video packet to reach the destination node D. Upon the reception of this packet, nodes A and B verify that they are within the forwarding area of the node S, and thus they compute the DFD values equal to 0.1ms and 0.3ms, respectively. The other neighbours out of the forwarding area of the node S just discard the packet.

Node A calculates the lower additional delay than the mode B, since it has the best trade-off between progress and link quality. After 0.1ms, node A sends the packet, which suppresses the packet transmission of node B. At the same time, the received packet by node A acknowledges the successful reception to node S, creating the persistent route $P_{SN,DN}$, as shown in Figure 38(b). The same broadcasted packet is also received by nodes C and E, which have not previously overheard this packet, and they calculate the DFD equal to 0.2ms and 0.4ms, respectively. Hence, node E relays the packet further, as depicted in Figure 38(c). Finally, when node D overhears any packet with its address, it immediately sends an ACK message, as shown in Figure 38(d). The acknowledgement serves not only to acknowledge the reception to the node E, but also to suppress other potential relay nodes that scheduled the packet for transmitting.

5.4.2 Persistent Route Mode

The transmission of all video packets in contention-based forwarding mode causes additional delays and interferences, and it also means that the DN receives a larger number of duplicate packets. For instance, packet duplication occurs when multiple RN_i within the same PPA do not overhear each other's transmission. The above issues reduce the video quality level based on the user's experience, being undesirable for many multimedia FANET applications. Hence, XLinGO avoids the drawbacks of broadcast transmissions by introducing the persistent route mode, i.e., it also supports the trans-

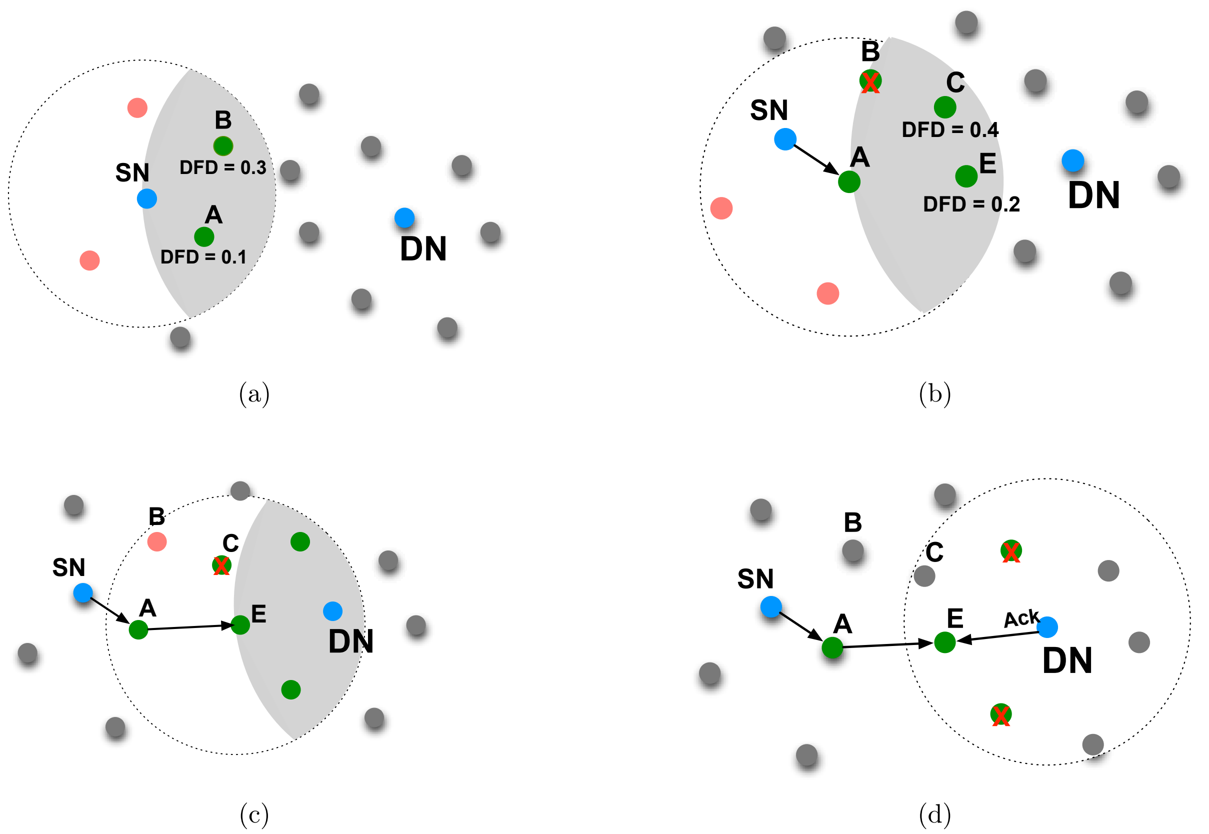

Figure 38: Routing Example with XLinGO in Contention-based Forwarding Mode

mission of unicast packets. For instance, XLinGO builds a reliable persistent route $P_{SN,DN}$ between SN and DN via multiple F by means of contention-based forwarding mode, such as explained in Section 5.4.1. In particular, after the SN has received a passive acknowledgment from F, it immediately sends subsequent video packets to the same destination by unicast to F until some of a given node detects that the $P_{SN,DN}$ is not reliable or does not exist anymore due to network changes or node mobility.

5.4.2.1 Recovery Mechanism for the Persistent Route Mode

Video content must be delivered with packet delivery guarantee even in the presence of continuous topology changes [22]. To cope with that, existing beaconless OR protocols [59, 81, 84–87] and also our initial studies [108–110, 121, 122] rely on periodical persistent route reconstruction to detect topology changes and to prevent suboptimal routing. Our recent study [111] relies on a recovery mechanism to detect and respond to route failures, allowing a smoother operation in harsh and mobile networks environments, as it is frequently the case in multimedia FANET applications. This is because beaconless OR protocols that rely on periodic route reconstruction as soon as one of the forwarding nodes from a given persistent route $P_{SN,DN}$ is no longer available to forward packets, a burst of packets might be lost until the protocol re-establishes the route, which reduces the video quality for longer periods. In this context, the route reconstruction interval should be adjusted according to the desired degree of robustness and energy consumption. From the energy consumption point-of-view, the persistent route reconstruction must occur with low frequency. From the robustness point-of-view, high frequency of route reconstruction provides better robustness. However, it is not trivial to find the appropriate route reconstruction interval to provide robustness, QoE support, and reduced overhead. In this way, XLinGO relies on a recovery mechanism, which considers link quality and PRR to detect and quickly react to route failures, providing a smoother operation in harsh environments and mobile networks.

In particular, for the recovery mechanism, XLinGO considers that every node that establishes a given $P_{SN,DN}$ should continually assess whether its forwarding node is still a reliable or available to transmit packets. Algorithm 5 describes the main operations for the recovery mechanism. Each forwarder that establishes a given persistent route $P_{SN,DN}$ must acknowledge the reception of a set of w packets within a given window, since acknowledging every packet that composes a video increases overhead and interference leads to waste of scarce network resources, such as energy and bandwidth. Based on this observation, each node must monitor the link quality and PRR perceived by its forwarder node, by receiving a reply message from it. After receiving w packets in a given window, the forwarder node sends an ACK message, which piggybacks the exponential average of link quality (LQE_{avg}) and also PRR for the last w received packets (lines 14 – 22). This average is used to highlight the importance of the most recent information.

Let us illustrate the behaviour of the recovery mechanism by using Figure 39. As soon as F_2 receives a given number of w packets from F_1, it must compute the PRR, and also the exponential average for the link quality $w(e_j)$ perceived in the last w received packets. Afterwards, the node F_2 must send an ACK message to F_1, and piggyback those information. Hence, F_1 can evaluate whether F_2 is still a reliable or valid next-hop for forwarding the subsequent packets.

Any node from $P_{SN,DN}$ must return to the contention-based forwarding mode to find a new reliable forwarder, preventing suboptimal routing. This may happen whenever a given node detects that the link quality perceived by its forwarder is below $w(e_j)_{bad}$, as well as when its forwarder has a PRR lower than PRR_{th} (lines 23 – 25). This is because such forwarder node cannot provide reliable multimedia dissemination anymore, which is explained by means of our calibration experiments. These experiments showed that when a given link e_j experiences a link quality $w(e_j)$ lower than $w(e_j)_{bad}$, it provides video dissemination with a poor video quality level, as can be seen in Figure 34(b).

In addition, any node that establishes a given path $P_{SN,DN}$ must consider the route is not valid any more, as long as it does not receive any ACK message from its forwarder node within a certain period of time, i.e., $timeOut_{ack}$ (line 26). In such case, a node must also return to the contention-based forwarding mode to re-establish $P_{SN,DN}$.

Algorithm 5 XLinGO Persistent Route Mode

StartUp

Let t = current time

Let LQE_{temp} = a queue to save the last w link quality $w(e_j)$ values

Let LQE_{avg} = exponential average for the $w(e_j)$ perceived in the last w packets

Let $w(e_j)_{bad}$ = link quality threshold used to define that a given F is not reliable anymore

Let PRR = packet reception rate for the last w received multimedia packets

Let PRR_{th} = PRR threshold to define that a given F is not reliable anymore

Let $waitingAck$ = a timer used to consider that a given F is not valid anymore

Let $timeOut_{ack}$ = the maximum waiting time required to consider that a given F is not valid anymore

On SN receiving a multimedia packet from application layer

unicast(pkt, src_{addr}, $dest_{addr}$, $nextHop_{addr}$)

$sentPkts$ ++

if $sentPkts == w$ **then**

    set $waitingAck$ timer to fire at t + $timeOut_{ack}$

end if

On F receiving multimedia packet from SN

LQE_{temp}.enqueue(getLQE(pkt))

$recPkts$ ++

if $recPkts == w$ **then**

    $LQE_{avg} \leftarrow$ computeExponetialAverage(LQE_{temp})

    LQE_{temp}.clear()

    $PRR \leftarrow$ computePRR()

    sendAck(LQE_{avg}, PRR)

end if

unicast(pkt, src_{addr}, $dest_{addr}$, $nextHop_{addr}$)

On SN receiving an ACK message from F

if $ackmsg.LQE_{avg} < w(e_j)_{bad}$ OR $ackmsg.PRR < PRR_{th}$ **then**

    return to the contention-based forwarding mode

end if

On $waitingAck$ timer timeout

return to the contention-based forwarding mode

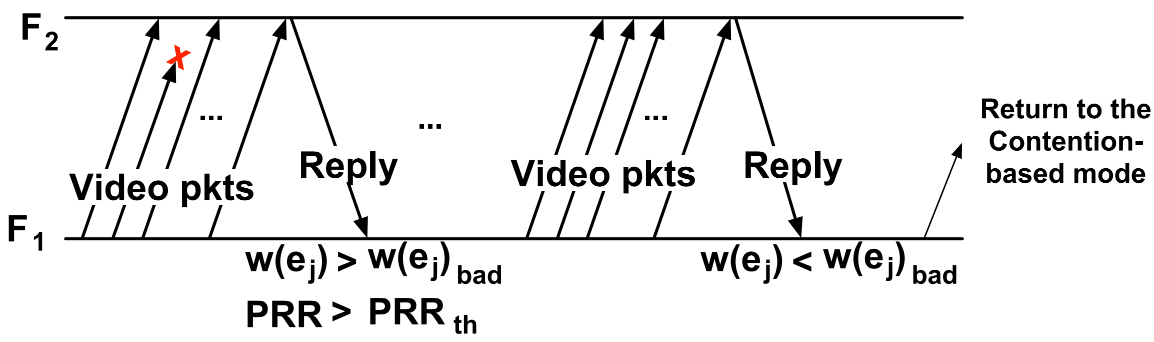

Figure 39: Time Diagram of the Mechanism Employed to Recover from Route Failures

5.4.2.2 Complexity and Overhead Analysis of the Persistent Route Mode Algorithm

In this section, we analyse the communication overhead and computational complexity for the persistent route mode algorithm introduced above.

- *Communication overhead.* The communication overhead to the persistent route mode introduced by our algorithm is dependent of the parameter w, where w is the number of received packets required to send an ACK message. For instance, a small w value, i.e., high sampling frequency, provides detailed information about the link, but increases the overhead, which leads to higher energy and bandwidth consumption. On the other hand, a large w value, i.e., low sampling frequency, provides only coarse grained information about the link, decreasing the responsiveness of the system, as well as the message overhead. In this context, some studies on LQE have reported that three continuous packets provide accurate link-quality status for high sampling rates, such as experienced in multimedia transmissions [127].

- *Computational complexity.* The proposed algorithm has a computational complexity value of $O(n)$. This is explained because each F has to read all values from the queue LQE_{temp} in order to compute the exponential average for link quality the values (LQE_{avg}), and the LQE_{temp} queue has the size of n.

5.5 Summary

This chapter introduced the XLinGO protocol to provide efficient, robust, and reliable video dissemination over multimedia FANET scenarios. XLinGO enables simultaneous multi-flow video dissemination with QoE assurance to be delivered to multimedia platforms for further processing and analysis. Those videos can guide rescue operations, and allow appropriate action to be taken based on visual information. XLinGO relies on a beaconless OR approach with two operational modes (i.e., contention-based forwarding and persistent route modes) to establish a persistent route $P_{SN,DN}$ between the SN

and DN via multiple forwarding nodes, where the persistent route mode reduces delays and maximizes system performance. It combines a set of cross-layer and human-related parameters for routing decisions, namely packet delivery rate, QoE, queue length, link quality, geographical location, and residual energy. It also relies on a recovery mechanism to react faster in route failure situations, providing a smoother operation in harsh environments and mobile networks.

CHAPTER 6

Performance Evaluation

Algorithms and protocols are usually implemented and evaluated with the aid of a network simulator, which provides more flexibility for testing those solutions. This enables us to conduct different and large-scale experiments, as well as providing reproducible performance evaluations composed of mobile nodes. Moreover, simulation experiments provide a suitable way for testing and debugging the functionality of algorithms and protocols. Hence, an event-driven simulation is required to allow the evaluation of different parameters before the real deployment in a more comprehensive manner, while reducing costs, time, and human resources [128].

In terms of performance evaluation, solutions involving multimedia transmission and management require the evaluation of video content from the user's perspective, by using QoE metrics, such as Peak Signal to Noise Ratio (PSNR), Mean Squared Error (MSE), the Structural Similarity Index Metric (SSIM), Video Quality Metric (VQM), and Mean Opinion Score (MOS). This is because Quality of Service (QoS) metrics do not reflect the user's perception in the same way as the QoE metrics do, and thus the QoS metrics fail in reflecting the subjective factors involved the human visual system [21]

This chapter has six sections organized as follows. Section 6.1 discusses particular features of our proposed Mobile MultiMedia Wireless Sensor Network (M3WSN) simulation environment, which is used for our performance evaluation [129]. Section 6.2 describes the QoE metrics used to evaluate the quality level of the transmitted videos. Section 6.3 discusses the simulation results of the MEVI protocol and compares them to well-known hierarchical routing protocols. Section 6.4 introduces the simulation methodology and discusses the results for the proposed QoE-aware redundancy mechanism. Section 6.5 shows the performance evaluation results for XLinGO. Section 6.6 summarizes the results achieved by our simulations.

6.1 Mobile MultiMedia Wireless Sensor Network (M3WSN) OMNeT++ Framework

This section describes our proposed the Mobile MultiMedia Wireless Sensor Network (M3WSN) OMNeT++ framework [129], which is an extension of the Castalia framework [130]. It fully supports the delivery, control, and evaluation of real video sequences in fixed and mobile network scenarios. The M3WSN framework integrates the functionalities of the WiSE-MNet [131] and WVSN models [132], following their initial efforts to model WMSNs, including moving objects, object detection, Field of View (FoV), cover-set, and application criticality.

Figure 40 depicts the overall M3WSN framework architecture, where wireless channel, physical process, and node modules comprise the M3WSN architecture. More specifically, the wireless channel simulates the behaviour of wireless links, and interconnects different nodes. One important aspect of the wireless channel is to estimate the average path loss between two nodes, or in general, two points in space. In this context, M3WSN considers the lognormal shadowing model has to give accurate estimates for average path loss, since empirical studies have shown that the lognormal shadowing model provides more accurate multi-path channel models than Nakagami and Rayleigh for indoor environments [133, 134]. The lognormal shadowing consider path loss exponent (rate at which signal decays), and X_σ a zero-mean Gaussian Random Variable (in dB) with standard deviation σ (shadowing effects). In the most general case, X_σ is a random process that is a function of time. For instance, it is possible to set a unit disk communication mode by setting σ to 0, i.e., transmissions within a certain range from a transmitter are perfectly received, and outside this range not received at all. In this way, M3WSN enables the definition of wireless parameters to allow dynamic wireless channel variations, link asymmetry, and irregular radio ranges, as expected in a real wireless network environment.

Each node is also interconnected with one or more physical processes, which model a sensed-data generation to feed the sensor manager. This is because existing simulators usually feed random numbers to nodes, or each node to have a static value as sensing data. Hence, the M3WSN physical process corresponds to events occurring in the external environment that have spatial correlation of data, and also variability over time. In addition, the sensor manager is responsible for providing the application module with new samples from the physical processes.

Each node is the composition of communication module, sensor manager, application module, resource manager, and mobility manager. From the standpoint of the network layer, the application module is equivalent to the application layer of the Internet architecture. The communication module uses a simplified network stack composed of three layers, namely radio (physical layer), MAC, and routing. The sensor manager is responsible for providing the application module with new samples from the physical processes. The mobility manager enables and controls mobility within the simulation area.

The resource manager models the use of local resources, such as energy consumption, memory usage, and CPU states. In this way, M3WSN provides a generic simulation network environment for designing network protocols and distributed algorithms for mobile and static wireless networks.

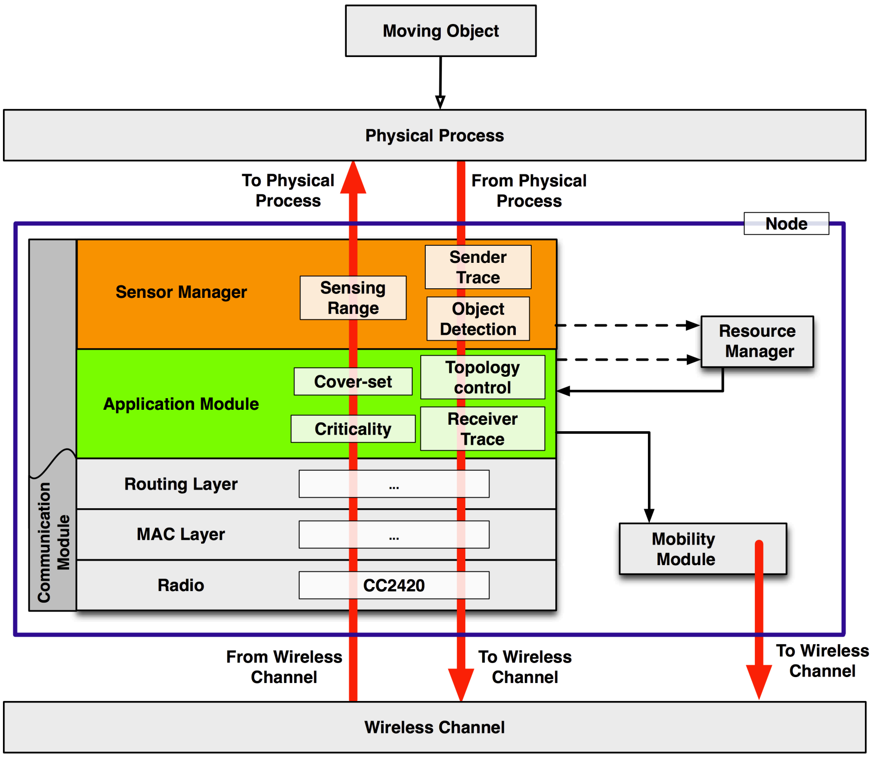

Figure 40: M3WSN Framework Architecture

M3WSN defines the sensing range of nodes equipped with a camera by means of a triangle, such as the FoV of a given camera sensor, as shown in Figure 41(a). FoV depends on the direction of the camera (V), angle of view (θ) and depth of view (d). Thus, the sensing range of a camera node is limited, and depends on the direction of the camera, its range of angle θ, and depth of view d. On the other hand, non-camera nodes have a sensing range defined by a disk, as can be seen in Figure 41(b). Hence, they can sense scalar physical measurements in an omni-directional way.

At the physical process module, M3WSN includes moving objects on a ground plane with different types of motion, e.g., linear, circular, random, and others, which models movement of a target (intruder) in a 2D plane. The moving objects allow simulation scenarios for intrusion detection applications. M3WSN represents a moving object as a box, which enables object detection. In other words, the moving object has a defined area (bounding box) that can be used by the nodes for detection of a given object within its sensing range, as shown in Figure 41(c).

We ported Evalvid [135] to M3WSN, since it provides video-related information, such as frame type, received/lost, delay, jitter, and decoding errors, as well as inter and intra-frame dependency of the received/distorted videos. This video-related information enables the creation of new assessment and optimization solutions for fixed and mobile

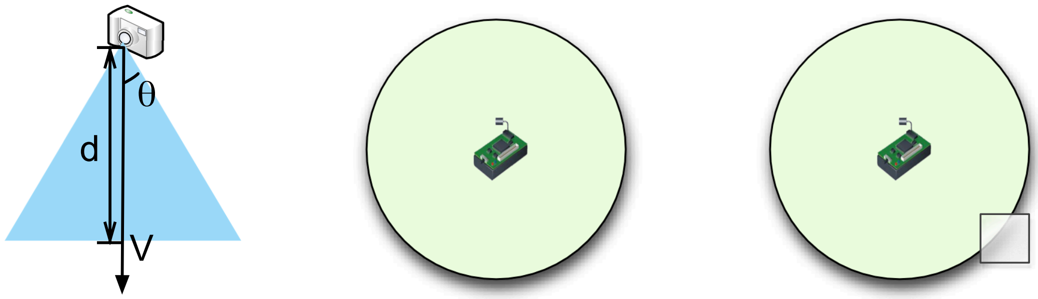

(a) Sensing Range of Camera Nodes (b) Sensing Range of Non-camera Nodes (c) Intrusion Detection

Figure 41: Sensing Range and Object Detection

WMSN scenarios. Before transmitting a real video sequence via Evalvid, we need a video source, for example from a video library [48], YouTube, or one created by the user.

Once the video has been encoded, trace files have to be produced. The trace files contain all relevant information for transmission, and the evaluation tools provide routines to read and write these trace files for multimedia evaluation. More specifically, there are three kinds of trace files. Two of them are created at the source side, namely video and sender traces. On the other hand, the destination node creates the receiver traces. Figure 42 illustrates the steps to generate the trace files, and reconstruct the transmitted video based on these trace files and original videos. More information on how to create these trace files can be found in [135].

The video trace is created once, and contains all relevant information about every frame that composes the video. This information includes frame number, type and size; number of segments in case of (optional) frame segmentation; and the time to transmit each frame. The source node has to create a sender trace file for every video transmission, based on information from the video trace file. The sender trace file is generated with the help of the input routines and data structures provided by Evalvid, which contains information about every packet generated before the transmission. The information consists of time stamp, the packet id and the packet size. Both video trace and sender trace files together represent a complete video transmission (at the sender side) and contain all the information needed for further evaluations. The destination node creates a receiver trace file for every received video, which is created with the help of the output routines of Evalvid. The receiver trace file also contains the time stamp, packet id, and payload size.

We implemented the creation of sender traces at the sensor manager module, because it supports a camera retrieving a video. On the other hand, the receiver trace is created at the application layer module, because it represents the application layer receiving multimedia packets and reconstructing the video. We can also define the energy consumption rate for retrieving each frame, and this value could be chosen for a real camera.

According to the M3WSN architecture, the mobility manager enables and controls node mobility within the simulation area. In this context, M3WSN relies on BonnMotion

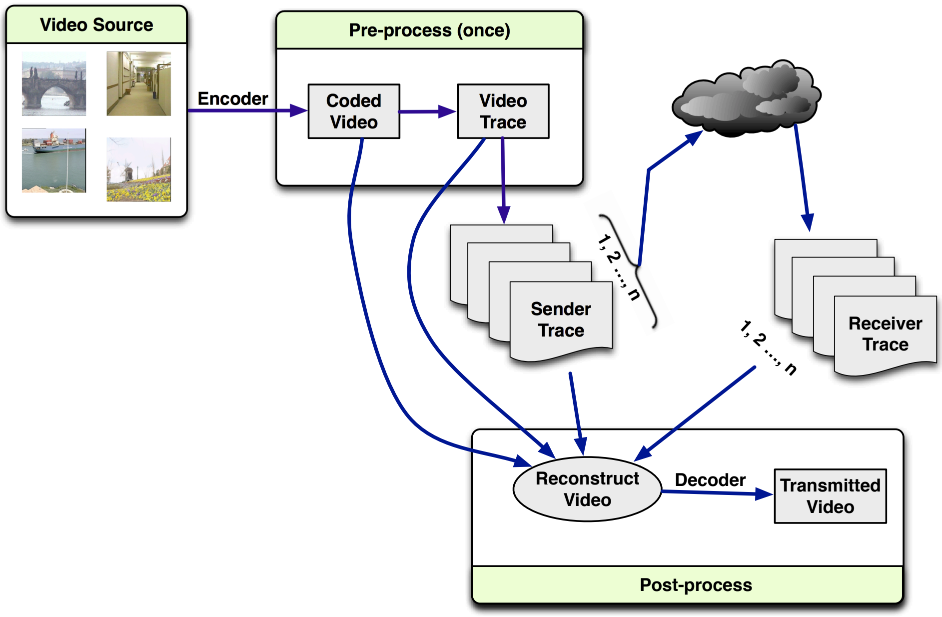

Figure 42: Video Transmission Procedure

[136], which is a simulator-independent tool to generate mobility traces for different mobility models. It is implemented in the mobility manager module to fully support different mobility traces. For instance, BonnMotion generates mobility traces for different mobility models, including, Random Waypoint model, Gauss-Markov model, Reference Point Group Mobility model, and others. At the resource manager, the M3WSN framework allows the configuration of the energy required to receive and transmit each packet, such as in the Castalia framework. In contrast to Castalia, M3WSN enables the configuration of the energy consumption required to move at a given speed, to sense physical scalar data measurements, and also to retrieve each video frame, making the simulation more realistic for mobile and static wireless multimedia network applications.

6.2 Performance Metrics

In this thesis, we used different video quality metrics as performance criteria to show the effects of packet loss during the transmission of video flows. Moreover, we use two metrics to analyse the energy-efficiency of the proposed protocols.

6.2.1 Video Quality Assessment

Solutions involving multimedia transmission must evaluate the video content from the user's perspective. In this context, over the last decade the focus has shifted away from pure network point-of-view assessment, i.e., QoS metrics, to a more end-user centric focus, i.e., QoE metrics, since QoE schemes can overcome limitations related to the human visual system. This is because QoS schemes alone are not enough to assess the quality level of multimedia applications, because they fail in capturing subjective aspects of video content related to human's experience and subjectivity [137].

Regarding to the assessment of video quality based on the user's perspective, there are basically two QoE approaches, namely, objective and subjective. It should be noted that hybrid methods will not be detailed in this thesis. Objective approaches estimate/predict the video quality level by means of mathematical models or signal processing algorithms. The main objective metrics are the following: PSNR [138], MSE, SSIM [139], and VQM [140]. Objective metrics fail in capturing all the details that might affect the user's experience. This problem is addressed by carrying out subjective evaluations. MOS [141] is one of the most widely used approaches for subjective video evaluation. In the following section, we explain the QoE metrics used for our video quality assessment.

SSIM metric improves the performance of the traditional PSNR and MSE metrics. This is because both PSNR and MSE metrics do not correlate well with the subjective perceptions of humans. Therefore, SSIM is a metric, which involves frame-to-frame measuring of three components, namely, luminance, contrast, and structural similarity. It also measures the structural distortion of the video, and seeks to obtain a better correlation with the user's subjective impression. Hence, it combines these components into a single value, called index. The SSIM index is a decimal value between 0 and 1, where 0 means no correlation with the original image (low video quality level), and 1 means exactly the same image (high video quality level).

The VQM method defines a set of computational models, which also has been shown to have superior performance than traditional PSNR and MSE metrics. VQM uses the same features of the human's eye to perceive video quality, including colour and block distortion, as well as blurring and global noise. More specifically, this model employs a linear combination with seven parameters. Four are extracted from spatial gradients, two are obtained from a chrominance vector, and the last is derived from absolute temporal and contrast details. VQM values closest to 0 correspond to the best possible video quality level, i.e., exactly the same image compared to original video. The MSU Video Quality Measurement Tool is used (VQMT) [142] to measure SSIM and VQM values for each transmitted video during the simulations.

Moreover, subjective evaluation captures all the details that might affect the human's experience. In this context, MOS is one of the most frequently used metrics for subjective evaluation, and is recommended by the International Telecommunication Union - Telecommunication Standardization Sector (ITU-T). MOS requires human observers rating the overall video quality level in accordance with a predefined scale. The MOS evaluation can be done by following the Single Stimulus (SS) or Double Stimulus (DS) methods defined by the ITU-R BT.500-11 recommendations [141].

When the SS approach is used, human observers only watch the video once, and then give a score. The choice of a SS paradigm fits well to a large number of emerging wireless multimedia applications [143]. When the DS method is applied into the MOS evaluation system, viewers watch an unimpaired reference video, and then they will watch same video impaired. Afterwards, he/she rates the second video using an impairment scale. For both approaches, in general, the MOS scale goes from 1 to 5, where 5 is the best possible score, as shown in Table 5.

Table 5: MOS Scale According to ITU-R BT.500-11 Recommendations [141]

MOS	Quality	Impairment
1	Bad	Very annoying
2	Poor	Annoying
3	Fair	Slightly annoying
4	Good	Perceptible, but not annoying
5	Excellent	Imperceptible

6.2.2 Energy-Efficiency Assessment

Two metrics were employed to evaluate the network lifetime: the entire lifetime of the network, and also the saturation time. We define the network lifetime as the time spent by nodes until the time when only 10% of the network nodes remain alive. The saturation time is similar to the network lifetime, although it starts from the moment of the first node run out of energy resources. The saturation time is useful to assess the capacity of routing protocols to dynamically adapt to new topologies resulting from the death of the nodes.

Moreover, we used an ad-hoc metric called of Energy-Quality Index (EQI) to measure the energy-efficiency of the proposed protocols [144]. EQI is designed as a "figure-of-merit" to benchmark different transmission schemes in terms of their energy consumption vs. image quality gain. In other words, it represents the trade-off between the video quality achieved ($\Delta SSIM$) and the spent energy (E) at the intermediate nodes along a path. The values of SSIM and E are standardized with the number of hops. The EQI for any scheme is defined as:

$$EQI = \frac{\Delta SSIM}{\Delta E} \tag{6.1}$$

6.3 Performance Evaluation of the MEVI Protocol over Static WMSN Scenarios

In this section, we first describe the simulation scenario for the performance evaluation of hierarchical routing protocols under static WMSN scenarios. Afterwards, we analyse the obtained simulation results in terms of video quality level, energy-efficiency, reliability, and scalability.

6.3.1 Simulation Scenarios

Simulations were carried out and repeated 33 times with different randomly generated seeds to provide a confidence interval of 95% (vertical bars in graphics) in order to show the impact and benefits of MEVI for dissemination of video content with static WMSNs. Table 6 summarizes the simulation parameters used for simulations conducted to evaluate the performance of MEVI compared to PEMuR, LEACH, MEVI, as well as LEACH and MEVI variations in a small (scenario 1) and large scale (scenario 2) scenarios.

In our simulations, we considered that some nodes (sensor nodes SN_i) are continuously monitoring physical scalar sensor data to predict an event occurrence, by means of existing models or methods and defined by an expert [14]. As soon as there is an event occurrence, another set of nodes (camera nodes CN_i) must transmit multimedia data, e.g., video streaming, audio or still image, with QoE assurance to headquarters or IoT platform. In this context, multimedia content provides more precise information than simple scalar data, enabling specialists, mobile users, or computer vision software to visually verify the real impact of the event, avoid false-positive alarms, take consciousness of what is happening in the environment, plan actions, detect objects or intruders, and analyse scenes. More specifically, each SN_i periodically collects physical scalar data measurements, and sends it to a given CN_i. Each CN_i receives the data packets from a set of SN_i, aggregates them into a single packet, assigns slot$_k$ for each SN_i according to the TDMA schedule, and sends the aggregate packet to the DN. Afterwards, a given CN_i triggers the multimedia transmission based on the SR of a given SN_i.

It is important to mention that the M3WSN framework enables to configure the energy consumption for retrieving each frame that composes a video, as expected in a realistic simulation scenario. In this context, we set this value according to the values from a CMUcam3 [145], since we consider that CN_i are equipped with a CMOS camera, such as CMUcam3. In addition, the framework also enables the definition of the energy consumption for transmitting packets, and thus we configured this value based on TelosB datasheet [146], because we consider that nodes are equipped with a CC2024 radio transceiver. We also set the simulation parameters to allow wireless channel temporal variations, link asymmetry, and irregular radio range, as expected in a real wireless network environment.

Regarding video parameters, we encode video sequences with a MPEG-4 codec at 200 kbps, 30 frames per second, and in a Quarter Common Intermediate Format (QCIF), i.e., 176x144. In addition, the decoder uses Frame-Copy as the error concealment method to replace each lost frame with the last received one, which is expected to generate less severe impact by frame losses on the video quality. Existing works classified video sequences according to their motion into three categories, namely low, median, and high. For instance, Aguiar et al. classified the Container video sequence (taken from Video Trace Library [48]) with low movement [51], which means that there is a small moving region of interest on a static background. In the case of the Container video sequence there is a ship crossing a lake. This video characteristic is required for many WMSN applications, such as environmental monitoring, smart parking, and others. Hence, these factors explain our option for transmitting the Container video sequence.

Table 6: Simulation Parameters for Different Hierarchical Routing Protocols

Parameters	Scenario 1	Scenario 2
Field size	40x40	80x80
DN location	20,40	40,80
Transmission power for multi-hop protocols	-10dbm	-3 dbm
Transmission power for single-hop protocols	-1dbm	0 dbm
Total number of nodes	100	
Number of CN_i	25	
Location of CN_i	Grid	
Location of SN_i	Uniform	
Initial energy (E_0) for SN_i	10 J	
Soft threshold	50 C	
Hard threshold	90 C	
Number of time-slots in each superframe (n_{slot})	14	
Time-slot duration (t_{slot})	1 Second	
Round duration (R)	30 Seconds	
Maximum hop count (HC_{max})	8 hops	
MAC protocol	CSMA/CA	
Radio model	CC2420 Transceiver	
Path loss model	Lognormal shadowing model	
Video sequence	Container	
Video length	10 seconds	
Video encoding	MPEG-4	
Video format	QCIF (176 x 144)	
Total number of frames	300 frames	
Frame rate	30 fps	
GoP size	30 frames	
Error concealment method	Frame-Copy	

Figure 43 depicts the topology for scenarios 1 and 2. In this context, hierarchical routing protocols with heterogeneous nodes, such as MEVI and one LEACH variation implemented by us, consider 25 CN_i placed in a grid topology of 5x5, which are represented by black circles in Figure 43. On the other hand, 75 SN_i are uniformly distributed in the field, which are represented by blue circles in Figure 43.

We consider that any of these 100 nodes deployed in the field can act as a CN_i or SN_i, and they are periodically elected in a distributed way for hierarchical routing protocols that consider a network composed of homogeneous nodes, such as LEACH and PEMuR. It is important to mention that we consider a network composed of 25% of nodes acting as a CN_i, for a network composed of both homogeneous or heterogeneous nodes capabilities. This is a reasonable assumption, since many hierarchical routing protocols, such as LEACH and PEMuR, also considered this value.

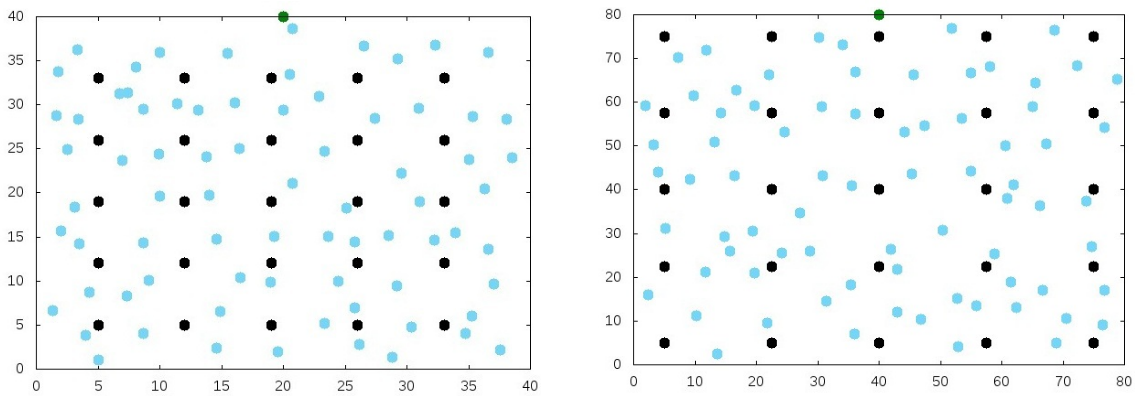

(a) Topology for Scenario 1 (b) Topology for Scenario 2

Figure 43: Simulation Topology for Different Hierarchical Routing Protocols for Static WMSN Scenarios

Figure 44 illustrates the network stack executed on each node. On the application layer, we implemented an application to retrieve video flows or physical scalar sensor data, depending on the node type. We used UDP on the transport layer, and implemented different hierarchical routing protocols at the network layer, namely PEMuR, LEACH, MEVI, as well as LEACH and MEVI variations. Nodes are equipped with CC2420 transceiver, using different transmission power, depending on the scenario characteristics. In addition, our simulations rely on the traditional CSMA/CA MAC protocol without RTS/CTS messages and retransmissions.

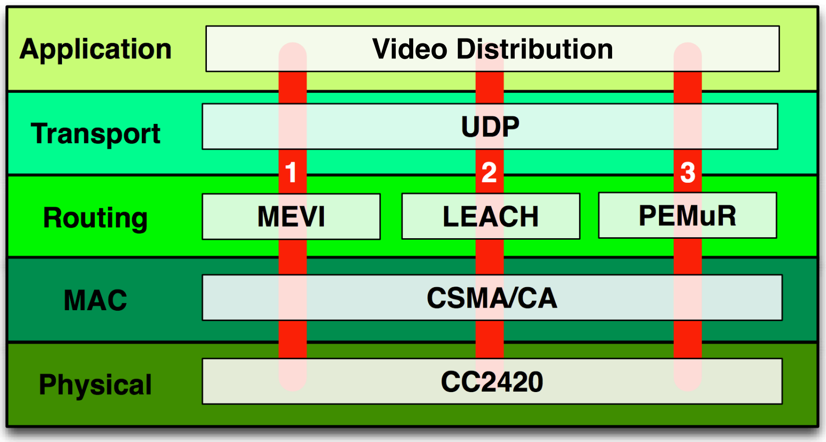

Figure 44: Network Stack for the Performance Evaluation of Different Hierarchical Routing Protocol for Static WMSN Scenarios

We conducted simulations with different hierarchical routing protocols for static WMSNs in order to compare the results in terms of scalability, energy-efficiency, reliability, and also the video quality level of each transmitted videos.

- **PEMuR** follows the PEMuR description [65], where nodes periodically create clusters in a centralized way by transmitting beacon, schedule, advertisement, identifier, and also join messages. Moreover, nodes classify routes based only on remaining energy.

- **LEACH** takes into account the traditional LEACH implementation to periodically perform cluster formation [64], i.e., nodes have homogeneous capabilities and transmit beacon, join, and schedule messages for cluster formation. In addition, nodes consider an event-based multimedia transmission after the TDMA period, according to the SR index.

- **LEACH fixed CN_i** considers heterogeneous node capabilities, i.e., it considers fixed CN_i. Additionally, it follows the traditional LEACH implementation for cluster formation. This LEACH variation can be used to evaluate the benefits of our proposed cluster formation scheme with reduced signalling overhead.

- **MEVI** follows all the MEVI description and operation principles, such as introduced in Chapter 4. More specifically, it considers cluster formation scheme with low overhead. It finds a subset of reliable camera nodes CN_i to establish multiple paths $P_{SN,DN}$ in order to connect each pair of SN to DN via multiple CN_i, and score each possible path based on end-to-end link quality estimation. MEVI triggers multimedia transmission according to the SR index. Finally, it schedules multimedia transmission via multiple-paths according to the frame relevance and PQ, providing load balance and QoE-awareness.

- **MEVI single-hop** implements a single-hop communication between CN_i and DN. Hence, it can be used to show the limitations of single-hop communication, and the benefits of our proposed cluster formation with reduced overhead compared to LEACH.

- **MEVI hop-count** considers the MEVI description and operation principles, but it scores each possible path based only on the number of hops. It is useful to highlight the benefits of using the proposed cross-layer mechanism to select routes based on network conditions and energy issues. This MEVI variation implements the traditional route discovery proposed in Ad-hoc On-demand Distance Vector routing protocol (AODV) [147], Ad-hoc On-demand Multipath Distance Vector (AOMDV) [148], and the AOMDV extension proposed by Hurni and Braun [149].

- **MEVI-LQ** considers the MEVI description, but it selects single-paths according to the proposed LQ metric, which score each possible path $P_{SN,DN}$ between CN_i and DN via multiple CN_i. LQ is computed according to Eq. 4.1 by taking into account multiple cross-layer single-hop metrics, namely RE_t, LQI, and HC. It is important to highlight that LQ uses metrics similar to some existing works [69, 70]. This MEVI variation can be used to evaluate the benefits of using end-to-end link quality estimation, such as implemented in the pure MEVI implementation.

- **MEVI-PQ** follows the MEVI description, but it considers the proposed PQ metric to score each possible path based on end-to-end link quality estimation, and does not include the video-aware mechanism to schedule packet transmission via multiple paths. More specifically, PQ is computed according to Eq. 4.2, which considers cross-layer single-hop metrics, i.e., RE_t and *LQI*, and also end-to-end link quality metrics, i.e., *DL* and *CL*. This MEVI variation is used to evaluate the video-aware mechanism to schedule packet transmission via multiple paths by using frame priority and also PQ information, such as used in the pure MEVI implementation.

6.3.2 Simulation-Based Result Analysis

In this section, we analyse the obtained simulation experiments, where first, we introduce the simulation results for scenarios 1 and 2 in order to show the scalability of MEVI compared to existing hierarchical routing protocols for static WMSNs. Afterwards, we describe the simulation results for scenario 1 and 2 in order to assess the energy-efficiency of MEVI against existing hierarchical routing protocols. Finally, we introduce the video quality results for MEVI.

6.3.2.1 Scalability Assessment

Figures 45 and 46 show the video quality level measured by means of SSIM and VQM according to the distance between the SN and the DN for both small and large-scale scenarios, i.e., scenarios 1 and 2, respectively. This is because we aim to evaluate the scalability of hierarchical routing protocols, namely LEACH, LEACH fixed CN_i, MEVI-LQ, MEVI single-hop, MEVI hop-count, and PEMuR.

We analysed the video quality level according to the distance, since it fluctuates depending on the distance between SN and DN. For instance, a further distant node suffers a higher packet loss, because more hops are needed to reach the DN, causing inference or buffer overflow. It is important to highlight that SSIM values range from 0 to 1, and VQM values range from 0 to 5, but in Figures 45 and 46 we established an interval from 0.5 to 1 for SSIM, and from 0 to 3 for VQM, in order to enlarge the differentiation between protocols. Moreover, VQM values closer to 0 and SSIM values closer to 1 correspond to the best possible video quality level, i.e., the received video has exactly the same image compared to original video.

Let us first analyse the SSIM of SN closer to the DN, i.e., SN with distance between 0m and 11m to DN, as shown in Figure 45(a). Those nodes delivered the video with similar quality level regardless of the protocols. This is because multi-hop hierarchical routing protocols, such as, MEVI-LQ, MEVI hop-count, and PEMuR, require few hops to reach DN, e.g., 1 or 2 hops. Moreover, for single-hop hierarchical routing protocols, i.e., LEACH, LEACH fixed CN_i, and MEVI single-hop, the source nodes are close to the DN, and also they use higher transmission power in order to reach the DN. Those issues reduce the packet loss ratio, which improve the video quality level. Moreover, VQM results confirm the SSIM results for the same reasons as explained above.

Nodes have a nominal transmission range of around 40m for parameters of scenario 1, which is defined based on the physical parameters of the antenna, such as transmission power, antenna gain, and receiver sensitivity. In this context, for distances between 11m and 26m, single-hop protocols still delivering video flows with higher quality level, i.e., SSIM around 0.9 and VQM around 0.5 for VQM. In contrast to that multi-hop protocols delivered videos with reduced quality level, i.e., SSIM ranging from 0.5 to 0.9 and VQM raging from 0.5 to 2.5. This is because for single-hop protocols the SN sends multimedia packets using higher transmission power directly addressed to the DN, which is still in the transmission range of SN. PEMuR has the worst performance, since it selects routes based only on remaining energy, which is not an appropriate metric to select reliable routes.

For distances above 26m under conditions of scenario 1, MEVI-LQ increases the SSIM in 20% and VQM in 60% compared to other protocols. This is because MEVI-LQ delivers the video across multiple hops, and relies on a cross-layer single-hop metric to select reliable routes based on network conditions, namely LQI, remaining energy, and number of hops. On the other hand, for single-hop protocols, such as LEACH, LEACH fixed CN_i, and MEVI single-hop, source nodes are not able to deliver video flows to the DN with higher reliability, even using higher transmission power. This is because DN is not anymore in the transmission range of SN. Moreover, PEMuR and MEVI hop-count select routes based on remaining energy or number of hops, respectively. This makes such proposals unreliable, since they do not consider cross-layer information to select reliable routes, which causes higher packet loss ratio and also lower video quality level.

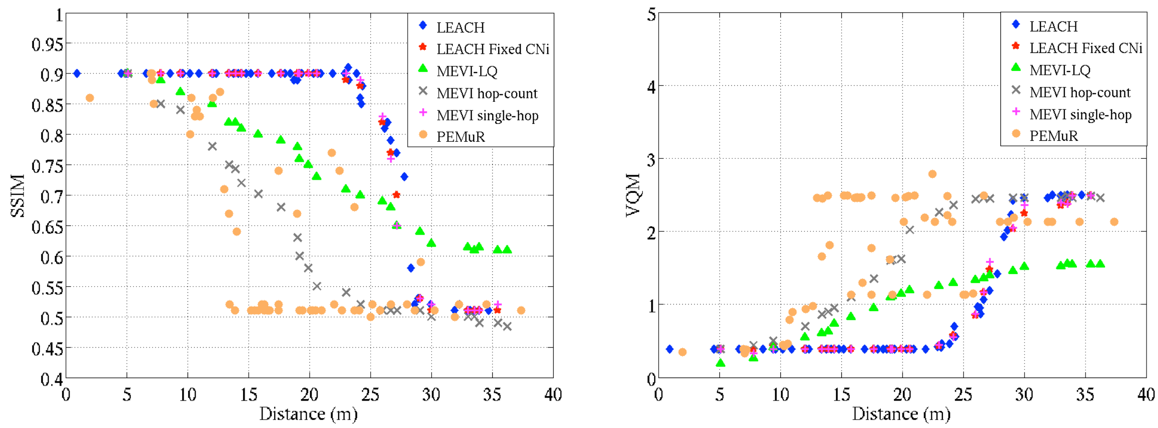

(a) SSIM Results (b) VQM Results

Figure 45: Video Quality Level According to the Distance Between SN and DN for Scenario 1

We also evaluated those hierarchical routing protocols in a large-scale scenario, such as expected in many multimedia smart city and environmental monitoring applications. In this way, we analysed if those protocols are still able to disseminate video flows with good quality level regardless the distance between the SN and the DN. In this context, delivered videos have a similar video quality regardless of protocols for distances from 0m to 20m, as shown in Figure 46. This is because protocols require a few hops to reach the DN, reducing packet loss ratio and improving the video quality level. It is important to mention that some source nodes from scenario 1 with distances between 0m and 20m delivered the video with worst quality level compared to scenario 2. This is because for scenario 2, nodes used higher transmission power than for scenario 1, which increases the number of neighbourhoods and also reduces the number of hops.

For distances longer than 40m, DN is not anymore within the transmission range of SN, which is an essential assumption for single-hop protocols, such as LEACH, LEACH fixed CN_i, and MEVI single-hop. Hence, those protocols are not able to disseminate multimedia packets even using the higher transmission power, since the radio range is about 45m for parameters of scenario 2. On the other hand, MEVI-LQ and MEVI hop-count are still able to deliver video flows to DN, because packets are transmitted via multiple hops. It is important to note that MEVI-LQ increases SSIM and VQM by around 20% compared to MEVI hop-count. This improvement is because it relies on multiple hops with a cross-layer solution to select reliable routes, which decreases the packet loss ratio and increases the video quality level. Moreover, the worse performance of MEVI hop-count compared to MEVI-LQ under conditions of scenario 2 is because routes are selected based only on the number of hops, which is not an appropriate metric to select routes to transmit video packets with reliability.

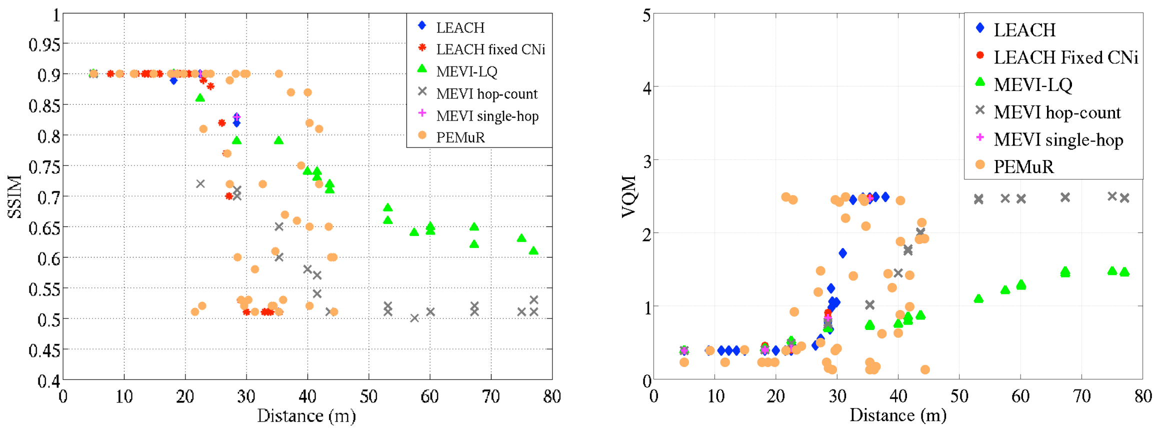

(a) SSIM Results (b) VQM Results

Figure 46: Video Quality Level According to the Distance Between SN and DN for Scenario 2

Figure 47 shows the SSIM for all videos transmitted by each node deployed for scenarios 1 and 2, where the yellow colour represents the best video quality level (i.e., SSIM equals to 1), and the red colour represents the worst video quality level (i.e., SSIM equals to 0). We have the same observation for the results of Figure 47 compared to results of Figures 45 and 46.

It is important to highlight that there are only 25 source nodes (circles in the Figure 47) transmitting video flows with MEVI-LQ and MEVI single-hop protocols for both scenarios 1 and 2. This is because both protocols consider heterogeneous node capabilities, and both scenarios have 25 CN_i placed in a grid topology of 5x5, as depicted in Figure 43. On the other hand, LEACH and PEMuR consider a network composed of nodes with homogeneous capabilities, and thus nodes periodically decide by themselves to become CN_i or SN_i. For these reasons, LEACH and PEMuR have more than 25 source nodes (circles in the Figure 47) transmitting video flows.

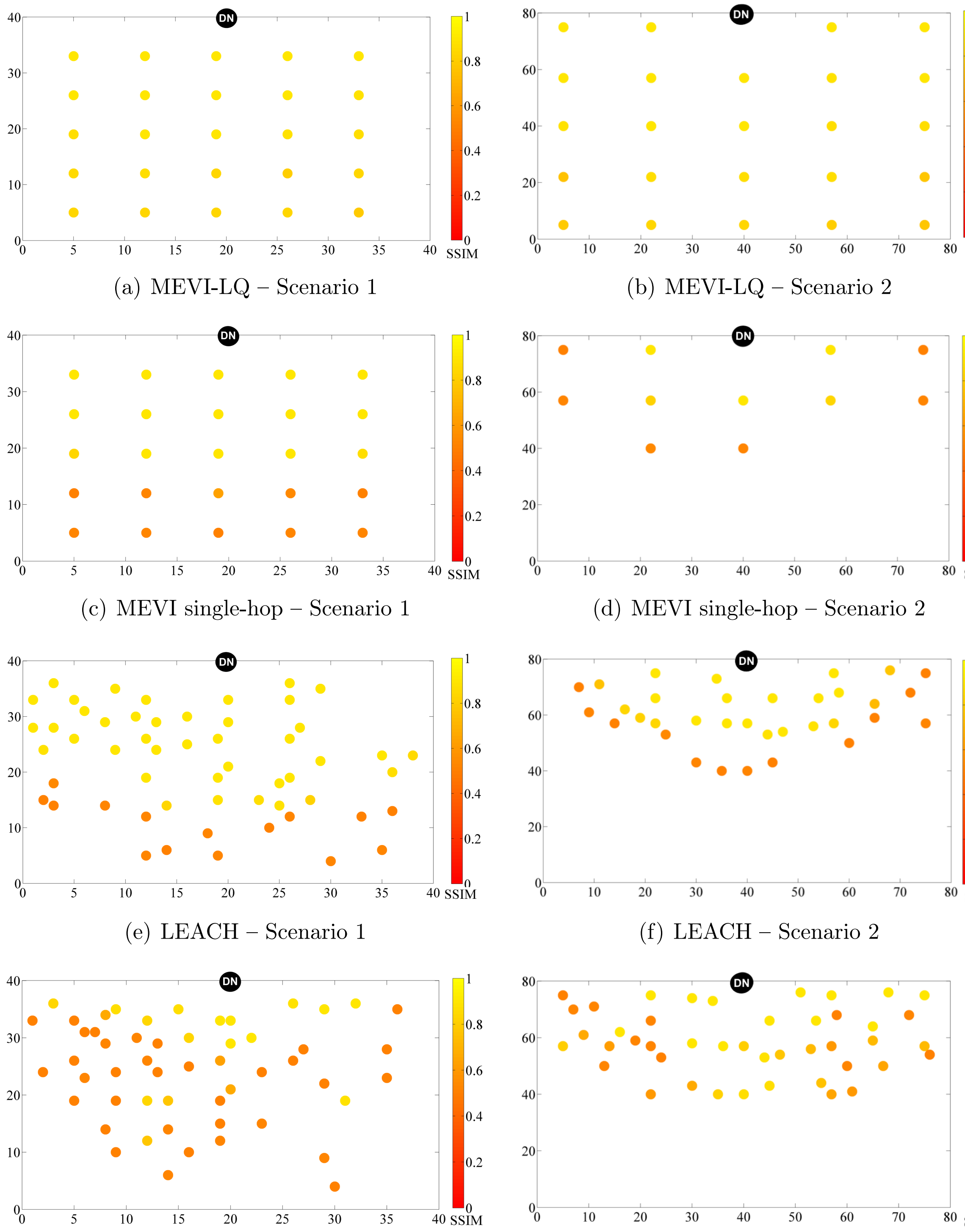

(a) MEVI-LQ – Scenario 1

(b) MEVI-LQ – Scenario 2

(c) MEVI single-hop – Scenario 1

(d) MEVI single-hop – Scenario 2

(e) LEACH – Scenario 1

(f) LEACH – Scenario 2

(g) PEMuR – Scenario 1

(h) PEMuR – Scenario 2

Figure 47: SSIM in Colour Scale for Each Node that Composes Scenarios 1 and 2

Based on the conducted simulation experiments, we conclude that single-hop hierarchical routing protocols, such as LEACH, LEACH fixed CN_i, and MEVI single-hop, do not provide multimedia transmission with high scalability compared to multi-hop hierarchical routing protocols, such as MEVI-LQ, MEVI hop-count, and PEMuR. This is because for longer distances between SN and DN, DN does not receive video flows. This happens only when the source nodes rely on single-hop hierarchical routing protocols.

As mentioned before, we consider an environmental monitoring WMSN application, which typically requires videos with a small moving region of interest on a static background. For instance, the Container video sequence (taken from the Video Trace Library [48]) has a static background, i.e. the lake, with a ship and a bird crossing the lake. Hence, to show the impact of transmitting video streams with different hierarchical routing protocols from the user point-of-view, we selected a random frame (i.e., Frame 266) from the transmitted videos for each routing protocol, as displayed in Figure 48. The frame number 266 is the moment when a bird is fling across the scene. Hence, for environmental monitoring WMSN applications, this small moving region of interest is useful to provide more precise information, enabling users and authorities (e.g., police) to visually verify the real impact of the event, take consciousness of what is happening in the environment, and plan actions according to rich visual information.

We can visually observe that MEVI delivered the video frame with a good quality level from the user perspective, since the frame has only few distortions and the bird appears to be in the same position compared to the original frame. This can be concluded by comparing the frame transmitted by MEVI-LQ (Figure 48(b)) to the original frame (Figure 48(a)). On the other hand, the frame 266 transmitted by MEVI single-hop, MEVI hop-count, LEACH, LEACH fixed CN_i, and PEMuR has a low video quality level from the user perspective, as shown in Figures 48(c), 48(d), 48(e), 48(f), and 48(g) respectively. For instance, there is a higher distortion in the ship and on the lake compared to the original frame. This happens because those hierarchical routing protocols are not reliable enough to provide multimedia dissemination with quality level support, which cause a higher packet loss ratio. In addition, the bird does not appearing at the same position compared to the original frame, since the frame 266 was lost, and thus the decoder reconstructed the frame 266 based of the previously received frames.

Figure 49 shows the SSIM values for all frames that compose the Container video sequence transmitted from a given node for scenario 1. This result illustrates the ability of hierarchical routing protocols to deliver frames with good quality level support. Single-hop protocols have almost the same video quality level, since the SN transmits the video with the same transmission power at the same distance. On the other hand, MEVI-LQ increases the SSIM in 20% and VQM 40% compared to other protocols. This is because MEVI-LQ relies on a cross-layer metric to select reliable paths. Finally, DN receives all video frames with a low quality level when the SN relies on PEMuR to forward packets, due to PEMuR relies only on remaining energy to select routes, which is not an appropriate metric (alone) to disseminate video packets with reliability.

(a) Original frame

(b) MEVI-LQ

(c) MEVI single-hop

(d) MEVI hop-count

(e) LEACH

(f) LEACH fixed CN_i

(g) PEMuR

Figure 48: Frame number 266 from Container Video Sequence Transmitted from a Given Node via Different Hierarchical Routing Protocols

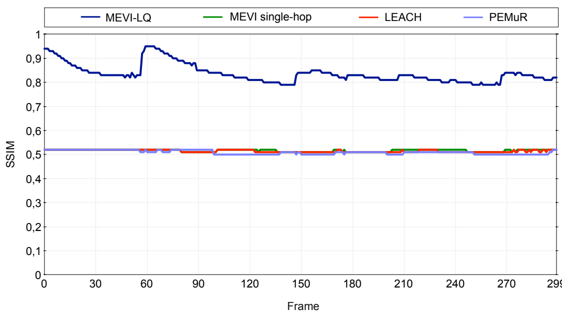

(a) SSIM Results

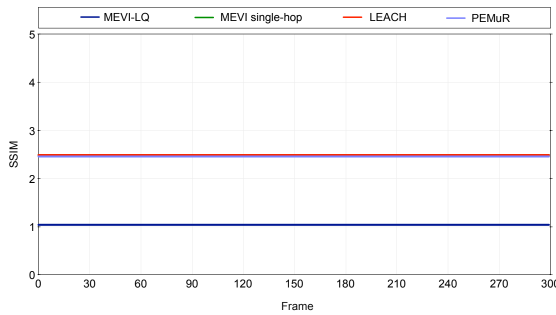

(b) VQM Results

Figure 49: SSIM for all Frames that Composes the Container Video Sequence Transmitted by a Specific Node under Conditions of Scenario 1

6.3.2.2 Reliability Assessment

In this section, we first introduce the experiments conducted to find the appropriate value to PQ_{min}, which impacts on the performance of the video-aware mechanism to schedule packet transmissions via multiple paths used by MEVI. This is because in some cases, an alternative path experiences a higher packet loss rate, and thus it is unable to provide reliable multimedia transmissions. In this way, as soon as MEVI detects that an alternative path has a PQ value lower than PQ_{min}, it must send the following video packets via a single path, in order to ensure the multimedia delivery with a minimal video quality level. Based on results of Figure 50, a video transmitted through a path with PQ below 0.4 obtains poor video quality level from the user perspective, and for this reason we selected PQ_{min} equal to 0.4.

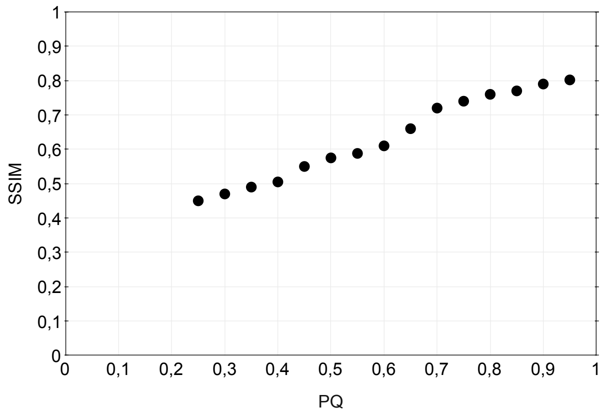

Figure 50: SSIM According to Different PQ Value

Figure 51 shows the results collected with SSIM and VQM with respect to the number of hops under conditions of scenario 2. We can see a higher and similar video quality level for routes up to 2 hops, regardless of hierarchical routing protocols, as shown in Figure 51(a). This happens because the SN is closer to DN and requires less hops, which decreases interference and the number of packet dropped at intermediate buffer. More specifically, MEVI improves the SSIM in 5% compared to other protocols, and in the worst case it has the same video quality level.

On the other hand, MEVI hop-count selects routes based on the number of hops, which makes it unreliable. This can be explained because some hops might experience bad link quality communications or high packet loss ratio, due to both noise and interference. Moreover, MEVI-LQ increases the video quality compared to MEVI hop-count, since it considers single-hop link quality estimation. However, the videos delivered by MEVI-LQ still have a lower video quality compared to MEVI-PQ, since MEVI-PQ considers the proposed PQ metric to score each possible path based on end-to-end link quality estimation. Finally, MEVI provides a gain of 12% in terms of SSIM compared to MEVI hop-count and MEVI-LQ. This is because it evaluates the end-to-end link quality communication with a minimal signalling overhead and includes a video-aware mechanism to schedule packet transmissions via multiple paths, which increase the packet delivery ratio. Moreover, MEVI provides higher reliability, since it uses the single-path communication when the alternative routes are not reliable enough for video dissemination.

VQM results confirm the observations for SSIM results. For instance, MEVI improves the VQM in 10%, and in the worst case it has a similar video quality for routes up to 2 hops, shown in Figure 51(b). On the other hand, for routes with more than 3 hops, MEVI increases the VQM by 40%, 30% and 10% compared to MEVI hop-count, MEVI-LQ, and MEVI-PQ, respectively. Based on SSIM and VQM results, we confirm the benefits of MEVI in assuring a higher video quality level based on the user perception for disseminating video flows.

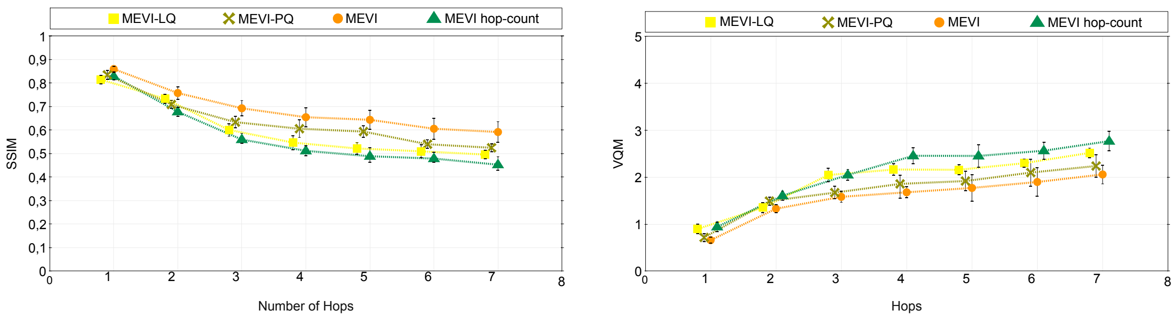

(a) SSIM Results (b) VQM Results

Figure 51: Video Quality Level According to the Number of Hops for Scenario 2

Once again, to show the benefits of transmitting video streams via MEVI from the standpoint of the end-user, we selected another random frame (i.e., frame 257) from the transmitted videos for each routing protocol, as shown Figure 52. Frame 257 is the moment when two birds are flying across the scene. The benefits of transmitting the video sequence via MEVI are evident by comparing it (see Figure 52(b)) with the other protocols (see Figures 52(d), 52(e), and 52(c)) and also with the original frame (see Figure 52(a)). For instance, the frame 257 transmitted via MEVI hop-count, MEVI-LQ, and MEVI-PQ have a higher distortion in the ship and also on the lake compared to the original frame (see Figure 52(a)), and also compared to the frame 257 transmitted via our protocol (see Figure 52(b)).

In addition, the birds also do not appear in the same position when transmitted by MEVI hop-count, MEVI-LQ, and MEVI-PQ, since the frame 257 was lost, and thus the decoder reconstructed it based on the previously received frames. On the other hand, the frame transmitted via MEVI presents only few distortions, and the bird appears in the same position. This is because MEVI relies on a mechanism to protect priority frames by transmitting them via reliable paths, enhancing the video quality level from the human perspective. In addition, MEVI scores each possible path in an end-to-end fashion by means of a cross-layer approach with a minimum overhead.

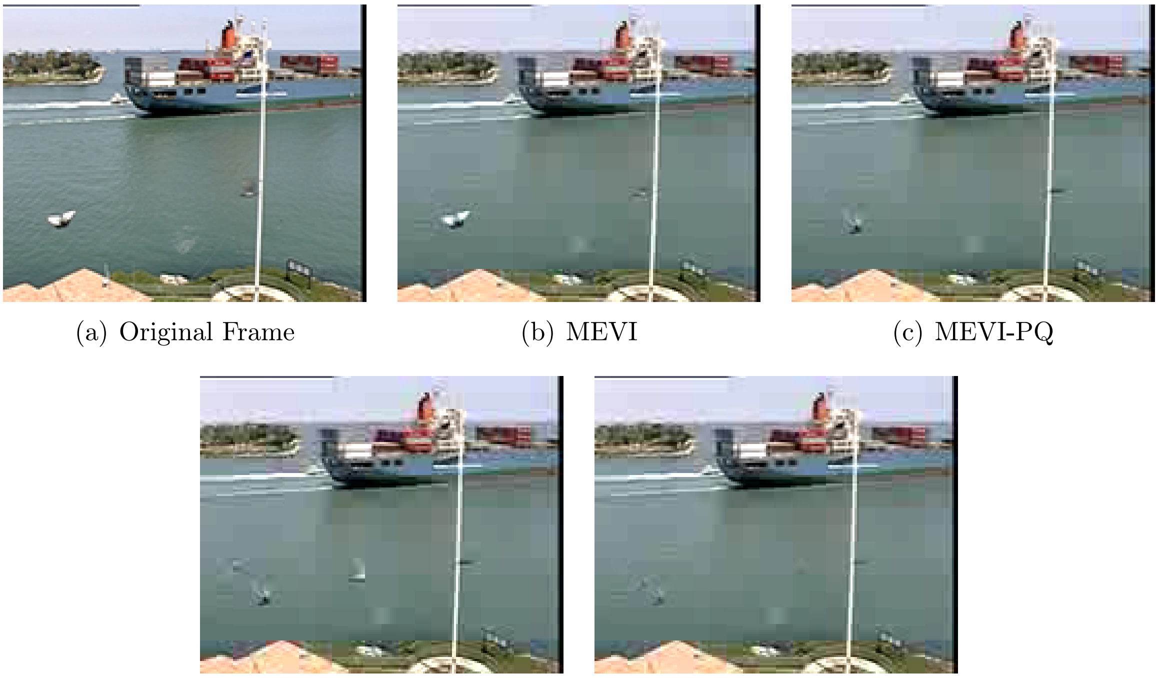

(a) Original Frame (b) MEVI (c) MEVI-PQ

(d) MEVI hop-count (e) MEVI-LQ

Figure 52: Frame number 257 from Container Video Sequence Transmitted from a Given Node via Different Hierarchical Routing Protocols

6.3.2.3 Energy-efficiency Assessment

Figure 53 shows the number of nodes that are still alive for the small (scenario 1) and large scale (scenario 2) scenarios. We only analyse results for one MEVI version, since the network lifetime for all MEVI versions is the same. Hence, the number of nodes alive is the same for all the MEVI versions. In PEMuR and LEACH, a different set of nodes is elected as CN_i in each round. In the hierarchical architecture, CN_i consumes more energy to transmit or to forward packets to the DN. Hence, MEVI and LEACH fixed CN_i never have a network with less than 25 nodes, which is the number of CN_i, which has more energy resources.

MEVI increases the network lifetime in 70% compared to LEACH for both scenarios 1 and 2, as shown in Figure 53(a) and 53(b), respectively. This is because CN_i in LEACH uses higher transmission, i.e., 0 dbm, power to send packets to the DN, which requires higher energy consumption. In contrast to CN_i in LEACH, CN_i in MEVI uses transmission power equal to -10 or -3 dbm. In addition, in every round LEACH elects a different set of CN_i and SN_i. Finally, LEACH includes a higher signalling overhead for cluster formation, increasing the energy consumption of nodes in LEACH.

PEMuR has the worst network lifetime, since it includes more control messages for cluster formation compared with the original LEACH. PEMuR is a multi-hop routing protocol, and thus each CN_i has to forward a higher number of multimedia packets, which consumes more energy compared to LEACH. Finally, MEVI increases the network lifetime in 50% compared to LEACH fixed CN_i. This is because MEVI considers a cluster formation with low signalling overhead, reducing the energy consumption.

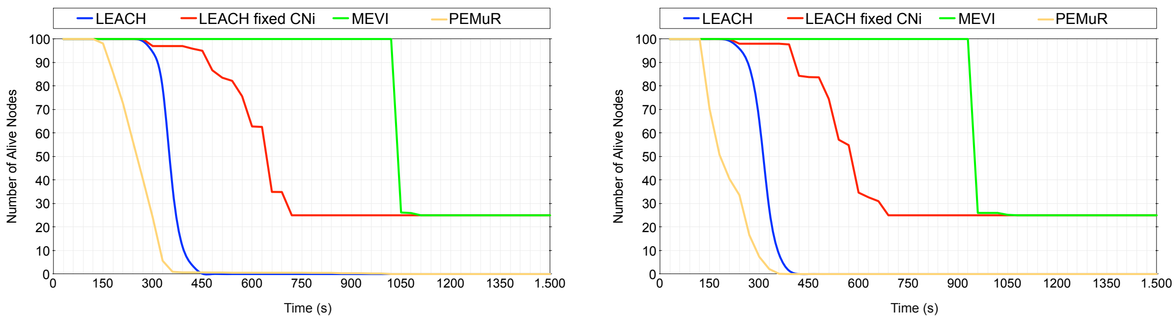

(a) Scenario 1 (b) Scenario 2

Figure 53: Network Lifetime

Figure 54 illustrates the energy costs incurred to provide a certain video quality level measured by means of the EQI metric. We can see that MEVI increases the Energy Quality Index (EQI) in 10% compared to other hierarchical routing protocols. Hence, we conclude that the proposed protocol provides the best trade-off between the video quality per unit of spent energy. This is because MEVI the end-to-end link quality communication, which improves the packet delivery. Additionally, it avoids alternative paths with low reliability.

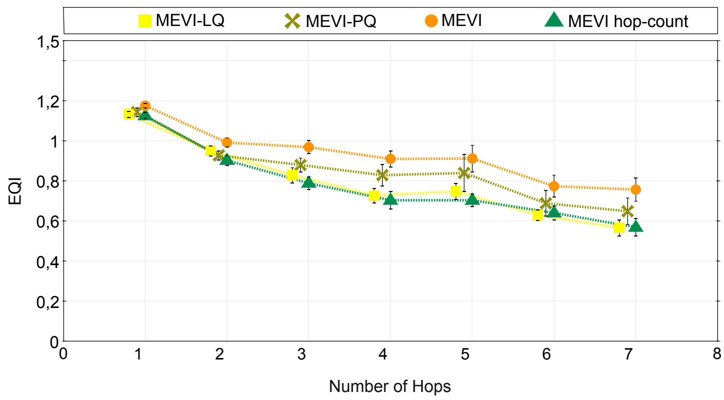

Figure 54: EQI According to the Number of Hops for Scenario 2

6.3.3 Summary

Simulation experiments were conducted to show the impact and benefits of MEVI for disseminating video content for a large and small field size compared to existing hierarchical routing protocols, namely PEMuR, LEACH, MEVI, as well as LEACH and MEVI variations, in terms of scalability, reliability, energy-efficiency, and video quality level of each transmitted video. Based on the simulation results, we found that MEVI increases the network lifetime by at least 60% for small and large-scale scenarios compared to PEMuR, LEACH, MEVI, as well as LEACH and MEVI variations.

In terms of scalability, MEVI is still able to deliver video for large-scale field sizes, unlike the related protocols that are not able to send video flows on a large-scale scale scenario. Simulation results also showed that the MEVI protocol provides multimedia distribution with a higher quality level compared to other approaches. More specifically, our protocol has a SSIM gains of 10% and a VQM gains between 10% and 40%. The results achieved in this section are summarized in Table 7.

Table 7: Comparison Among Different Hierarchical Routing Protocols Based on Conducted Simulation Experiments

Algorithms	Scalability	Reliability	Energy-efficiency	QoE assurance
MEVI	High	High	High	High
LEACH	Low	Medium	Low	Low
LEACH fixed CN_i	Low	Medium	Medium	Low
MEVI single-hop	Low	Medium	Medium	Low
MEVI hop-count	High	Medium	Medium	Medium
MEVI-LQ	High	Medium	Medium	Medium
MEVI-PQ	High	Medium	Medium	Medium
PEMuR	Medium	Medium	Low	Low

6.4 Performance Evaluation of the QoE-aware Redundancy Mechanism

In this section, we describe the simulation scenario description and also the main parameters used for the performance evaluation of the proposed QoE-aware redundancy mechanism. Afterwards, we analyse the obtained simulation results in terms of video quality level, overhead, and also energy-efficiency.

6.4.1 Simulation Scenarios

For the experiments conducted in this section, we implemented the QoE-aware redundancy mechanism for intrusion detection WMSN application, where a set of sensor nodes performs intrusion detection, e.g., by using vibration sensors. On the other hand, another set of camera sensor nodes only transmits real-time videos from the intruder area, as soon as the scalar sensor detected it. As mentioned before, the M3WSN framework enables to set the energy consumption for retrieving each frame that composes a video. In this context, we set this value according to the values from CMUcam3 [145]. Additionally, it is also possible to define the energy consumption for transmitting packets, and thus we configured this value based on TelosB datasheet [146].

Simulations were carried out and repeated 33 times with different randomly generated seeds to provide a confidence interval of 95% (vertical bars in graphics). We set the simulation parameters to allow wireless channel temporal variations, link asymmetry, and irregular radio range, as expected in a real wireless network environment. Table 8 summarizes the simulation parameters used for simulations conducted to evaluate different packet redundancy mechanisms.

Simulation starts with an intruder located at (0,0), and during the simulation the intruder moves according to the random waypoint mobility model. As soon as the sensor node detects an intruder, the camera node must send the video flows to DN. This is because real time video flows enable users and authorities (e.g. the police) to monitor, detect, and predict the intruder's moving direction. Moreover, they allow the authorities to take precise decisions based on valuable visual information.

Table 8: Simulation Parameters for Different Packet Redundancy Mechanisms

Parameters	Scenario 1	Scenario 2
Field size	40x40	100x100
DN location	20, 0	50,100
Type of movement of intruder	Random mobility	Random mobility
Initial location of intruder	0,0	0,0
Intruder velocity	1.5 m/s	2.0 m/s
Total number of nodes	100	200
Number of CN_i	25	64
Location of CN_i	Grid	Grid
Location of SN_i	Uniform	Uniform
Initial energy for SN_i	14 J	20 J
Transmission power	-15 dBm	-10 dBm
MAC protocol	CSMA/CA	
Radio model	CC2420 Transceiver	
Path loss model	Lognormal shadowing model	
Video sequence	Hall	
Video length	12 seconds	
Video Encoding	H.264	
Format	QCIF (176 x 144)	
Total number of frames	300 frames	
Frame rate	26 fps	
GoP size	30 frames	
Error Concealment Method	Frame-Copy	
Redundancy (r)	80 %, 100 %	

We encoded the video sequences with H.264 codec at 200 kbps, 26 frames per second, and in a QCIF (176x144). The decoder uses Frame-Copy as the error concealment method to replace each lost frame with the last received one, which is expected to make less severe impact of frame losses on the video quality. Existing works on multimedia area classify the videos into three categories, according to their motion and complexity levels, i.e. low, median, and high. For example, Aguiar et al. classify the Hall video sequence (taken from the Video Trace Library [48]) as low movement, which means that there is a small moving region on a static background, i.e. men walking in a hall [51]. Hence, we selected the Hall video sequence, since it has similar motion and complexity for the video intrusion detection application.

Figure 55 illustrates the network stack executed on each camera node. At the application layer, we implemented different redundancy solutions to transmit each video flows, namely, simple redundancy, QoE-aware redundancy, and without redundancy. UDP is used at the transport layer, and MEVI at the network layer. Nodes are equipped with CC2420 transceiver, using transmission power of -15 or -10dBm, and relying on the traditional CSMA/CA MAC protocol without RTS/CTS messages and retransmissions.

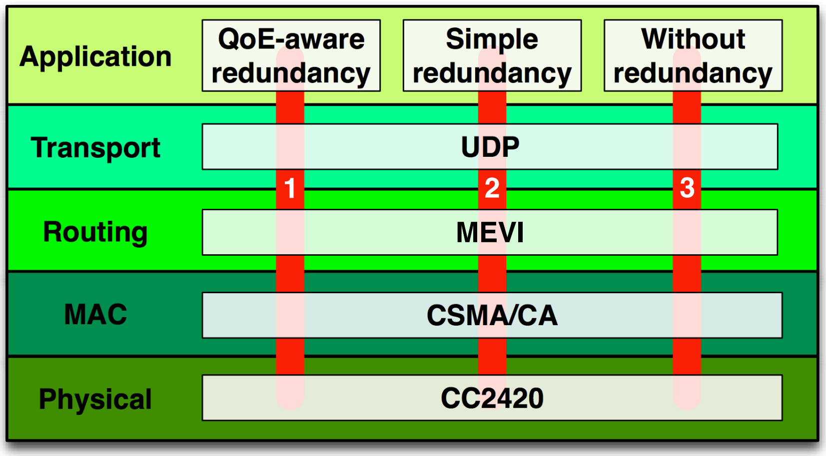

Figure 55: Network Stack for the Performance Evaluation of Different Redundancy Mechanisms

We conducted simulations with different redundancy schemes to compare the results. The first experiment servers as a baseline results, and it was performed without any enhancement (**without redundancy**). The second simulation implements a non-QoE approach (**simple-FEC**), such as performed by some the existing redundancy schemes [57–63] that add redundant packets in a black-box manner, i.e., without considering the frame importance from the user perspective. More specifically, the simple redundancy mechanism statically added a fixed amount of packet redundancy to all frames that compose a given video sequence. Finally, the last experiment uses the proposed **QoE-aware redundancy mechanism** [90,91], which adds redundant packets depending on the frame type and the location of the P-frame within the GoP.

6.4.2 Simulation-Based Result Analysis

In this section, we analyse the conducted simulation experiments in terms of the video quality level of each transmitted video, overhead, and energy-efficiency. First, we introduce the simulation results to select some parameters for the proposed QoE-aware redundancy mechanism. Afterwards, we describe the simulation results for scenarios 1 and 2 in order to analyse the obtained results.

6.4.2.1 QoE-aware Redundancy Mechanism Parameters Definition

As mentioned earlier, P-frames earlier in the GoP, i.e., P-frames with a relative position p lower than X_1, have their packets encoded to add $r\%$ of packet redundancy for the set of n_{pkts} original packets. This is because the loss of P-frames earlier in the GoP cause impairments over a longer period, since subsequent frames are directly or indirectly impaired until the decoder receives the next I-frame, as presented by Greengrass et al. [45, 53]. For instance, X_1 equals to 50% means that the proposed redundancy mechanism adds $r\%$ of redundant packets only to 50% of P-frames in each GoP.

It should be noted that X_1 should be defined based on both video motion and complexity levels. This is because a GoP may be composed of video frames with different sizes, depending on the video spatial and temporal levels. For instance, a given video with larger I-frames will be fragmented into several packets, i.e., videos with high spatial complexities, such as the Flower video sequence downloaded from the YUV library [48]. In this context, the dropping probability of an I-frame increases, which produces different impact on the user perception when a packet is dropped in the network. The same process occurs with P- and B-frames for videos with high temporal complexity, such as the Football video sequence downloaded from the YUV library. Aguiar et al. showed that the video called Mobile has the biggest I-frame size, and consequently, it has a highest spatial complexity, while the video Football has the smallest ones [51].

In this context, we first analyse our QoE-aware redundancy mechanism with different values for X_1 and r. We defined the packet redundancy r equals to 80% or 100%, and also $X_1\%$ equals to 60% or 50%. Table 9 summarizes eight possible configurations for these values, and also the packet overhead included by the proposed QoE-aware redundancy mechanism.

Table 9: Possible Configurations for the QoE-aware Redundancy Mechanism

	Redundancy for the first 60 % of P-frames	Redundancy for the last 40 % of P-frames	Network Overhead
Configuration #1	80%	0%	96 packets
Configuration #2	80%	40%	152 packets
Configuration #3	100%	0%	159 packets
Configuration #4	100%	50%	215 packets
	Redundancy for the first 50 % of P-frames	Redundancy for the last 50 % of P-frames	Network Overhead
Configuration #5	80%	0%	84 packets
Configuration #6	80%	40%	152 packets
Configuration #7	100%	0%	145 packets
Configuration #8	100%	50%	213 packets

Let us use Figure 56 to illustrate four possible configurations of the QoE-aware redundancy mechanism with r equals to 100%, and $X_1\%$ equals to 60% or 50%. More specifically, the proposed mechanism adds $r\%$ of redundant packets to I-frames and also to the first $X_1\%$ P-frames of each GoP. On the other hand, the possible configurations for sending the remaining P-frames are the following: (i) the proposed mechanism encodes the last 100 - $X_1\%$ P-frames with $r/2$ redundant packets, i.e., configurations #2, #4, #6, and #8 (ii); and the mechanism sends the last 100 - $X_1\%$ P-frames without packet redundancy, i.e. configurations #1, #3, #5, and #7.

For these 8 configurations introduced in Table 9, we analysed the average values of SSIM according to the distance between SN and DN, as shown in Figure 57. This is because a further distant node suffers a higher packet loss, because more hops are needed to reach the DN, causing inference or buffer overflow. Moreover, nodes with similar distances have different SSIM values, but the difference is below 0.05, since nodes with similar distances select routes with different numbers of hops.

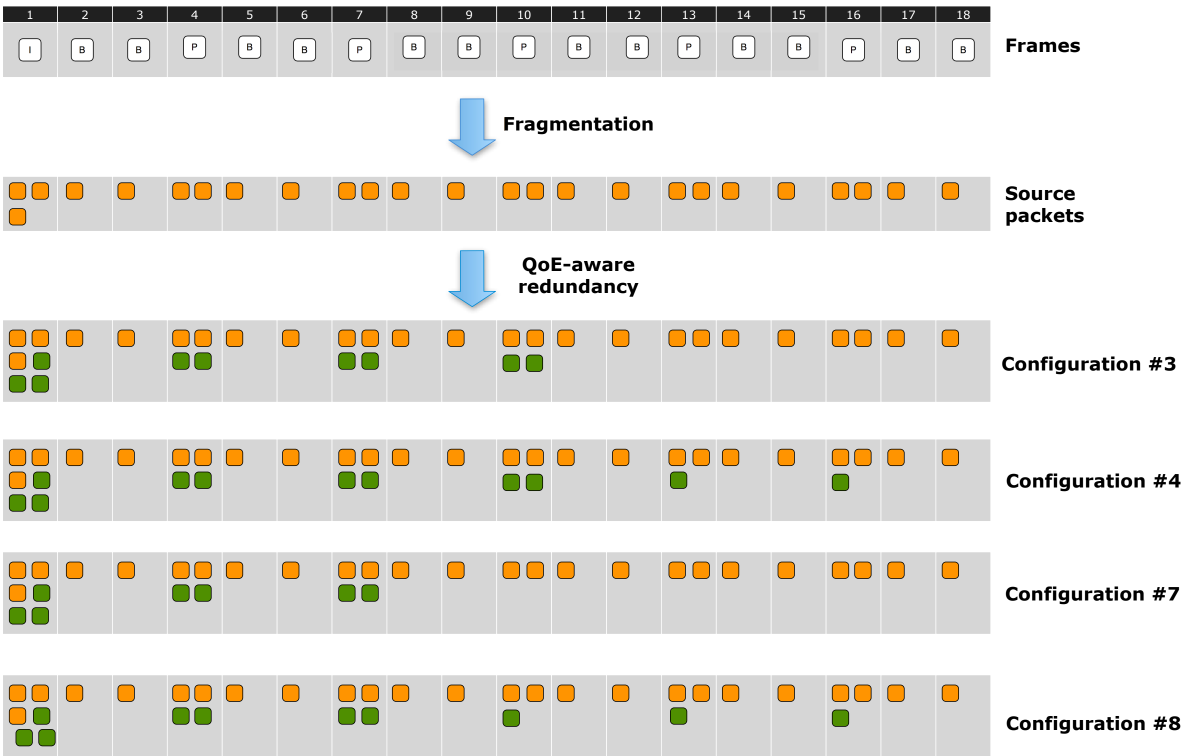

Figure 56: Possible Configurations for the QoE-aware Redundancy Mechanism

Let us first analyse the results with r equals to 80%. Afterwards, we divided results into two groups in order to analyse the impact of adding redundant packets to the last 100 - $X_1\%$ of P-frames. In the first group, the mechanism sends the last 100 - $X_1\%$ of P-frames without packet redundancy, such as happened in configurations #1 and #5. In the second group, the mechanism adds $r/2\%$ of redundant packets for the last 100 - $X_1\%$ of P-frames, i.e., configurations #2 and #6.

Configurations #2 and #6 have almost the same video quality level, because for the Hall video sequence both configurations create the same number of redundant packets. Hence, we conclude that by adding 80% of redundant packets for the first 50% or 60% of P-frames, and also 40% of redundant packets for the last 50% or 40% of P-frames have no benefit for improving the video quality level (in terms of SSIM measurements). On the other hand, configuration #1 improves the video quality level in less than 0.06 for some distances compared to configuration #5. This is because the proposed mechanism adds redundant packets to more P-frames, i.e., it sends the first 60% of P-frames with packet redundancy. By analysing the results of configurations #1, #2, #5, and #6, we conclude that the configurations of the second group, i.e., configurations #2 and #6, improve video quality level in less than 0.09 in some distances. This is because both configurations #2 and #6 add redundant packets to all P-frames, increasing the error resilience and also the video quality level.

Let us analyse when the QoE-aware redundancy mechanism adds 100% of redundant packets to the set of n_{pkts} original packets, i.e., configurations #3, #4, #7, and #8. It is possible to group the results with 100% of redundant packets in a similar way to results with 80% of redundant packets. More specifically, in the first group (configurations #3 and #7), the mechanism sends the last P-frames without redundancy. On the other hand, in the second group, i.e., configurations #4 and #8, it sends the last P-frames with a redundancy of $r/2$. We can see that configurations #4 and #8 improve the video quality level compared with scenarios #3 and #7, for the same reasons explained for the results with 80% of redundant packets.

In applications that support videos with low motion and complexity levels, we believe that the best trade-off between video quality, network overhead, and energy-efficiency is to use either configurations #5 or #7, even if both configurations do not delivered video with the best quality level compared to other configurations. However, both configurations delivered videos without a significant difference to other configurations. This is because the other configurations create more redundant packets, which increase interference, buffer overflow, and also energy consumption.

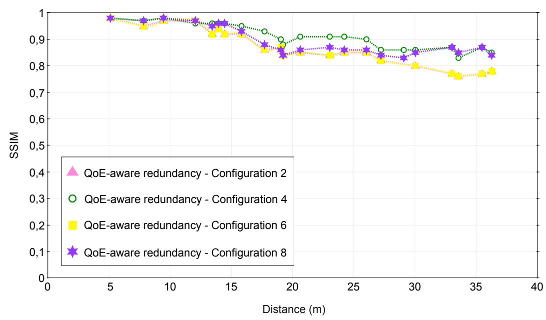

(a) The mechanism sends the last 100 - X_1% P-frames without packet redundancy

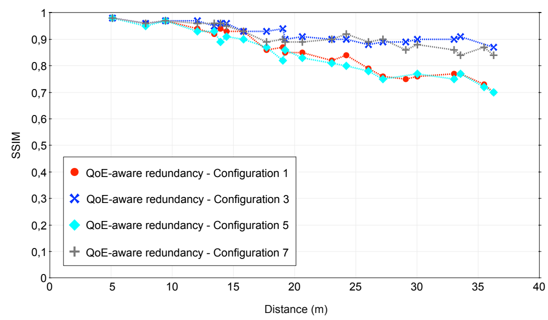

(b) The mechanism sends the last 100 - X_1% of P-frames with r% of redundant packets

Figure 57: SSIM According to the Distance for Different Configurations of the QoE-aware Redundancy Mechanism

6.4.2.2 Simulation Results for Scenario 1

Figure 58 shows the video quality level measured by means of SSIM and VQM according to the distance between SN and DN for scenario 1. SN transmitted videos without redundancy, with simple redundancy, and with the proposed QoE-aware redundancy mechanisms. The SN added 80% and 100% of redundant packets to the original set of n_{pkts} packets, in order to analyse the impact of increasing the parameter r.

We can see that for distances below 25m and when the packet redundancy is equal to 80%, the simple and the QoE-aware redundancy mechanisms improve the SSIM in 10% compared with transmitted the video without packet redundancy, as shown Figure 58(a). For distances above 25m, both simple and QoE-aware redundancy mechanisms enhance the SSIM in 20%. It is important to note that for almost all distances between SN and DN, the simple and also the QoE-aware redundancy mechanisms provided multimedia distribution with similar video quality level. However, the simple redundancy mechanism includes a higher packet overhead compared to the proposed QoE-aware redundancy, as depicted in Figure 59.

Figure 58(b) presents the VQM results according to the distances between SN and DN. VQM results also demonstrate the benefits of using a packet redundancy scheme in a similar way than SSIM results, for both the standard and QoE-aware approaches. By adding 80% of redundant packets, the redundancy mechanisms kept the VQM values below 1 for distances of less than 30m, and around 1.5 for distances above. It is important to mention that VQM values closest to 0 correspond to the best possible video quality level, i.e., exactly the same image compared to original video.

Let us analyse the results of adding 80% and 100% of redundant packets. We conclude that in some cases it is possible to increase the video quality up to 12%. However, when the redundancy r is equal to 100%, it includes an extra packet overhead compared to the case of 80% of redundancy without substantially increase the video quality level.

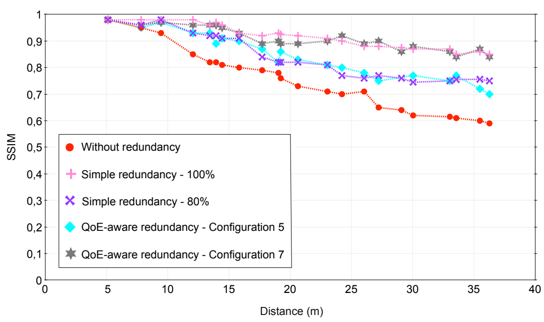

(a) SSIM Results

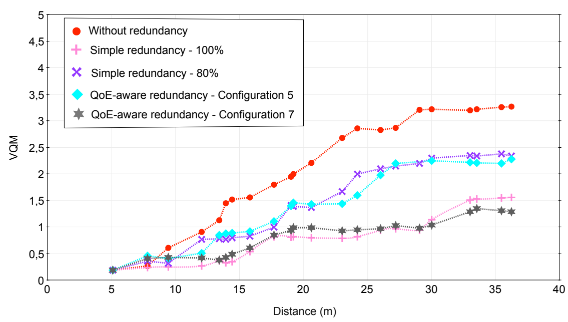

(b) VQM Results

Figure 58: Video Quality Level According to the Distance Between SN and DN for Scenario 1

We conclude that our proposal reduces the overhead compared to the simple redundancy mechanism, while keeping the transmitted video with a good quality based on the user perspective. This is because it adds redundant packets based on video frame importance in order to reduce the packet overhead compared to a simple redundancy mechanism, as shown in Figure 59. For instance, simple redundancy mechanisms [57–63] add redundant packets in a black-box manner, i.e., without considering the frame importance from the QoE/human point-of-view. More specifically, a simple redundancy scheme statically adds a fixed amount of packet redundancy to all frames that composes a given video sequence.

Figure 59 shows the overhead created by the simple and QoE-aware redundancy mechanisms, which add redundant packets to protect frames during loss or link error periods. The proposed QoE-aware redundant mechanism adds redundant packets based on the frame importance from the user experience. Hence, the proposed QoE-aware redundancy mechanism minimizes the overhead, which causes less interference and also reduces the packet loss rate.

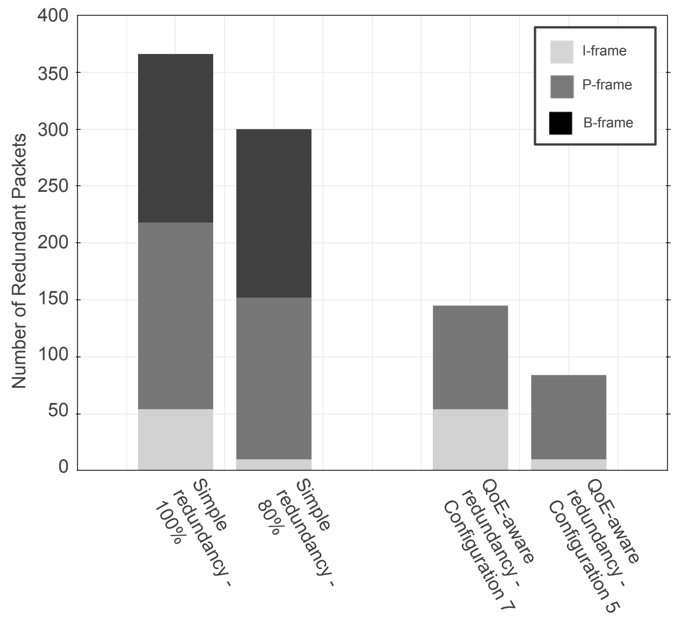

Figure 59: Packet Overhead Introduced by Different Redundancy Mechanisms

6.4.2.3 Simulation Results for Scenario 2

Figure 60 shows the video quality level according to the number of hops between SN and DN for scenario 2. The SN transmitted videos without redundancy, with simple redundancy, and with the proposed QoE-aware redundancy mechanisms. The SN added 80% of redundant packets to the set of n_{pkts} original packets, since a redundancy equal to 100% includes an extra packet overhead without substantially increasing the video quality level, as introduce above.

In Figure 60(a), we can see higher and similar SSIM values for routes up to 3 hops, regardless of the redundancy scheme. This is because the SN is closer to DN, which has reduced interference and number of packet dropped at intermediate buffer. On the other hand, redundancy mechanisms improve the SSIM in 25% compared to transmitting the video without packet redundancy for routes with more than 3 hops. This is because packet-level redundancy is applied as an error-control scheme for handling packet losses in real-time communications. In this way, redundant packets are used to reconstruct a lost frame, in order to improve the video quality level. It should be noted that the simple and the QoE-aware redundancy mechanisms provide multimedia distribution with a similar video quality level. However, the simple redundancy schemes includes a higher overhead. In contrast to simple redundancy scheme, the QoE-aware redundancy approach achieves multimedia dissemination with a lower overhead, while keeping the video with similar quality level, which will bring many benefits for a resource-constrained system.

Figure 60(b) shows the VQM results according to the number of hops. The VQM results confirm the SSIM results, demonstrating the benefits of the proposed QoE-aware redundancy mechanism. The simple and the QoE-aware redundancy approaches kept low VQM values, i.e., high video quality level, for videos transmitted with redundant packets. However, the QoE-aware redundancy mechanism reduces the number of redundant packets (overhead), while keeping videos with an acceptable quality level.

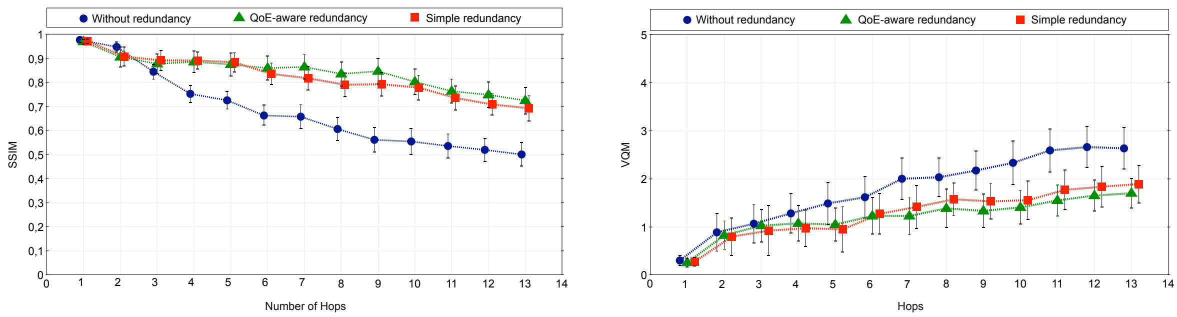

(a) SSIM Results (b) VQM Results

Figure 60: Video Quality Level According to the Number of Hops for Scenario 2

For the energy analysis, we present the energy consumption for transmitting the Hall video sequence along all nodes that compose a given path. We assumed a scenario without node failures during communication caused by hardware or software failures or duty cycles, as well as we do not consider the energy consumption to retrieve each video frame. Figure 61 shows the energy consumption to transmit the Hall video sequence according to the number of hops between SN and DN for different transmission schemes. We can see that our mechanism adds low energy consumption (around 20%) compared to transmitting video content without packet redundancy. On the other hand, the simple mechanism requires more energy to transmit all video packets. More specifically, a simple redundancy mechanism consumes 100% more energy compared to transmitting video content without packet redundancy, and also it consumes 60% more energy compared to the proposed QoE-aware redundancy scheme. This is because the QoE-aware redundant mechanism adds redundant packets only to priority frames, which reduces the overhead as shown Figure 59. On the other hand, the simple redundancy mechanism adds redundant packets in a black-box manner, i.e., without considering the frame importance from a users perspective, which increases the overhead and also the energy consumption.

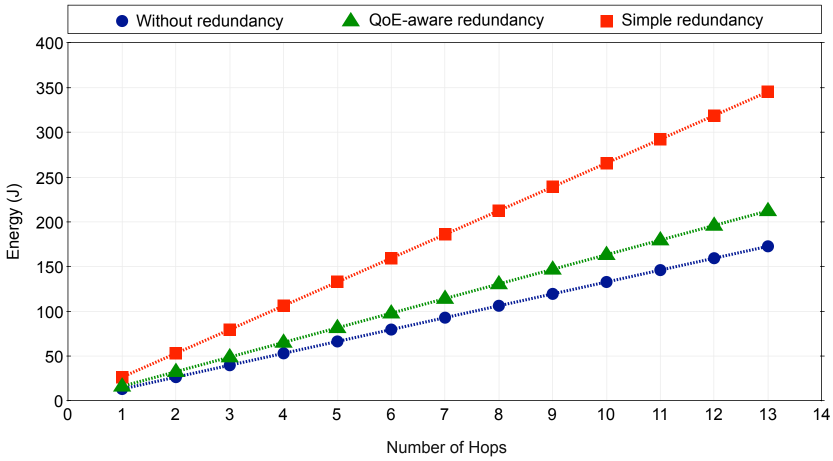

Figure 61: Energy Consumption According to the Number of Hops for Scenario 2

Figure 62 illustrates the energy costs incurred to provide a certain video quality level measured by means of the EQI metric. Transmitting a given video flow without a packet redundancy scheme achieves higher EQI for routes up to 3 hops, since it has a reduced energy cost with higher video quality level compared to redundancy schemes. On the other hand, simple and QoE-aware redundancy mechanisms increase the EQI by around 15% when compared to a solution without redundant packets for routes with more than 3 hops. This is because both schemes protect the priority frames during loss or link error periods, which increase the video quality level based on the user perspective. In addition, intermediate nodes spend energy to forward packets that are not useful to reconstruct some frames received at the destination node, due to the hierarchical structure of MPEG/h.264. In this case, nodes waste scarce network resources, such as energy and bandwidth.

It is important to highlight that the QoE-aware redundancy scheme increases the EQI in 10% compared to the simple redundancy mechanism. In this way, the proposed QoE-aware redundancy mechanism provides the best trade-off between video quality level achieved per unit of energy spent. This is because the proposed redundancy scheme reduces the overhead, i.e., reduces the energy spent to forward redundant packets at intermediate nodes, while keeping the video with similar quality level compared to simple redundancy schemes. Moreover, our proposal increases the video quality level compared to solutions without redundant packets, since we protect the priority frames during loss or link error periods. The energy-efficiency provided by the proposed redundancy mechanism brings many benefits for a resource-constrained system.

Figure 63 shows the SSIM values for all frames that compose the Hall video sequence for a given node with 5 hops to reach DN. This results help to illustrate the ability of our QoE-aware redundancy mechanism to deliver all video frames with quality level support. We can see a poor video quality for the first GoP (i.e., frames 0 to 29), regardless of the mechanisms. This is because the DN does not received the first I-frame and also some P-frames, and thus the decoder can not reconstruct the first 30 frames with a reasonable degree of quality.

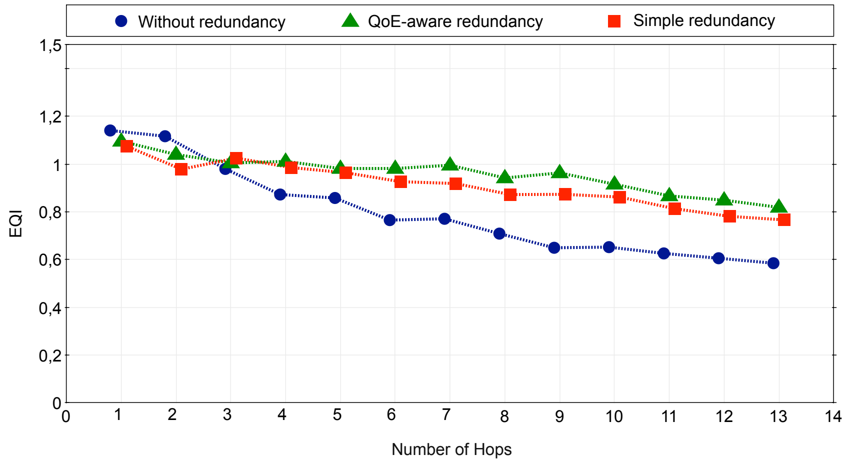

Figure 62: EQI According to the Number of Hops for Scenario 2

Transmitting the videos without redundant packets provide a bad video quality for the entire video sequences, since it does not protect priority frames, i.e., I- and P-frames, during loss or link error periods. For instance, it increases the likelihood of losing an I-frame, which is used as reference to decode all the other frames within each GoP, and thus it reduces the video quality level for the entire GoP.

Moreover, simple and QoE-aware redundancy schemes deliver frames with higher quality level than transmitting the video without redundant packets, since both schemes protect priority frames during loss or link error periods. However, the proposed QoE-aware redundancy mechanism disseminates the first 149 frames with better quality level measured in terms of SSIM when compared to the simple-redundancy scheme, since the simple scheme adds more redundant packets, which increase interference, leading to a higher packet loss rate. Finally, the QoE-aware redundancy mechanism ensures a good video quality level for almost the entire video frames. This is because it protects only priority frames, which reduces the overhead and also the interference.

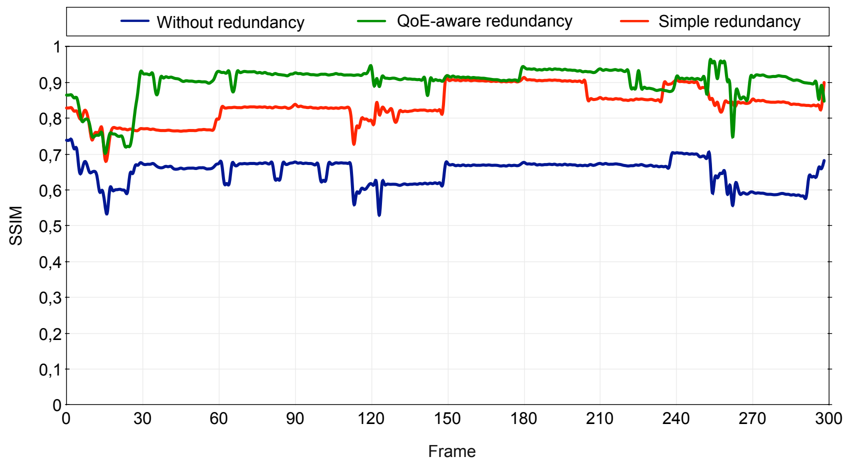

Figure 63: SSIM for all the Frames that Composes the Hall Video Sequence Transmitted by a Specific Node under Conditions of Scenario 2

As mentioned before, we consider intrusion detection WMSN applications to analyse the performance of our proposed packet redundancy mechanism. This application typically requires videos with a small moving region of interest on a static background, such as the Hall video sequence (taken from the Video Trace Library [48]). More specifically, it has a static background, i.e., a Hall, with a small moving region of interest, i.e., a men walking in a hall.

Hence, to show the impact of transmitting video streams with a packet redundancy scheme from the standpoint of the end-user, a frame was randomly selected (i.e., Frame 258) from the transmitted videos, as displayed in Figure 64. The frame 258 is the moment when a man (the intruder in our application) was walking along a hall. The benefits of transmitting the frame using redundancy mechanisms are visible by analysing all the frames of Figure 64. By comparing each transmitted frame with the original frame (see Figure 64(a)), it is possible to see a higher distortion for the frame transmitted without using any packet redundancy scheme, as shown in Figure 64(b). The frame sent with packet redundancy equals to 80% achieves lower distortion compared to the original frame, as shown in Figures 64(f) and 64(c). Finally, the frame has almost the same quality as the original one by sending with redundancy equals to 100%, as shown in Figures 64(d) and 64(c). From the user perspective, the proposed QoE-aware redundancy mechanism keeps the video with an acceptable quality level, while the network overhead is significantly reduced compared to simple redundancy mechanisms, saving scarce network resources, such as bandwidth and energy.

(a) Original Frame

(b) Without Redundancy

(c) Simple Redundancy – 100%

(d) QoE-aware Redundancy - Configuration #7

(e) Simple Redundancy – 80%

(f) QoE-aware Redundancy – Configuration #5

Figure 64: Frame Number 258 for the Hall Video Sequence Transmitted for a Given Node with Different Redundancy Mechanisms for Scenario 2

6.4.3 Summary

Simulation experiments were conducted to show the impacts and benefits of our proposed QoE-aware redundancy mechanism for disseminating video content. Based on the simulation results, we conclude that our proposed QoE-aware redundancy mechanism provides the following advantage, such as expected for many wireless multimedia applications. It achieved similar video quality level compared with non-QoE-aware redundancy schemes, while reducing the transmission of redundant packets, which brings many benefits in a resource-constrained system.

More specifically, it protects priority frames during loss or link error periods, as well as achieves high resilience and reliability without wasting more bandwidth and energy. Moreover, it reduces the overhead compared with non-QoE redundancy mechanisms, which also minimizes the delay. This is because it reduces the number of redundant packets that has to be buffered before the encoding and decoding process at the application layer, as well as in intermediate forwarding nodes. Finally, it decreases the energy consumption at the source node, as well as indirectly preserving energy of intermediate nodes. The results achieved in this section are summarized in Table 10.

Table 10: Comparison Among Different Packet Redundancy Mechanisms Based on Conducted Simulation Experiments

Algorithms	Robustness	Overhead	Energy-efficiency	QoE assurance
Without redundancy	Low	None	Low	Medium/Low
QoE-aware redundancy	High	Low	High	High
Simple redundancy	High	High	Medium	High

6.5 Performance Evaluation of the XLinGO Protocol over Multimedia FANET Scenarios

In this section, we first describe the simulation scenario description for the performance evaluation of the proposed XLinGO routing protocol for video disseminations over multimedia FANET scenarios compared to well known beaconless OR protocols, namely BLR, MRR, BOSS, as well as XLinGO variations. Afterwards, we analyse the obtained simulation results in terms of video quality level and signalling overhead of each transmitted video flows via different beaconless OR protocols.

6.5.1 Simulation Scenarios

Simulations were carried out and repeated 33 times with different randomly generated seeds to provide a confidence interval of 95% (vertical bars in graphics) in order to show the impact and benefits of XLinGO for video dissemination over multimedia FANET scenarios. Table 11 summarizes the simulation parameters used to evaluate the performance of XLinGO compared to well known beaconless OR protocols. The simulations last for 200 seconds and run with the lognormal shadowing path loss model. We set the simulation parameters to allow wireless channel temporal variations, link asymmetry, and irregular radio range, as expected in a real wireless network environment. More specifically, we take pathLossExponent as the indicator of the channel condition in a wireless environment, which is an indicator used to approximate signal attenuation in a wireless environment. Its value is normally in the range of 2 to 6 (indoor), where 2 is for a good channel, 6 is for lossy environment [134]. In addition, it is possible to set a non-uniform radio range mode by setting σ different to 0. In our simulations, each SN sends a total number of 10 videos per simulation.

Table 11: Simulation Parameters for Different Beaconless OR Protocols

Parameters	Scenario 1	Scenario 2
Field Size	40x40	100x100
DN Location	38,38	50,0
SN Location	5,5	Moving
RN_i Location	Uniform Deployment	Moving
Node mobility model	Without mobility	Random Waypoint mobility model
Maximum speed limit (s_{max})	Without mobility	1, 5, 10, 15, and 20 m/s
Transmission power	-15dbm	12 dbm
Total number of nodes	30 and 40 nodes	40 nodes
Redundancy mechanism	QoE-aware redundancy mechanism	
Redundancy (r)	80%	
MAC protocol	CSMA/CA	
Radio model	CC2420 and IEEE 802.11 Transceiver	
Path loss model	Lognormal shadowing model	
Video sequence	Hall, Container, UAV_1, and UAV_2	
Video length	10 seconds	
Video encoding	H.264	
Video format	QCIF (176 x 144), and CIF (352x288)	
Total number of frames	300 frames	
Frame rate	30 fps	
GoP size	30 frames	
Error concealment method	Frame-Copy	

In our simulations, we consider that group of UAVs that are equipped with cameras can be used to set up a temporary multimedia FANET. In such scenario, source nodes are responsible for capturing video flows and transmitting them to DN in a multi-hop fashion. At the beginning of every data transmission in beaconless OR, each SN broadcasts video packets to its neighbours $N(SN)$. Then, the forwarding selection process selects one of those neighbours as the F, i.e., next hop. In this way, multimedia dissemination over FANETs provide visual information, as soon as the standard fixed network infrastructure is unavailable due to a natural disaster, such as an earthquake or hurricane. This description could also be applied to various multimedia applications, such as safety & security, environmental monitoring, natural disaster recovery, and others.

For scenario 1, we deployed n nodes over a 40×40 m flat terrain with one SN located at $(5,5)$, one DN located at $(38,38)$, and $(n-2)$ RN_i deployed uniformly. They are equipped with a CC2420 radio transceiver, using transmission power of -15 dBm, and relying on the traditional CSMA/CA MAC protocol without RTS/CTS messages and retransmissions. We encoded the video sequences with H.264 codec at 200 kbps, 30 frames per second, GoP size of 18 frames, and in a QCIF (176x144). The decoder uses frame-copy as the error concealment method to replace each lost frame with the last received one, which is expected to generate less severe impact by frame losses on the video quality [51].

For scenario 2, the network topology is generated with the DN located at $(50,0)$. The other $n-1$ nodes are moving using the random waypoint mobility model over the entire flat terrain. The mobility traces are generated by means of the BonnMotion mobility trace generator tool. The nodes are equipped with IEEE 802.11 radio, use a transmission power of 12dBm, and rely on CSMA/CA as a MAC protocol. We encoded the video with H.264 codec at 300 kbps, 30 frames per second, GoP size of 18 frames, and Common Intermediate Format (CIF), i.e., 352x288. The decoder also uses frame-copy for error concealment. In addition, the proposed recovery mechanism considers $time-out = 0.5$s and $PRR_{th} = 30\%$ to detect topology or channel changes.

We selected the Hall and Container video sequences, since they have similar characteristics as a UAV stationary in a certain area to capture a video. The UAV_1, UAV_2, and Highway video sequences have similar motion and complexity levels, compared to the case of a mobile node capturing video flows while it is flying from point A to point B. It is important to mention that video UAV_2 has a higher motion level than the video UAV_1 caused by UAV instability during the flight. We downloaded the Hall, Container, and Highway video sequence from the YUV video trace library [48], while we downloaded UAV_1 and UAV_2 video sequences from YouTube [150]. Video sequences with these characteristics can be captured and transmitted in a typical natural disaster recovery application with UAVs equipped with cameras. For these reasons, we decided to use these video sequences in our evaluations. Figure 65 shows one frame from each video used for our simulations. It is important to mention that we selected a set of transmitted videos via LinGO, BLR, and MRR to make available at [151]. In addition, we selected another set of videos transmitted via XLinGO, BLR, BOSS, and MRR together with original videos to make available at [150].

Figure 66 illustrates the network stack executed on each node for the experiments conducted to evaluate beaconless OR protocols to disseminate multimedia content over FANETs. We implemented an application to retrieve video flows and applied the QoE-aware redundancy mechanism to add 80% of redundant packets only to priority frames,

(a) Hall

(b) Container

(c) Highway

(d) UAV_1

(e) UAV_2

Figure 65: Snapshots of the Selected Videos

and we used UDP at the transport layer. We implemented different beaconless OR protocol at the network layer, namely XLinGO, BLR, BOSS, MRR, as well as XLinGO variation. Nodes are equipped with CC2420 or IEEE 802.11 radio transceiver, using different transmission power, depending on the scenario characteristics. In addition, our simulations rely on the traditional CSMA/CA MAC protocol without RTS/CTS messages and retransmissions.

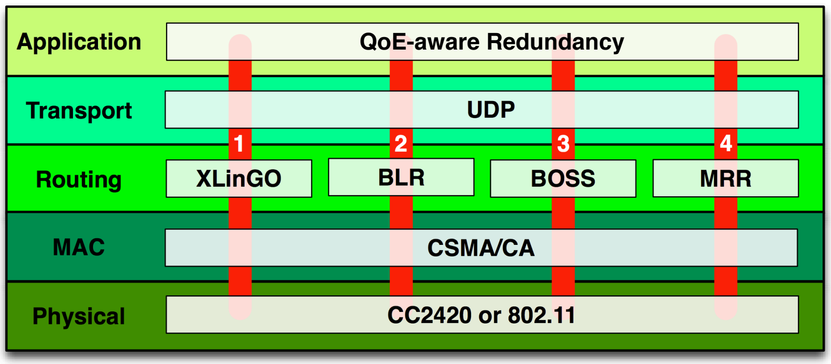

Figure 66: Network Stack for the Performance Evaluation of Different Beaconless OR Protocol for Multimedia FANETs

We conducted simulations with different beaconless OR protocols for video dissemination over multimedia FANET scenarios, in order to compare the results in terms of reliability, robustness, and also the video quality level of transmitted videos.

- **LinGO** follows our initial XLinGO definition [108–110], which combines link quality, geographical information, and energy to compute the DFD based on Eq. 5.1.

In addition, it relies on periodic route reconstruction in time intervals called Link Validity time Estimation (LIVE). During the LIVE interval, instead of the nodes broadcasting the packets, they must transmit video packets in a unicast fashion. This XLinGO variation is used to show the benefits of considering the recovery mechanism to react to topology changes, and also the benefits of using queue length for routing decision in a scenario with simultaneous multiple video flow transmissions.

- **XLinGO** follows all the XLinGO description and operation principles, such as introduced in Chapter 5. More specifically, it combines a set of cross-layer, video, and human-related parameters for routing decisions, namely PRR, QoE, queue length, link quality, geographical location, and residual energy. It combines link quality, geographical information, and queue length to compute the DFD function according to Eq. 5.2. It also relies on a recovery mechanism to react faster to route failure situations.

- **BLR** follows the BLR description [80–82], where it only considers geographical information to compute the DFD, and relies on periodic route reconstruction.

- **MRR** follows the MRR specifications [87, 88], but without the location update mechanism, since in our simulations we consider a static DN. In this way, nodes compute the DFD function based on geographical information, RSSI, and energy to compute the DFD. It also relies on a periodic route reconstruction.

- **BOSS** follows the BOSS specifications [83,84]. More specifically, it relies on a tree-way handshake and only considers geographical information to compute the DFD, as well as relies on periodic route reconstruction.

6.5.2 Simulation-Based Result Analysis

In this section, we analyse the obtained simulation experiments in terms of objective and subjective QoE metrics for each transmitted video. More specifically, we first introduce the simulation results to select some parameters for the proposed XLinGO protocol. Afterwards, we describe the simulation results to analyse the impact of permanent and transient node failures, signalling overhead for different beaconless OR protocols, impact of the mechanism to recover from route failure, as well as the impact of node mobility and different numbers of video flows.

6.5.2.1 XLinGO Parameters under Conditions of Scenario 1

The coefficients (i.e., $\Phi_{LQE}, \Phi_{progress}, \Phi_{energy}$) of the DFD function computed based on Eq. 5.1 affect the XLinGO performance. We defined 10 combinations with different coefficient values to show the performance in terms of video quality level, as shown in Table 12. For instance, combination #1 only gives priority to geographical information

($\Phi_{progress}$), and thus it ignores link quality (Φ_{LQE}) and energy (Φ_{energy}). Combinations #2 to #9 give the same priority to energy ($\Phi_{energy} = 0.1$), since energy is not the most important metric in our experiments. These 8 combinations differ from each other with regard to priorities for link quality (Φ_{LQE}) and geographical information ($\Phi_{progress}$). Finally, combination #10 gives priority only to link quality (Φ_{LQE}), in order to show the impact of considering only link quality. Based on simulation results, we choose one configuration for the following simulations.

Table 12: Coefficient Combinations for DFD function

Combinations #	Φ_{LQE} (Link Quality)	$\Phi_{progress}$ (Geographical information)	Φ_{energy} (Energy)
1	0	1	0
2	0.1	0.8	0.1
3	0.2	0.7	0.1
4	0.3	0.6	0.1
5	0.4	0.5	0.1
6	0.5	0.4	0.1
7	0.6	0.3	0.1
8	0.7	0.2	0.1
9	0.8	0.1	0.1
10	1	0	0

Figure 67 shows the results of the video quality levels measured by means of SSIM and VQM for these 10 different coefficient combinations under conditions of scenario 1. We can observe that the combination #1 has bad performance for both SSIM and VQM results. This is because each node only considers progress to compute the DFD function, i.e., each node chooses the forwarder node that is closer to the DN. However, the most distant node suffers from poor channel quality due to the unreliable nature of wireless links, as experienced in multimedia FANET scenarios. These issues lead to higher packet loss rate, which reduces the video quality level. It is worth noting that this combination is similar to existing beaconless OR approaches that only consider progress to compute the DFD, such as BLR.

In addition, combination #10 has bad performance for both SSIM and VQM results. This is because each node computes the DFD function based only on link quality, e.g., measured by means of SNR, LQI, or RSSI, and thus a given node that received packet with a higher link quality computes a shorter DFD value and forwards the received packet faster. However, typically a given node that received a packet with higher link quality value provides short progress towards the DN, which increases the number of hops and interferences. This leads to a higher packet loss ratio and also a bad video quality level. Finally, combinations #2 to #9 perform better than both combinations #1 and #10. This is because combinations #2 to #9 have different weights for link quality and progress parameters, and thus XLinGO selects forwarder nodes closer to DN with a reliable link, and sufficient energy to forward packets with a reduced packet loss ratio. We conclude that XLinGO achieves the best results by tuning the coefficients for link quality and progress, such as achieved by combination #6. For these reasons, we choose a XLinGO combination with similar priority for progress and link quality for the next simulations, in order to compare with the results of XLinGO with BLR, BOSS, MRR, and XLinGO variation.

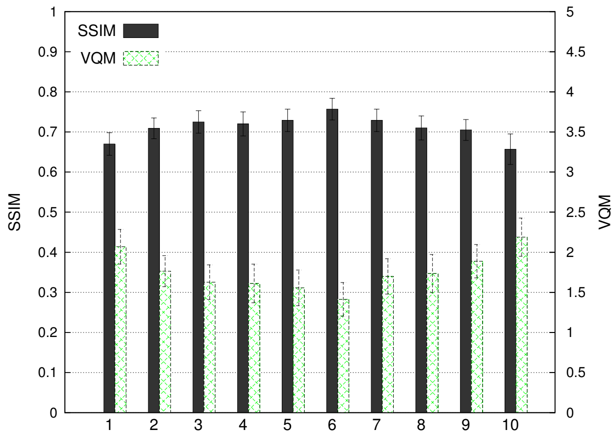

Figure 67: Video Quality Level for Different XLinGO Coefficient Combinations

We also performed simulations to show the benefits of the QoE-aware redundancy mechanism for XLinGO, BLR, and MRR. Figure 68 shows the impact of the QoE-aware redundancy mechanism for a network composed of 30 static nodes deployed in the simulation area for scenario 1. The mechanism improves the video quality in 20% compared to multimedia transmissions without packet redundancy. This is because it adds redundant packets based on the frame importance, protecting priority frames in loss and link error periods. It also achieves robust video transmissions over a bandwidth-limited and unreliable networking environment with reduced overhead. Moreover, XLinGO increases the video quality in 18% and 55% compared to BLR and MRR, respectively. For these reasons, we use the QoE-aware redundancy mechanism for any beaconless OR protocols in the following simulations, in order to analyse only the impact of routing decision to disseminate simultaneous multiple video flows without any external factor.

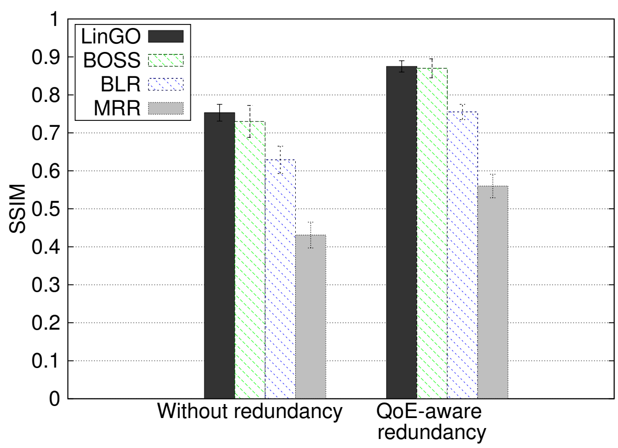

Figure 68: Impact of Redundancy Mechanism for Different Beaconless OR Protocols

6.5.2.2 Impact of Transient and Permanent Node Failures under Conditions of Scenario 1

In this section, we evaluate the reliability and robustness of beaconless OR protocols that rely on periodic route reconstruction. In this way, we evaluate the performance of LinGO compared to BLR and MRR by deploying 30 and 40 static nodes, and the topology changes are caused by individual node failures, as well as wireless channel variations. We defined two scenarios, where one has temporary node failures and another one has permanent node failures. For both scenarios, we created the worst-case scenario for topology changes, where the SN established the persistent route and 10% of 1-hop SN neighbours that have individual node failures. For instance, Figure 69 depicts a network composed of 30 static nodes uniformly deployed over a 40×40 m flat terrain, where the SN and DN are deployed on the corner of the field size in order to make the distance between them bigger. Green circles in Figure 69(a) represent the SN neighbours for different random-generated seeds. On the other hand, red circles in Figure 69(b) represents the 10% of 1-hop SN neighbours that have individual node failures, which are the most used nodes by SN to forward packets when they rely on LinGO, MRR, and BLR as routing protocol.

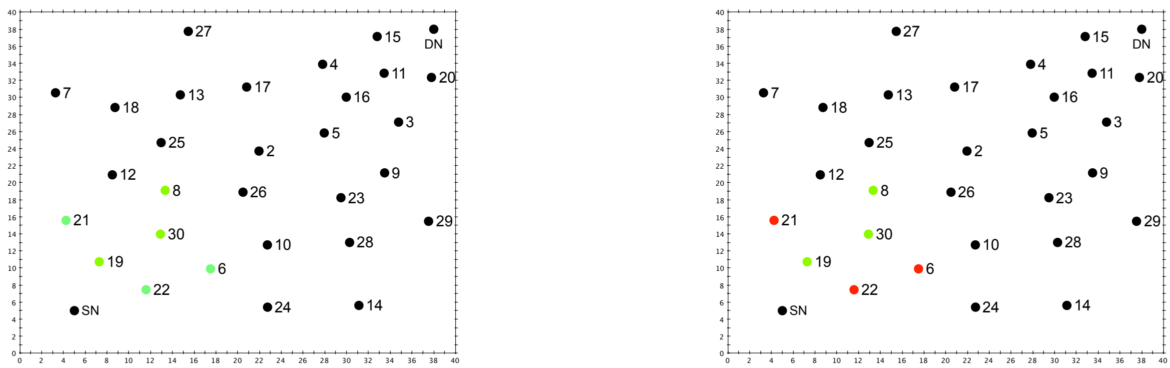

(a) Scenario Composed of 30 Nodes Without Node Failures

(b) Scenario Composed of 30 Nodes With Node Failures

Figure 69: Network Topology Composed of 30 Static Nodes

Figure 70 shows the video quality level for 10 video flows transmitted for a network composed of 30 and 40 nodes. First, we performed simulations for each protocol only with wireless channel changes, i.e., without node mobility or failures, to serve as a baseline video quality level. Afterwards, we performed simulations for each protocol with transient node failures in order to analyse its impact on the video quality level, where the transient node failures happened during the transmissions of videos 6 and 7.

First, we conclude that in contrast to BLR and MRR without node failures, LinGO without node failures keeps the video quality high and constant independent of wireless channel conditions, i.e., LinGO baseline keeps the $SSIM$ around 0.87 for videos 1 – 10. In addition, LinGO has smaller confidence intervals than MRR and BLR, which means LinGO has a small variation in the video quality for different random-generated seeds. This is explained because LinGO builds a reliable persistent route by taking into account multiple metrics, which protects frames during link error periods. For instance, LinGO reduces loss of I- and P-frames by up to 50% compared to BLR and MRR, which are the priority frames and their losses increase video distortion. Hence, LinGO enables single flow video disseminations with QoE support in scenarios with topology changes caused by only channel quality variations.

For video transmissions that experienced transient node failures, during the transmission of video 6, nodes established the persistent route $P_{SN,DN}$ connecting the pair of SN to DN via multiple relays F. Afterwards, 10% of 1-hop SN neighbours have individual transient failures lasting until the end of the video 7, i.e., those nodes turn-off their radios. In this way, the next-hop of SN is not available anymore to forward subsequent packets, which creates controlled topology changes to evaluate how LinGO reacts to temporary topology changes compared to BLR and MRR. Besides the topology changes caused by node failures, a burst of packets might be lost until the SN re-establishes the persistent route $P_{SN,DN}$, since one of the nodes from the persistent route might be not available anymore to forward subsequent packets. In the worst case, the loss of a burst of packets during the $LIVE$ interval occurs, because this is the time interval required to reconstruct the persistent route $P_{SN,DN}$. On the other hand, videos 1 – 5 and 8 – 10 transmitted without any node failures have similar video quality level compared to the baseline transmission regardless of the beaconless OR, as shown in Figure 70.

We can see that video 6 transmitted via LinGO in presence of node failures (LinGO - Fail) decreases the video quality by 5% compared to the baseline video transmission (LinGO), as shown Figure 70(a). It is important to notice that the video quality is still better than BLR and MRR without any node failure, since LinGO reacted better to topology changes caused by transient node failures. In addition, when video 6 is transmitted via BLR and MRR with transient node failures (BLR- and MRR - Fail), it decreases the video quality by up to 10% compared to the baseline video quality level of those protocols (BLR and MRR). This is because both BLR and MRR are not able to re-establish a reliable persistent route $P_{SN,DN}$ in case of topology changes.

Finally, video 7 transmitted via LinGO in presence of lower node density (LinGO - Fail), due to 10% of node turned-off their radios, has similar quality level compared to the baseline video transmissions. This is because LinGO is able to re-establish the persistent route in a scenario with lower node density. Moreover, when video 7 is transmitted via BLR and MRR in presence of transient node failures (BLR- and MRR - Fail), it reduces the video quality by 10% compared to the baseline video transmission, because those protocols do not adapt well in presence of topology changes.

We also analysed the impact of node density, by comparing results of Figure 70(a) with Figure 70(b). We can see that when the number of nodes increases, the impact of node failures on the video quality level decreases, regardless of the beaconless OR protocols. This is because the nodes have more neighbours, and thus the SN has more and reliable neighbours to reconstruct the persistent route. Hence, these issues increase the likely of nodes reconstruct a reliable persistent route $P_{SN,DN}$, enabling network nodes to adapt better to topology changes.

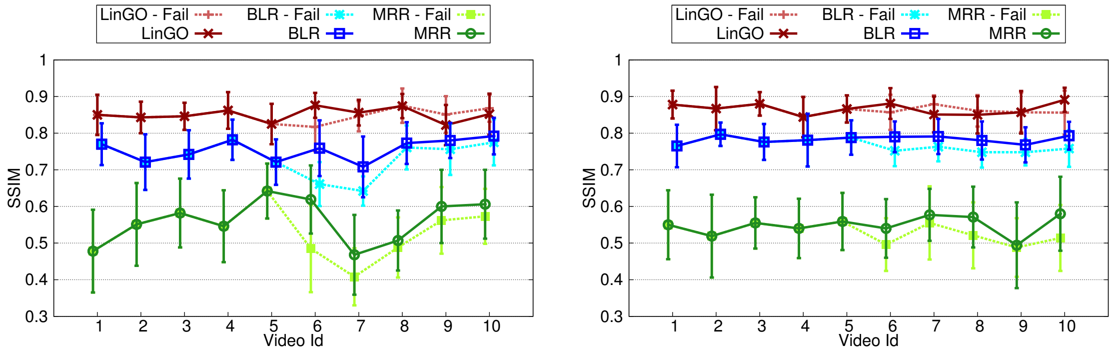

(a) Scenario Composed of 30 Nodes (b) Scenario Composed of 40 Nodes

Figure 70: Video Quality in Presence of Transient Node Failures with $LIVE$ Value of 2 and Different Number of Nodes

Figure 71 shows the video quality level over 10 videos transmitted for a network composed of 30 and 40 nodes. We performed simulations for each protocol without node mobility or failures to serve as a baseline video quality level. Hereafter, we performed simulations in presence of permanent node failures, where permanent node failures happened during the transmissions of videos $6 - 10$.

We can see that videos 6 and 7 transmitted via LinGO in presence of permanent node failures reduced the SSIM by 7% compared to the baseline video quality. In addition, videos 6 and 7 transmitted via BLR and MRR in presence of permanent node failures reduced the SSIM by 14% compared to the baseline transmission. This is explained for the same reason as we discussed for transient node failures, since those videos are transmitted under the same conditions. On the other hand, videos $8 - 10$ transmitted via LinGO with permanent node failure decreased the video quality by 5% compared to baseline SSIM. Those videos transmitted via BLR and MRR under permanent node failures decreased the SSIM by 10% compared to baseline video transmission. This is because those videos are transmitted in a scenario with permanent node failures, which happened during the transmissions of videos $6 - 10$. Finally, the impact of permanent node failures decreases as soon as the node density increases.

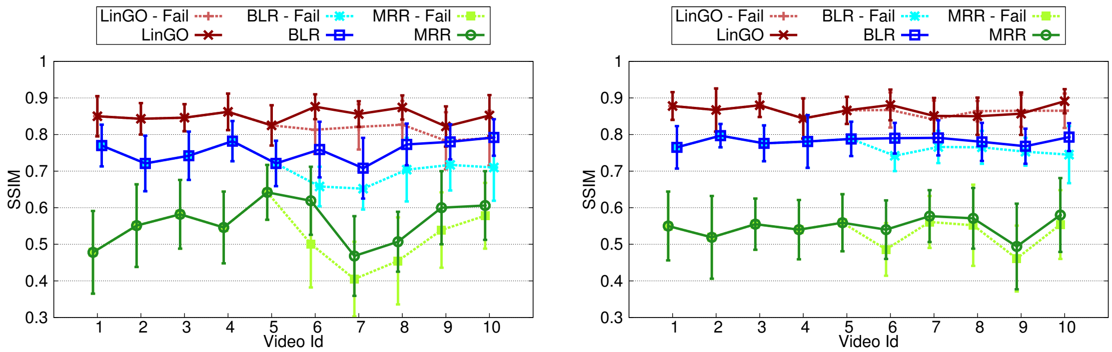

(a) Scenario with 30 Nodes (b) Scenario with 40 Nodes

Figure 71: Video Quality in Presence of Permanent Node Failures with $LIVE$ Value of 2 and Different Number of Nodes

6.5.2.3 Impact of the Mechanism to Recover from Route Failures under Conditions of Scenario 1

In this section, we used a simple simulation scenario to validate the mechanism to recover from route failures. In this way, we evaluate the performance of XLinGO with the recovery mechanism compared to periodic route reconstruction by deploying 30 static nodes, and the topology changes are caused by individual node failures, as well as wireless channel variations. Hence, we created temporary node failures in a similar way as explained in Section 6.5.2.2.

More specifically, we defined three configurations to transmit the Hall video sequence via XLinGO: i) **XLinGO** does not have node failures and recovery mechanism; ii) **XLinGO – Failure** relies on periodic route reconstruction, such as performed in LinGO, BLR, MRR, and BOSS, and experiences node failures. iii) **XLinGO – Recovery** considers the recovery mechanism and experiences node failures. Finally, the original video in the plot represents an errorless video transmission, which is used as a benchmark video quality. This is because video coding and decoding also introduce impairments in the video quality even in the absence of packet losses. Thus, it helps to see exactly the quality loss due to packet loss.

Figure 72(a) shows the SSIM for all frames that compose the Hall video sequence for those three XLinGO configurations, and also the original video. XLinGO without node failures keeps the video quality level high and constant, i.e., $SSIM$ around 0.94 for all frames, which is similar to the video quality provided by the benchmark video quality. This can be explained by the fact that XLinGO builds a reliable persistent route $P_{SN,DN}$, which protects all video frames during link error periods. Hence, XLinGO enables video disseminations with QoE support in scenarios with dynamic topologies caused by only channel quality variations. Frames 0 – 17 have a good quality level when transmitted by XLinGO – Failure and XLinGO – Recovery. This is because DN received frame 0, i.e., it is an I-frame for the first GoP from frames 0 to 17. In addition, the decoder relies on frame-copy as error concealment method to replace each lost frame with the last received one, enabling it to reconstruct those frames with a good quality.

On the other hand, XLinGO transmitted video frames 18 – 89 with bad quality in scenarios with node failures and without a mechanism to recover from route failures (i.e., XLinGO – Failure). The reason for this is that nodes established the persistent route $P_{SN,DN}$ and 10% of network nodes have a node failure. Apart from the topology changes caused by node failures, bursts of packets were lost until the SN has re-established the $P_{SN,DN}$, since one of the nodes from the $P_{SN,DN}$ is no longer available to forward packets. In the worst case, the packet loss lasts during the interval for route reconstruction. In our experiments, XLinGO – Failure reconstructs routes every 3 seconds, and this explains the poor video quality for frames 18 – 89. Afterwards, frames 90 – 299 have similar quality level compared the benchmark video quality level, since XLinGO enables the SN to reconstruct another reliable persistent route.

XLinGO transmitted only frames 18 – 35 with poor quality level, in scenarios with node failures and a mechanism to recover from route failures (i.e., XLinGO – Recovery). This is because the proposed recovery mechanism has a time-out value of 0.3s, which is the time required to detect that one of the forwarder nodes is no longer available to forward packets. As soon as the time-out expires, the node must return to the contention-based forwarding mode, and re-establish a reliable $P_{SN,DN}$. Moreover, frames 36 – 299 have similar quality level compared to the benchmark video quality level.

Aguiar et al. classified the Hall video sequence as a low motion video flow, which means that there is a small moving region on a static background [51]. More specifically, static background makes the frame losses less severe than in a scenario with more motions. Hence, we also carried out simulations with the SN transmitting the UAV_1 video sequences to analyse how the proposed recovery mechanism performs with more dynamic video sequences, as shown Figure 72(b). SSIM values for the UAV_1 video sequence have higher variations than the results for Hall video sequence, due to UAV_1 video has more motion level than the Hall video sequence. It is important to highlight that all XLinGO configurations have similar behaviour for both videos for same reasons as explained above, which means that XLinGO – Recovery react faster to route failure situations, such as expected in multimedia FANET applications.

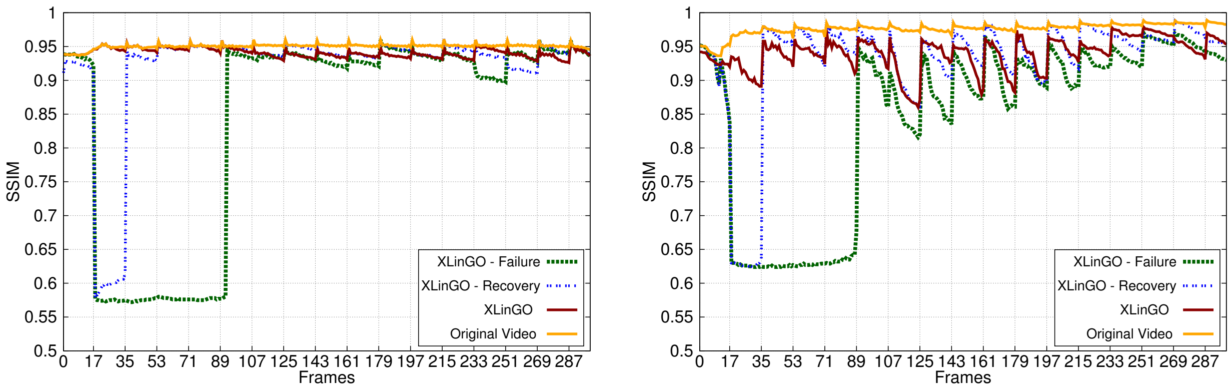

(a) Hall Video Sequence

(b) UAV_1 Video Sequence

Figure 72: SSIM for All Frames for the Compose the Hall and UAV_1 Video Sequence Transmitted by a Specific SN under Conditions of Scenario 1 with Transient Node Failures

Let us summarise the results to analyse the impact of the proposed mechanism to recover from route failures. In a scenario without any node failure, XLinGO transmits the Hall video with SSIM equal to 0.94. On the other hand, XLinGO - Failure transmits the entire video with an SSIM value of 0.84. Finally, the video transmitted by XLinGO - Recovery has a SSIM value of 0.91. Hence, the proposed recovery mechanism reduces the video quality level less than periodic route reconstruction schemes. This is because the proposed mechanism enables XLinGO to quickly detect and respond to topology changes, and thus it enables multimedia dissemination with robustness and QoE assurance. Moreover, Hall and UAV_1 have similar quality level regardless the transmission scheme, since the maximum SSIM value for those videos area different.

Based on simulation results presented in Sections 6.5.2.2 and 6.5.2.3, we conclude

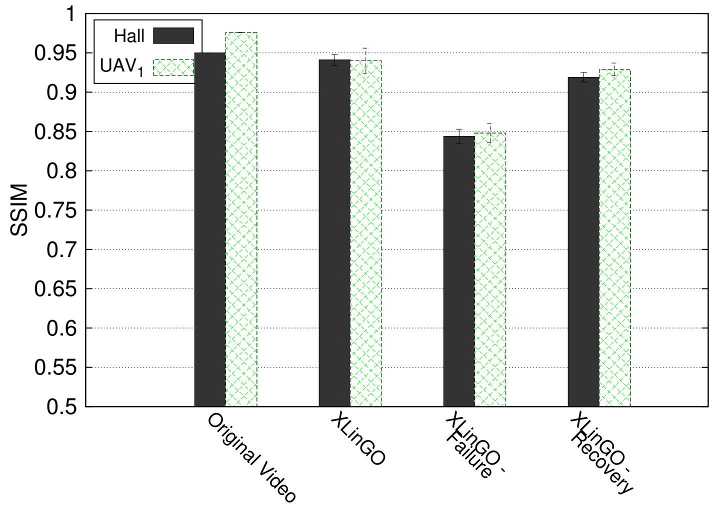

Figure 73: Overall Video Quality for Hall and UAV_1 Video Sequences Transmitted by a Specific SN under Conditions of Scenario 1 with Transient Node Failures

that in periodic route reconstruction as soon as one of the forwarding nodes from a given persistent route is no longer available to forward packets, a burst of packets might be lost until the protocol re-establishes the route, which reduces the video quality for longer periods. Moreover, the route reconstruction interval should be adjusted according to the desired degree of robustness and energy consumption. From the energy consumption point-of-view, the persistent route reconstruction must occur with low frequency. On the other hand, from the robustness point-of-view, high frequency of route reconstruction provides better robustness. However, it is not trivial to find the appropriate route reconstruction interval to provide robustness, QoE support, and reduced overhead. In this way, XLinGO relies on a recovery mechanism, which considers link quality and PRR to detect and quickly react to route failures, providing a smoother operation in harsh environments and mobile networks, such as experienced in multimedia FANET scenarios.

6.5.2.4 Impact of Node Mobility and Number of Video Flows under Conditions of Scenario 2

In this section, we evaluate the reliability of XLinGO compared to LinGO [110], BLR [81], BOSS [84], and MRR [87] in a scenario composed of mobile nodes and also simultaneous multiple video flow transmissions. This involves deployment of 40 nodes with two configurations under conditions of scenario 2. The first configuration has one static DN, two mobile SNs transmitting simultaneous video flows, and 37 possible mobile relay nodes RN_i. The second configuration has one static DN, three SNs transmitting simultaneous video flows, and 36 possible mobile RN_i. For both configurations, each SN transmits a different video sequence, i.e., UAV_1, UAV_2, Highway, Hall, and Container.

Figure 74 shows the quality level of each video transmitted via XLinGO, LinGO, BLR, BOSS, and MRR. For the simulations conducted for this section, we defined the minimum speed limit (s_{min}) equal to 0, and six different maximum speed limits (s_{max}), i.e., 0 (static network), 1, 5, 10, 15, and 20 m/s. In this way, we can analyse the impact of the moving speed on the final video quality level.

In the case of video flows transmitted through LinGO, BLR, MRR, and BOSS, as soon as the s_{max} increases, the video quality level decrease, as shown results of Figure 74(a). This is because these protocols rely on periodic route reconstruction, and thus as soon as a two forwarders F from a given persistent route $P_{SN,DN}$ quickly move out of each other's transmission range, causing route failures. Hence, a burst of packets might be lost until the SN has recreated the persistent route, increasing packet loss rate, and consequently reducing the video quality level.

Moreover, we conclude that XLinGO provides multimedia dissemination with a high quality level compared to LinGO, BLR, MRR, and BOSS regardless of the moving speed, as shown results of Figure 74(a). For instance, more than 75% of the transmitted videos via BLR and MRR have a video quality lower than 0.8, for s_{max} values of 0 – 20 m/s. This is because BLR only considers geographical information to compute the DFD, and due to the unreliability of the wireless channels, the most distant node might suffer from a bad connection, increasing the packet loss ratio for BLR. In addition, MRR selects a forwarding node that receives a packet with a weak signal, reducing reliability and quality level of videos transmitted via MRR. Finally, videos transmitted via BOSS have a higher quality compared to BLR and MRR, even if BOSS only considers geographical information for routing decisions like BLR. This is because BOSS considers a three-way handshake mechanism to select F, and also full data payload size for the RTS control message size. However, videos transmitted via BOSS have a video quality lower than videos transmitted via LinGO and XLinGO, since both LinGO and XLinGO efficiently combines multiple metrics for forwarding decisions.

Videos transmitted via LinGO have video quality lower than videos transmitted via XLinGO, because XLinGO considers queue length to compute the DFD, which avoids the selection of forwarder nodes F to composed the persistent route $P_{SN,DN}$ with a heavy traffic load. Hence, the *queueLength* metric helps to prevent buffer overflow, minimizing packet loss, delay, and jitter, as well as providing load balancing. In addition, LinGO considers periodic route reconstruction, leading to higher packet loss ratio in case of route failures, as shown in the results of the recovery mechanism in Section 6.5.2.3.

The SSIM measured for each video flows transmitted via XLinGO ranges from 0.82 to 0.974 regardless of the moving speed, as shown in Figure 74(a). For instance, for maximum speed s_{max} values between 0 and 10 m/s, XLinGO delivers more than 75% of the transmitted videos with a high quality level, i.e., a SSIM higher than 0.9. On the other hand, for s_{max} values above 15 m/s, 75% of the transmitted videos via XLinGO have SSIM better than 0.86. This is because in contrast to LinGO, BLR, BOSS, and MRR, XLinGO efficiently combines multiple metrics for forwarding decisions, and also considers a mechanism to recover from route failures.

The results of Figure 74(a) and 74(b) can be compared to analyse the impact of the number of simultaneous video flow transmissions. When the number of multimedia

SN increases, the quality level of the videos transmitted via LinGO, BLR, BOSS, and MRR decreases. This is because in contrast to XLinGO, these protocols do not prevent the forwarding selection mechanism from selecting F with heavy traffic load. This increases the probability of queue overflows in intermediate F. Hence, we conclude that XLinGO provides multimedia dissemination with QoE assurance in a scenario composed of mobile nodes, different moving speed, multiple multimedia SN, and also videos with different motion and complexity levels.

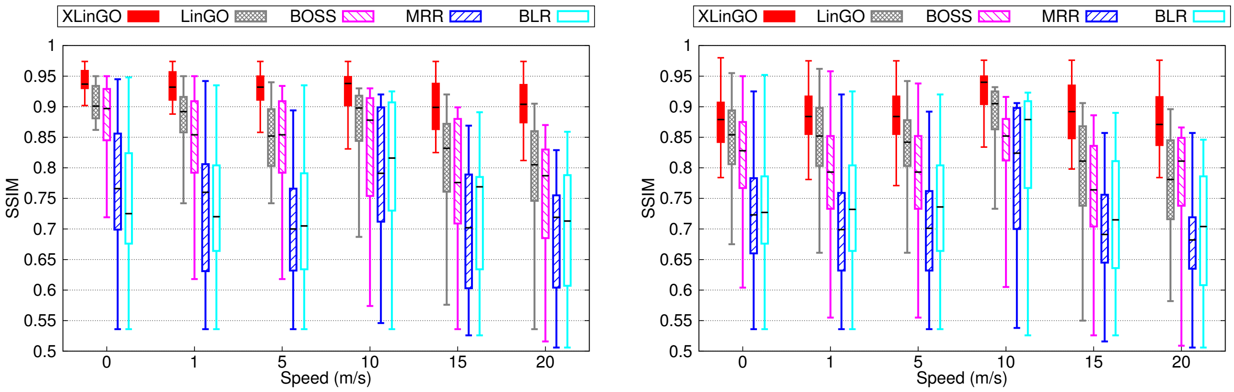

(a) Scenario Composed of 2 Multimedia SN (b) Scenario Composed of 3 Multimedia SN

Figure 74: Video Quality for a Scenario with a Different Number of Multimedia SN, Moving Speed, and Videos with Different Motion and Complexity Levels

Results of Figure 74(a) can also be explained based on the frame loss rate, as shown in Figure 75. In this way, let us analyze the frame loss ratio for speed limit s_{max} value of 20m/s and with 2 simultaneous video flow transmissions. Based on the frame loss ratio evaluation, XLinGO has an overall frame loss rate of 17.8%, which is 48%, 61%, 57%, 70% lower than LinGO, BLR, BOSS, and MRR, respectively. From the I-frame loss perspective, XLinGO only lost 13.6% of I-frames, which is 55%, 70%, 62%, 75% lower than LinGO, BLR, BOSS, and MRR, respectively. XLinGO lost 19.4% of P-frames, which is 60%, 63%, 62%, 75% lower than LinGO, BLR, BOSS, and MRR, respectively. We conclude that XLinGO transmits video packets with a reduced frame loss rate, and thus it protects priority frames, i.e., I- and P-frames, in periods of congestion and link errors. The frame loss ratio for other s_{max} also confirms that XLinGO protects priority frames during congestion and link error periods.

Figure 76 shows the number of packets dropped at intermediate node's queue for videos transmitted via XLinGO, LinGO, BLR, BOSS, and MRR. BLR has the lowest number of dropped packets in an intermediate queues. This is because BLR only considers geographical information to compute the DFD, and due to the unreliability of wireless channels, the most distant node might suffer from a bad connection.

On the other hand, MRR has the higher number of packets dropped at intermediate buffers, since it considers forwarding area as a rectangle. In particular, MRR selects forwarder nodes closer to boundaries of the rectangle, which does not mean that the forwarder provides geographical advance towards the DN, i.e., MRR does not select

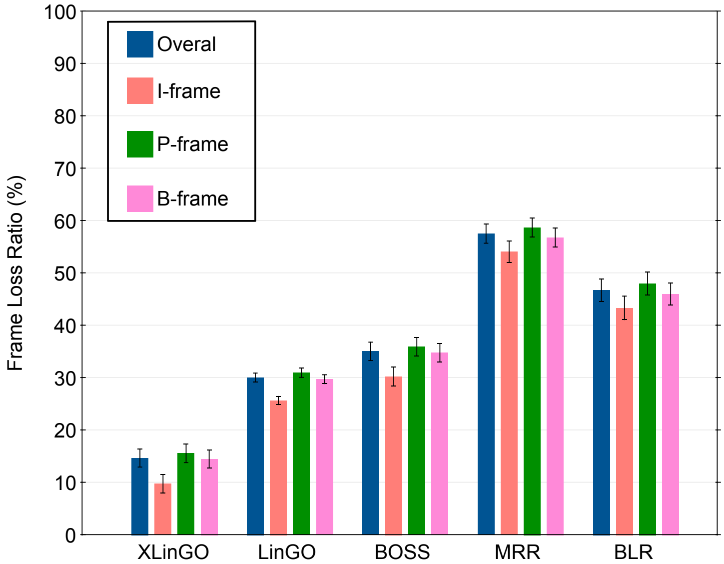

Figure 75: Frame Loss Ratio for Videos Transmitted in a Scenario with s_{max} equals to 20m/s and with 2 Simultaneous Video Flows Transmissions

forwarder closer to the DN. In this way, it increases the number of hops, interferences, and buffer overflow, which decreases video quality level. Finally, XLinGO has lower packet loss rate in intermediate node's buffers than LinGO, BLR, BOSS, and MRR. This is because XLinGO avoids selecting F with heavy traffic load, which prevents buffer overflow, minimizes packet loss, delay and jitter, and also provides load balancing. The number of packets dropped at intermediate buffers increases, as soon as the number of SN increases, as shown in Figure 76. This is because more packets are transmitted, which increases interference.

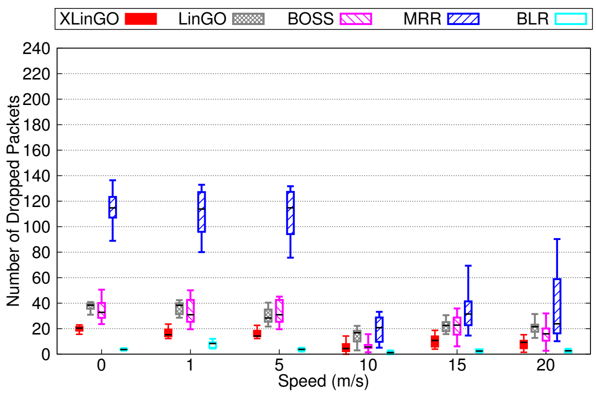

(a) Scenario Composed of 2 Multimedia SN

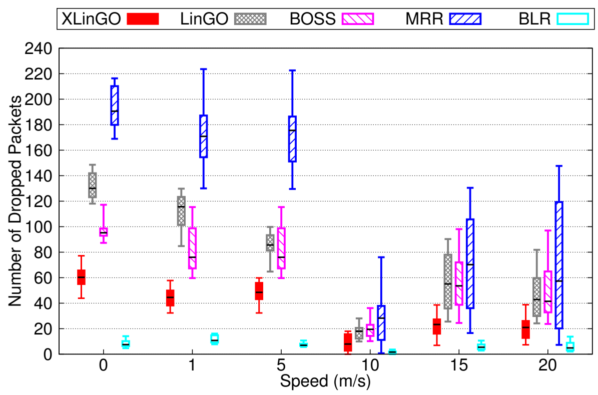

(b) Scenario Composed of 3 Multimedia SN

Figure 76: Number of Dropped Packets at Intermediate Buffers for a Scenario with Different Number of Multimedia Source Nodes and Moving Speeds

6.5.2.5 Signalling Overhead Evaluation under Conditions of Scenario 1

In this section, we analyse the signalling overhead introduced by each beaconless OR protocol for the experiments conducted for Section 6.5.2.4. For the signalling overhead evaluation, we counted the number of control messages required to transmit a given video flow. Figure 77 shows the number of control messages transmitted to deliver a given video flow via XLinGO, LinGO, BLR, BOSS, and MRR.

Persistent route creation may fail, and BLR defines a recovery strategy to deal with this situation, where the SN broadcasts a control packet and all of its neighbours reply with a control packet indicating their positions. Then, SN chooses the RN_i closer to the DN as the forwarder node F. On the other hand, LinGO and MRR do not include any control packet in the system, since they define a simple recovery strategy, where the SN must repeat the contention-based forwarding mode. Moreover, it is important to highlight that MRR includes an extra overhead and delay for a location update mechanism, because the nodes need to transmit control packets to find the DN's location. However, we implemented only the routing algorithm, because we consider a static DN. BOSS includes overhead, since it considers a tree-way handshake mechanisms in order to help the forwarding selection.

The proposed XLinGO protocol adds more control packets than LinGO, XLinGO, BLR, and MRR. This is because the XLinGO persistent route mode considers a recovery mechanism to detect and quickly react to route failures, where every node should continually assess whether the persistent route $P_{SN,DN}$ is still reliable or available to transmit packets, such as introduced in Section 5.4.2. In particular, after the SN has received a passive acknowledgment from F, it immediately sends subsequent video packets to the same destination by unicast to F until some of a given node detects that the $P_{SN,DN}$ is not reliable or does not exist anymore due to network changes or node mobility. Each forwarder that composes a given persistent route $P_{SN,DN}$ must acknowledge the reception of a set of w packets within a given window, and thus any node from $P_{SN,DN}$ must return to the contention-based forwarding mode to find a new reliable forwarder as soon as it detects that the link quality perceived by its forwarder is below $w(e_j)_{bad}$ or it does not receive any ACK message from its forwarder node within a certain period of time, i.e., $timeOut_{ack}$. Hence, the communication overhead to the persistent route mode introduced by our algorithm is dependent of the parameter w. It is important to highlight that although XLinGO introduces higher packet overhead, it provides the best video quality. Hence, we conclude that XLinGO provides the best trade-off between the video quality per unit of spent energy.

6.5.2.6 Subjective Video Quality Evaluation

In our subjective evaluation, 25 observers evaluated the videos, including undergraduate and postgraduate students as well as university staff. They had normal vision, and their age ranged from 18 to 45 years. We implemented a software to play the videos

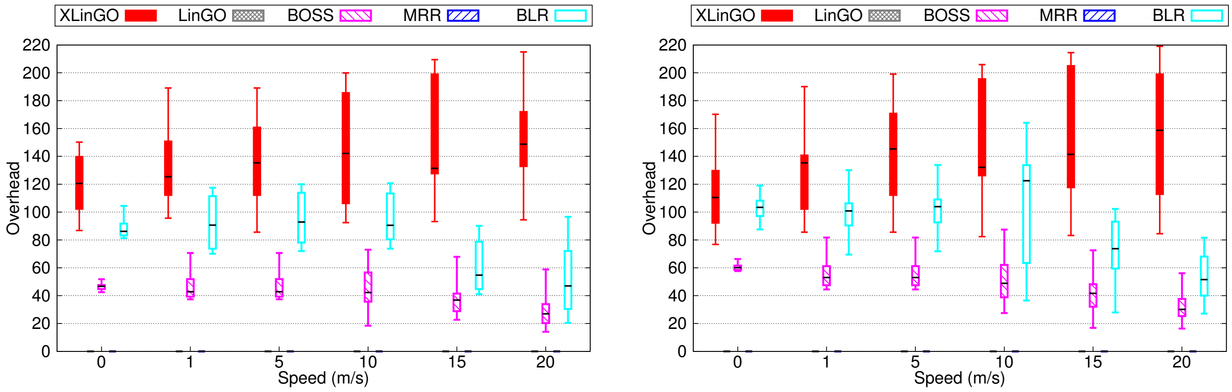

(a) Scenario with 2 multimedia source nodes

(b) Scenario with 3 multimedia source nodes

Figure 77: Signalling Overhead for a Scenario with Different Number of Multimedia Source Nodes and Moving Speeds

in a random order at the centre of the monitor against a neutral grey background, as recommended by ITU. The software runs on a Desktop PC Intel Core i5, 4GB RAM, and a 21" LCD monitor to display the video sequences for the observer to score them.

Figure 78 shows the subjective video quality evaluation by means of the MOS metric. Those results indicate that LinGO provides higher video quality compared to BLR and MRR in scenarios involving videos with similar motion and complexity. This is explained by the fact that BLR and MRR have a higher frame loss rate than LinGO. For instance, LinGO reduces the losses of I- and P-frames for Hall and Highway video sequences by up to 30%, since it relies on multiple metrics to establish a reliable virtual backbone protecting the frames of link error periods. Those issues increase the video quality level, as required in many multimedia FANET applications with QoE support.

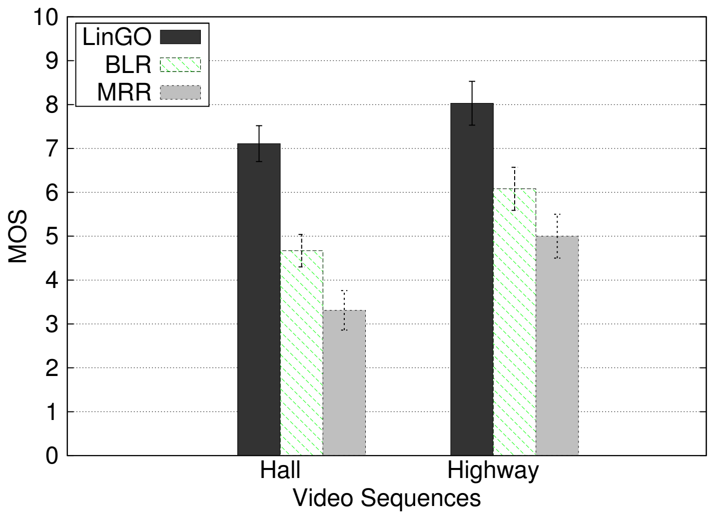

Figure 78: Subjective Video Quality Evaluation

We selected a random frame (i.e., Frame 143) from the UAV_1 video sequence transmitted by each protocol, to show the impact of transmitting video streams via XLinGO compared to LinGO, BLR, MRR, and BOSS from the standpoint of the end-user, as displayed in Figure 79. Frame number 143 is the moment when the church tower appears in the scene (as shown in Figure 79(a)).

This frame transmitted via XlinGO has the same quality compared to the original frame, as it can be seen in Figure 79(b), makes the benefits of XLinGO for video transmission evident. Moreover, apart from distortions in the frames transmitted via LinGO, BLR, MRR, and, BOSS, the buildings do not appear in the same position compared to the original frame (as it can be seen in Figure 79(c), 79(d), 79(e), and 79(f), respectively). This is because frame 143 was lost, and the decoder reconstructed it based on the previously received frames.

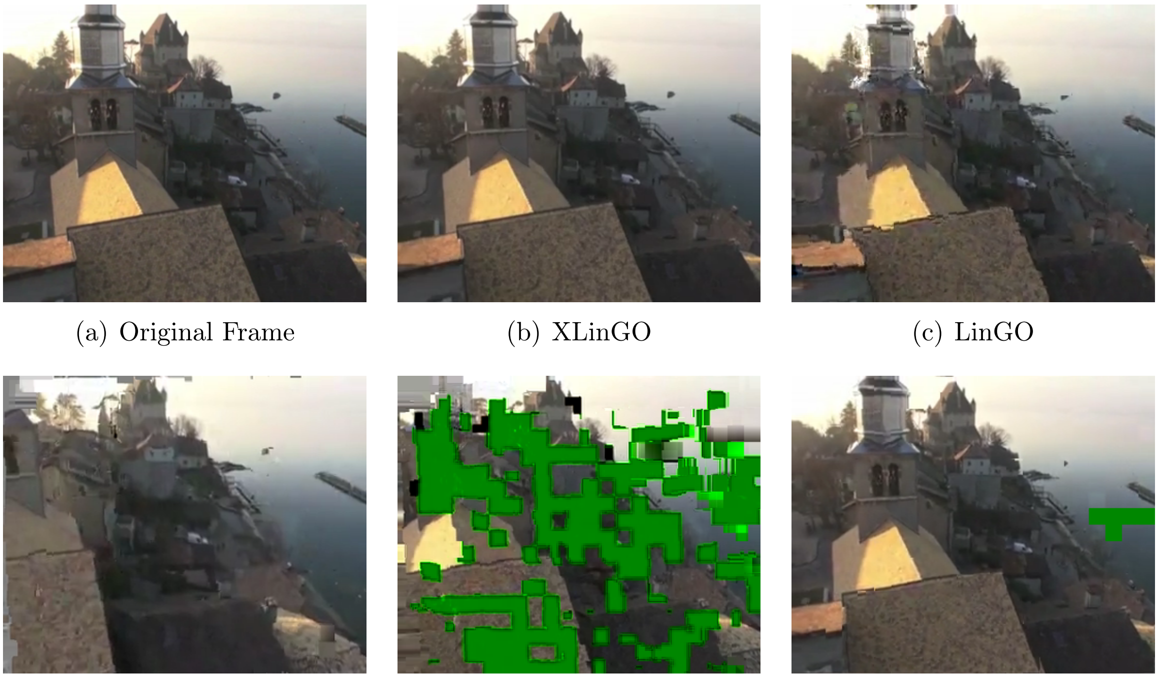

(a) Original Frame (b) XLinGO (c) LinGO

(d) BLR (e) MRR (f) BOSS

Figure 79: Frame Number 143 from UAV Video Sequence Transmitted from a Given Node via Different Beaconless OR for Scenario 2

Figure 80 shows the SSIM values for each frame of the UAV_1 video sequence for the selected videos in Figure 79. Let us analyse the quality level of frame 143 transmitted by different beaconless OR protocol, as depicted in Figure 79. Frame number 143 transmitted via XLinGO, LinGO, BLR, BOSS, and MRR has SSIM equal to 0.97, 0.69, 0.58, 0.61, and 0.29, respectively. First, these SSIM results can be attributed to the fact that the DN received frame number 143 transmitted via XlinGO correctly. Second, frame 143 is an I-frame, which was lost when transmitted through LinGO, BLR, BOSS, and MRR. Hence, there is a higher distortion for a long period, since the I-frame has more information to update the scene. Moreover, the distortion propagates in subsequent frames, because the decoder uses the I-frame as a reference frame for all the other frames within the GoP [51]. Error propagation explains the poor video quality for the entire video transmitted via LinGO, BLR, BOSS, and MRR. Third, the decoder uses Frame-Copy as an error concealment method, which means that the decoder must replace each lost frame with the last one that was correctly received. Hence, frame number 143 was reconstructed based on frame numbers 130, 120, 131, and 73 when transmitted via LinGO, BLR, BOSS, and MRR, respectively. This is because they are the last frames received correctly by the DN.

This result also helps us to illustrate the ability of XLinGO to deliver all video frames with quality level support. We can see that frames transmitted by XLinGO have similar and constant quality level compared to the baseline video quality level (original video). This is because XLinGO builds a reliable persistent route PSN, DN between SN and DN via multiple F by taking into account cross-layer multiple metrics for routing decision, namely energy, queue length, link quality, and geographical information. XLinGO also considers a recovery mechanism to deal with route failures and node mobility, providing a smoother operation in harsh environments and mobile networks, such as experienced in multimedia FANET scenarios. In addition, the video quality of frames transmitted by LinGO, BLR, BOSS, and MRR have a higher difference compared to the baseline video quality level.

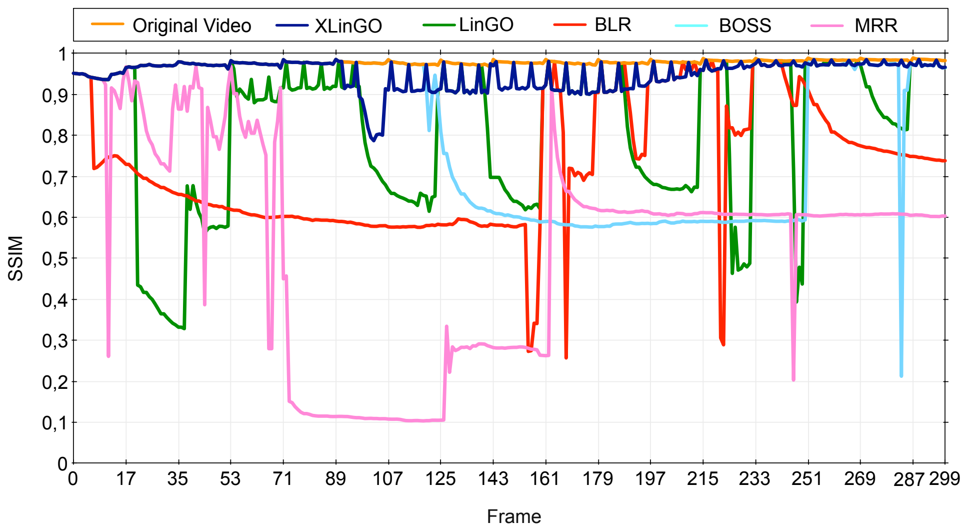

Figure 80: SSIM for All Frames for the Compose the UAV_1 Video Sequence Transmitted by a Specific SN

Figure 81 shows the overall SSIM value for the entire video from Figure 80. XLinGO, LinGO, BLR, BOSS, and MRR reduced the SSIM in 3%, 16%, 25%, 16, and 45%, respectively, compared to the benchmark video quality level. In addition, the SSIM for videos transmitted by LinGO, BLR, BOSS, and MRR is 13%, 23%, 13%, and 40% lower than XLinGO. Hence, we conclude that XLinGO enables simultaneous multiple video disseminations with QoE support.

6.5.3 Summary

From our performance evaluation analysis, we identified that LinGO, BLR, BOSS, and MRR perform poorly compared to XLinGO in a scenario composed of mobile nodes, multiple flows, and videos with different motion and complexity levels. This is because

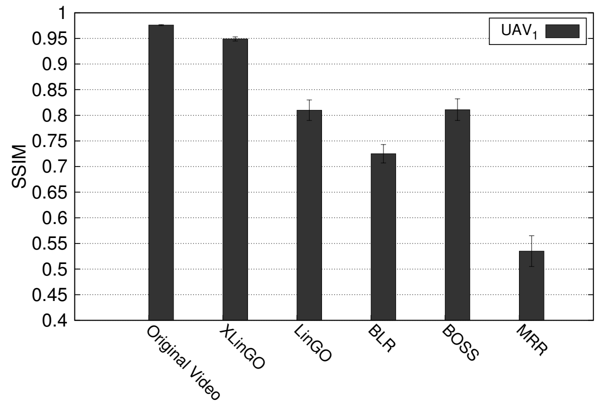

Figure 81: Overall Video Quality for the UAV_1 Video Sequences Transmitted by a Specific SN

XLinGO builds a reliable persistent route by combining link quality, geographical information and queue capacity. Hence, it selects forwarder nodes closer to DN with a reliable link, and enough queue size to forward packets with a reduced packet loss ratio. This performance is desirable for many FANET multimedia applications, such as safety & security, environmental monitoring, and natural disaster recovery. The results achieved are summarized in Table 13.

Table 13: Comparison Among Different Beaconless OR Protocols Based on Conducted Simulation Experiments

Algorithms	Reliability	Robustness	Overhead	QoE assurance
XLinGO	High	High	High	High
LinGO	High	Medium	None	Medium
BLR	Medium	Medium	Medium	Medium
BOSS	Medium	Medium	Medium	Medium
MRR	Low	Low	None	Low

6.6 Performance Evaluation Summary

In this thesis, we introduced contributions on different layers of the communication stack. At application layer, we introduce a QoE-aware packet redundancy mechanism to reduce the impact of the unreliable and lossy nature of wireless environment. At the network layer, we introduce two routing protocols, namely MEVI and XLinGO. Both protocols enable multimedia dissemination with energy-efficiency, robustness, scalability, reliability and QoE support. Based on the simulation results, we conclude that our proposals achieved our goal of how to provide multimedia distribution with high energy-efficiency, reliability, robustness, scalability, and QoE support over wireless ad-hoc networks.

The proposed redundancy mechanism achieves good results for both static and mobile wireless ad hoc networks, bringing many benefits for a resource constrained system to provide multimedia distribution with robustness and QoE support, as well as without increase the energy and bandwidth consumption. In addition, MEVI perform well for WMSN applications that is possible to rely on a fixed network infrastructure, where some static nodes are continuously monitoring physical scalar sensor data to predict an event occurrence, and another set of static nodes transmit multimedia data in case of event occurrence. This is because it relies on a hierarchical network architecture with heterogeneous nodes, as expected for many WMSN scenarios. Finally, XLinGO performs well for multimedia FANET applications, which can be deployed as soon as the fixed standard telecommunications infrastructure might be damaged or does not exist anymore, caused by natural disaster, such as Hurricane Sandy in New York/USA (2012), flooding in Rio de Janeiro/Brazil (2013) or any other disaster environments. This is because XLinGO does not require a stable end-to-end connection from the source to the destination, and thus packets are forwarded even during continuous topology changes.

CHAPTER 7

Conclusions and Outlook

The proliferation of multimedia content and the demand for new audio or video services have fostered the development of a new era based on multimedia information [15, 16], which allowed the evolution of WMSNs [4–7] and also FANETs [8–10]. Those networks enable a large class of scenarios in both civilian and military areas, which require visual and audio information, such as, environmental monitoring, intruder detection, video surveillance, safety & security, smart parking, traffic control, natural disaster recovery, smart cities, and other multimedia applications.

Multimedia content must be transmitted with QoE assurance to headquarters or IoT platforms for further processing and analysis, such as provided by the semantic system [11], sensor4cities [12,13], i-SCOPE [100], and other platforms. Hence, multimedia content has the potential to enhance the level of collected information compared to simple scalar data. For instance, it enables the end user or end system to take appropriate actions and be aware of the environmental conditions based on rich visual information.

In this context, live multimedia services require real-time video transmissions with a low frame loss rate, tolerable end-to-end delay, and jitter to support video dissemination with QoE support. Multimedia content should be delivered with, at least, a minimum video quality level from the user's point-of-view [21, 22]. Further, frames with different priorities compose a compressed video, and from a human's experience, the loss of high priority frames causes severe video distortions. Thus, a key principle in a QoE-aware approach is the transmission of high priority frames (protect them) with a minimum packet loss ratio, as well as network overhead.

Moreover, the routing service must find a set of reliable routes between the pair of source and destination nodes via multiple forwarding nodes with a minimal overhead. The protocol must prevent the selection of forwarding nodes with heavy traffic load or low residual energy. It also has to adapt to topology changes and be aware of QoE requirements in order to recover or maintain the video quality with acceptable level, providing reliability and robustness under scenarios with topology changes.

In the following, we describe the main challenges and contributions of this thesis in Section 7.1. In Section 7.2, we outline promising research topics for future work related to our contributions.

7.1 Main Contributions and Thesis Summary

In this thesis, we consider two classes of applications. The first class of applications consists of WMSN application that relies on fixed network infrastructure to accurately monitor physical scalar measurements, and also collect multimedia data in the case of an event occurrence [17–20]. The second class of applications consist of multimedia FANET [8–10] to explore, sense, and also send multimedia data from the hazardous area. Multimedia FANET can be deployed in case of a natural disaster, e.g., earthquake or hurricane, where the recovery process demands a rapid deployment of a communication system to monitor the hazard area that rescuers cannot reach easily. This is because the standard communication infrastructure might be damaged or does not work anymore.

The main research contributions of this thesis are driven by the research question how to provide multimedia distribution with high energy-efficiency, reliability, robustness, scalability, and QoE support over wireless ad-hoc networks. In this way, we address several problem domains with contributions on different layers of the communication stack. We studied application level redundancy schemes and routing protocols for multimedia distributions over wireless ad-hoc networks that make use of cross-layer multiple metrics for decision-making. As result, we proposed and designed two routing protocols and one application level redundancy mechanism. Their performance and behaviour for multimedia distribution with QoE support was evaluated by means of simulation experiments. Based on the simulation results, we conclude that our cross-layer optimizations for multimedia distribution over WMSN and multimedia FANETs achieved results that filled the goal of our initial research question.

In Chapter 2, we first investigate in a more depth way error correction schemes, application-level packet redundancy mechanisms, hierarchical routing protocols, and also OR protocols. More specifically, we describe their drawbacks to provide multimedia transmission with scalability, reliability, energy-efficiency, load balancing, and QoE support. First, we conclude that among the existing error control schemes to handle packet losses in real-time multimedia communication, application-level redundancy mechanisms offer a suitable approach to provide multimedia distribution with quality level assurance and robustness, as well as without adding delay and considering end-to-end reverse channel. However, existing redundancy mechanisms [57–63] add redundant packets in a black-box manner, i.e., without considering the frame importance from a user's perspective, which increases the overhead and the usage of scarce resources, such as battery and bandwidth.

Hierarchical network architectures with heterogeneous nodes have proven to be more beneficial than flat architectures in terms of lower energy consumption, greater functionality, better scalability, and reliability for WMSN applications that is possible to rely on a fixed network infrastructure. However, existing hierarchical routing protocols [64–76] should create clusters with low overhead, and also trigger multimedia transmissions only in case of event occurrence, which increases network lifetime. Moreover, node-disjoint multiple paths together with a route selection scheme that considers cross-layer end-to-end link quality estimation improves scalability, reliability, and energy-efficiency. Existing hierarchical routing protocols also do not consider a video-aware scheduling mechanism to protect priority frames in loss or link error periods.

Finally, routing protocols that rely on end-to-end routes or in a fixed network infrastructure might not be a feasible approach to forward the packets from the event area, as soon as the standard fixed network infrastructure is not available due to some natural disaster. In this way, beaconless OR appears as a promising routing scheme for multimedia FANET applications. This is because nodes do not need to proactively broadcast beacon messages to be aware of their neighbours, saving scarce resources, such as battery and bandwidth. However, existing beaconless OR protocols [59, 80–88] do not consider cross-layer multiple metrics to compute the DFD function in order to assure robust and reliable video dissemination. In addition, nodes might also deal with route failures, providing a smoother operation in harsh environments and mobile networks.

In Chapter 3, we discuss motivations towards an application-level packet redundancy mechanism. Hence, we introduced our proposed QoE-aware packet redundancy scheme [90, 91], which enables video dissemination with a similar video quality level compared to standard packet-level redundancy mechanisms. The proposed QoE-aware packet redundancy mechanism has a realistic assumption that not all packets are equal or have the same degree of importance, which are key parameters to reduce the number of redundant packets needed for the decoding process. More specifically, the proposed mechanism adds redundant packets depending on the frame type and the location of the P-frame within the GoPs. Based on simulation results described in Section 6.4, we conclude that our proposed QoE-aware redundancy mechanism protects priority frames during loss or link error periods, as well as achieves high resilience and reliability without wasting more bandwidth and energy. It also reduces the overhead compared with non-QoE redundancy mechanisms, which also minimizes the delay and energy consumption. Finally, the proposed redundancy mechanism achieves good results for both static and mobile wireless ad-hoc networks, bringing many benefits for a resource constrained system to provide multimedia distribution with robustness and QoE support without increase the consumption of scarce network resources, such as bandwidth and energy.

In Chapter 4, we discuss motivations towards a hierarchical routing protocol for WMSN composed of heterogeneous static nodes. The advantages of using a hierarchical architecture with heterogeneous nodes are as follows: i) nodes have different roles or functionalities to reduce energy consumption; ii) some nodes perform data aggregation, avoiding unnecessary data transmission; and iii) a set of nodes may turn-off the radio after transmitting their data packets, and as a result, reduce their energy consumption and avoid communication conflicts. In this context, we introduce the MEVI operation principles [95–97], which creates clusters with reduced overhead and find a set of reliable multiple paths to forward multimedia packets.

The MEVI behavior was evaluated in a serie of simulation experiments , and compared against well-known hierarchical routing protocols, namely PEMuR, LEACH, MEVI, as well as LEACH and MEVI variations, in a small and large scale scenarios. Based on the simulation results introduced in Section 6.3, we found that MEVI increases the network lifetime by at least 60% for small and large-scale scenarios compared to PEMuR, LEACH, MEVI, as well as LEACH and MEVI variations. In terms of scalability, MEVI is still able to deliver video for large-scale field sizes, unlike the related protocols that are not able to send video flows on a large-scale scale scenario. Simulation results also showed that MEVI provides multimedia distribution with a higher quality level compared to other approaches, i.e. it provides a SSIM gains of 10% and a VQM gains between 10% and 40%. This behavior is desirable for many WMSN applications that relies on fixed network infrastructure to accurately monitor physical scalar measurements, and also collect multimedia data in the case of an event occurrence, such as safety & security, environmental monitoring, smart parking, traffic control, and other smart cities applications.

In Chapter 5, we introduce our contributions towards a beaconless OR protocol for multimedia dissemination over multimedia FANET applications, the XLinGO protocol [108–111, 121, 122]. In contrast to MEVI, i.e., a routing protocol that relies on existing end-to-end routes, in XLinGO forwarding decisions are not taken by the sender of a packet, but in a completely distributed manner at the possible relay nodes. In XLinGO, the sender sends a packet not only to a single next-hop, but to multiple neighbours simultaneously. Afterwards, one or more of the receiving nodes forward the packet towards the destination, based on a coordination method to select the best candidate to forward packets. Hence, the routing mechanism forwards the packet towards the destination on a based on hop-by-hop routing decision at the receiver side. In other words, in XLinGO forwarding decisions are performed by the receiver of a packet based only on information contained in the packet, as well as in local information, such as node position and direction. In this context, the coordination method relies on a DFD calculation at the receiver side to select the forwarding node, i.e., the candidate node with best conditions compute the shortest DFD value, and thus such node transmits the packet faster, creating the persistent route. With the introduction of the XLinGO, we have targeted the designing of an efficient and reliable beaconless OR protocol for simultaneous multi-flow video transmissions. We found out that XLinGO must select forwarder nodes closer to the destination with a reliable link, as well as sufficient queue and energy capacity to forward packets from simultaneous multi-flows and mobile nodes with a reduced packet loss ratio. To achieve such performance, XLinGO takes multiple metrics into account to compute the DFD, including link quality, geographical information, remaining energy, and queue length. Furthermore, we found out that XLinGO with periodic route reconstruction, as soon as one of the forwarding nodes from a given route is no longer available to forward packets, a burst of packets might be lost until the protocol re-establishes the route, which reduces the video quality for longer periods. The route reconstruction interval should be adjusted according to the desired degree of robustness and energy consumption. From the energy consumption point-of-view, the persistent route reconstruction must occur with low frequency. From the robustness point-of-view, high frequency of route reconstruction provides better robustness. However, it is not trivial to find such value in order to provide robustness, QoE support, and reduced overhead. In this way, XLinGO relies on a recovery mechanism, which considers link quality and PRR to detect and quickly react to route failures, providing a smoother operation in harsh environments and mobile networks, such as experienced in multimedia FANET scenarios.

We evaluated XLinGO behaviour in a series of simulation experiments, and compared it against well-known beaconless OR protocols, namely BLR, MRR, BOSS, as well as XLinGO variation, in order to analyse the impacts and benefits for simultaneous multi-flow video dissemination for a scenario composed of mobile nodes and videos with different mobility and complexity levels. Based on simulation results described in Section 6.5, we identified that LinGO, BLR, BOSS, and MRR perform poorly compared to XLinGO in a scenario composed of mobile nodes, multiple flows, and videos with different motion and complexity levels. This performance is desirable for many multimedia FANET applications deployed in case of a natural disaster, where the standard communication infrastructure might be damaged or does not work anymore, such as safety & security, environmental monitoring, and natural disaster recovery.

We can summarize the main conclusions from the work performed in this thesis as follows. QoE-aware packet redundancy mechanisms achieve robust video distribution by transmitting redundant packets together with the original sequence, and thus when the original packet is lost, it can be recovered from redundant packets. Recovered packets help to reconstruct a corresponding video frame, which might be considered as a lost frame in a scenario that does not add redundant packets. Moreover, routing protocols that consider end-to-end routes may be appropriate for many scenarios, but also have significant shortcomings in others. The routing service must consider cross-layer multiple metrics for routing decision with the aims to provide the best trade-off between progress together with transmission reliability and load balancing. The routing service must also consider on a recovery mechanism to deal with route failures, providing a smoother operation in harsh environments and mobile networks. In this context, we proposed two routing protocols, MEVI and XLinGO. Both protocols provide multimedia transmissions with scalability, reliability and QoE support for small and large-scale and videos with different motion and complexity levels.

MEVI performs well for WMSN applications that are possible to rely on a fixed network infrastructure. For such application some static nodes are continuously monitoring physical scalar sensor data to predict an event occurrence, and another set of static node transmits multimedia data in case of event occurrence. In this way, MEVI relies on hierarchical network architecture with heterogeneous nodes and considers existing end-to-end routes to forward scalar or multimedia packets. On the other hand, XLinGO can be used as soon as the fixed standard telecommunications infrastructure might be damaged or does not exist anymore, and thus multimedia FANET applications can be deployed.

First, nodes are no longer required to transmit proactively beacon messages to announce themself, which saves network resources. The second advantage is that XLinGO relies on completely stateless forwarding decisions at receivers of a packet, where a sending node does not have to route packets towards an outdated network topology, and XLinGO proofs to be almost unaffected even by highest rate of topology changes. These two characteristics make XLinGO especially suited for multimedia FANETs with frequently changing topology.

7.2 Outlook

In the following, we briefly elaborate on possible future work in the field of routing protocols as studied in this thesis, as well as packet redundancy mechanisms. First of all, we evaluated the proposed QoE-aware redundancy mechanism with MEVI and XLinGO by means of simulation experiments. In order to fully evaluate the advantages and drawbacks of our contributions, testbed experiments and long-term real-world deployment in the two classes of applications considered in this thesis can be applied to outline advantages and drawbacks, but also to provide further potential improvements. For testbed experiments, we can use the Testbed Management Architecture (TARWIS) infrastructure [152], which has been developed by University of Bern. TARWIS enables to schedule and control experiments via a user-friendly web interface and to provide experiment data for testbed evaluations. All sensors are controlled via dedicated mesh nodes running an embedded Linux version called ADAM, which is tailored to resource-constrained devices. In addition, we can also propose an analytical model for XLinGO and MEVI in order to provide more insight about their performance benefit.

The QoE-aware redundancy mechanism introduced in Chapter 3 adds redundant packets based on frame importance. However, it can be extended to add redundant packets based on a utility function that combines sensing relevance and frame importance. This is because source nodes may have different sensing relevance based on application requirements, e.g., a sensor node capturing video flows closer to the event area has higher sensing relevance than other nodes, since it generates more accurate and detailed video information. Hence, sensing relevance of source nodes can be exploited to assure transmission with high reliability for the most relevant sources based on application requirements. For instance, video packets from low-relevant source nodes can be transmitted without redundancy or with lower packet redundancy. In this way, we can save energy and bandwidth over the network with potential low impact to the overall monitoring quality, since corruptions of low-relevant nodes might have low impact based on the user perspective. In addition, we can adaptive the amount of redundant packets by considering sensing relevance, frame importance, and path quality. More specifically, the sender calculates the appropriate amount of packet redundancy for different video frame types to avoid network congestion and the unnecessary packet redundancy when the sender transmits video streaming to the receiver over wireless networks.

XLinGO must consider the link expiration time estimation, position prediction, and moving direction in a 3D plane for routing decision. In this way, we avoid the selection of a forwarder node that is moving in opposite direction in a 3D plane than its previous hop, which avoids loops and prevents suboptimal routing. We also enhance the nodes connectivity in XLinGO for multimedia FANET in 3D environments by adding link expiration time estimation, position prediction, and moving direction to compute the DFD, offering a higher packet delivery rate and higher video quality level.

We consider that several issues need to be studied and understood in order to extend MEVI and XLinGO by taking into consideration the characteristics and requirements of human centric multimedia network systems, such as human-centric schemes, video characteristics, and context-awareness for decision making. For instance, online QoE assessment and user experience can be measured and integrated into MEVI and XLinGO protocols, in order to support routing decisions to improve the user satisfaction on watching real-time video flows.

References

[1] L. Zhou and H.-C. Chao, "Multimedia Traffic Security Architecture for the Internet of Things," *IEEE Network*, vol. 25, no. 3, pp. 35–40, 2011.

[2] L. Atzori, A. Iera, and G. Morabito, "The Internet of Things: A Survey," *Computer Networks*, vol. 54, no. 15, pp. 2787–2805, 2010.

[3] J. M. Jornet and I. F. Akyildiz, "The Internet of Multimedia Nano-Things," *Nano Communication Networks*, vol. 3, no. 4, pp. 242–251, 2012.

[4] I. Almalkawi, M. Guerrero Zapata, J. Al-Karaki, and J. Morillo-Pozo, "Wireless Multimedia Sensor Networks: Current Trends and Future Directions," *Sensors (Basel)*, vol. 10, no. 7, pp. 6662–6717, 2010.

[5] I. Akyildiz, T. Melodia, and K. Chowdhury, "A survey on wireless multimedia sensor networks," *Computer Networks*, vol. 51, no. 4, pp. 921–960, 2007.

[6] ——, "Wireless Multimedia Sensor Networks: Applications and Testbeds," *Proceedings of the IEEE*, vol. 96, no. 10, pp. 1588–1605, 2008.

[7] D. Costa and L. Guedes, "A Survey on Multimedia-based Cross-layer Optimization in Visual Sensor Networks," *Sensors (MDPI)*, vol. 11, no. 5, pp. 5439–5468, 2011.

[8] İ. Bekmezci, O. K. Sahingoz, and Ş. Temel, "Flying Ad-Hoc Networks (FANETs): A survey ," *Ad Hoc Networks*, vol. 11, no. 3, pp. 1254–1270, 2013.

[9] S. Morgenthaler, T. Braun, Z. Zhao, T. Staub, and M. Anwander, "UAVNet: A mobile wireless mesh network using Unmanned Aerial Vehicles," in *Proceedings of the 3rd International Workshop on Wireless Networking and Control for Unmanned Autonomous Vehicles (Wi-UAV'12)*. Anaheim, USA: IEEE, Dec. 2012, pp. 1603–1608.

[10] A. Shaw and K. Mohseni, "A Fluid Dynamic Based Coordination of a Wireless Sensor Network of Unmanned Aerial Vehicles: 3D Simulation and Wireless Communication Characterization," *IEEE Sensors Journal*, vol. 11, no. 3, pp. 722–736, 2011.

[11] E. Macias, J. Lloret, A. Suarez, and M. Garcia, "Architecture and Protocol of a Semantic System Designed for Video Tagging with Sensor Data in Mobile Devices," *Sensors*, vol. 12, no. 2, pp. 2062–2087, 2012.

[12] P. Lima, T. Fonseca, D. Rosário, K. Machado, and E. Cerqueira, "Monitoramento Ambiental Através de Redes de Sensores Sem Fio e Redes Sociais," in *Proceedings of the Salão de Ferramentas of the 30th Brazilian Symposium on Computer Networks and Distributed Systems (SBRC'12).* Ouro Preto, Brazil: SBC, May 2012, pp. 938–945.

[13] D. Rosário, P. Lima, K. Machado, E. Cerqueira, Z. Zhao, and T. Braun, "Demo Abstract: Disseminating WMSN Data by Using Social Network and Web," in *Proceedings of the 10th European Conference on Wireless Sensor Networks (EWSN'13)*, Ghent, Belgium, Feb. 2013.

[14] O. Penha and E. Nakamura, "Fusing Light and Temperature Data for Fire Detection," in *Proceedings of the IEEE Symposium on Computers and Communications (ISCC'10).* Riccione, Italy: IEEE, Jun. 2010, pp. 107–112.

[15] D. Rosário, K. Machado, A. Abelém, D. Monteiro, and E. Cerqueira, *Recent Advances and Challenges in Wireless Multimedia Sensor Networks*, ser. Mobile Multimedia - User and Technology Perspectives. Dian Tjondronegoro (Ed.): InTech, Jan. 2012, pp. 74–96.

[16] E. Cerqueira, A. Santos, D. Rosário, T. Braun, and M. Gerla, *Multimedia Human-Centric Networking: Concepts, Technologies and Trends*, ser. Tutorials of the 32th Brazilian Symposium on Computer Networks and Distributed Systems (SBRC'14). Carlos Maziero (Ed.): SBC, May 2014.

[17] M. Pechoto, J. Ueyama, and J. de Alburqueque, "E-noé: Rede de Sensores Sem Fio para Monitorar Rios Urbanos," in *Proceedings of the Congresso Brasileiro Sobre Desastres Naturais.* Rio Claro, Brazil: SBC, May 2012.

[18] D. Hughes, J. Ueyama, E. Mendiondo, N. Matthys, W. Horré, S. Michiels, C. Huygens, W. Joosen, K. Man, and S.-U. Guan, "A Middleware Platform to Support River Monitoring Using Wireless Sensor Networks," *Journal of the Brazilian Computer Society*, vol. 17, no. 2, pp. 85–102, 2011.

[19] Libelium, "Smart Water: Wireless Sensor Networks to Detect Floods and Respond," [OnLine] Available: http://www.libelium.com/smart_water_wsn_flood_detection/. (Access date: Jun. 2014).

[20] A. Jamakovic, D. Dimitrova, M. Anwander, T. Macicas, T. Braun, J. Schwanbeck, T. Staub, and B. Nyffenegger, "Real-World Energy Measurements of a Wireless Mesh Network," in *Proceedings of the Energy Efficiency in Large Scale Distributed Systems Conference.* Vienna, Austria: Springer, Apr. 2013, pp. 218–232.

[21] R. Serral-Gracià, E. Cerqueira, M. Curado, M. Yannuzzi, E. Monteiro, and X. Masip-Bruin, "An Overview of Quality of Experience Measurement Challenges for Video Applications in IP Networks," in *Wired/Wireless Internet Communications*, ser. Lecture Notes in Computer Science, E. Osipov, A. Kassler, T. Bohnert, and X. Masip-Bruin, Eds. Springer Berlin Heidelberg, 2010, vol. 6074, pp. 252–263.

[22] S. Ickin, K. Wac, M. Fiedler, L. Janowski, J.-H. Hong, and A. Dey, "Factors Influencing Quality of Experience of Commonly Used Mobile Applications," *Communications Magazine*, vol. 50, no. 4, pp. 48–56, 2012.

[23] N. Baccour, A. Koubâa, C. Noda, H. Fotouhi, M. Alves, H. Youssef, M. Zúñiga, C. Boano, K. Römer, D. Puccinelli, T. Voigt, and L. Mottola, *Radio Link Quality Estimation in Low-Power Wireless Networks.* Springer, 2013.

[24] A. Avizienis, J.-C. Laprie, B. Randell, and C. Landwehr, "Basic Concepts and Taxonomy of Dependable and Secure Computing," *Dependable and Secure Computing, IEEE Transactions on*, vol. 1, no. 1, pp. 11–33, 2004.

[25] S. Ehsan and B. Hamdaoui, "A Survey on Energy-Efficient Routing Techniques with QoS Assurances for Wireless Multimedia Sensor Networks," *IEEE Communications Surveys & Tutorials*, vol. 14, no. 2, pp. 265 – 278, 2012.

[26] M. Radi, B. Dezfouli, K. Bakar, and M. Lee, "Multipath Routing in Wireless Sensor Networks: Survey and Research Challenges," *Sensors (MDPI)*, vol. 12, no. 1, pp. 650–685, 2012.

[27] D. Macedo, L. Correia, A. Santos, A. Loureiro, and J. Nogueira, "A Rule-based Adaptive Routing Protocol for Continuous Data Dissemination in WSNs," *Journal of Parallel and Distributed Computing*, vol. 66, no. 4, pp. 542–555, 2006.

[28] M. Naderi, H. Rabiee, M. Khansari, and M. Salehi, "Error control for Multimedia Communications in Wireless Sensor Networks: A Comparative Performance Analysis," *Ad Hoc Networks*, vol. 10, no. 6, pp. 1028–1042, 2012.

[29] A. Abu-Baker, H. Huang, E. Johnson, and S. Misra, "Green Diffusion: Data Dissemination in Sensor Networks Using Solar Power," in *Proceedings of the IEEE Consumer Communications and Networking Conference (CCNC'11).* Las Vegas, USA: IEEE, Jan. 2011, pp. 803–807.

[30] J. Solobera, "Libelium Technologies Incorporated - Detecting Forest Fires using Wireless Sensor Networks with Waspmotes," [OnLine] Available: http://www.libelium.com/libeliumworld/articles/101031032811. (Access date: Jun. 2014).

[31] D. Costa and L. Guedes, "Exploiting the Sensing Relevancies of Source Nodes for Optimizations in Visual Sensor Networks," *Multimedia Tools and Applications*, vol. 64, no. 3, pp. 549–579, 2013.

[32] H. Park, J. Lee, S. Oh, Y. Yim, S.-H. Kim, and K.-D. Nam, "Quality-based Event Reliability Protocol in Wireless Sensor Networks," in *Proceedings of the IEEE Consumer Communications and Networking Conference (CCNC'11).* Las Vegas, USA: IEEE, Jan. 2011, pp. 730–734.

[33] V. Adzic, H. Kalva, and B. Furht, "A Survey of Multimedia Content Adaptation for Mobile Devices," *Multimedia Tools and Applications*, vol. 51, no. 1, pp. 379–396, 2011.

[34] X. Qiu, H. Liu, D. Ghosal, B. Mukherjee, J. Benko, W. Li, and R. Bajaj, "Enhancing the Performance of Video Streaming in Wireless Mesh Networks," *Wireless Personal Communications*, vol. 56, no. 3, pp. 535–557, 2011.

[35] Y. Andreopoulos, N. Mastronarde, and M. van der Schaar, “Cross-layer Optimized Video Streaming over Wireless Multihop Mesh Networks,” *IEEE Journal on Selected Areas in Communications*, vol. 24, no. 11, pp. 2104–2115, 2006.

[36] M. Lindeberg, S. Kristiansen, T. Plagemann, and V. Goebel, “Challenges and Techniques for Video Streaming over Mobile Ad hoc Networks,” *Multimedia Systems*, vol. 17, no. 1, pp. 51–82, 2011.

[37] C. Ververidis, J. Riihijarvi, and P. Mahonen, “Evaluation of Quality of Experience for Video Streaming over Dynamic Spectrum Access Systems,” in *Proceedings of the IEEE International Symposium on a World of Wireless Mobile and Multimedia Networks (WoWMoM'10)*. Montreal, Canada: IEEE, Jun. 2010, pp. 1–8.

[38] D. Rosário, E. Cerqueira, A. Neto, A. Riker, R. Immich, and M. Curado, “A QoE Handover Architecture for Converged Heterogeneous Wireless Networks,” *Wireless Networks (winet)*, vol. 19, no. 8, pp. 2005–2020, 2013.

[39] H. Wu and A. A. Abouzeid, “Error Resilient Image Transport in Wireless Sensor Networks,” *Computer Networks*, vol. 50, no. 15, pp. 2873–2887, 2006.

[40] L. Hanzo, P. Cherriman, and J. Streit, “Video compression and communications,” *IEEE Press*, 2007.

[41] D. Rodrigues, E. Cerqueira, and E. Monteiro, “Quality of Experience Adaptation Controllers for Voice and Video in Wireless Networks,” in *Wired/Wireless Internet Communications*. Springer, 2011, pp. 350–361.

[42] D. Le Gall, “MPEG: A Video Compression Standard for Multimedia Applications,” *Communications of the ACM*, vol. 34, no. 4, pp. 46–58, 1991.

[43] G. Gualdi, A. Prati, and R. Cucchiara, “Video streaming for mobile video surveillance,” *IEEE Transactions on Multimedia*, vol. 10, no. 6, pp. 1142–1154, 2008.

[44] Y. Xu, “Optimising Video Streaming Over Multi-hop Wireless Networks: A Queueing Model Analytical Approach,” Ph.D. dissertation, University of Otago, 2013.

[45] J. Greengrass, J. Evans, and A. Begen, “Not All Packets are Equal, Part I: Streaming Video Coding and SLA Requirements,” *IEEE Internet Computing*, vol. 13, no. 1, pp. 70–75, 2009.

[46] D. J. L. Gall, “The MPEG video compression algorithm,” *Signal Processing: Image Communication*, vol. 4, no. 2, pp. 129–140, 1992.

[47] J. Watkinson, *The MPEG handbook*. Taylor & Francis US, 2004.

[48] V. T. Library, “YUV Video Sequences,” [online] http://trace.eas.asu.edu/yuv/ (accessed date: Jun. 2014).

[49] E. Aguiar, A. Riker, M. Mu, S. Zeadally, E. Cerqueira, and A. Abelem, “Real-time QoE Prediction for Multimedia Applications in Wireless Mesh Networks,” in *Proceedings of the 4th IEEE International Workshop on Future Multimidia Networking (FMN 2012)*. Las Vegas, USA: IEEE, Jan. 2012, pp. 592–596.

[50] E. Aguiar, B. Pinheiro, J. a. Figueirêdo, E. Cerqueira, A. Abelém, and R. Gomes, *Trends and Challenges for Quality of Service and Quality of Experience for Wireless Mesh Networks*, ser. Wireless Mesh Networks. Nobuo Funabiki (Ed.): InTech, 2011, pp. 127–148.

[51] E. Aguiar, A. Riker, A. Abelém, E. Cerqueira, and M. Mu, "Video Quality Estimator for Wireless Mesh Networks," in *Proceedings of the 20th International Workshop on Quality of Service (IWQoS'12)*. Coimbra, Portugal: IEEE, Jun. 2012, pp. 1–9.

[52] R. Immich, E. Cerqueira, and M. Curado, "Adaptive Video-aware FEC-based Mechanism with Unequal Error Protection Scheme," in *Proceedings of the 28th Annual ACM Symposium on Applied Computing (SAC'13)*. Coimbra, Portugal: ACM, Mar. 2013, pp. 981–988.

[53] J. Greengrass, J. Evans, and A. C. Begen, "Not All Packets are Equal, Part 2: The Impact of Network Packet Loss on Video Quality," *IEEE Internet Computing*, vol. 13, no. 2, pp. 74–82, 2009.

[54] C. Zhang, J. Zhang, G. Wei, and P. Ren, "An Efficient Cooperative ARQ Protocol for Wireless Relay Networks," *Computer Communications*, vol. 36, no. 1, pp. 105–112, 2012.

[55] P. Hurni and T. Braun, "Link-Quality Aware Run-Time Adaptive Forward Error Correction Strategies in Wireless Sensor Networks," IAM, University of Bern, IAM-11-003, Tech. Rep., 2011.

[56] M. van der Schaar, S. Krishnamachari, S. Choi, and X. Xu, "Adaptive Cross-layer Protection Strategies for Robust Scalable Video Transmission over 802.11 WLANs," *IEEE Journal on Selected Areas in Communications*, vol. 21, no. 10, pp. 1752–1763, 2003.

[57] P. Sarisaray-Boluk, V. C. Gungor, S. Baydere, and A. E. Harmanci, "Quality Aware Image Transmission over Underwater Multimedia Sensor Networks," *Ad Hoc Networks*, vol. 9, no. 7, pp. 1287–1301, 2011.

[58] Y. Yang, Y. Chen, and W. Yi, "Cross-layer FEC for Reliable Transfer of Variable-length Coded Data in WMSNs," *IET Conference Proceedings*, pp. 380–384(4), 2010.

[59] M. Chen, V. Leung, S. Mao, and Y. Yuan, "Directional Geographical Routing for Real-time Video Communications in Wireless Sensor Networks," *Computer Communications*, vol. 30, no. 17, pp. 3368–3383, 2007.

[60] L. Rizzo, "Effective erasure codes for reliable computer communication protocols," *ACM SIGCOMM Computer Communication Review*, vol. 27, no. 2, pp. 24–36, 1997.

[61] D. Costa, L. Guedes, F. Vasques, and P. Portugal, "Redundancy-Based Semi-Reliable Packet Transmission in Wireless Visual Sensor Networks Exploiting the Sensing Relevancies of Source Nodes," *WSEAS Transactions on Communications*, vol. 12, no. 9, pp. 468–478, 2013.

[62] M.-F. Tsai, C.-K. Shieh, T.-C. Huang, and D.-J. Deng, "Forward-Looking Forward Error Correction Mechanism for Video Streaming over Wireless Networks," *IEEE Systems Journal*, vol. 5, no. 4, pp. 460–473, 2011.

[63] M.-F. Tsai, T.-C. Huang, C.-H. Ke, C.-K. Shieh, and W.-S. Hwang, "Adaptive Hybrid Error Correction Model for Video Streaming over Wireless Networks," *Multimedia systems*, vol. 17, no. 4, pp. 327–340, 2011.

[64] W. Heinzelman, A. Chandrakasan, and H. Balakrishnan, "Energy-efficient Communication Protocol for Wireless Microsensor Networks," in *Proceedings of the 33rd Annual Hawaii International Conference on System Sciences*. Hawaii, USA: IEEE, Nov. 2000, pp. 10–pp.

[65] D. Kandris, M. Tsagkaropoulos, I. Politis, A. Tzes, and S. Kotsopoulos, "Energy Efficient and Perceived QoS Aware Video Routing over Wireless Multimedia Sensor Networks," *Ad Hoc Networks*, vol. 9, no. 4, pp. 591– 607, 2011.

[66] D. Kandris, P. Tsioumas, A. Tzes, G. Nikolakopoulos, and D. Vergados, "Power Conservation Through Energy Efficient Routing in Wireless Sensor Networks," *Sensors*, vol. 9, no. 9, pp. 7320–7342, 2009.

[67] K. Lin, M. Chen, and X. Ge, "Adaptive Reliable Routing Based on Cluster Hierarchy for Wireless Multimedia Sensor Networks," *EURASIP Journal on Wireless Communications and Networking*, vol. 2010, p. 3, 2010.

[68] K. Lin, J. Rodrigues, H. Ge, N. Xiong, and X. Liang, "Energy Efficiency QoS Assurance Routing in Wireless Multimedia Sensor Networks," *IEEE Systems Journal*, vol. 5, no. 4, pp. 495–505, 2011.

[69] A. Lari and B. Akbari, "Network-adaptive Multipath Video Delivery over Wireless Multimedia Sensor Networks based on Packet and Path Priority Scheduling," in *Proceedings of the International Conference on Broadband, Wireless Computing, Communication and Applications (BWCCA'10)*. Fukuoka, Japan: IEEE, Nov. 2010, pp. 351–356.

[70] A. Jayashree, G. Biradar, and V. Mytri, "Energy Efficient Prioritized Multipath QoS Routing Over WMSN," *International Journal of Computer Applications*, vol. 46, no. 17, pp. 33 – 39, 2012.

[71] I. Politis, M. Tsagkaropoulos, T. Dagiuklas, and S. Kotsopoulos, "Power Efficient video Multipath Transmission over Wireless Multimedia Sensor Networks," *Mobile Networks and Applications*, vol. 13, no. 3-4, pp. 274–284, 2008.

[72] Y. Sun, H. Ma, L. Liu, and Y. Zheng, "ASAR: An Ant-based Service-aware Routing Algorithm for Multimedia Sensor Networks," *Frontiers of Electrical and Electronic Engineering in China*, vol. 3, no. 1, pp. 25–33, 2008.

[73] L. Cobo, A. Quintero, and S. Pierre, "Ant-based Routing for Wireless Multimedia Sensor Networks Using Multiple QoS Metrics," *Computer networks*, vol. 54, no. 17, pp. 2991–3010, 2010.

[74] M. Heissenbüttel, T. Braun, D. Jörg, and T. Huber, "A Framework for Routing in Large Ad-Hoc Networks with Irregular Topologies," in *Proceedings of the Fourth Annual Mediterranean Ad Hoc Networking Workshop (Med-Hoc-Net'05)*. Porquerolles, France: Springer, Jun. 2005, pp. 119–128.

[75] M. Heissenbüttel, T. Braun, T. Huber, and D. Jörg, "Routing in Large Wireless Multihop Networks with Irregular Topologies," in *Proceedings of the 5th Scandinavian Workshop on Wireless Ad-hoc Networks (ADHOC'05*. Stockholm, Sweden: IEEE, May. 2005, pp. 1–5.

[76] M. Heissenbüttel and T. Braun, "Ants-Based Routing in Large Scale Mobile Ad-Hoc Networks," in *Proceedings of the 5th Kommunikation in verteilten Systemen (KiVS'03)*. Leipzig, Germany: IEEE, Feb. 2003, pp. 91–99.

[77] X. Mao, S. Tang, X. Xu, X.-Y. Li, and H. Ma, "Energy-efficient Opportunistic Routing in Wireless Sensor Networks," *IEEE Transactions on Parallel and Distributed Systems*, vol. 22, no. 11, pp. 1934–1942, 2011.

[78] M. Lu, P. Steenkiste, and T. Chen, "Video Transmission over Wireless Multihop Networks Using Opportunistic Routing," in *Proceedings of the Packet Video*. Lausanne, Switzerland: IEEE, Nov. 2007, pp. 52–61.

[79] H. Seferoglu and A. Markopoulou, "Video-aware Opportunistic Network Coding over Wireless Networks," *IEEE Journal on Selected Areas in Communications*, vol. 27, no. 5, pp. 713–728, Jun. 2009.

[80] M. Heissenbüttel, T. Braun, T. Bernoulli, and M. Wälchli, "BLR: Beacon-less Routing Algorithm for Mobile Ad Hoc Networks," *Computer communications*, vol. 27, no. 11, pp. 1076–1086, 2004.

[81] T. Braun, M. Heissenbüttel, and T. Roth, "Performance of the Beacon-less Routing Protocol in Realistic Scenarios," *Ad Hoc Network*, vol. 8, no. 1, pp. 96–107, jan. 2010.

[82] M. Heissenbüttel, T. Braun, M. Wälchli, and T. Bernoulli, "Optimized Stateless Broadcasting in Wireless Multi-Hop Networks," in *Proceedings of the Annual IEEE International Conference on Computer Communications (INFOCOM'06)*. Barcelona, Spain: IEEE, Mar. 2006, pp. 1–6.

[83] J. A. Sanchez, R. Marin-Perez, and P. M. Ruiz, "BOSS: Beacon-less On Demand Strategy for Geographic Routing inWireless Sensor Networks," in *Proceedings of theIEEE Internatonal Conference on Mobile Adhoc and Sensor Systems (MASS'07)*. Pisa, Italy: IEEE, Jun. 2007, pp. 1–10.

[84] J. Sanchez, P. Ruiz, and R. Marin-Perez, "Beacon-less Geographic Routing Made Practical: Challenges, Design Guidelines, and Protocols," *IEEE Communications Magazine*, vol. 47, no. 8, pp. 85–91, 2009.

[85] H. Zhang and H. Shen, "Energy-efficient Beaconless Geographic Routing in Wireless Sensor Networks," *IEEE Transactions on Parallel and Distributed Systems*, vol. 21, no. 6, pp. 881–896, 2010.

[86] P. Spachos and D. Hatzinakos, "Data Relevance Dynamic Routing Protocol for Wireless Visual Sensor Networks," in *Proceedings of the 18th International Conference on Digital Signal Processing (DSP'13)*. Santorini, Greece: IEEE, Jul. 2013, pp. 1–6.

[87] M. Al-Otaibi, H. Soliman, and J. Zheng, "A Multipath Routeless Routing Protocol with an Efficient Location Update Mechanism," *International Journal of Internet Protocol Technology*, vol. 6, no. 1/2, pp. 75–82, 2011.

[88] M. Al-Otaibi and H. Soliman, "Efficient Geographic Routeless Routing Protocols with Enhanced Location Update Mechanism," *International Journal of Sensor Networks*, vol. 8, no. 3/4, pp. 160–171, 2010.

[89] N. Baccour, A. Koubâa, L. Mottola, M. A. Zúñiga, H. Youssef, C. A. Boano, and M. Alves, "Radio Link Quality Estimation in Wireless Sensor Networks: A Survey," *ACM Transactions on Sensor Networks (TOSN)*, vol. 8, no. 4, pp. 34:1–34:33, sep 2012.

[90] Z. Zhao, T. Braun, D. Rosário, E. Cerqueira, R. Immich, and M. Curado, "QoE-aware FEC Mechanism for Intrusion Detection in Multi-tier Wireless Multimedia Sensor Networks," in *Proceedings of the 1st International Workshop on Wireless Multimedia Sensor Networks (WiMob'12 WS-WMSN)*. Barcelona, Spain: IEEE, Oct. 2012, pp. 697–704.

[91] D. Rosário, Z. Zhao, T. Braun, and E. Cerqueira, "A Cross-layer QoE-based Approach for Event-Based Multi-tier Wireless Multimedia Sensor Networks," *Submitted*, 2014.

[92] L. Biard and D. Noguet, "Reed-Solomon Codes for Low Power Communications," *Journal of Communications*, vol. 3, no. 2, pp. 13–21, 2008.

[93] J.-S. Ahn, J.-H. Yoon, and K.-W. Lee, "Performance and Energy Consumption Analysis of 802.11 with FEC Codes over Wireless Sensor Networks," *Communications and Networks, Journal of*, vol. 9, no. 3, pp. 265–273, 2007.

[94] E. Aguiar, A. Riker, E. Cerqueira, A. Abelém, M. Mu, T. Braun, M. Curado, and S. Zeadally, "A Real-time Video Quality Estimator for Emerging Wireless Multimedia Systems," *Wireless Networks*, pp. 1–18, 2014.

[95] D. Rosário, R. Costa, H. Paraense, K. Machado, E. Cerqueira, and T. Braun, "A Smart Multi-Hop Hierarchical Routing Protocol for Efficient Video Communication over Wireless Multimedia Sensor Network," in *Proceedings of the 2nd IEEE International Workshop on Smart Communication Protocols and Algorithms (ICC'12 WS-SCPA)*. Ottawa, Canada: IEEE, Jun. 2012, pp. 8113–8117.

[96] D. Rosário, R. Costa, H. Paraense, K. Machado, E. Cerqueira, T. Braun, and Z. Zhao, "A Hierarchical Multi-hop Multimedia Routing Protocol for Wireless Multimedia Sensor Networks," *Network Protocols and Algorithms (NPA)*, vol. 4, no. 2, pp. 44–64, 2012.

[97] D. Rosário, R. Costa, A. Santos, T. Braun, and E. Cerqueira, "QoE-aware Multiple Path Video Transmission for Wireless Multimedia Sensor Networks," in *Proceedings of the 31th Brazilian Symposium on Computer Networks and Distributed Systems (SBRC'13)*. Brasilia, Brazil: SBC, May 2013, pp. 31–44.

[98] K. Machado, D. Rosário, E. Nakamura, A. Abelém, and E. Cerqueira, "Design of a Routing Protocol using Remaining Energy and Link Quality Indicator (REL)," in *Proceedings of the 6th Latin America Networking Conference (LANC'11)*. Quito, Equator: ACM, Jun. 2011, pp. 33–39.

[99] K. Machado, D. Rosário, E. Cerqueira, A. A. Loureiro, A. Neto, and J. N. de Souza, "A Routing Protocol Based on Energy and Link Quality for Internet of Things Applications," *Sensors (Basel)*, vol. 13, no. 2, pp. 1942–1964, 2013.

[100] i SCOPE, "i-SCOPE - Interoperable Smart City service Thought an Open Source Platform for Urban Ecosystems," [OnLine] Available: http://www.iscopeproject.net/. (Access date: Jun. 2014).

[101] J.-O. Fajardo, F. Liberal, I.-H. Mkwawa, L. Sun, and H. Koumaras, "QoE-driven Dynamic Management Proposals for 3G VoIP Services," *Computer Communications*, vol. 33, no. 14, pp. 1707–1724, 2010.

[102] E. Gürses and Ö. B. Akan, "Multimedia Communication in Wireless Sensor Networks," *Annales des télécommunications*, vol. 60, no. 7-8, pp. 872–900, 2005.

[103] N. Baccour, A. Koubâa, M. Jamâa, D. Rosário, H. Youssef, M. Alves, and L. Becker, "RadiaLE: a Framework for Designing and Assessing Link Quality Estimators," *Ad Hoc Networks*, vol. 9, no. 7, pp. 1165–1185, 2011.

[104] M. Butt, A. Akbar, K.-H. Kim, M. Javed, C.-S. Lim, and Q. Taj, "LABILE: Link Quality-based Lexical Routing Metric for Reactive Routing Protocols in IEEE 802.15. 4 Networks," *The Journal of Supercomputing*, vol. 62, no. 1, pp. 84–104, 2012.

[105] N. Baccour, A. Koubâa, H. Youssef, M. B. Jamâa, D. Rosário, M. Alves, and L. B. Becker, "F-LQE: A Fuzzy Link Quality Estimator for Wireless Sensor Networks," in *Proceedings of the European Conference on Wireless Sensor Networks (EWSN'10)*. Coimbra, Portugal: Springer, Feb. 2010, pp. 240–255.

[106] C. Gomez, A. Boix, and J. Paradells, "Impact of LQI-based Routing Metrics on the Performance of a One-to-one Routing Protocol for IEEE 802.15. 4 Multihop Networks," *Journal on Wireless Communications and Networking (EURASIP)*, vol. 2010, no. 1, p. 205407, 2010.

[107] N. Baccour, A. Koubâa, M. Ben Jamaa, H. Youssef, M. Zuniga, and M. Alves, "A Comparative Simulation Study of Link Quality Estimators in Wireless Sensor Networks," in *Proceedings of the IEEE International Symposium on Modeling, Analysis & Simulation of Computer and Telecommunication Systems (MASCOTS'09)*. London, England: IEEE, Sep. 2009, pp. 1–10.

[108] Z. Zhao, D. Rosário, T. Braun, E. Cerqueira, H. Xu, and L. Huang, "Topology and Link Quality-aware Geographical Opportunistic Routing in Wireless Ad-hoc Networks," in *Proceedings of the 9th Internation Conference on Wireless Communications & Mobile Computing Conference (IWCMC'13)*. Sardinia, Italy: IEEE, Jul. 2013, pp. 1522–1527.

[109] D. Rosário, Z. Zhao, T. Braun, E. Cerqueira, A. Santos, and Z. Li, "Assessment of a Robust Opportunistic Routing for Video Transmission in Dynamic Topologies," in *Proceedings of the IFIP Wireless Days conference (WD'13)*. Valencia, Spain: IEEE, Nov. 2013, pp. 1–6.

[110] D. Rosário, Z. Zhao, A. Santos, T. Braun, and E. Cerqueira, "A Beaconless Opportunistic Routing Based on a Cross-Layer Approach for Efficient Video Dissemination in Mobile Multimedia IoT Applications." *Computer Communication (comcom)*, 2014.

[111] D. Rosário, Z. Zhao, T. Braun, E. Cerqueira, and A. Santos, "Opportunistic Routing for Multi-flow Video Dissemination over Flying Ad-Hoc Networks," in *Proceedings of the EEE International Symposium on a World of Wireless, Mobile and Multimedia Networks (WoWMoM'14)*. Sydney, Australia: IEEE, Jun. 2014.

[112] ——, "A Comparative Simulation Analysis of Beaconless OR Protocols for Video Dissemination over FANETs," in *Submitted*, 2014.

[113] L. Lin, Q. Sun, J. Li, and F. Yang, "A Novel Geographic Position Mobility Oriented Routing Strategy for UAVs," *Journal of Computational Information Systems*, vol. 8, no. 2, pp. 709–716, 2012.

[114] E. Ancillotti, R. Bruno, M. Conti, and A. Pinizzotto, "Load-aware Routing in Mesh Networks: Models, Algorithms and Experimentation," *Computer Communications*, vol. 34, no. 8, pp. 948–961, 2011.

[115] Y. Xu, J. Deng, M. Nowostawski, and M. Purvis, "Optimized Routing for Video Streaming in Multi-hop Wireless Networks using Analytical Capacity Estimation," *Journal of Computer and System Sciences*, 2013.

[116] C.-J. Hsu, H.-I. Liu, and W. K. G. Seah, "Survey Paper: Opportunistic routing - A review and the challenges ahead," *Computer Network*, vol. 55, no. 15, pp. 3592–3603, oct. 2011.

[117] S. Biswas and R. Morris, "ExOR: Opportunistic Multi-hop Routing for Wireless Networks," in *Proceedings of the ACM SIGCOMM Computer Communication Review (SIGCOMM'05)*, vol. 35, no. 4. New York, USA: ACM, 2005, pp. 133–144.

[118] R. Prasad and M. Ruggieri, *Applied Satellite Navigation Using GPS, GALILEO, and Augmentation Systems*. Artech House, 2005.

[119] P. Huang, H. Chen, G. Xing, and Y. Tan, "SGF: A State-free Gradient-based Forwarding Protocol for Wireless Sensor Networks," *ACM Transactions on Sensor Networks (TOSN)*, vol. 5, no. 2, pp. 14:1–14:25, 2009.

[120] J. Jubin and J. D. Tornow, "The DARPA Packet Radio Network Protocols," *Proceedings of the IEEE*, vol. 75, no. 1, pp. 21–32, 1987.

[121] Z. Zhao, D. Rosário, T. Braun, and E. Cerqueira, "Context-aware Opportunistic Routing in Mobile Ad-hoc Networks Incorporating Node Mobility," in *Proceedings of the IEEE Wireless Communications and Networking Conference (WCNC'14)*. Istanbul, Turkey: IEEE, Apr. 2014.

[122] Z. Zhao, T. Braun, D. Rosário, and E. Cerqueira, "CAOR: Context-aware Adaptive Opportunistic Routing in Mobile Ad-hoc Networks," in *Proceedings of the 7th IFIP Wireless and Mobile Networking Conference (WMNC'14)*. Vilamoura, Portugal: IEEE, May 2014.

[123] J. Nonnenmacher and E. W. Biersack, "Scalable Feedback for Large Groups," *IEEE/ACM Transactions on Networking (ToN)*, vol. 7, no. 3, pp. 375–386, 1999.

[124] G. Zhou, T. He, S. Krishnamurthy, and J. A. Stankovic, "Impact of Radio Irregularity on Wireless Sensor Networks," in *Proceedings of the 2nd international conference on Mobile systems, applications, and services (MobiSys'04)*. Boston, USA: ACM, Jun. 2004, pp. 125–138.

[125] L. Shu, Y. Zhang, L. T. Yang, Y. Wang, M. Hauswirth, and N. Xiong, "TPGF: Geographic Routing in Wireless Multimedia Sensor Networks," *Telecommunication Systems*, vol. 44, no. 1-2, pp. 79–95, 2010.

[126] C. Palazzi, M. Roccetti, and S. Ferretti, "A-bombunication Architecture for Safety and Entertainment," *IEEE Transactions on Intelligent Transportation Systems*, vol. 11, no. 1, pp. 90–99, 2010.

[127] T. Anagnostopoulos, C. Anagnostopoulos, and S. Hadjiefthymiades, "An Adaptive Location Prediction Model Based on Fuzzy Control," *Computer Communications*, vol. 34, no. 7, pp. 816–834, 2011.

[128] T. Steinbach, H. D. Kenfack, F. Korf, and T. C. Schmidt, "An extension of the OMNeT++ INET Framework for Simulating Real-Time Ethernet with High Accuracy," in *Proceedings of the 4th International Workshop on OMNeT++ (OMNeT++'11)*. Barcelona, Spain: ICST, Mar. 2011, pp. 375–382.

[129] D. Rosario, Z. Zhao, C. Silva, E. Cerqueira, and T. Braun, "An OMNeT++ Framework to Evaluate Video Transmission in Mobile Wireless Multimedia Sensor Networks," in *Proceedings of the 6th International Workshop on OMNeT++ (OMNeT++'13)*. Cannes, France: ICST, Mar. 2013, pp. 277–284.

[130] A. Boulis, "Castalia, a Simulator for Wireless Sensor Networks and Body Area Networks, Version 2.2," *User manual, NICTA*, Aug. 2009.

[131] C. Nastasi and A. Cavallaro, "WiSE-MNet: an Experimental Environment for Wireless Multimedia Sensor Networks," in *Proceedings of Sensor Signal Processing for Defence (SSPD'11)*. London, England: IET, Sep. 2011, pp. 1–5.

[132] C. Pham and A. Makhoul, "Performance Study of Multiple Cover-Set Strategies for Mission-Critical Video Surveillance with Wireless Video Sensors," in *Proceedings of the IEEE 6th International Conference on Wireless and Mobile Computing, Networking and Communications (WiMob'10)*. Niagara Falls, Canada: IEEE, Oct. 2010, pp. 208–216.

[133] M. Zuniga and B. Krishnamachari, "Analyzing the Transitional Region in Low Power Wireless Links," in *Proceedings of the First Annual IEEE Communications Society Conference on Sensor and Ad Hoc Communications and Networks (SECON'04)*, Oct 2004, pp. 517–526.

[134] Z. Zhao, B. Mosler, and T. Braun, "Performance Evaluation of Opportunistic Routing Protocols: A Framework-based Approach Using OMNeT++," in *Proceedings of the 7th Latin American Networking Conference (LANC '12)*. ACM, Oct. 2012, pp. 28–35.

[135] Evalvid, "EvalVid - A Video Quality Evaluation Tool-set," [OnLine] Available: http://www2.tkn.tu-berlin.de/research/evalvid/fw.html. (Access date: Jun. 2014).

[136] N. Aschenbruck, R. Ernst, E. Gerhards-Padilla, and M. Schwamborn, "BonnMotion: a Mobility Scenario Generation and Analysis Tool," in *Proceedings of the 3rd International ICST Conference on Simulation Tools and Techniques (SIMUTools'10)*. Malaga, Spain: ICST, Mar. 2010, pp. 51:1–51:10.

[137] M. Mu, P. Romaniak, A. Mauthe, M. Leszczuk, L. Janowski, and E. Cerqueira, "Framework for the Integrated Video Quality Assessment," *Multimedia Tools and Applications*, vol. 61, no. 3, pp. 1–31, 2012.

[138] K. J. Ma, R. Bartoš, and S. Bhatia, "Review: A Survey of Schemes for Internet-based Video Delivery," *Journal of Network and Computer Applications*, vol. 34, no. 5, pp. 1572–1586, Sep. 2011.

[139] Z. Wang, A. C. Bovik, H. R. Sheikh, and E. P. Simoncelli, "Image Quality Assessment: From Error Visibility to Structural Similarity," *IEEE Transactions on Image Processing*, vol. 13, no. 4, pp. 600–612, 2004.

[140] M. H. Pinson and S. Wolf, "A New Standardized Method for Objectively Measuring Video Quality," *IEEE Transactions on Broadcasting*, vol. 50, no. 3, pp. 312–322, 2004.

[141] "ITU-R recommendation BT.500-11. methodology for the subjective assessment of the quality of television pictures," international Telecommunication Union, Geneva, Switzerland, pp. 53–56, 2002.

[142] D. Vatolin, A. Moskvin, O. Petrov, and N. Trunichkin, "MSU Video Quality Measurement Tool," [OnLine] Available: http://www.download3k.com/Install-MSU-Video-Quality-Measurement-Tool.html. (Access date: Jun. 2014).

[143] K. Seshadrinathan, R. Soundararajan, A. C. Bovik, and L. K. Cormack, "Study of Subjective and Objective Quality Assessment of Video," *IEEE transactions on Image Processing*, vol. 19, no. 6, pp. 1427–1441, 2010.

[144] P. Boluk, S. Baydere, and A. Harmanci, "Robust Image Transmission over Wireless Sensor Networks," *Mobile Networks and Applications*, vol. 16, no. 2, pp. 149–170, 2011.

[145] A. Rowe, C. Rosenberg, and I. Nourbakhsh, "A Low Cost Embedded Color Vision System," in *Proceedings of the International Conference on Intelligent Robots and Systems (RSJ'02)*. IEEE, Sep. 2002, pp. 208–213.

[146] Memsic, "Telosb Datasheet," [OnLine] Available: http://memsic.com/support/documentation/wireless-sensor-networks/category/7-datasheets.html?download=152%3Atelosb. (Access date: Jun. 2014).

[147] C. Perkins, E. Belding-Royer, and S. Das, "Ad hoc on demand distance vector (aodv) routing (rfc 3561)," *IETF MANET Working Group*, 2003.

[148] M. K. Marina and S. R. Das, "On-demand Multipath Distance Vector Routing in Ad Hoc Networks," in *Proceedings of the 79th International Conference on Network Protocols*. IEEE, Nov. 2001, pp. 14–23.

[149] P. Hurni and T. Braun, "Energy-Efficient Multi-path Routing in Wireless Sensor Networks," in *Proceedings of the 7th International Conference on Ad-hoc Networks & Wireless (ADHOC-NOW'08)*. Sophia-Antipolis, France: LCNS, Sep. 2008, pp. 72–85.

[150] GERCOM, "A Set of Videos Transmitted via LinGO, BLR, BOSS, and MRR, together with the Original Videos," 2013, https://plus.google.com/117765468529449487870/videos. Acessado em 10 de Setembro de 2013.

[151] ——, "A Set of Videos Transmitted via LinGO, BLR, and MRR, together with the Original Videos," [online] http://cds.unibe.ch/research/M3WSN/videos.zip and accessed at Jul. 2013.

[152] P. Hurni, M. Anwander, G. Wagenknecht, T. Staub, and T. Braun, "TARWIS: a Testbed Management Architecture for Wireless Sensor Network Testbeds," in *Proceedings of the 7th International Conference on Network and Services Management (NOMS'11)*. ACM, Apr. 2011, pp. 320–323.

List of Publications

List of papers with main contributions:

1. D. Rosário, K. Machado, A. Abelém, D. Monteiro, and E. Cerqueira, *Recent Advances and Challenges in Wireless Multimedia Sensor Networks*, ser. Mobile Multimedia - User and Technology Perspectives. Dian Tjondronegoro (Ed.): InTech, jan 2012 b, pp. 74–96.

2. E. Cerqueira, A. Santos, D. Rosário, T. Braun, and M. Gerla, *Multimedia Human-Centric Networking: Concepts, Technologies and Trends*, ser. Tutorials of the 32th Brazilian Symposium on Computer Networks and Distributed Systems (SBRC'14). Carlos Maziero (Ed.): SBC, May 2014.

3. D. Rosário, Z. Zhao, A. Santos, T. Braun, and E. Cerqueira, "A Beaconless Opportunistic Routing Based on a Cross-Layer Approach for Efficient Video Dissemination in Mobile Multimedia IoT Applications." *Computer Communication*, 2014.

4. D. Rosário, R. Costa, H. Paraense, K. Machado, E. Cerqueira, T. Braun, and Z. Zhao, "A Hierarchical Multi-hop Multimedia Routing Protocol for Wireless Multimedia Sensor Networks," *Network Protocols and Algorithms (NPA)*, vol. 4, no. 2, pp. 44–64, 2012.

5. D. Rosário, Z. Zhao, T. Braun, E. Cerqueira, and A. Santos, "Opportunistic Routing for Multi-flow Video Dissemination over Flying Ad-Hoc Networks," in *Proceedings of the EEE International Symposium on a World of Wireless, Mobile and Multimedia Networks (WoWMoM'14).* Sydney, Australia: IEEE, Jun. 2014.

6. D. Rosário, Z. Zhao, T. Braun, E. Cerqueira, and A. Santos, "A Comparative Simulation Analysis of Beaconless OR Protocols for Video Dissemination over FANETs," in *Submitted*, 2014.

7. Z. Zhao, D. Rosário, T. Braun, E. Cerqueira, H. Xu, and L. Huang, "Topology and Link Quality-aware Geographical Opportunistic Routing in Wireless Ad-hoc Networks," in *Proceedings of the 9th Internation Conference on Wireless Communications & Mobile Computing Conference (IWCMC'13)*. Sardinia, Italy: IEEE, Jul. 2013, pp. 1522–1527.

8. D. Rosário, Z. Zhao, T. Braun, E. Cerqueira, A. Santos, and Z. Li, "Assessment of a Robust Opportunistic Routing for Video Transmission in Dynamic Topologies," in *Proceedings of the IFIP Wireless Days conference (WD'13)*. Valencia, Spain: IEEE, Nov. 2013, pp. 1–6.

9. D. Rosário, R. Costa, A. Santos, T. Braun, and E. Cerqueira, "QoE-aware Multiple Path Video Transmission for Wireless Multimedia Sensor Networks," in *Proceedings of the 31th Brazilian Symposium on Computer Networks and Distributed Systems (SBRC'13)*. Brasilia, Brazil: SBC, May 2013, pp. 31–44.

10. D. Rosário, Z. Zhao, C. Silva, E. Cerqueira, and T. Braun, "An OMNeT++ Framework to Evaluate Video Transmission in Mobile Wireless Multimedia Sensor Networks," in *Proceedings of the 6th International Workshop on OMNeT++*. Cannes, France: ICST, Mar. 2013, pp. 277–284.

11. D. Rosário, R. Costa, H. Paraense, K. Machado, E. Cerqueira, and T. Braun, "A Smart Multi-Hop Hierarchical Routing Protocol for Efficient Video Communication over Wireless Multimedia Sensor Network," in *Proceedings of the 2nd IEEE International Workshop on Smart Communication Protocols and Algorithms (ICC'12 WS-SCPA)*. Ottawa, Canada: IEEE, Jun. 2012, pp. 8113–8117.

12. Z. Zhao, T. Braun, D. Rosário, E. Cerqueira, R. Immich, and M. Curado, "QoE-aware FEC Mechanism for Intrusion Detection in Multi-tier Wireless Multimedia Sensor Networks," in *Proceedings of the 1st International Workshop on Wireless Multimedia Sensor Networks (WiMob'12 WS-WMSN)*. Barcelona, Spain: IEEE, Oct. 2012, pp. 697–704.

13. D. Rosário, Z. Zhao, T. Braun, and E. Cerqueira, "A Cross-layer QoE-based Approach for Event-Based Multi-tier Wireless Multimedia Sensor Networks," *Submitted*, 2014.

List of papers with minor contributions:

1. D. Rosário, E. Cerqueira, A. Neto, A. Riker, R. Immich, and M. Curado, "A QoE Handover Architecture for Converged Heterogeneous Wireless Networks," *Wireless Networks (winet)*, vol. 19, no. 8, pp. 2005–2020, 2013.

2. K. Machado, D. Rosário, E. Cerqueira, A. A. Loureiro, A. Neto, and J. N. de Souza, "A Routing Protocol Based on Energy and Link Quality for Internet of Things Applications," *Sensors (Basel)*, vol. 13, no. 2, pp. 1942–1964, 2013.

3. K. Machado, D. d. Rosário, E. Nakamura, A. Abelém, and E. Cerqueira, "Design of a Routing Protocol using Remaining Energy and Link Quality Indicator (REL)," in *Proceedings of the 6th Latin America Networking Conference (LANC'11).* Quito, Equator: ACM, Jun. 2011, pp. 33–39.

4. Z. Zhao, D. Rosário, T. Braun, and E. Cerqueira, "Context-aware Opportunistic Routing in Mobile Ad-hoc Networks Incorporating Node Mobility," in *Proceedings of the IEEE Wireless Communications and Networking Conference (WCNC'14).* Istanbul, Turkey: IEEE, Apr. 2014.

5. Z. Zhao, T. Braun, D. Rosário, and E. Cerqueira, "CAOR: Context-aware Adaptive Opportunistic Routing in Mobile Ad-hoc Networks," in *Submitted to 7th IFIP Wireless and Mobile Networking Conference (WMNC'14).* Vilamoura, Portugal: IEEE, May 2014.

6. P. Lima, T. Fonseca, D. Rosário, K. Machado, and E. Cerqueira, "Monitoramento Ambiental Através de Redes de Sensores Sem Fio e Redes Sociais," in *Proceedings of the Salão de Ferramentas of the 30th Brazilian Symposium on Computer Networks and Distributed Systems (SBRC'12).* Ouro Preto, Brazil: SBC, May 2012, pp. 938–945.

7. D. Rosário, P. Lima, K. Machado, E. Cerqueira, Z. Zhao, and T. Braun, "Demo Abstract: Disseminating WMSN Data by Using Social Network and Web," in *Proceedings of the 10th European Conference on Wireless Sensor Networks (EWSN'13)*, Ghent, Belgium, Feb. 2013.

Curriculum Vitae

Personal Details	
Name	Denis Lima do Rosário
Date of Birth	October 1, 1986
Address	Av. Conselheiro Furtado 1663, apto 403 66040-100, Belém-pa
Nationality	Brazilian
Education	
2010-2014	PhD Student and Researcher in Electrical Engineering at Federal University of Pará–Brazil. Joint-supervision undertaken by the Institute of Computer Science and Applied Mathematics of the University of Bern–Switzerland.
Mar. 2012 to Nov. 2013	Visiting Researcher at University of Bern, Switzerland.
2008-2010	Master degree in Automation and systems Engineering, by the Federal University of Santa Catarina, Brazil.
Feb. – Aug. 2009	Visiting Researcher at School of Engineering of the Polytechnic Institute of Porto, Portugal.
2004-2007	Bachelor in Computer Engineering, by the Institute of Higher Studies of Amazon, Brazil.

Erklärung

gemäss Art. 28 Abs. 2 RSL 05

Name/Vorname: Lima do Rosário, Denis

Matrikelnummer: ....

Studiengang: Informatik

Bachelor ☐ Master ☐ Dissertation ☒

Titel der Arbeit: Cross-layer Optimizations for Multimedia Distribution over Wireless Multimedia Sensor Networks and Flying Ad-Hoc Networks with Quality of Experience Support

LeiterIn der Arbeit: Prof. Dr. Eduardo Coelho Cerqueira
Prof. Dr. Torsten Braun

Ich erkläre hiermit, dass ich diese Arbeit selbständig verfasst und keine anderen als die angegebenen Quellen benutzt habe. Alle Stellen, die wörtlich oder sinngemäss aus Quellen entnommen wurden, habe ich als solche gekennzeichnet. Mir ist bekannt, dass andernfalls der Senat gemäss Artikel 36 Absatz 1 Buchstabe r des Gesetztes vom 5. September 1996 über die Universität zum Entzug des auf Grund dieser Arbeit verliehenen Titels berechtigt ist.

Ich gewähre hiermit Einsicht in diese Arbeit.

Belém, 2.6.2014
Ort/Datum

Denis Lima do Rosário
Unterschrift